Extensions of Retrospective Cost Adaptive Control: Nonsquare Plants, and Robustness Modifications

by

Erol Dogan Sumer

A dissertation submitted in partial fulfillment
of the requirements for the degree of
Doctor of Philosophy
(Aerospace Engineering)
in The University of Michigan
2013

Doctoral Committee:

Professor Dennis S. Bernstein, Chair
Professor Anouck R. Girard
Professor Ilya V. Kolmanovsky
Professor Semyon M. Meerkov

To my beloved grandmother, Durefsan Ozsubasi

ACKNOWLEDGEMENTS

It is difficult to put into words my gratitude for those who supported me in this long journey, but I will try my best:

I am deeply grateful to my future wife, Duygu Kanver; for your love, patience and support made the writing of this dissertation much more pleasant than how it would have been without you. I hereby pledge to return the favor by being there with you when you write your own PhD dissertation in a few years.

Special thanks to my advisor, Dennis Bernstein. Thanks to your valuable guidance, I am now on the verge of becoming a "Doctor of Philosophy". Your intellect and insight into science and engineering never cease to amaze me, even at times when I disagree with you.

I am deeply indebted to Galatasaray Educational Foundation (GEV) and Arcelor-Mittal S.A, whose financial support made my dreams of higher education come true. I am especially grateful to Mr. Sait Bingol and Mr. Adnan Ozturk who played major role in the arrangement of this scholarship. I can only repay my debt of gratitude to you by providing the same support to my younger fellows from the Galatasaray community in the future.

Finally, I would like to thank my parents, Hasan Sumer and Jeyan Sumer, and my brother, Uygur Sumer. Simply put, I wouldn't be the man I am today without either one of you.

TABLE OF CONTENTS

LIST OF FIGURES

Figure

LIST OF TABLES

Table

CHAPTER I

Introduction

1.1 Control System Design

Control system design consists of choosing the controlled plant inputs so that the performance outputs of the plant meet a set of predefined control objectives in the presence of uncontrolled exogenous inputs entering the plant. A plant is any process that takes inputs and generates outputs, as shown in Figure 1.1.

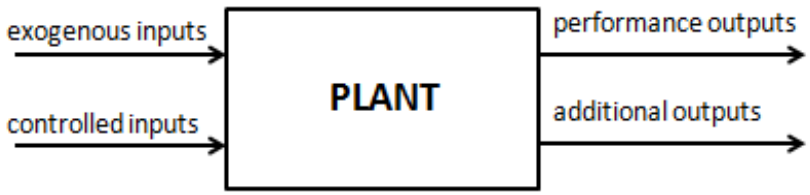

Figure 1.1: A plant is a system that takes inputs and generates outputs.

Cruise control in the modern automobiles is one of the most popular control system applications. For cruise control, the plant is the automobile, and the task is to choose the control input acting on the automobile in order to regulate the output of the automobile, in the presence of exogenous forces disturbing the vehicle. Specifically, the goal is to choose the gas pedal angle so that the vehicle maintains a desired speed, in the presence of aerodynamical and gravitational forces acting on the vehicle.

Two main approaches are commonly used (sometimes jointly) in addressing the control system design: Feedforward and Feedback control. Feedforward, or open-loop control refers to the control system design in which the choice of the control input does not depend on the plant output. For example, for the automobile, a primitive feedforward cruise control strategy would be to adjust the gas pedal angle α based on the desired speed level v. This can be done by going on a test drive with the vehicle and recording the throttle angles $\alpha_1, \ldots, \alpha_k$ for a predefined set of speed levels $v_1, \ldots, v_k$. A feedforward cruise control scheme can then be implemented by building a mechanism that adjusts the throttle angle according to the desired speed level set by the driver. While this approach may work in ideal conditions, one critical aspect of the problem that was overlooked in this approach is the presence of exogenous, or disturbance forces acting on the vehicle. For instance, if you did your test drive and recorded the α_i values on a flat road on a wind-free day, then it is very unlikely that your feedforward cruise controller will accurately maintain the desired speed when your vehicle is climbing on a windy day. A command-feedforward control system is shown in Figure 1.2.

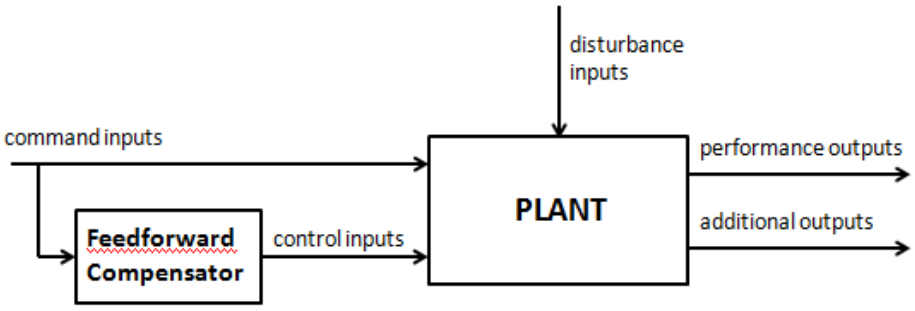

Figure 1.2: Command-feedforward control architecture.

On the other hand, in feedback control, the control input is chosen based on measured values of plant outputs. An immediate prerequisite for feedback control is thus the use of sensors to measure the outputs, which in turn increases the cost to imple-

ment the control system. However, feedback control performs better than feedforward control in the presence of external disturbances, is less sensitive to uncertainty in the plant parameters, and is applicable to a broader range of plants [32, 62, 94, 95]. An output feedback control architecture is shown in Figure 1.3.

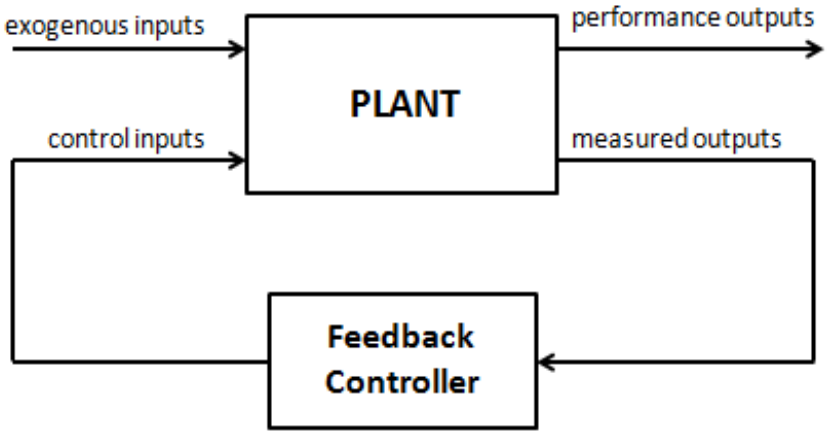

Figure 1.3: Output-feedback control architecture.

1.2 Feedback Control

We interact with feedback control systems very frequently in our daily environment. In our homes, we interact with refrigerators and air conditioning units which utilize feedback control to regulate the ambient temperature. Modern vehicles are equipped with feedback control systems such as cruise control or traction control systems. In fact, while driving, the human brain acts like an output-feedback controller; the eyes read the speed measurements from the speedometer, the brain compares the measured speed with the speed limit, and uses the feet to regulate the speed by pressing the brake or gas pedals.

The common objectives in feedback control are command following, disturbance rejection, or the combination of both. The goal of command following is to have the output of the plant follow a command trajectory. In disturbance rejection, the goal

is to cancel the effect of external disturbances from the output of the plant. Finally, combined command following and disturbance rejection problem consists of having the output of the plant follow a command trajectory in the presence of external disturbances. For instance, cruise control is a combined command following and disturbance rejection problem, where the goal is to have the vehicle speed remain near the commanded value in the presence of gravitational, frictional, and aerodynamic disturbances acting on the vehicle.

One of the major benefits of feedback control is that it inherently reduces the effect of disturbances and sensitivity of the control system to uncertainty in the plant, assuming that the closed-loop stability is maintained. Therefore, in control systems, the feedback gains must be as large as possible, but not larger, as too much feedback may cause instability. The fundamental challenge in feedback control is thus to design a controller that provides enough feedback in order to attenuate the disturbances and reduce sensitivity, while maintaining closed-loop stability. If the exogenous inputs are outputs of an unforced linear system, then the feedback controller can be designed using the internal model principle [23, 29, 30, 31, 52], which consists of designing a controller with high gain at the exogenous signal frequencies and small gain in other frequencies. An integrator, which has infinite gain at DC, is the simplest internal model controller. On the other hand, if the exogenous inputs are broadband, then LQR/LQG techniques can be used to minimize the H_2 cost of the closed-loop system [81, 90, 95, 117]. However, these methods may require a complete and exact model of the plant dynamics as well as a complete and exact model of the disturbance and sensor-noise statistics and frequency spectrum. Therefore, any uncertainty in the plant model or disturbance spectrum could lead to poor closed-loop performance, or worse, instability.

1.3 Adaptive Control

In many applications of control, a model of the plant that is sufficiently accurate for feedback control synthesis is not available. A model with sufficient fidelity may be lacking due to either complex physics that are not amenable to first principles analysis or the inability to collect a sufficient amount of quality data for empirical modeling. Even if a sufficiently accurate model is available, the plant may undergo unexpected changes that cannot be accounted for prior to control-system operation.

The underlying motivation for feedback is uncertainty, yet uncertainty in the parameters of a plant can degrade performance and lead to instability. The goal of robust control is to design controllers that account for prior uncertainty in the plant model [25, 71, 95, 117]. Robust control thus trades performance for stability.

In contrast to robust control, the goal of adaptive control is to avoid the need to sacrifice performance for modeling uncertainty by modifying the controller online to the actual plant. Although there is not an established definition of adaptive control, it is generally understood to be a form of highly robust nonlinear control that does not a priori sacrifice performance for uncertainty. In daily use, "to adapt" evokes a modification according to changing circumstances. In [4], an adaptive controller is defined as *a controller with adjustable parameters and a mechanism for adjusting the parameters*. This definition invokes the use of an update mechanism (or update law) that adjusts the parameters of the control law. Typically, this update mechanism is driven by the performance output of the plant, and the updated controller parameters are used to compute the control input, as shown for a feedback architecture in Figure 1.4.

Adaptive control for linear systems primarily focuses on adaptive stabilization, adaptive pole placement, adaptive command following, and model reference adaptive control (MRAC) [4, 7, 21, 34, 45, 46, 47, 50, 65, 66, 75, 79, 91, 105]. Extensions of adaptive control to nonlinear systems include adaptive backstepping control, adaptive

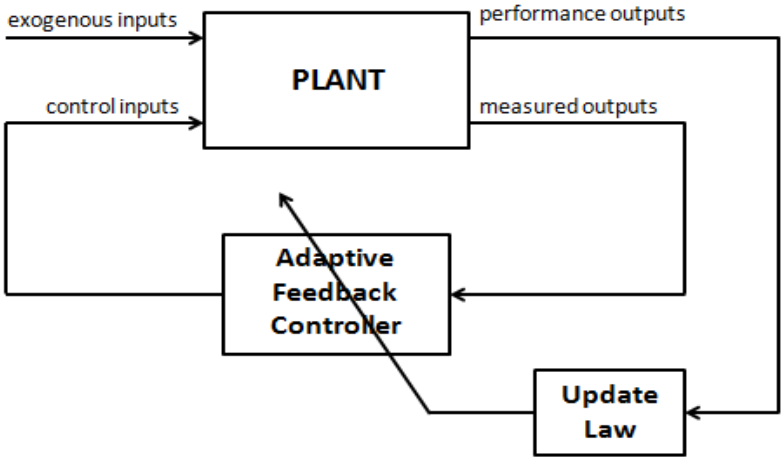

Figure 1.4: Adaptive feedback control architecture.

feedback linearization of nonlinear systems, and adaptive nonlinear stabilization using control Lyapunov functions [53, 58, 60, 116].

For control applications requiring disturbance rejection, adaptive feedforward control algorithms such as filtered-X LMS have been developed [26, 63, 64]. These algorithms do not require knowledge of the disturbance spectrum, but require a direct measurement of the disturbance signal. For applications in which measurements of only the plant response are available, feedback control is needed. For systems with harmonic disturbances having known spectrum, such as active noise and vibration control in helicopters, harmonic steady-state algorithms can be used [82]. For disturbance rejection in the presence of harmonic disturbances with unknown spectra, adaptive feedback control methods have been developed [10, 11, 43, 110]. A more challenging problem is adaptive disturbance rejection without feedforward measurements in the presence of broadband disturbances. Within the context of adaptive feedback control, adaptive LQG control is considered in [18, 50, 83].

Adaptive control may depend on prior modeling information, such as bounds on the model order and plant parameters, or it may entail explicit on-line system identification. These approaches are known, respectively, as direct and indirect adaptive control. Adaptive controllers can be further classified as either digital [2, 4, 34, 51, 66, 105]

or continuous-time [45, 46, 47, 50, 79, 91]. Although most plants are naturally modeled in continuous time, the modeling data used by an adaptive controller is typically based on sampled data. In addition, most control applications are confined to a fixed, bounded sample rate, while controllers developed in discrete time can be directly transformed into embedded code.

In this dissertation, we focus on retrospective cost adaptive control (RCAC), which is a digital, direct adaptive control algorithm. The earliest version of RCAC is given in [110], where the authors develop a gradient update law based on a retrospective performance variable that is computed using ARMARKOV system representations. The retrospective performance of a plant is a function of time and a controller. In particular, the retrospective performance is the performance output that would have been obtained at current time assuming that a specific controller was used over a past window of time. The underlying idea behind RCAC is to solve for the retrospectively-optimized controller minimizing the retrospective performance at each time step, and compute the control input at each time step by using the retrospectively-optimized controller. Applications and extensions of the ARMARKOV-based method are given in [1, 37, 42, 86].

In [43], a specialization of the ARMARKOV-based RCAC is considered. With this specialization, the controller update is carried out using only the first nonzero Markov parameter of the plant. Using this specialization, asymptotic command following and disturbance rejection capabilities as well as stability properties of RCAC are rigorously shown for minimum phase square plants, that is, plants with equal number of inputs and outputs. In [87, 88], RCAC update law is reformulated as an optimization problem which involves an instantaneous cost function that depends on the retrospective performance. Furthermore, an alternative to the ARMARKOV based representations is shown in [87, 88] by defining the retrospective performance in terms of the time-series numerator coefficients of the plant. Finally, in [36], RCAC update

law is reformulated as the solution of a cumulative cost function. Asymptotic convergence properties for SISO, possibly nonminimum-phase (NMP) plants are shown in [36] for both instantaneous and cumulative update laws, and these results are shown for a MRAC extension of RCAC in [41]. This dissertation thus focuses on and extends the instantaneous and cumulative update laws developed in [36, 43, 87, 88].

1.4 Adaptive Control of Nonsquare Plants

Most adaptive controllers, including MRAC, have the restrictive assumption that the plant is minimum phase. The gradient-based method in [43] considers MIMO, square plants, and shows convergence and stability results for MIMO, square plants, assuming all the transmission zeros of the plant are minimum-phase. RCAC developed in [87, 88, 110] is applicable to NMP plants, but it is assumed that the NMP transmission zeros of the plant, if any, are known.

Zeros of nonsquare (tall or wide) plants are considered in [24, 59], where it is shown that nonsquare plants generically have no transmission zeros. This suggests that nonsquare systems are generically minimum phase. Does this mean that it is easier to apply adaptive control schemes to nonsquare plants than to square plants?

To be specific, consider the open-loop systems shown in Figures 1.5 and 1.6. In Figure 1.5, the transfer functions from u to z_1, and u to z_2 are NMP. However, the MIMO transfer matrix from u to $z = \begin{bmatrix} z_1 & z_2 \end{bmatrix}^{\mathrm{T}}$ given by

$$G(z) = \begin{bmatrix} \frac{z-2}{z^2} \\ \\ \frac{z-3}{z^2} \end{bmatrix} \tag{1.1}$$

has no transmission zeros, and therefore is minimum phase. Similarly, in Figure 1.6, the SISO channels are NMP, but the MIMO transfer matrix is minimum phase.

Let us assume that, for RCAC, it is indeed easier to control nonsquare plants since

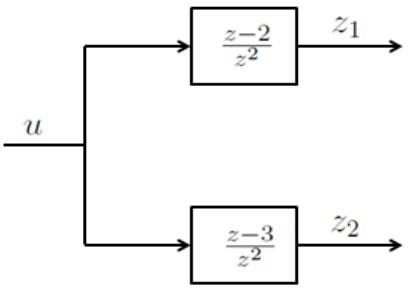

Figure 1.5: A 2×1 tall system. The transfer function from u to z_1 is NMP, the transfer function from u to z_2 is NMP, but the transfer matrix from u to $z \stackrel{\triangle}{=} [z_1 \ z_2]^{\mathrm{T}}$ has no transmission zeros.

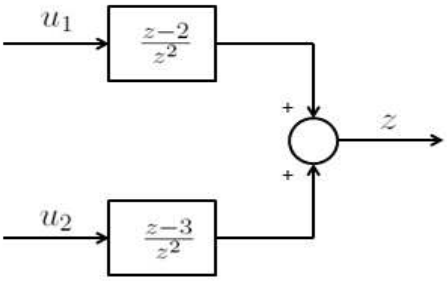

Figure 1.6: A 1×2 wide system. The transfer function from u_1 to z is NMP, the transfer function from u_2 to z is NMP, but the transfer matrix from $u \stackrel{\triangle}{=} [u_1 \ u_2]^{\mathrm{T}}$ to z has no transmission zeros.

they generically have no transmission zeros. If this assumption held, then, in order to control a SISO plant, all we would need to do is to add one more sensor or actuator to the system, thus obtain either a wide or a tall plant, and apply RCAC without worrying about the NMP zeros of the plant.

In this dissertation, we investigate adaptive control of MIMO nonsquare systems with RCAC, and we demonstrate that nonsquare plants are not easier to control than square plants, as far as the zero structure is concerned. In particular, contrary to the intuitive expectation, we show that, the fact that the nonsquare plant is minimum phase does not guarantee closed-loop stability and signal boundedness properties, unlike the square case. Specifically, we show that, due to the nature of the RCAC update law, retrospective cost adaptive control involves two implicit squaring operations; one performed by pre-compensating the plant, the other performed by post-compensating the plant. In the wide case, pre-compensation leads to squaring-down, which incorporates additional zeros due to squaring, which we call "input-subspace zeros". Similarly, in the tall case, post-compensation changes the zero structure and incorporates additional zeros, which we call output-subspace zeros. We show that if

the nonsquare plant has NMP subspace zeros, then RCAC may attempt to cancel these zeros, which leads to unbounded control input in the wide case, and unbounded control input and performance output in the tall case.

1.5 Robust Adaptive Control

Although adaptive control reduces the need for plant modeling, it usually does not eliminate it completely. This modeling information may be obtained through either an offline identification process, leading to direct adaptive control, or a simultaneous identification process, leading to indirect adaptive control. In either case, it stands to reason that the less modeling information an adaptive controller needs, the more robust it is to model uncertainty. It may therefore be tempting to think that an adaptive controller is inherently robust to any modeling information that it does not require. This reasoning, however, is not completely accurate.

All practical adaptive controllers inevitably require that the plant dynamics satisfy certain assumptions. The most common assumptions made in adaptive control include passivity, positive realness, or that the plant is minimum phase. Consequently, the fact that an adaptive controller does not require a particular modeling information does not imply that it is unconditionally robust to uncertainty in that modeling information. For example, most adaptive controllers do not require specific knowledge of plant poles and zeros, but, uncertainty in pole-zero configurations, or the presence of unmodeled dynamics in the plant may lead to a violation of the assumptions and thus destabilize the adaptive system.

The publication in 1985 of [84] challenged the robustness of adaptive control methods to uncertainty in plant dynamics. In particular, [84] presented two counterexamples (known as the Rohrs counterexamples) showing the fragility of model reference adaptive control (MRAC) schemes. These counterexamples considered plants with high-frequency unmodeled dynamics that can induce a large, unknown phase shift

in the plant's open-loop response. The presence of unknown dynamics was shown to result in drifting control parameters and unbounded plant response. These counterexamples initially dampened enthusiasm for adaptive control and led to a cautionary view of these techniques. However, [84] encouraged the development of robustness modifications that overcame the instability observed in these counterexamples [4, 48, 49, 50, 77, 78, 79, 80, 91, 106].

Among the robustness modifications, the most common are leakage modifications [4, 50, 78, 79] and parameter projection [34, 50, 76, 80]. Leakage modifications eliminate parameter drift by adding a penalty term into the cost function which penalizes the distance from the controller to an a priori known stabilizing controller. If the plant is asymptotically stable, the stabilizing controller is typically chosen to be zero. On the other hand, parameter projection eliminates parameter drift by constraining the controller parameters to lie inside an a priori defined bounded convex set in the parameter space. Each of these modifications is essentially based on constraining the control parameters so that they do not depart too far away from an a priori determined set of stabilizing controllers. These modifications led to a relaxation in the adaptive control assumptions such as passivity, positive realness, known relative degree, and persistent excitation.

Within the context of RCAC developed in [36, 41, 43, 87, 88, 110], the relative degree, and the NMP zeros of the plant, if any, are assumed to be known. For RCAC, the presence of unmodeled dynamics may therefore lead to two violations: It may induce additional unknown NMP zeros due to sampling [3], or it may increase the relative degree of the plant. Fortunately for RCAC, or for any sampled-data based digital adaptive control scheme, the relative degree of a sampled-data system is almost always equal to one, regardless of the relative degree of the underlying continuous-time plant. Therefore, unmodeled dynamics in the continuous-time plant generically do not change the relative degree of the sampled-data plant and do not lead to a

violation of the known relative degree assumption. However, unknown NMP zeros contributed by unmodeled dynamics stand as a major robustness challenge for RCAC.

The RCAC schemes developed in this dissertation incorporate a performance-dependent control penalty that prevents the controller from destabilizing the closed-loop system in the presence of unknown NMP zeros. This robustness modification was originally developed for a variation of RCAC, where the controller update consisted of an intermediate step of reconstructing the retrospective controls [19]. In this dissertation, we remove the intermediate step of reconstructing the retrospective controls and, as in [36, 41, 43, 87, 88, 110], we directly update the controller. We do this for an instantaneous cost function as in [87, 88] as well as for a cumulative cost function as in [36, 41]. In addition, and unlike [19], we modify the cost function by filtering the data used in the retrospective performance, which allows the algorithm to work for plants with known NMP zeros without the need to use the robustness modification. This new robust RCAC scheme was originally developed and applied to Rohrs counterexamples in [100]. Further applications of robust RCAC to flexible structures are presented for a centralized control architecture in [98], and for a decentralized control architecture in [99]. Finally, in addition to the robustness modification presented in [98, 99, 100], which penalizes the distance of the control parameters from the origin, a novel feature of the robustness modification developed in this dissertation is the additional flexibility of penalizing the distance between the controller to any a priori known stabilizing controller. This additional flexibility allows RCAC to control unstable, possibly *not strongly stabilizable* [111] plants with unknown NMP zeros, provided a stabilizing controller is known in advance.

1.6 Dissertation Outline

In Chapter II, we present a review of the instantaneous and cumulative RCAC update laws developed in [36, 88]. We reformulate the instantaneous update law

given in [88] as a recursive gradient update. We also reformulate the cumulative update law given in [36] using quadratic minimization lemma [5] as in [88], and then derive the RLS update equations, which is how the update law is presented in [36]. Next, we provide a summary of the Markov-parameter-based, time-series-coefficients-based, and NMP-zero-based controller construction techniques that have been developed in [36, 88, 110]. Then, we present a summary of closed-loop stability and convergence properties of the instantaneous and cumulative RCAC update laws. Finally, we present an application of the instantaneous RCAC to road-following preview control for a vehicle, which was published in [104].

In Chapter III, we investigate RCAC for nonsquare plants. Except for the limited investigation of RCAC for SIMO and MISO plants provided in [97], RCAC for nonsquare plants has not been studied before. We start the main discussion by providing motivating examples that consider nonsquare plants with no transmission zeros, and demonstrate that the fact that the plant is minimum phase does not guarantee closed-loop stability and signal boundedness properties, unlike the square case. Then, we show that, in the wide case, the control signal generated by RCAC lies inside a subspace that is contained within the input space, which we call the "input subspace". Next, we make a stability analysis for the instantaneous controller update, and demonstrate that, in the case where $d = 1$, the controller update is static, therefore stability is irrelevant, and, in the case where $d = 2$, the controller update is globally exponentially stable under a weak persistency assumption. In this chapter, we also provide sufficient conditions for convergence of the adaptive controller, which shows that, if the performance output lies inside a specific "output subspace", then the controller converges. These results point out the existence of two implicit squaring operations performed on the nonsquare plant: one performed by pre-compensating the plant, the other performed by post-compensating the plant. In the wide case, pre-compensation leads to squaring-down, which incorporates additional zeros due

to squaring, which we call "input-subspace zeros". Similarly, in the tall case, post-compensation changes the zero structure and incorporates additional zeros, which we call "output-subspace zeros". We show that if the nonsquare plant has NMP subspace zeros, then RCAC attempts to cancel these zeros, which leads to unbounded control input in the wide case, and unbounded control input and performance output in the tall case. In light of these findings, we extend the retrospective cost function to include a performance dependent control penalty in order to prevent the controller from generating an unbounded control input. The analysis and results presented in this chapter are submitted to the International Journal of Control.

In Chapter IV, we modify the RCAC update laws of [36, 88] to include a performance-dependent control penalty. We call this modification the "η-modification" because of the similarities of the technique with the ϵ-modification developed in [78] for continuous-time adaptive control. This modification penalizes the distance between the adaptive controller and an a priori known stabilizing controller on the regressor directions. Therefore, this modification pushes the control input toward the input signal that would have been generated by the stabilizing controller. In the open-loop stable case, a simple choice for the stabilizing controller is the zero-gain controller. In this case, the η-modification prevents the control input from growing without bound. We present numerical examples demonstrating RCAC with η-modification for both SISO and MIMO plants. Finally, we apply robust RCAC to the celebrated Rohrs counterexamples in order to determine its ability to address the effects of unmodeled dynamics and unknown NMP sampling zeros. We show that the unmodified RCAC update laws of Chapter II exhibit instability when the unknown sampling zero is NMP. However, we show that the robust RCAC update law with η-modification is able to follow the sinusoidal command despite the unmodeled modes, the unknown sinusoidal disturbance, and the unknown NMP sampling zero contributed by the unmodeled dynamics. The algorithms and results presented in this chapter appear in

[100].

In Chapter V, we numerically investigate asymptotic command following and disturbance rejection capabilities of RCAC with η-modification. This numerical investigation includes a large-scale simulation with random control parameters, whose results suggest that the phase mismatch between an FIR filter involved in the retrospective cost optimization and the open-loop plant plays critical role in the asymptotic convergence of the performance output to zero. This numerical evidence motivates the development of two system identification methods to fit IIR transfer functions with FIR transfer functions to minimize the phase mismatch. These identification methods lead to a new phase-matching-based controller construction technique in addition to the Markov-parameter, NMP-zero, and time-series-based construction methods given in Chapter II. We demonstrate the phase-matching-based construction on mass-spring-dashpot systems in the presence of multi-tone sinusoidal disturbances. The algorithms and results presented in this chapter appear in [97, 98, 102, 103].

Finally, in Chapter VI, we consider RCAC in the presence of aliasing, due to either the high frequency free response of the plant, or the high-frequency content in the disturbances. We show that the intersample command-following performance may be nonzero due to aliasing of disturbances. We demonstrate that if the disturbance frequency is larger than the Nyquist frequency, then RCAC converges to an internal model controller with high gain at the aliased disturbance frequency. Therefore, the samples of the performance output converge to zero, but the actual continuous-time performance output is not zero between two consecutive sampling instants. Nevertheless, the numerical examples suggest that RCAC is able to stabilize the plant despite the high-frequency dynamics, and does not destabilize the closed-loop system because of disturbance aliasing, provided the controllability of unstable modes is not lost due to sampling [57]. The results presented in this chapter appear in [101].

CHAPTER II

Retrospective Cost Adaptive Control

2.1 Introduction

This chapter presents a review of the instantaneous and cumulative RCAC update laws developed in [36, 88]. We reformulate the instantaneous update law given in [88] as a recursive gradient update. We introduce the cumulative update law given in [36] using the quadratic minimization lemma [5] as in [88], and then derive the RLS update equations. Next, we provide a summary of the Markov-parameter-based, time-series-coefficients-based, and NMP-zero-based controller construction techniques that have been developed in [36, 88, 110]. Finally, we review the closed-loop stability and convergence properties of the instantaneous and cumulative RCAC update laws, and demonstrate the algorithm in a road-following preview control application.

2.2 Problem Statement

Consider the multivariable (MIMO) discrete-time system

$$x(k+1) = Ax(k) + Bu(k) + D_1 w(k), \tag{2.1}$$

$$y(k) = Cx(k) + D_2 w(k), \tag{2.2}$$

$$z(k) = E_1 x(k) + E_0 w(k), \tag{2.3}$$

where $k \geq 0$, $x(k) \in \mathbb{R}^n$, $z(k) \in \mathbb{R}^{l_z}$ is the measured performance variable to be minimized, $y(k) \in \mathbb{R}^{l_y}$ contains additional measurements that are available for control, $u(k) \in \mathbb{R}^{l_u}$ is the input signal, $w(k) \in \mathbb{R}^{l_w}$ is the exogenous signal. The system (2.1)–(2.3) can represent a sampled-data application arising from a continuous-time system with sample and hold operations with the sampling period h, where $y(k)$ represents $y(kh)$, $z(k)$ represents $z(kh)$, and so on. The operator matrix from u to z is thus given by

$$G_{zu}(\mathbf{q}) \triangleq E_1(\mathbf{q}I - A)^{-1}B, \tag{2.4}$$

$$G_{zw}(\mathbf{q}) \triangleq E_1(\mathbf{q}I - A)^{-1}D_1, \tag{2.5}$$

$$G_{yu}(\mathbf{q}) \triangleq C(\mathbf{q}I - A)^{-1}B, \tag{2.6}$$

$$G_{yw}(\mathbf{q}) \triangleq C(\mathbf{q}I - A)^{-1}D_1, \tag{2.7}$$

where $\mathbf{q}$ is the shift operator which accounts for possibly nonzero initial conditions. Furthermore, for a positive integer i, $H_i \triangleq E_1A^{i-1}B$ is the i^{th} Markov parameter of G_{zu}.

We represent (2.1), (2.3) as the time series model

$$z(k) = \sum_{i=1}^{n} \alpha_i z(k-i) + \sum_{i=d}^{n} \beta_i u(k-i) + \sum_{i=0}^{n} \gamma_i w(k-i), \tag{2.8}$$

where $\{\alpha_1, \ldots, \alpha_n\} \in \mathbb{R}$, $\{\beta_d, \ldots, \beta_n\} \in \mathbb{R}^{l_z \times l_u}$, $\{\gamma_0, \ldots, \gamma_n\} \in \mathbb{R}^{l_z \times l_w}$, and d is the smallest positive integer i such that the H_i is nonzero. Note that $H_d = \beta_d$, and d is the *relative degree* of G_{zu}.

Now, consider the output-feedback controller

$$x_{\mathrm{c}}(k+1) = A_{\mathrm{c}}(k)x_{\mathrm{c}}(k) + B_{\mathrm{c}}(k)y(k), \tag{2.9}$$

$$u(k) = C_{\mathrm{c}}(k)x_{\mathrm{c}}(k), \tag{2.10}$$

where $x_{\mathrm{c}} \in \mathbb{R}^{n_{\mathrm{c}}}$. The output feedback control (2.9), (2.10) is represented by $u = G_c(\mathbf{q}, k)y$, where

$$G_c(\mathbf{q}, k) \stackrel{\triangle}{=} C_{\mathrm{c}}(k)(\mathbf{q}I - A_{\mathrm{c}}(k))^{-1}B_{\mathrm{c}}(k). \tag{2.11}$$

The closed-loop system with output feedback (2.9), (2.10) is thus given by

$$\tilde{x}(k+1) = \tilde{A}(k)\tilde{x}(k) + \tilde{D}_1(k)w(k), \tag{2.12}$$

$$y(k) = \tilde{C}\tilde{x}(k) + D_2w(k), \tag{2.13}$$

$$z(k) = \tilde{E}_1\tilde{x}(k) + E_0w(k), \tag{2.14}$$

where $\tilde{x} \stackrel{\triangle}{=} \left[\begin{array}{cc} x^{\mathrm{T}} & x_c^{\mathrm{T}} \end{array} \right]^{\mathrm{T}}$,

$$\tilde{A}(k) = \left[\begin{array}{cc} A & BC_{\mathrm{c}}(k) \\ B_{\mathrm{c}}(k)C & A_{\mathrm{c}}(k) \end{array} \right], \tilde{D}_1(k) = \left[\begin{array}{c} D_1 \\ B_{\mathrm{c}}(k)D_2 \end{array} \right],$$

$$\tilde{C} = \left[\begin{array}{cc} C & 0_{l_y \times n_{\mathrm{c}}} \end{array} \right], \quad \tilde{E}_1 = \left[\begin{array}{cc} E_1 & 0_{l_z \times n_{\mathrm{c}}} \end{array} \right].$$

The closed-loop system (2.12)–(2.14) is described by the operator matrices

$$\tilde{G}_{zw}(\mathbf{q}, k) \stackrel{\triangle}{=} \tilde{E}_1(\mathbf{q}I - \tilde{A}(k))^{-1}\tilde{D}_1(k), \tag{2.15}$$

$$\tilde{G}_{yw}(\mathbf{q}, k) \stackrel{\triangle}{=} \tilde{C}(\mathbf{q}I - \tilde{A}(k))^{-1}\tilde{D}_1(k). \tag{2.16}$$

The goal is to develop an adaptive output feedback controller to minimize the performance measure $z^{\mathrm{T}}z$ in the presence of the exogenous signal w with limited modeling information about the dynamics and exogenous signal. The components of the exogenous signal w can represent either command signals to be followed, external disturbances to be rejected, or both. For instance, if $D_1 = 0$ and $E_0 \neq 0$, then the

objective is to have the output $E_1 x$ follow the command signal $-E_0 w$. On the other hand, if $D_1 \neq 0$ and $E_0 = 0$, then the objective is to reject the disturbance w from the performance variable z. In this case, we say that w is a *matched disturbance* if $\mathcal{R}(D_1) \subseteq \mathcal{R}(B)$, where $\mathcal{R}(\cdot)$ denotes range, and w is an *unmatched disturbance* if it is not matched. Furthermore, if $D_1 = \begin{bmatrix} \hat{D}_1 & 0 \end{bmatrix}$, $E_0 = \begin{bmatrix} 0 & \hat{E}_0 \end{bmatrix}$, and $w = \begin{bmatrix} w_1 & w_2 \end{bmatrix}^{\mathrm{T}}$, then the objective is to have $E_1 x$ follow the command $-\hat{E}_0 w_2$ while rejecting the disturbance $\hat{D}_1 w_1$. Lastly, if D_1 and E_0 are empty matrices, then the objective is to achieve $z(k) \to 0$ as $k \to \infty$ with no exogenous signals. A block diagram of the adaptive control architecture is shown in Figure 2.1.

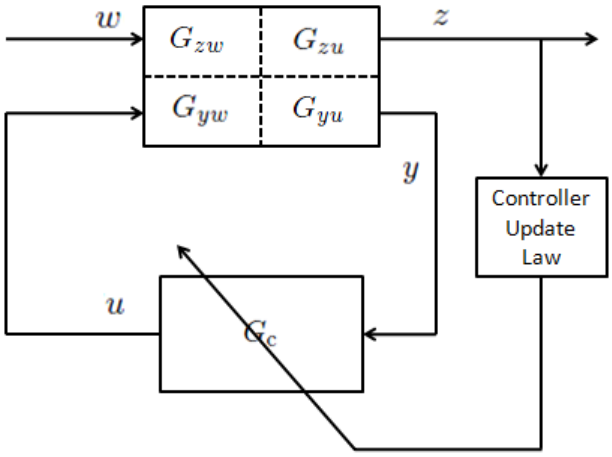

Figure 2.1: Adaptive Control Problem

The model reference adaptive control (MRAC) problem can be formulated in terms of (2.1)–(2.3), where $z \triangleq y_0 - y_{\mathrm{m}}$ is the command-following error between the plant output y_0 and the output y_{m} of a reference model G_{m} whose input is the reference signal r. For MRAC, the measurement of the reference signal r is assumed to be available for feedforward compensation, as shown in Figure 2.2.

For the adaptive controller (2.9), (2.10), the closed-loop state matrix $\tilde{A}(k)$ may be time-varying. To monitor the ability of the adaptive controller to stabilize the

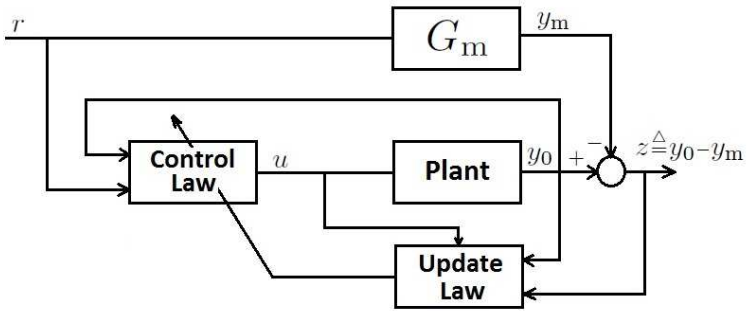

Figure 2.2: MRAC Problem

plant, we compute the spectral radius $\mathrm{spr}(\tilde{A}(k))$ at each time step. If the controller converges, and $\mathrm{spr}(\tilde{A}(k))$ converges to a number less than 1, then the asymptotic closed-loop system is internally stable.

2.3 Retrospective Cost Adaptive Control

In this section, we describe the retrospective cost adaptive control algorithms developed in [43, 36, 40, 41, 88].

2.3.1 Control Law

We represent (2.9), (2.10) by

$$u(k) = \theta^{\mathrm{T}}(k)\phi(k-1), \tag{2.17}$$

where

$$\theta(k) \triangleq \begin{bmatrix} N_1(k) \\ \vdots \\ N_{n_c}(k) \\ M_1(k) \\ \vdots \\ M_{n_c}(k) \end{bmatrix} \in \mathbb{R}^{n_c(l_u+l_y)\times l_u}, \quad \phi(k-1) \triangleq \begin{bmatrix} y(k-1) \\ \vdots \\ y(k-n_c) \\ u(k-1) \\ \vdots \\ u(k-n_c) \end{bmatrix} \in \mathbb{R}^{n_c(l_u+l_y)}. \quad (2.18)$$

The control law (2.17) can be reformulated as

$$u(k) = \Phi(k-1)\Theta(k), \quad (2.19)$$

where

$$\Phi(k-1) \triangleq I_{l_u} \otimes \phi^{\mathrm{T}}(k-1) \in \mathbb{R}^{l_u \times l_u n_c(l_u+l_y)}, \quad (2.20)$$

$$\Theta(k) \triangleq \mathrm{vec}(\theta(k)) \in \mathbb{R}^{l_u n_c(l_u+l_y)}, \quad (2.21)$$

"$\otimes$" denotes the Kronecker product, and "vec" is the column-stacking operator [5].

2.3.2 Retrospective Performance

For a positive integer r, we define

$$G_{\mathrm{f}}(\mathbf{q}^{-1}) \triangleq K_1\mathbf{q}^{-1} + K_2\mathbf{q}^{-2} + \cdots + K_r\mathbf{q}^{-r}, \quad (2.22)$$

where $K_i \in \mathbb{R}^{l_z \times l_u}$ for $1 \leq i \leq r$. Next, for $k \geq 1$, we define the *retrospective performance variable*

$$\hat{z}(\hat{\Theta}, k) \triangleq z(k) + \Phi_{\mathrm{f}}(k-1)\hat{\Theta} - u_{\mathrm{f}}(k) \in \mathbb{R}^{l_z}, \tag{2.23}$$

where

$$\Phi_{\mathrm{f}}(k-1) \triangleq G_{\mathrm{f}}(\mathbf{q}^{-1})\Phi(k-1) \in \mathbb{R}^{l_z \times l_u n_{\mathrm{c}}(l_u+l_y)}, \tag{2.24}$$

$$u_{\mathrm{f}}(k) \triangleq G_{\mathrm{f}}(\mathbf{q}^{-1})u(k) \in \mathbb{R}^{l_z}, \tag{2.25}$$

for $k \leq 0$, $u(k) = 0$, $\Phi(k-1) = 0$, and, for $k \geq 1$, $\hat{\Theta}(k) \in \mathbb{R}^{l_u n_{\mathrm{c}}(l_u+l_y)}$ is an optimization variable. Necessary modeling information for constructing the finite-impulse-response (FIR) transfer matrix $G_{\mathrm{f}}(\mathbf{q}^{-1})$ is discussed in Section 2.4.

2.3.3 Instantaneous Update Law

For $k \geq 1$, we define the instantaneous cost function

$$J_{\mathrm{ins}}(\hat{\Theta}, k) \triangleq \hat{z}^{\mathrm{T}}(\hat{\Theta}, k)R_1(k)\hat{z}(\hat{\Theta}, k) + \alpha(k)(\hat{\Theta} - \Theta(k-1))^{\mathrm{T}}R_2(k)(\hat{\Theta} - \Theta(k-1)), \tag{2.26}$$

where, for all $k \geq 1$, $\alpha(k) > 0$, $R_1(k) \in \mathbb{R}^{l_z \times l_z}$ is positive definite, and $R_2(k) \in \mathbb{R}^{l_u n_{\mathrm{c}}(l_u+l_y) \times l_u n_{\mathrm{c}}(l_u+l_y)}$ is positive definite. Now, substituting (2.23) into (2.26) yields

$$J_{\mathrm{ins}}(\hat{\Theta}, k) = \hat{\Theta}^{\mathrm{T}}\Gamma_1(k)\hat{\Theta} + \Gamma_2^{\mathrm{T}}(k)\hat{\Theta} + \Gamma_3(k), \tag{2.27}$$

where

$$\Gamma_1(k) \triangleq \Phi_{\mathrm{f}}^{\mathrm{T}}(k-1)R_1(k)\Phi_{\mathrm{f}}(k-1) + \alpha(k)R_2(k) \in \mathbb{R}^{l_u n_{\mathrm{c}}(l_u+l_y)\times l_u n_{\mathrm{c}}(l_u+l_y)}, \tag{2.28}$$

$$\Gamma_2(k) \triangleq 2\Phi_{\mathrm{f}}^{\mathrm{T}}(k-1)R_1(k)\left[z(k) - u_{\mathrm{f}}(k)\right] - 2\alpha(k)R_3(k)\Theta(k-1) \in \mathbb{R}^{l_u n_{\mathrm{c}}(l_u+l_y)}. \tag{2.29}$$

Since $\Gamma_1(k)$ is positive definite, $J_{\mathrm{ins}}(\hat{\Theta}(k), k)$ has the unique global minimizer

$$\Theta(k) = -\frac{1}{2}\Gamma_1^{-1}(k)\Gamma_2(k), \tag{2.30}$$

which is the instantaneous RCAC update law.

The instantaneous update law (2.30) requires the on-line inversion of a positive-definite matrix of size $l_u n_{\mathrm{c}}(l_u + l_y) \times l_u n_{\mathrm{c}}(l_u + l_y)$. The following result provides an alternative recursive computation which requires the on-line inversion of a positive-definite matrix of size $l_z \times l_z$.

Proposition 2.3.1. *Let $R_1(k) = I_{l_z}$, $R_2(k) = I_{l_u n_{\mathrm{c}}(l_u+l_y)}$. For each $k \geq 1$, the unique global minimizer of the instantaneous cost function* (2.26) *is given by*

$$\Theta(k) = \Theta(k-1) - \Phi_{\mathrm{f}}^{\mathrm{T}}(k-1)\Psi^{-1}(k)\hat{z}(\Theta(k-1), k), \tag{2.31}$$

where

$$\Psi(k) \triangleq \alpha(k)I + \Phi_{\mathrm{f}}(k-1)\Phi_{\mathrm{f}}^{\mathrm{T}}(k-1). \tag{2.32}$$

Proof Substituting (2.29) into (2.30) and using (2.23) and (2.28) yields

$$\begin{aligned}
\Theta(k) &= \Gamma_1^{-1}(k)[\alpha(k)\Theta(k-1) - \Phi_{\mathrm{f}}^{\mathrm{T}}(k-1)(z(k) - u_{\mathrm{f}}(k))] \\
&= \Gamma_1^{-1}(k)[\alpha(k)\Theta(k-1) - \Phi_{\mathrm{f}}^{\mathrm{T}}(k-1)(z(k) - u_{\mathrm{f}}(k))] \\
&\quad + \Gamma_1^{-1}(k)\Phi_{\mathrm{f}}^{\mathrm{T}}(k-1)\Phi_{\mathrm{f}}(k-1)\Theta(k-1) \\
&\quad - \Gamma_1^{-1}(k)\Phi_{\mathrm{f}}^{\mathrm{T}}(k-1)\Phi_{\mathrm{f}}(k-1)\Theta(k-1) \\
&= \Gamma_1^{-1}(k)[\alpha(k)I + \Phi_{\mathrm{f}}^{\mathrm{T}}(k-1)\Phi_{\mathrm{f}}(k-1)]\Theta(k-1) \\
&\quad - \Gamma_1^{-1}[\Phi_{\mathrm{f}}^{\mathrm{T}}(k-1)(z(k) - u_{\mathrm{f}}(k)) + \Phi_{\mathrm{f}}^{\mathrm{T}}(k-1)\Phi_{\mathrm{f}}(k-1)\Theta(k-1)] \\
&= \Theta(k-1) - \Gamma_1^{-1}(k)\Phi_{\mathrm{f}}^{\mathrm{T}}(k-1)\hat{z}(\Theta(k-1), k). \qquad (2.33)
\end{aligned}$$

Next, applying the matrix inversion lemma to (2.28) and using (2.32) yields

$$\Gamma_1^{-1}(k) = \frac{1}{\alpha(k)}[I - \Phi_{\mathrm{f}}^{\mathrm{T}}(k-1)\Psi^{-1}(k)\Phi_{\mathrm{f}}(k-1)]. \qquad (2.34)$$

Now, substituting (2.34) into (2.33) yields

$$\begin{aligned}
\Theta(k) &= \Theta(k-1) - \frac{1}{\alpha(k)}\Phi_{\mathrm{f}}^{\mathrm{T}}(k-1)\Psi^{-1}(k)\Psi(k)\hat{z}(\Theta(k-1), k) \\
&\quad + \frac{1}{\alpha(k)}\Phi_{\mathrm{f}}^{\mathrm{T}}(k-1)\Psi^{-1}(k)\Phi_{\mathrm{f}}(k-1)\Phi_{\mathrm{f}}^{\mathrm{T}}(k-1)\hat{z}(\Theta(k-1), k) \\
&= \Theta(k-1) - \frac{1}{\alpha(k)}\Phi_{\mathrm{f}}^{\mathrm{T}}(k-1)\Psi^{-1}(k)[\alpha(k)\hat{z}(\Theta(k-1), k) \\
&\quad + \Phi_{\mathrm{f}}(k-1)\Phi_{\mathrm{f}}^{\mathrm{T}}(k-1)\hat{z}(\Theta(k-1), k) - \Phi_{\mathrm{f}}(k-1)\Phi_{\mathrm{f}}^{\mathrm{T}}(k-1)\hat{z}(\Theta(k-1), k)] \\
&= \Theta(k-1) - \Phi_{\mathrm{f}}^{\mathrm{T}}(k-1)\Psi^{-1}(k)\hat{z}(\Theta(k-1), k). \qquad \square
\end{aligned}$$

Stability of the closed-loop adaptive system with the instantaneous RCAC update law is analyzed in [43] for minimum-phase plants. The results of [43] are extended to nonminimum-phase (NMP) plants in [36]. The closed-loop stability properties of the instantaneous RCAC are summarized in Section 2.5 for convenience.

2.3.4 Cumulative Update Law

For $k \geq 1$, we define the cumulative cost function

$$J_{\mathrm{cum}}(\hat{\Theta}, k) \triangleq \sum_{i=1}^{k} \lambda^{k-i} \hat{z}^{\mathrm{T}}(\hat{\Theta}, i) R_1(i) \hat{z}(\hat{\Theta}, i) + \lambda^k (\hat{\Theta} - \Theta(0))^{\mathrm{T}} P_0^{-1} (\hat{\Theta} - \Theta(0)), \quad (2.35)$$

where $\lambda \in (0, 1]$, and $P_0 \in \mathbb{R}^{l_u n_{\mathrm{c}}(l_u+l_y) \times l_u n_{\mathrm{c}}(l_u+l_y)}$ is positive definite. Substituting (2.23) into (2.35) yields

$$J_{\mathrm{cum}}(\hat{\Theta}(k), k) = \hat{\Theta}^{\mathrm{T}} \mathcal{C}_1(k) \hat{\Theta} + \mathcal{C}_2^{\mathrm{T}}(k) \hat{\Theta} + \mathcal{C}_3(k), \quad (2.36)$$

where $\mathcal{C}_1(0) = P_0^{-1}$, $\mathcal{C}_2(0) = -2P_0^{-1}\Theta(0)$, and, for all $k \geq 1$,

$$\mathcal{C}_1(k) \triangleq \sum_{i=1}^{k} \lambda^{k-i} \Phi_{\mathrm{f}}^{\mathrm{T}}(i-1) R_1(i) \Phi_{\mathrm{f}}(i-1) + \lambda^k P_0^{-1}, \quad (2.37)$$

$$\mathcal{C}_2(k) \triangleq \sum_{i=1}^{k} 2\lambda^{k-i} \Phi_{\mathrm{f}}^{\mathrm{T}}(i-1) R_1(i) [z(i) - u_{\mathrm{f}}(i)] - 2\lambda^k P_0^{-1} \Theta(0). \quad (2.38)$$

Since $\mathcal{C}_1(k)$ is positive definite, the cumulative cost function (2.35) has the unique global minimizer

$$\Theta(k) = -\frac{1}{2} \mathcal{C}_1^{-1}(k) \mathcal{C}_2(k), \quad (2.39)$$

which is the cumulative RCAC update law. To reduce memory usage, $\mathcal{C}_1(k)$ and $\mathcal{C}_2(k)$ can be computed recursively using

$$\mathcal{C}_1(k) = \lambda \mathcal{C}_1(k-1) + \Phi_{\mathrm{f}}^{\mathrm{T}}(k-1) R_1(k) \Phi_{\mathrm{f}}(k-1), \quad (2.40)$$

$$\mathcal{C}_2(k) = \lambda \mathcal{C}_2(k-1) + 2\Phi_{\mathrm{f}}^{\mathrm{T}}(k-1) R_1(k) [z(k) - u_{\mathrm{f}}(k)]. \quad (2.41)$$

The cumulative update law (2.39) involves the on-line inversion of a positive-

definite matrix of size $l_u n_c(l_u + l_y) \times l_u n_c(l_u + l_y)$. The following result provides an alternative recursive computation that requires the on-line inversion of a positive-definite matrix of size $l_z \times l_z$.

Proposition 2.3.2. *For all $k \geq 1$, let $R_1(k) = I$, and define $P(k) \stackrel{\triangle}{=} \mathcal{C}_1^{-1}(k)$ with $P(0) = P_0$. Then, for all $k \geq 1$, $P(k)$ satisfies*

$$P(k) = P(k-1) - P(k-1)\Phi_{\mathrm{f}}^{\mathrm{T}}(k-1)\Lambda^{-1}(k)\Phi_{\mathrm{f}}(k-1)P(k-1), \tag{2.42}$$

where

$$\Lambda(k) \stackrel{\triangle}{=} I_{l_z} + \Phi_{\mathrm{f}}(k-1)P(k-1)\Phi_{\mathrm{f}}^{\mathrm{T}}(k-1). \tag{2.43}$$

Furthermore, for each $k \geq 1$, let $\Theta(k)$ be the unique global minimizer of the cumulative cost function (2.35) *given by* (2.39)*. Then, for all $k \geq 1$,*

$$\Theta(k) = \Theta(k-1) - P(k-1)\Phi_{\mathrm{f}}^{\mathrm{T}}(k-1)\Lambda^{-1}(k)\hat{z}(\Theta(k-1), k). \tag{2.44}$$

Proof It follows from (2.40) that

$$P^{-1}(k) = P^{-1}(k-1) + \Phi_{\mathrm{f}}^{\mathrm{T}}(k-1)\Phi_{\mathrm{f}}(k-1). \tag{2.45}$$

Applying the matrix inversion lemma to (2.45) and using (2.43) yields

$$\begin{aligned} P(k) &= P(k-1) \\ &\quad - P(k-1)\Phi_{\mathrm{f}}^{\mathrm{T}}(k-1)[I_{l_z} + \Phi_{\mathrm{f}}(k-1)P(k-1)\Phi_{\mathrm{f}}^{\mathrm{T}}(k-1)]^{-1}\Phi_{\mathrm{f}}(k-1)P(k-1) \\ &= P(k-1) - P(k-1)\Phi_{\mathrm{f}}^{\mathrm{T}}(k-1)\Lambda^{-1}(k)\Phi_{\mathrm{f}}(k-1)P(k-1). \end{aligned}$$

Hence, (2.42) holds. Next, since $P(k) = \mathcal{C}_1^{-1}(k)$, it follows from (2.39), (2.41), and

(2.42) that

$$
\begin{aligned}
\Theta(k) &= -\frac{1}{2}P(k)\mathcal{C}_2^{\mathrm{T}}(k) \\
&= -\frac{1}{2}P(k-1)\mathcal{C}_2^{\mathrm{T}}(k-1) - P(k-1)\Phi_{\mathrm{f}}^{\mathrm{T}}(k-1)[z(k) - u_{\mathrm{f}}(k)] \\
&\quad + \frac{1}{2}P(k-1)\Phi_{\mathrm{f}}^{\mathrm{T}}(k-1)\Lambda^{-1}(k)\Phi_{\mathrm{f}}(k-1)P(k-1)\mathcal{C}_2^{\mathrm{T}}(k-1) \\
&\quad + P(k-1)\Phi_{\mathrm{f}}^{\mathrm{T}}(k-1)\Lambda^{-1}(k)\Phi_{\mathrm{f}}(k-1)P(k-1)\Phi_{\mathrm{f}}^{\mathrm{T}}(k-1)[z(k) - u_{\mathrm{f}}(k)] \\
&= \Theta(k-1) - P(k-1)\Phi_{\mathrm{f}}^{\mathrm{T}}(k-1)\Lambda^{-1}(k)\Lambda(k)[z(k) - u_{\mathrm{f}}(k)] \\
&\quad - P(k-1)\Phi_{\mathrm{f}}^{\mathrm{T}}(k-1)\Lambda^{-1}(k)\Phi_{\mathrm{f}}(k-1)\Theta(k-1) \\
&\quad + P(k-1)\Phi_{\mathrm{f}}^{\mathrm{T}}(k-1)\Lambda^{-1}(k)\Phi_{\mathrm{f}}(k-1)P(k-1)\Phi_{\mathrm{f}}^{\mathrm{T}}(k-1)[z(k) - u_{\mathrm{f}}(k)] \\
&= \Theta(k-1) - P(k-1)\Phi_{\mathrm{f}}^{\mathrm{T}}(k-1)\Lambda^{-1}(k)[\Phi_{\mathrm{f}}(k-1)\Theta(k-1) + (I_{l_z} \\
&\quad + \Phi_{\mathrm{f}}(k-1)P(k-1)\Phi_{\mathrm{f}}^{\mathrm{T}}(k-1) - \Phi_{\mathrm{f}}(k-1)P(k-1)\Phi_{\mathrm{f}}^{\mathrm{T}}(k-1))[z(k) - u_{\mathrm{f}}(k)]] \\
&= \Theta(k-1) - P(k-1)\Phi_{\mathrm{f}}^{\mathrm{T}}(k-1)\Lambda^{-1}(k)\hat{z}(\Theta(k-1), k). \qquad \square
\end{aligned}
$$

Stability of the closed-loop adaptive system with the cumulative RCAC update law is analyzed in [36, 41]. The closed-loop stability properties of the cumulative RCAC are summarized in Section 2.5 for convenience.

2.4 Construction of G_{f}

In this section we present three constructions for G_{f} based on the available modeling information.

2.4.1 Construction of G_{f} Using Time-Series Coefficients

Assume that the relative degree d, the coefficients $\{\beta_d, \ldots, \beta_i\}$ corresponding to the time-series model (2.8) are known. Then, the time-series-based construction of

G_{f} is given by

$$G_{\mathrm{f}}(\mathbf{q}^{-1}) \triangleq \sum_{i=d}^{n} \beta_i \mathbf{q}^{-i}. \tag{2.46}$$

Note that the construction (2.46) captures the relative degree, the first nonzero Markov parameter, and the transmission zeros of G_{zu}.

2.4.2 Construction of G_{f} Using Markov Parameters

Expanding G_{zu} for $|z| > \rho(A)$ yields the Laurent series

$$G_{zu} = \sum_{i=1}^{\infty} H_i z^{-i} = \sum_{i=d}^{\infty} H_i z^{-i}, \tag{2.47}$$

where $\rho(A)$ denotes the spectral radius of A. For a positive integer $r \geq d$, the truncation

$$G_{\mathrm{f}}(\mathbf{q}^{-1}) \sum_{i=d}^{r} H_i \mathbf{q}^{-i} \tag{2.48}$$

yields the construction of G_{f} using Markov parameters. The Markov parameters contain information about the relative degree and the sign of the high-frequency gain corresponding to G_{zu}. Furthermore, it is shown in [88] that, as r increases, roots of the Markov-parameter-based construction (2.48) asymptotically approximate the NMP zeros of G_{zu} that are located at least $\rho(A)$ distance away from the origin. Therefore, if A is Lyapunov stable and r is sufficiently large, then the construction (2.48) contains information about the NMP zeros of G_{zu}. The advantage in using the construction (2.48) is that the time-series coefficients β_i need not be known. However, if $\rho(A) > 1$, then the construction (2.48) may not be able to capture all the NMP zeros of G_{zu}. As discussed in Section 2.5, for closed-loop stability, RCAC requires G_{f} to capture the NMP zeros of G_{zu}.

2.4.3 Construction of $G_{\rm f}$ Using NMP zeros

Assuming $l_z = l_u = 1$, we rewrite (2.4) as $G_{zu}(\mathbf{q}) = H_d \frac{N(\mathbf{q})}{D(\mathbf{q})}$, where $D(\mathbf{q})$ is a monic polynomial of degree n, $N(\mathbf{q})$ is a monic polynomial of degree $n-d$, and d is the relative degree of G_{zu}. Assume that H_d and the nonminimum-phase (NMP) zeros of G_{zu}, if any, are known. Now, consider the numerator factorization

$$N(\mathbf{q}) = \beta_{\rm U}(\mathbf{q})\beta_{\rm S}(\mathbf{q}), \tag{2.49}$$

where $\beta_{\rm U}(\mathbf{q})$ and $\beta_{\rm S}(\mathbf{q})$ are monic polynomials of orders $n_{\rm U}$ and $n_{\rm S} = n - d - n_{\rm U}$, respectively, and each NMP zero of $G_{zu}(\mathbf{q})$ is a root of $\beta_{\rm U}(\mathbf{q})$. Defining

$$\tilde{\beta}_{\rm U}(\mathbf{q}^{-1}) \stackrel{\triangle}{=} \mathbf{q}^{-n_{\rm U}-d}\beta_{\rm U}(\mathbf{q}), \tag{2.50}$$

the NMP-zero-based construction of $G_{\rm f}$ is given by

$$G_{\rm f}(\mathbf{q}^{-1}) = H_d\tilde{\beta}_{\rm U}(\mathbf{q}^{-1}). \tag{2.51}$$

The construction (2.51) requires information about d, H_d, and the NMP zeros of G_{zu} counting multiplicity.

Construction of $G_{\rm f}$ using NMP zeros is extended to MIMO plants in [39, 89]. This extension requires the knowledge of d, H_d, and the NMP transmission zeros of G_{zu} counting multiplicity.

2.5 Closed-Loop Stability Properties of RCAC

In this section, we present the convergence and stability properties of the instantaneous and cumulative algorithms developed in Section 2.3. Since the stability properties are dependent on whether or not G_{zu} is NMP, the results for minimum

phase and NMP plants are covered separately. The following assumptions are required for both the minimum phase and NMP cases.

(A1) $C = E_1$, $D_2 = E_0$, and thus $y = z$.

(A2) The performance variable y is measured and available for feedback.

(A3) The triple (A, B, C) is controllable and observable.

(A4) d is known.

(A5) There exists an integer $\bar{n}$ such that $n \leq \bar{n}$, and $\bar{n}$ is known.

(A6) The exogenous signal $w(k)$ is generated by

$$x_w(k+1) = A_w x_w(k), \quad w(k) = C_w x_w(k), \tag{2.52}$$

where $x_w \in \mathbb{R}^{n_w}$ and A_w has distinct eigenvalues, all of which are on the unit circle.

(A7) There exists an integer $\bar{n}_w$ such that $n_w \leq \bar{n}_w$ and $\bar{n}_w$ is known.

It should be noted that Assumption (A6) restricts the exogenous signal w to consist purely of steps and sinusoids.

2.5.1 Stability and Convergence Properties for Minimum-Phase Plants

We now make the following additional assumptions.

(A8) $l_u = l_y$.

(A9) If $\zeta \in \mathbb{C}$ and

$$\text{rank} \begin{bmatrix} A - \zeta I & B \\ C & 0 \end{bmatrix} < \text{normal rank} \begin{bmatrix} A - zI & B \\ C & 0 \end{bmatrix}, \tag{2.53}$$

then $|\zeta| < 1$.

(A10) H_d is nonsingular.

(A11) There exists $\bar{H}_d \in \mathbb{R}^{l_y \times l_u}$ such that $2H_d^{\mathrm{T}} H_d \leq H_d^{\mathrm{T}} \bar{H}_d + \bar{H}_d^{\mathrm{T}} H_d$, and $G_{\mathrm{f}}(\mathbf{q}^{-1}) = \bar{H}_d \mathbf{q}^{-d}$.

Assumption (A8) restricts the discussion to square G_{yu}. Assumption (A9) implies that the invariant zeros of G_{yu} are minimum phase. It follows from Assumption (A3) that the invariant zeros of G_{yu} are the transmission zeros of G_{yu}. Assumption (A11) provides the construction of G_{f} for which the following result is valid. For the SISO case, Assumption (A11) implies that RCAC has 6 dB downward, and infinite upward gain margin to uncertainty in H_d.

The following result is due to [43].

Theorem 2.5.1. *Consider the open-loop system* (2.1)–(2.3) *satisfying Assumptions (A1)–(A11) and the control law* (2.19) *with the instantaneous update law* (2.31). *Then, for all initial conditions* $x(0)$ *and* $\Theta(0)$, $\Theta(k)$ *is bounded,* $u(k)$ *is bounded,* $\lim_{k\to\infty} y(k) = 0$, *and* $x(k)$ *satisfying* (2.1) *is bounded. If, in addition, the open-loop dynamics matrix* A *is asymptotically stable and* $u(k) = 0$ *for all* $k \leq 0$, *then, for all* $x_w(0)$, *the zero solution of the closed-loop adaptive system is Lyapunov stable.*

2.5.2 Stability and Convergence Properties for NMP Plants

The following assumptions are required in addition to Assumptions (A1)–(A7).

(A12) $l_u = l_y = 1$.

(A13) If $\zeta \in \mathbb{C}$, $|\zeta| \geq 1$, and

$$\operatorname{rank} \begin{bmatrix} A - \zeta I & B \\ C & 0 \end{bmatrix} < n + 1, \tag{2.54}$$

then ζ is known.

(A14) H_d is known.

(A15) $G_{\mathrm{f}}(\mathbf{q}^{-1})$ is constructed as in (2.51).

(A16) A_w in (2.52) has no eigenvalue that coincides with a zero of G_{yu}.

Assumption (A12) limits the discussion to SISO G_{yu} and is thus more restrictive than Assumption (A8). Assumption (A3) and (A13) imply that the NMP zeros of G_{yu} are known, if any. Unlike the previous case of minimum-phase plants, it now follows from Assumption (A14) that the first nonzero Markov parameter H_d is known. For $i \in \{1, \ldots, n_{\mathrm{c}}\}$, define $\lambda_i(A_{\mathrm{c}}(k))$ to be the i^{th} instantaneous eigenvalue of the controller dynamics matrix $A_{\mathrm{c}}(k)$ at frozen time k. The following result is due to [36].

Theorem 2.5.2. *Consider the open-loop system* (2.1)–(2.3) *satisfying Assumptions (A1)–(A7), (A12)–(A16), and consider the control law* (2.19) *with the instantaneous update law* (2.31) *or the cumulative update law* (2.42)–(2.44). *Assume that there exists* $\varepsilon > 0$ *and* $k_1 > 0$ *such that, for all* $k \geq k_1$, *for all* $\zeta \in \mathbb{C}$, $|\zeta| \geq 1$ *satisfying* (2.54), *and for all* $i \in \{1, \ldots, n_{\mathrm{c}}\}$, $|\lambda_i(A_{\mathrm{c}}(k)) - \zeta| \geq \varepsilon$. *Then, for all initial conditions* $x(0)$, $x_w(0)$, *and* $\Theta(0)$, $\Theta(k)$ *is bounded,* $u(k)$ *is bounded, and* $\lim_{k\to\infty} y(k) = 0$.

Theorem 2.5.2 guarantees global asymptotic convergence of y to zero and boundedness of Θ and u. However, it should be noted that Theorem 2.5.2 does not claim that the closed-loop adaptive system is Lyapunov stable.

Furthermore, Theorem 2.5.2 involves the assumption that there exist $\varepsilon > 0$, $k_1 > 0$, such that, for all $k \geq k_1$, the poles of the instantaneous controller are located at least a distance ε away from each NMP zero of G_{yu}. Although this assumption cannot be verified a priori, numerical examples suggest that if Assumption (A15) is satisfied, then the asymptotic unstable pole-zero cancellation does not occur [39, 88, 89, 100].

2.6 Application of RCAC to Adaptive Road-Following Preview Control for an Automobile

In this section, we consider a tracking problem for a car moving at a constant speed. We assume that radius of curvature information is available at each point along a road that is piecewise straight and circular. We assume that the only control input is the steering angle. In addition, we assume that the road friction is sufficient to avoid skidding. Under these assumptions, we apply the instantaneous RCAC as discussed in section 2.3. The required modeling information for RCAC is provided by system identification methods; no additional knowledge about car parameters such as cornering stiffness or moment of inertia is required. Furthermore, since RCAC can use multiple measurements, which can represent both feedback and feedforward signals, we take advantage of this flexibility by including a preview estimate of time-to-departure, which is based on current and future radius-of-curvature information.

Since RCAC requires only limited modeling information, we implement RCAC in simulation using only data obtained from the simulation platform. In particular, we perform Markov parameter identification using the CarSim simulation environment [72], and then implement the instantaneous RCAC within the CarSim environment using the Markov parameter based construction of G_{f} as outlined in Section 2.4.

2.6.1 Problem Setup

We consider the problem of having a car track a specified road while moving at a constant speed. We assume that the radius-of-curvature at each point along the road is known in advance. This information facilitates the use of preview control within a feedforward control setting. However, the bank and inclination of the road are unknown. For simplicity, the road is *piecewise circular*, which means that it consists of segments that are either straight or arcs of circles. We assume that the road is free

of bumps and the ambient wind is zero.

The only available control input is assumed to be the front wheel steering. The speed of the car is maintained at a given constant value without explicit reference to throttle or braking commands. For feedback control we assume that the lateral displacement of the car from the center of lane and its derivative are known.

We model the problem as the linear discrete-time system (2.1)–(2.3), where the control input u is the steering angle, while the exogenous signal w represents the curvature, bank angle, and inclination angle along the road. Our goal is to minimize the performance vector z, which consists of the displacement h from the center of the lane, and its derivative $\dot{h}$. As described in Section 2.4, RCAC requires specific, limited modeling information relating to (2.1)-(2.3).

Let c denote the center of mass of the car, $O_{\rm A}$ denote a point on the center of the lane, $\rm F_A$ be a road-fixed frame, and $\rm F_B$ be a car-fixed frame, as shown in Figure 2.3. Let $\vec{r}_{{\rm c}/O_{\rm A}}$ denote the position of c relative to $O_{\rm A}$, and $\vec{v}_{{\rm c}/O_{\rm A}/{\rm A}}$ denote the velocity with respect to $\rm F_A$. We resolve these vectors as $\vec{r}_{{\rm c}/O_{\rm A}}\Big|_{\rm A} = \begin{bmatrix} h \\ d \end{bmatrix}$, $\vec{v}_{{\rm c}/O_{\rm A}/{\rm A}}\Big|_{\rm A} = \begin{bmatrix} \dot{h} \\ \dot{d} \end{bmatrix}$, $\vec{v}_{{\rm c}/O_{\rm A}/{\rm A}}\Big|_{\rm B} = \begin{bmatrix} v_x \\ v_y \end{bmatrix}$.The speed of the car $V_{\rm car}$ is then given by

$$V_{\rm car} = \sqrt{v_x^2 + v_y^2} = \sqrt{\dot{h}^2 + \dot{d}^2} = \frac{v_x}{\cos(\beta)}, \tag{2.55}$$

where β is the sideslip angle.

We assume that measurements of h and $\dot{h}$ are available, so that $y(k) = z(k) = \begin{bmatrix} h(k) & \dot{h}(k) \end{bmatrix}^{\rm T}$. When we use preview, we assume that measurements of v_x and β are available as well as knowledge of the radius-of-curvature and road width at each point on the road surface. We then use this data to extrapolate and thus estimate the time-to-departure $T_{\rm dep}$, and define the preview variable $\xi_{T_{\rm dep}}$, which is

further discussed in Section 2.6.2. The performance vector is then extended to $z(k) = \begin{bmatrix} h(k) & \dot{h}(k) & \xi_{T_{\rm dep}}(k) \end{bmatrix}^{\rm T}$. We do not assume that additional output measurements such as yaw rate or roll angle are available.

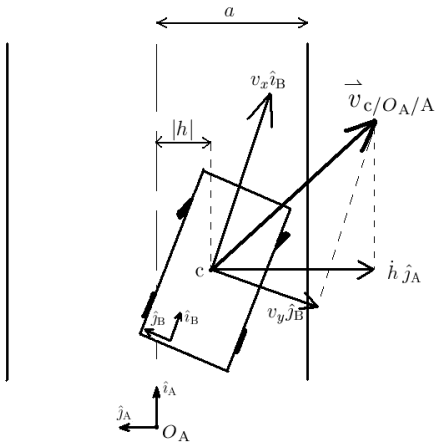

Figure 2.3: Illustration of the car-road model on a straight track.

The simulation architecture is shown in Figure 2.4. In order to apply RCAC, we require specific modeling information, which we obtain from parameter estimation based on simulation. In practice, this modeling data would be obtained from road tests. For identification and implementation of RCAC, CarSim is interfaced with Simulink. Since all required modeling data are obtained by system identification methods, there is no need to specify the state space matrices in (2.1)–(2.3).

2.6.2 Definition of the Preview Variable

In this section, we construct the preview variable $\xi_{T_{\rm dep}}$, which requires an estimate of $T_{\rm dep}$. The speed $V_{\rm car}$, the radius-of-curvature ρ, and width of the track $2a$ are assumed to be known and constant, as shown in Figure 2.5.

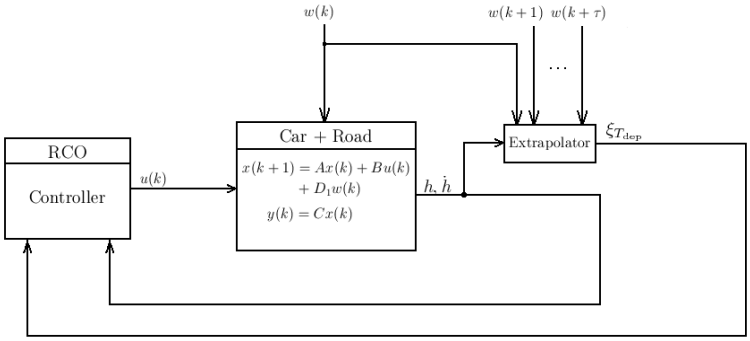

Figure 2.4: Block diagram of the control architecture. The retrospective cost optimization and extrapolation logic are handled by Matlab and Simulink, while the car-road model and the road database are provided by Carsim.

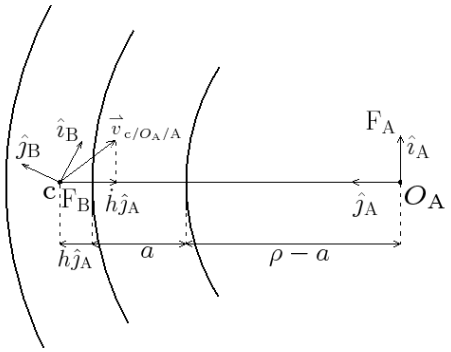

Figure 2.5: Illustration of the variables used to estimate $T_{\rm dep}$ on a curve with constant radius of curvature and road width.

We define the estimated preview tracking error $h_{\rm est}(k,T)$ by

$$h_{\rm est}(k,T) \stackrel{\triangle}{=} ((\rho + h(k))^2 + (V_{\rm car}T)^2 - 2(\rho + h(k))V_{\rm car}T\cos(\frac{\pi}{2} + \arcsin\frac{\dot{h}(k)}{V_{\rm car}}))^{-1} - \rho \tag{2.56}$$

where T is the preview period. For a straight road, $h_{\rm est}(k,T)$ is given by

$$\lim_{\rho\to\infty} h_{\rm est}(k,T) = \dot{h}(k)T + h(k).$$

Next, $\xi_T(k)$ is defined by

$$\xi_T(k) \stackrel{\triangle}{=} h_{\text{est}}(k,T)f(T), \tag{2.57}$$

where $f(T)$ is a monotonically decreasing positive nonnegative function for $T > 0$, and $\lim_{T\to\infty} f(T) = 0$. We choose $f(T) = e^{-T^2}$. We then estimate the time-to-departure T_{dep} as the minimum positive T_{dep} that satisfies

$$|h_{\text{est}}(k, T_{\text{dep}})| = a.$$

Finally, we obtain the preview variable $\xi_{T_{\text{dep}}}(k)$ by setting $T = T_{\text{dep}}$ in (2.57), so that

$$\xi_{T_{\text{dep}}}(k) = h_{\text{est}}(k, T_{\text{dep}})f(T_{\text{dep}}). \tag{2.58}$$

Since $f(T_{\text{dep}})$ is monotonically decreasing and nonnegative for all T_{dep}, minimizing $|\xi_{T_{\text{dep}}}(k)|$ maximizes T_{dep}. Note that $T_{\text{dep}} \to \infty$ as $\xi_{T_{\text{dep}}}(k) \to 0$.

We now demonstrate the extrapolation of T_{dep} under the assumption that ρ is constant. Suppose the vehicle is tracking the centerline of the curved track shown in Figure 2.5 with the present tracking error h and its derivative $\dot{h}$. Depending on ρ, a, and the direction of $\vec{v}_{\text{c}/O_{\text{A}}/\text{A}}$, the vehicle leaves the road from either the inner or outer edge. It can be shown that the car departs from the inner edge of the road if both

$$\dot{h} < 0 \tag{2.59}$$

and

$$0 < \cos^{-1}\left(\frac{|\dot{h}|}{V_{\text{car}}}\right) \leq \sin^{-1}\left(\frac{\rho - a}{\rho + h}\right). \tag{2.60}$$

Otherwise, the vehicle leaves from the outer edge. Note that, if $\vec{v}_{\text{c}/O_{\text{A}}/\text{A}}$ is constant and $\rho < \infty$, then the vehicle always leaves the track in finite time.

If (2.59) and (2.60) both hold, then T_{dep} is given by the minimum positive solution

of

$$V_{\text{car}}^2 T^2 - 2(\rho + h)|\dot{h}|T + (\rho + h)^2 - (\rho - a)^2 = 0.$$

Otherwise, T_{dep} is the positive solution of

$$V_{\text{car}}^2 T^2 - 2(\rho + h)\cos(\Psi(\dot{h}, V_{\text{car}}))V_{\text{car}}T + (\rho + h)^2 - (\rho + a)^2 = 0,$$

where

$$\Psi(\dot{h}, V_{\text{car}}) = \frac{\pi}{2} + \arcsin\frac{\dot{h}}{V_{\text{car}}}.$$

2.6.3 Markov Parameter Identification

We estimate H_i offline through least square identification in conjunction with a μ-Markov model structure [27], where H_i represents the ith Markov parameter from u to $y = \begin{bmatrix} h & \dot{h} \end{bmatrix}^{\text{T}}$. For identification, we apply a white noise steering input to the vehicle moving at 90 km/h along a straight road for 100 sec. We sample the input and outputs h and $\dot{h}$ with a sample interval T_{s} of 0.01 sec, yielding 10001 samples for each signal. We then apply least squares μ-Markov identification to the sampled signals to obtain estimates of H_i, each of which is a 2×1 matrix.

Next, we estimate the Markov parameters for $\xi_{T_{\text{dep}}}$. Let $H_{h,i}$ denote the estimate of the ith Markov parameter for h. Then, the estimate of the ith Markov parameter for $\xi_{T_{\text{dep}}}$ is

$$H_{\xi_{T_{\text{dep}}},i} = H_{h,\tau+i} f(T_{\text{dep}}), \tag{2.61}$$

where $\tau \triangleq \lfloor \frac{T_{\text{dep}}}{T_{\text{s}}} \rfloor$. Therefore, the Markov parameters for $\xi_{T_{\text{dep}}}$ are estimated by shifting $H_{h,i}$ back in time by T_{dep} seconds and scaling by $f(T_{\text{dep}})$.

The estimates of $H_{h,i}$ and $H_{\dot{h},i}$ are illustrated in Figures 2.6 and 2.7. Note that $H_{h,i}$ is almost linear, particularly for $i \geq 100$. Therefore, we approximate $H_{h,\tau+i}$ by

the least squares line fit to reduce implementation complexity.

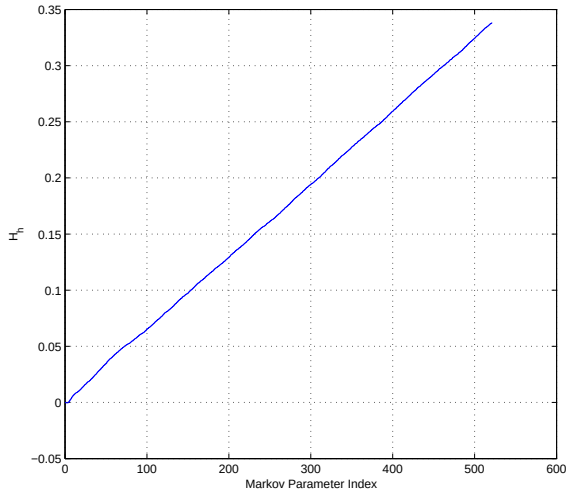

Figure 2.6: Markov parameter estimates for $H_{h,i}$, obtained through μ-Markov least-squares estimation.

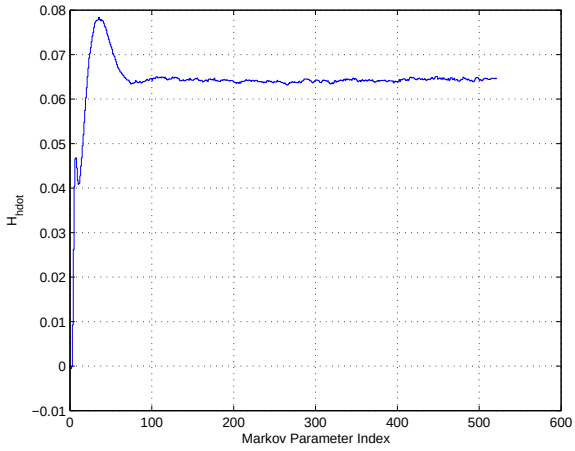

Figure 2.7: Markov parameter estimates for $H_{h,i}$, obtained through μ-Markov least-squares estimation.

2.6.4 Controller Parameter Tuning

In this section, we investigate by simulations the least amount μ of Markov parameters required to construct G_{f} in order to achieve closed-loop stability. We also

present simulation results with various values of n_c and μ, and compare the transient and tracking performances. In all simulations, we take $R_2(k) = I$ in (2.26).

We consider the track shown in Figure 2.8. We define the output and performance vectors $y = z = \begin{bmatrix} h & \dot{h} & \xi_{T_{\rm dep}} \end{bmatrix}^{\rm T}$. We take the adaptive controller order $n_c = 1$, learning rate $\alpha(k) \equiv 2000$, and $R_1(k) \equiv \mathrm{diag}(20, 20, 1)$ in (2.26).

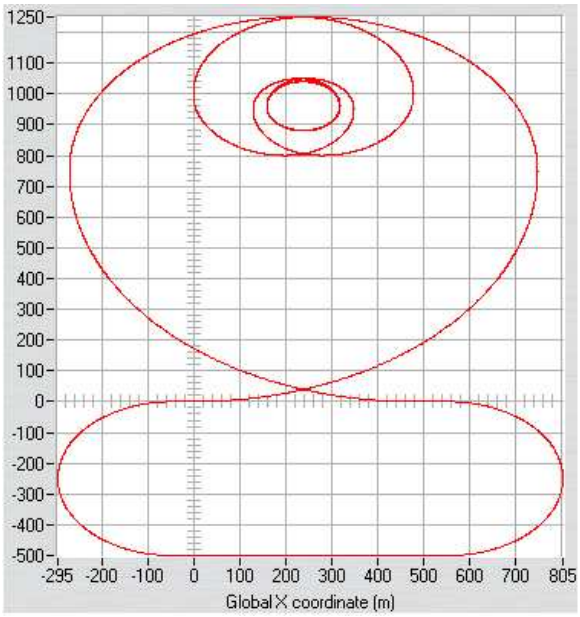

Figure 2.8: Spiral loop track. Starting from the origin, the track spirals inward first, then outward. After two 180-degree curves, the track ends at the origin.

We first set $\mu = 1$, so that only 1 Markov parameter estimate is used, that is, $G_{\rm f} = H_1 \mathbf{q}^{-1}$. We conclude by simulation that the vehicle cannot follow the track when $\mu = 1$.

Now, we choose $\mu = 2$ so that $G_{\rm f}(\mathbf{q}^{-1}) = H_1 \mathbf{q}^{-1} + H_2 \mathbf{q}^{-2}$, and keep the other parameters constant. Figure 2.9 shows that the performance variables do not diverge, although the tracking error is large.

To obtain better tracking, we now vary n_c and μ. Figure 2.10 shows that regardless of μ, we get poor transients as we increase n_c. Furthermore, n_c does not affect the tracking error significantly for $\mu = 10, 15$ and 20. Therefore, we conclude that $n_c = 1$ yields the best transient performance. On the other hand, increasing μ by keeping n_c

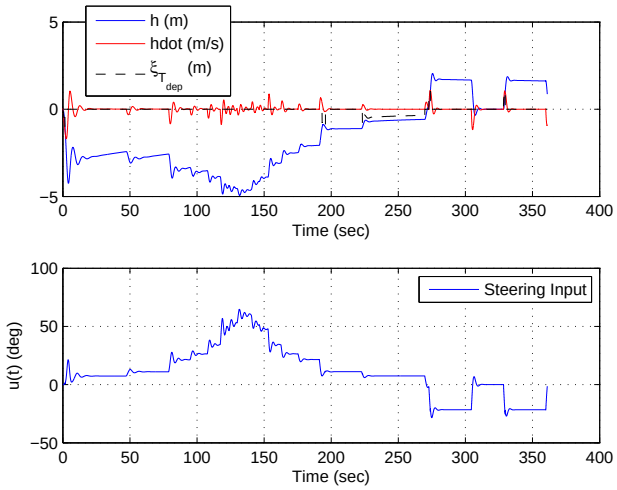

Figure 2.9: Steering input, and output variable plots with $\mu = 2$. We observe that the tracking error does not increase beyond 5 m.

constant leads to worse transient behavior, but improved tracking error. For $n_c = 1$, using $\mu = 15$ yields the best performance, although decreasing μ to 10 yields similar results.

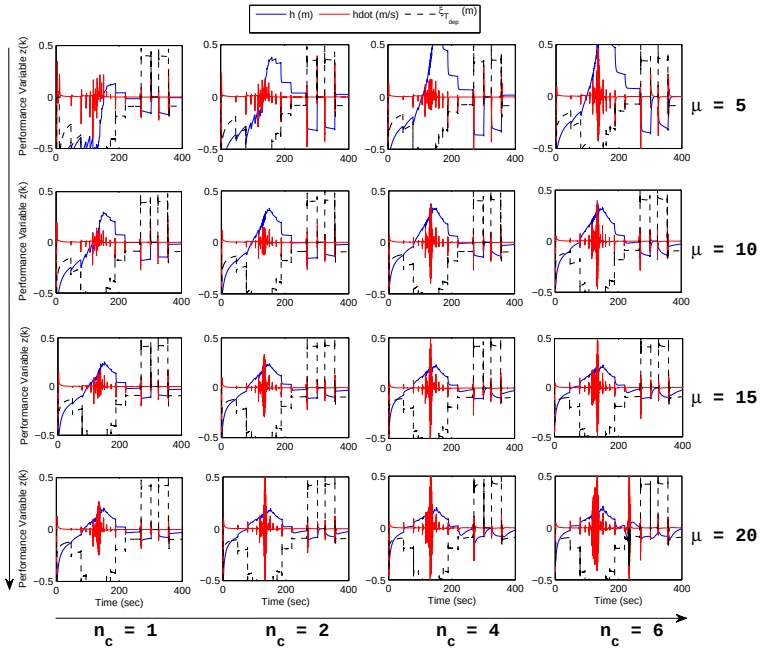

Figure 2.10: Simulation results obtained by varying the values of n_c and μ and keeping the remaining parameters constant. Each plot in a given row corresponds to the same μ, and each plot in a given column corresponds to the same n_c.

2.6.5 Numerical Examples

We now illustrate the performance of RCAC for various road types. For preview control, we extrapolate T_{dep} and define $\xi_{T_{\text{dep}}}$ under the assumption that ρ is constant, as shown in Section 2.6.2. The only exception is the last example, where we use preview information about ρ to extrapolate T_{dep}. It is assumed in each example that the car is moving at constant longitudinal speed $v_x = 90$ km/h. In each example, the weighting matrix $R_2(k)$ in (2.26) is set to be equal to I for all $k \geq 1$.

2.6.5.1 Circular Track

We consider a circular track with $\rho = 250$ m in the horizontal plane. Preview is not used, and thus $y = z = \begin{bmatrix} h & \dot{h} \end{bmatrix}^{\mathrm{T}}$. We take the adaptive controller order $n_{\text{c}} = 1$, learning rate $\alpha(k) \equiv 2000$, and $R_1(k) \equiv \text{diag}(1, 20)$. As shown in Figure 2.11, the vehicle follows the circular with a decreasing tracking error. The controller gains are shown in Figure 2.12.

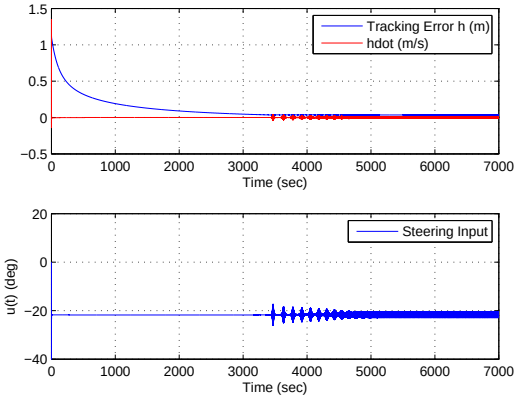

Figure 2.11: Steering input and closed-loop responses for the circular track.

2.6.5.2 Quasi-Circular Track

We now consider a flat, quasi-circular closed track consisting of six different circular arcs with radii 100, 150, and 250 m in the horizontal plane, as shown in Figure

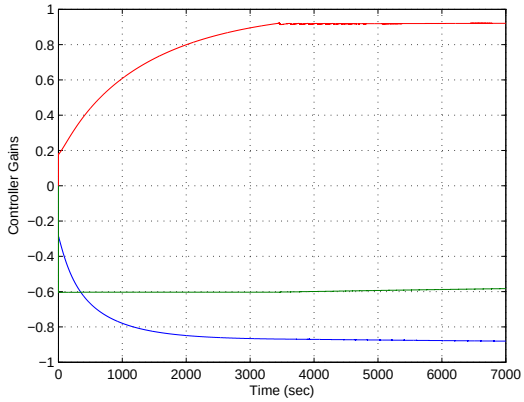

Figure 2.12: Adaptive controller gains. These traces show the time history the components of the controller gain matrix $\Theta(k)$ during the simulation on the circular track.

2.13. The simulation starts from the origin of the track coordinates, and the car moves in the counterclockwise direction. Preview is not used, and thus $y = z = \begin{bmatrix} h & \dot{h} \end{bmatrix}^{\mathrm{T}}$. We take $n_{\mathrm{c}} = 1$, $\alpha(k) \equiv 2000$, and $R_1 \equiv \mathrm{diag}(1, 20)$.

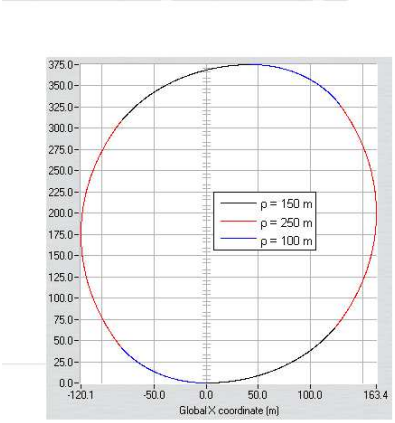

Figure 2.13: Quasi-circular track. This track has piecewise constant radius of curvature ranging from 100 m to 250 m, zero inclination, and zero banking.

The closed-loop responses are shown in Figure 2.14. Note that the tracking error does not exceed 1.25 m, and decreases as the car repeats the track. The controller gains plotted in Figure 2.15 show that the algorithm adapts to different radii of curvature.

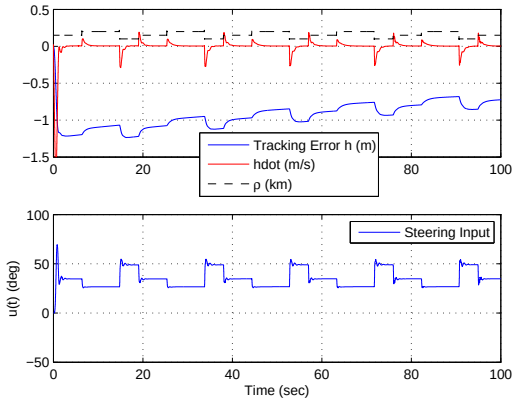

Figure 2.14: Steering input, closed-loop responses, and road radius of curvature. These results are obtained for the simulation on the quasi-circular track.

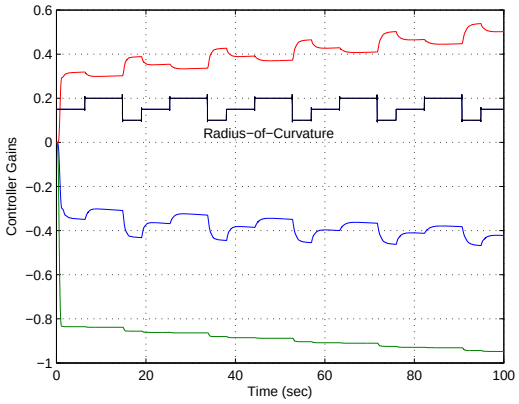

Figure 2.15: These traces show the time histories of the controller gains. The components adapt to various radii of curvature. These results are obtained for the simulation on the quasi-circular track.

2.6.5.3 Banked Road

We now consider the track shown in Figure 2.16. This track contains banked sections with bank angles specified as percentages shown in Figure 2.16. Colors indicate the bank direction. The simulation starts from the origin, and the car starts by moving to the right.

We first do not use preview, so that $y = z = \begin{bmatrix} h & \dot{h} \end{bmatrix}^{\mathrm{T}}$. We take n_{c}, $\alpha(k)$, and $R_1(k)$ as in Section 2.6.5.2. Figure 2.17 shows that the car remains on the road with a maximum tracking error about 1 m. Moreover, the steering input and $\dot{h}$ response

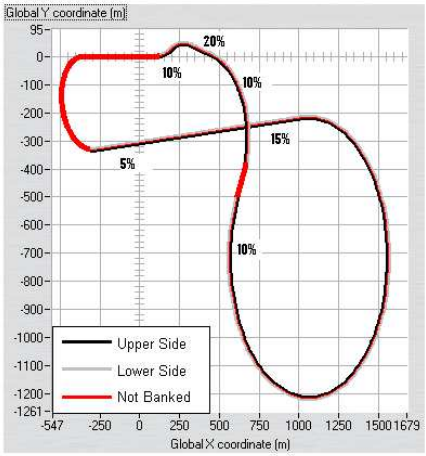

Figure 2.16: This track contains banked sections. Bank angles are illustrated with percentages and colors. Black represents the higher edge, while gray represents the lower edge of the road; red means the road is not banked. Radii of curvature on this track range from 100 m to 500 m.

are oscillatory.

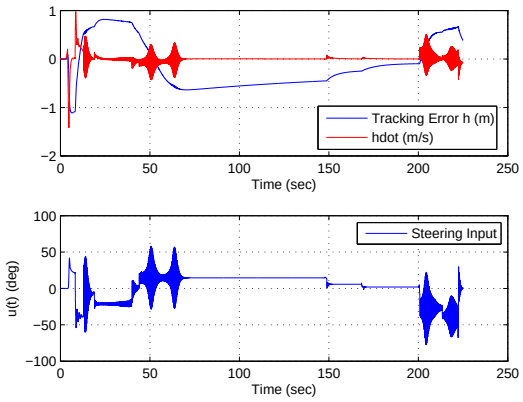

Figure 2.17: Steering input and closed-loop responses for the banked road of Figure 2.16. Preview is not used in this simulation.

Now, preview variable is added to the performance vector, so that $z = [\, h \;\dot{h}\; \xi_{T_{\rm dep}} \,]^{\rm T}$. $T_{\rm dep}$ is extrapolated under constant ρ assumption. We take $n_{\rm c} = 1$, $\alpha(k) \equiv 2000$, and $R_1 \equiv \mathrm{diag}(20, 20, 1)$. The closed-loop responses of h, $\dot{h}$, and $\xi_{T_{\rm dep}}$ are illustrated in Figure 2.18. The oscillatory behavior of $u(k)$ and $\dot{h}$ disappears, while the maximum

tracking error decreases to about 0.7 m.

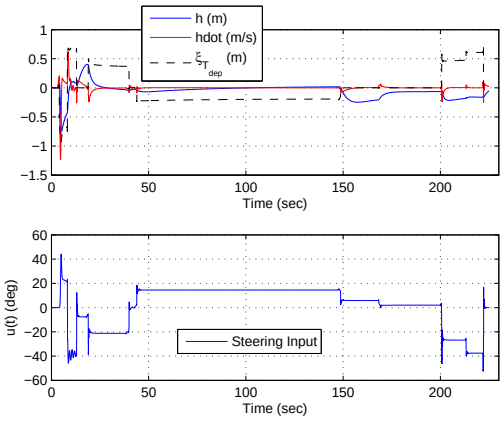

Figure 2.18: Steering input and closed-loop responses for the banked road of Figure 2.16. Preview variable is used in this simulation.

2.6.5.4 Inclined Road

Consider the track shown in Figure 2.19. This track has inclined sections as shown in Figure 2.20. The simulation starts from the origin and the car starts moving to the right.

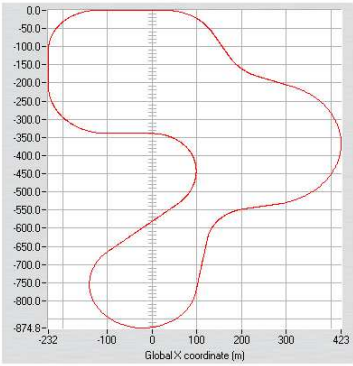

Figure 2.19: Inclined road. This track contains inclined sections as shown in Figure 2.20. The radii of curvature on this track range from 100 m to 168 m.

We first do not use the preview variable, and take n_c, $\alpha(k)$, and R_1 as in Section 2.6.5.2. Figure 2.21 shows that the car is kept on track with a maximum tracking

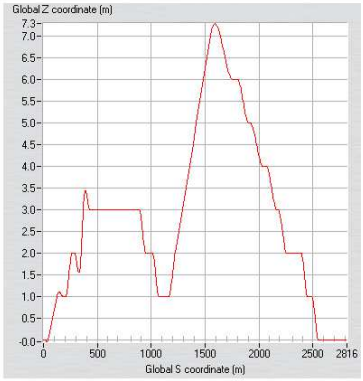

Figure 2.20: Elevation in the road with respect to the distance s along the road, where $s = 0$ at the origin of the inclined track shown in Figure 2.19.

error of about 1.2 m. We also note oscillations in $u(k)$ and $\dot{h}$.

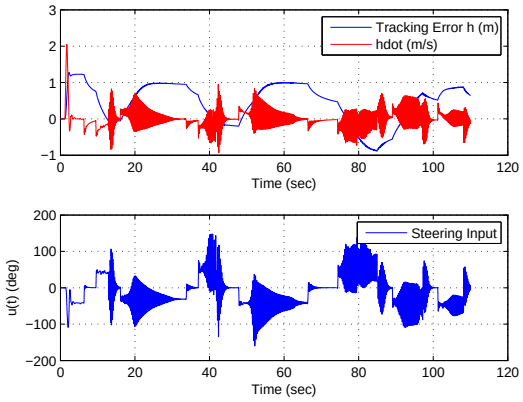

Figure 2.21: These simulation results are for the inclined road of Figures 2.19 and 2.20. Preview is not used in this simulation.

Preview variable is now added to the performance vector, and T_{dep} is estimated under the assumption that ρ is constant. We take n_{c}, $\alpha(k)$ as in Section 2.6.5.2, and $R_1 \equiv \text{diag}(20, 20, 1)$. The closed-loop responses are presented in Figure 2.22. The transient behavior of $u(k)$ and $\dot{h}$ are improved compared to Figure 2.21. We also note a significant improvement in the overall tracking error. Furthermore, as shown in Figure 2.23, preview control drives the car on the inside of the curve unlike control without preview.

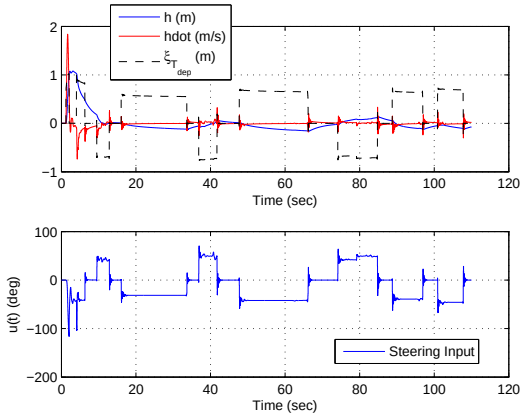

Figure 2.22: These simulation results are for the inclined road of Figures 2.19 and 2.20. Preview variable is used in this simulation.

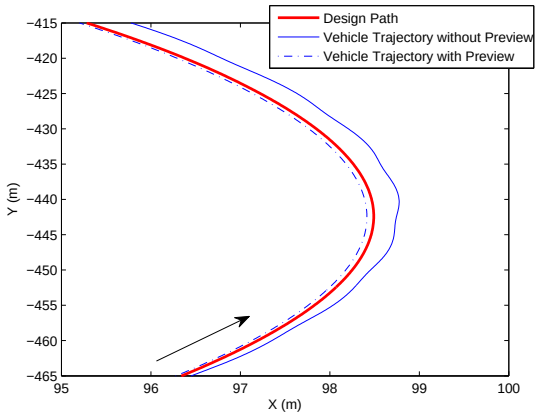

Figure 2.23: Tracking on a curved section of the inclined road. The adaptive control drives the car on the inside of the curve with a smaller tracking error when we include the preview variable.

2.6.5.5 Single Curve

We now consider a section of a track that consists of a straight road, followed by a curve with $\rho = 100$ m.

First, we do not use the preview variable, and we set the control parameters as in Section 2.6.5.2. Figure 2.24 shows that the control does not steer the car until the curve begins. The vehicle is driven on the outside of the curve with a maximum tracking error of about 0.5 m.

Now, we include the preview variable to the performance vector, and we extrap-

olate T_{dep} using current and preview ρ information. We set the control parameters as in Section 2.6.5.4. The control starts steering to the inside of the track before the curve begins, and keeps the vehicle on the inside of the curve, as shown in Figure 2.24. The tracking error remains less than 0.25 m throughout the simulation.

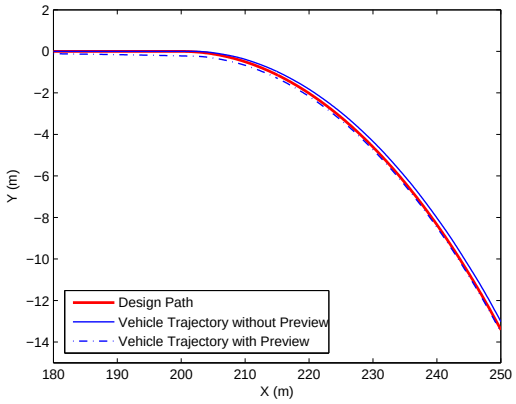

Figure 2.24: Trajectories with and without preview. Control without preview steers when the vehicle reaches the curve, and the vehicle is driven on the outside of the curve. On the other hand, preview control starts steering prior to the curve, and drives the vehicle on the inside of the curve with a smaller tracking error.

2.7 Conclusion

In this chapter, we presented a review of the instantaneous and cumulative RCAC update laws. We provided a summary of the Markov-parameter-based, time-series-coefficients-based, and NMP-zero-based controller construction techniques, and reviewed the closed-loop stability and convergence properties of RCAC. In the minimum phase case, RCAC leads to a Lyapunov stable closed-loop system, assuming that the plant is square. In the NMP, SISO case, signals are bounded, and the performance output asymptotically converges to zero.

CHAPTER III

On the Role of Subspace Zeros for Retrospective Cost Adaptive Control of Nonsquare Plants

3.1 Introduction

NMP zeros limit achievable control-system performance in various ways. These limitations are manifested as constraints on the closed-loop frequency response, pole locations, and step response [33, 38]. Analogous issues arise in discrete-time control [108], with the additional difficulty that sampling may give rise to NMP zeros [3].

Zeros in MIMO systems can be defined in terms of either a state space realization (invariant zeros) or a transfer function (transmission zeros) [24, 55, 70, 85, 92]. The presence of zeros in MIMO systems implies blocking of certain input signals [38, 95]. Associated with the zeros of MIMO systems are zero directions, which determine the directions along which each zero affects the response of the system. The zero directions are grouped in two categories; input zero directions, which determine the direction along which certain inputs are blocked, and output zero directions, which give rise to directions along which the output may be difficult to control [95].

The NMP zeros of a MIMO plant may limit achievable control-system performance in analogy with the SISO case [14, 15], however, the amount of reduction in total phases associated with a NMP zero depends on its zero directions. Surprisingly, if

the zero directions associated with a NMP zero satisfy certain conditions, then the NMP zero does not necessarily limit the roll-off rates of the open-loop gains and may have no effect on the phase margin [14].

Zeros of nonsquare (tall or wide) plants are considered in [24, 59], where it is shown that nonsquare plants generically have no transmission zeros. This suggests that nonsquare systems are generically minimum phase and therefore are easier to control than square systems. This is shown to be a misconception in [68] due to the fact that nonsquare plants may have zero-like properties that cannot be detected through transmission blocking. In addition, control techniques developed for square systems may not extend to, or may have poor performance in the nonsquare case. For example, since perfect command following is typically infeasible for tall plants [34], multivariable adaptive control methods, including MIMO extensions of MRAC, are formulated exclusively for square plants [50, 79].

Therefore, for plants that are not square, it is often desirable to transform the plant through squaring, where the plant is pre- or post-compensated, or augmented by additional actuators/sensors, so as to create a square plant with a desired zero structure [22, 54, 69, 109]. Specifically, it is shown in [109] that the zero structure of the squared plant is closely related to the invariant dynamical indices [28] and that the "squaring down and arbitrary zero assignment" problem has in general no solution. Nevertheless, in [109], it is shown that, if certain conditions are satisfied, then the zero placement problem admits a unique solution, which is obtained by using the Smith-Mcmillan form of the nonsquare transfer matrix. In [73, 74] the opposite case of "squaring up and zero assignment" is considered, where the underactuated plant is augmented with additional sensors (for wide plants) or actuators (for tall plants) to obtain a square, minimum phase plant. It should be noted, however, that the squaring-based zero-assignment methods require partial or full knowledge of the plant dynamics.

In this chapter, we focus on RCAC, which is a direct, discrete-time adaptive control algorithm. This approach was developed in [36, 43, 88, 110], where it was shown that, in the square case, RCAC requires knowledge of the first nonzero Markov parameter and the NMP transmission zeros of the plant, if any. A summary of RCAC algorithms developed in [36, 43, 88, 110] is given in Chapter II. Extensions of RCAC were given in [19, 20, 97, 102], where the need to know the NMP zeros of the square plant was removed by modifying the retrospective cost function with a performance-dependent control penalty. As shown in [20] for the SISO case, the price paid for this relaxed modeling requirement is the need to ensure that the Markov parameters used in RCAC provide a suitable approximation of the frequency response of the plant. Except for the limited investigation of RCAC for SIMO and MISO plants provided in [97], RCAC for nonsquare plants has not been studied.

The goal of the present chapter is thus to consider RCAC for nonsquare systems without explicitly squaring-down or squaring-up the plant. Contrary to the intuitive expectation, we show that the fact that the nonsquare plant is minimum phase does not guarantee closed-loop stability and signal boundedness properties, unlike the square case. Specifically, we show that, due to the nature of the RCAC update law, retrospective cost adaptive control involves two implicit squaring operations; one performed by pre-compensating the plant, the other performed by post-compensating the plant. In the wide case, pre-compensation leads to squaring-down, which incorporates additional zeros due to squaring, which we call "input-subspace zeros". Similarly, in the tall case, post-compensation changes the zero structure and incorporates additional zeros, which we call "output-subspace zeros". We show that if the nonsquare plant has NMP subspace zeros, then RCAC may attempt to cancel these zeros, which leads to unbounded control input in the wide case, and unbounded control input and performance output in the tall case. In light of these findings, we extend the retrospective cost function to include a performance-dependent control penalty in order

to prevent the controller from generating an unbounded control input.

3.2 Preliminaries and Problem Formulation

Consider the MIMO discrete-time system

$$x(k+1) = Ax(k) + Bu(k) + D_1 w(k), \tag{3.1}$$

$$y(k) = Cx(k) + D_2 w(k), \tag{3.2}$$

where (A, B, C) is minimal, $x(k) \in \mathbb{R}^n$, $y(k) \in \mathbb{R}^{l_y}$, $u(k) \in \mathbb{R}^{l_u}$, and $w(k) \in \mathbb{R}^{l_w}$. The goal is to develop an output feedback controller of the form

$$u(k) = \sum_{i=1}^{n_c} M_i(k) u(k-i) + \sum_{i=1}^{n_c} N_i(k) y(k-i), \tag{3.3}$$

where, for all $i \in \{1, \ldots, n_c\}$ and $k \geq 0$, $M_i(k) \in \mathbb{R}^{l_u \times l_u}$ and $N_i(k) \in \mathbb{R}^{l_u \times l_y}$, such that the performance variable y converges to zero in the presence of the exogenous signal w, which may be a sum of steps and sinusoids. The controller is activated at $k = 1$ with $M_i(k) = 0$ and $N_i(k) = 0$ for all $i \in \{1, \ldots, n_c\}$ and $k \leq 0$. We rewrite the control law (3.3) in regressor form

$$u(k) = \theta^{\mathrm{T}}(k) \phi(k-1), \tag{3.4}$$

where

$$\theta(k) \stackrel{\triangle}{=} \begin{bmatrix} M_1^{\mathrm{T}}(k) \\ \vdots \\ M_{n_c}^{\mathrm{T}}(k) \\ \\ N_1^{\mathrm{T}}(k) \\ \vdots \\ N_{n_c}^{\mathrm{T}}(k) \end{bmatrix} \in \mathbb{R}^{n_c(l_u+l_y)\times l_u}, \quad \phi(k-1) \stackrel{\triangle}{=} \begin{bmatrix} u(k-1) \\ \vdots \\ u(k-n_c) \\ \\ y(k-1) \\ \vdots \\ y(k-n_c) \end{bmatrix} \in \mathbb{R}^{n_c(l_u+l_y)}, \quad (3.5)$$

and $\theta(0) = 0$.

The components of the exogenous signal w can represent either command signals to be followed, external disturbances to be rejected, or both. For instance, if $D_1 = 0$ and $D_2 \neq 0$, then the objective is to have the output Cx follow the command signal $-D_2 w$. On the other hand, if $D_1 \neq 0$ and $D_2 = 0$, then the objective is to reject the disturbance w from the performance variable y. In this case, we say that w is a *matched disturbance* if $\mathcal{R}(D_1) \subseteq \mathcal{R}(B)$, where $\mathcal{R}(\cdot)$ denotes range, and w is an *unmatched disturbance* if it is not matched. Furthermore, if $D_1 = \begin{bmatrix} \hat{D}_1 & 0 \end{bmatrix}$, $D_2 = \begin{bmatrix} 0 & \hat{D}_2 \end{bmatrix}$, and $w = \begin{bmatrix} w_1 & w_2 \end{bmatrix}^{\mathrm{T}}$, then the objective is to have Cx follow the command $-\hat{D}_2 w_2$ while rejecting the disturbance $\hat{D}_1 w_1$. Lastly, if D_1 and D_2 are empty matrices, then the objective is to achieve $y(k) \to 0$ as $k \to \infty$ with no exogenous signals.

The open-loop system (3.1), (3.2) is characterized by the transfer matrix

$$y = G \begin{bmatrix} u \\ \\ w \end{bmatrix}, \quad (3.6)$$

where

$$G \stackrel{\triangle}{=} \left[\begin{array}{cc} G_{yu} & G_{yw} \end{array} \right] \in \mathbb{R}^{l_y \times (l_u + l_w)}(z) \tag{3.7}$$

and

$$G_{yu}(z) = C(zI - A)^{-1}B \in \mathbb{R}^{l_y \times l_u}(z), \tag{3.8}$$

$$G_{yw}(z) = C(zI - A)^{-1}D_1 + D_2 \in \mathbb{R}^{l_y \times l_w}(z). \tag{3.9}$$

We write $G_{yu} \sim \left[\begin{array}{c|c} A & B \\ \hline C & 0 \end{array}\right]$ to denote a *realization* of G_{yu}, and $G_{yu} \stackrel{\min}{\sim} \left[\begin{array}{c|c} A & B \\ \hline C & 0 \end{array}\right]$ to denote a *minimal realization* of G_{yu}. If $l_y = l_u$, then G_{yu} is *square*, whereas, if $l_y \neq l_u$, then G_{yu} is *nonsquare*. In particular, if $l_y > l_u$, then G_{yu} is *tall*, whereas, if $l_y < l_u$, then G_{yu} is *wide*.

Definition 3.2.1. *Let $F \in \mathbb{R}^{l_y \times l_u}(z)$ be a rational transfer matrix, and, for all $i \in \{1, \ldots, l_y\}$ and $j \in \{1, \ldots, l_u\}$, let $F_{ij}(z) = p_{ij}(z)/q_{ij}(z)$, where q_{ij} is not the zero polynomial, and $p_{ij}(z), q_{ij}(z) \in \mathbb{R}(z)$ are coprime. Then, the poles of F are the elements of the set*

$$\text{poles}(F) \stackrel{\triangle}{=} \bigcup_{i,j=1}^{l_y,l_u} \text{roots}(q_{ij}(z)),$$

and the normal rank *of F is the nonnegative integer*

$$\text{normal rank } F \stackrel{\triangle}{=} \max_{z \in \mathbb{C} \setminus \text{poles}(F)} \text{rank } F(z).$$

Now, define the *Rosenbrock system matrix* of $G_{yu} \overset{\min}{\sim} \left[\begin{array}{c|c} A & B \\ \hline C & 0 \end{array}\right]$ by

$$\Sigma(z) \overset{\triangle}{=} \begin{bmatrix} zI - A & B \\ C & 0 \end{bmatrix} \in \mathbb{R}^{(n+l_y)\times(n+l_u)}[z]. \tag{3.10}$$

The *transmission zeros* of G_{yu} are the elements of the set

$$\text{tzeros}(G_{yu}) \overset{\triangle}{=} \{\zeta \in \mathbb{C} : \text{ rank } \Sigma(\zeta) < \text{normal rank } \Sigma\}. \tag{3.11}$$

Definition 3.2.2. *Let* $\zeta \in \text{tzeros}(G_{yu})$.

(i) If $|\zeta| \geq 1$, *then* ζ *is a* nonminimum-phase (NMP) transmission zero *of* G_{yu}.

(ii) If $|\zeta| < 1$, *then* ζ *is a* minimum-phase transmission zero *of* G_{yu}.

(iii) If G_{yu} *has at least one NMP transmission zero, then* G_{yu} *is NMP.*

(iv) If G_{yu} *is not NMP, then* G_{yu} *is* minimum phase.

Expanding G_{yu} for $|z| > \rho(A)$ yields the Laurent series

$$G_{yu}(z) = \sum_{i=1}^{\infty} H_i z^{-i} = \sum_{i=d}^{\infty} H_i z^{-i},$$

where $\rho(A)$ is the spectral radius of A, $H_i \overset{\triangle}{=} CA^{i-1}B \in \mathbb{R}^{l_y \times l_u}$ is the i^{th} Markov parameter of G_{yu}, and d is the *relative degree*, which is the smallest integer i such that H_i is nonzero. For $j \in \{1, \ldots, l_y\}$ and $l \in \{1, \ldots, l_u\}$, let $H_{i,(j,l)}$ denote the (j, l) entry of H_i. Then, it follows from (3.1), (3.2) that $H_{i,(j,l)}$ is the impulse response at $k = i$ of the j^{th} output of G_{yu} for a unit impulse at $k = 0$ applied to the l^{th} input of G_{yu}. In practice, G_{yu} may be a sampled-data plant arising from a strictly proper continuous-time plant $T_{yu} \in \mathbb{R}^{l_y \times l_u}(s)$ under sample and hold operations with

sampling period h. In this case, the relative degree of G_{yu} is generically equal to 1. In particular, for a zero-order hold, $d > 1$ if and only if the step response of $T_{yu,(i,j)}$ at $t = h$ is zero for all $i \in \{1, \ldots, l_y\}$ and $j \in \{1, \ldots, l_u\}$. Aside from a lower bound on the required controller order to facilitate internal model control [43, 44], d and H_d are the only modeling information assumed to be available for controller synthesis. In particular, no modeling information about the poles and zeros of G_{yu} is required, and no knowledge of the amplitude, phase, or spectrum of the harmonic signal w is required. Throughout this chapter, we assume that H_d has full rank, that is, rank $H_d = \min(l_u, l_y)$. Furthermore, throughout the chapter, we write $\|\cdot\|$ to denote the *Euclidean norm* of a vector.

In the nonadaptive case, a sufficient condition for command following and disturbance rejection is [34, Lemma 5.2.2]

$$\text{normal rank } G_{yu} = l_y, \tag{3.12}$$

which is not satisfied if G_{yu} is tall. Furthermore, in the case where G_{yu} is wide, it follows from (3.12) that $l_u - l_y$ control inputs can be discarded without hindering command following and disturbance rejection capabilities. Therefore, multivariable MRAC is often formulated based on the assumption that G_{yu} is square [34, 43, 50]. In practice, this may incorporate the additional "squaring problem," where, given B (C), C (B) should be chosen so that G_{yu} is minimum phase [69]. Solving the squaring problem may require partial or full knowledge about the matrices A, B and C.

On the contrary, in this chapter, we focus mainly on the case where G_{yu} is non-square. Since (3.12) is a sufficient condition, there exist special cases where command following and/or disturbance rejection is possible with tall G_{yu}. For example, in a matched disturbance rejection problem, since $\mathcal{R}(D_1) \subseteq \mathcal{R}(B)$, u can be chosen to cancel w from (3.1). Another example is the case where the individual performance

outputs are chosen compatibly for a command following problem, for example, a step command following problem with $y(k) = \left[\begin{smallmatrix} y_0(k)-w \\ y_0(k)-y_0(k-1) \end{smallmatrix}\right]^{\mathrm{T}}$. On the other hand, for wide plants, it follows from (3.12) that both asymptotic command following and asymptotic disturbance rejection are achievable. Therefore, if a control technique is applicable to wide plants, there is no reason to discard certain control inputs to obtain a square plant.

3.3 Update Laws Based On Retrospective Cost Optimization

In this chapter, we present two RCAC update laws for the controller $\theta(k)$ in (3.4). For convenience, we rewrite the control law (3.4) as

$$u(k) = \Phi(k-1)\Theta(k), \tag{3.13}$$

where

$$\Phi(k-1) \triangleq I_{l_u} \otimes \phi^{\mathrm{T}}(k-1) \in \mathbb{R}^{l_u \times l_u n_{\mathrm{c}}(l_u+l_y)}, \tag{3.14}$$

$$\Theta(k) \triangleq \mathrm{vec}(\theta(k)) \in \mathbb{R}^{l_u n_{\mathrm{c}}(l_u+l_y)}, \tag{3.15}$$

"$\otimes$" denotes the Kronecker product, and "vec" is the column-stacking operator [5]. Note that $\Theta(0) = 0$. For simplicity of analysis, we implicitly set the FIR filter $G_{\mathrm{f}}(\mathbf{q}^{-1})$ in (2.22) to $H_d\mathbf{q}^{-d}$ throughout this chapter. Therefore, for control synthesis, the only modeling information we use is d and H_d.

3.3.1 Retrospective Performance

For $k \geq 0$, we define the *retrospective performance variable*

$$\hat{y}(\hat{\Theta}, k) \stackrel{\triangle}{=} y(k) + H_d \Phi(k-d-1)[\hat{\Theta} - \Theta(k-d)] \tag{3.16}$$

$$= y(k) - H_d u(k-d) + H_d \Phi(k-d-1)\hat{\Theta}, \tag{3.17}$$

where $\hat{\Theta}$ is an optimization variable. To understand the meaning of $\hat{y}(\hat{\Theta}, k)$, note that it follows from (3.1), (3.2) that

$$\begin{aligned} y(k) &= CA^d x(k-d) + \sum_{i=1}^{d} H_i u(k-i) + D_2 w(k) + \sum_{i=1}^{d} CA^{i-1} D_1 w(k-i) \\ &= CA^d x(k-d) + H_d \Phi(k-d-1)\Theta(k-d) + D_2 w(k) + \sum_{i=1}^{d} CA^{i-1} D_1 w(k-i). \end{aligned} \tag{3.18}$$

Replacing $\Theta(k-d)$ by $\hat{\Theta}$ in (3.18) yields

$$\begin{aligned} &CA^d x(k-d) + H_d \Phi(k-d-1)\hat{\Theta} + D_2 w(k) + \sum_{i=1}^{d} CA^{i-1} D_1 w(k-i) \\ &\qquad = y(k) - H_d \Phi(k-d-1)[\Theta(k-d) - \hat{\Theta}] \\ &\qquad = \hat{y}(\hat{\Theta}, k). \end{aligned} \tag{3.19}$$

Note that $x(k-d)$ and $\Phi(k-d-1)$ in (3.18) are independent of $\Theta(k-d)$, and thus are unchanged if $\hat{\Theta}$ is used instead of $\Theta(k-d)$. Consequently, it follows from (3.19) that the retrospective performance variable $\hat{y}(\hat{\Theta}, k)$ is the performance output that would have been obtained at time k if the controller $\hat{\Theta}$ had been used in place of $\Theta(k-d)$.

We now formulate two update laws based on $\hat{y}(\hat{\Theta}, k)$. In both cases, a quadratic cost function that depends on $\hat{y}(\hat{\Theta}, k)$ is minimized with respect to $\hat{\Theta}$. The algorithms

presented below are equivalent to the instantaneous and cumulative update laws of Chapter II with $G_{\rm f}(\mathbf{q}^{-1}) = H_d\mathbf{q}^{-d}$.

3.3.2 Instantaneous Update Law

For each $k \geq 1$, we define the *instantaneous cost function*

$$J_{\rm ins}(\hat{\Theta}, k) \triangleq \hat{y}^{\rm T}(\hat{\Theta}, k)\hat{y}(\hat{\Theta}, k) + \mu[\hat{\Theta} - \Theta(k-1)]^{\rm T}[\hat{\Theta} - \Theta(k-1)], \tag{3.20}$$

where $\mu > 0$ weights the distance between $\hat{\Theta}$ and the controller $\Theta(k-1)$ used at step $k-1$. Substituting (3.17) into (3.20) yields

$$J_{\rm ins}(\hat{\Theta}, k) = \hat{\Theta}^{\rm T}\Gamma_1(k)\hat{\Theta} + \Gamma_2^{\rm T}(k)\hat{\Theta} + \Gamma_3(k), \tag{3.21}$$

where

$$\Gamma_1(k) \triangleq \Phi^{\rm T}(k-d-1)H_d^{\rm T}H_d\Phi(k-d-1) + \mu I \in \mathbb{R}^{l_u n_{\rm c}(l_u+l_y)\times l_u n_{\rm c}(l_u+l_y)}, \tag{3.22}$$

$$\Gamma_2(k) \triangleq 2\Phi^{\rm T}(k-d-1)H_d^{\rm T}[y(k) - H_d u(k-d)] - 2\mu\Theta(k-1) \in \mathbb{R}^{l_u n_{\rm c}(l_u+l_y)}, \tag{3.23}$$

and $\Gamma_3(k) \in \mathbb{R}$. Since $\Gamma_1(k)$ is positive definite, $J_{\rm ins}(\hat{\Theta}, k)$ has the unique global minimizer

$$\Theta(k) = -\frac{1}{2}\Gamma_1^{-1}(k)\Gamma_2(k), \tag{3.24}$$

which is the instantaneous RCAC update law. Note that the only modeling information required to implement (3.24) is knowledge of d and H_d. We write (3.24) in recursive form as follows.

Lemma 3.3.1. *For each $k \geq 1$, the unique global minimizer of the instantaneous cost*

function (3.20) *is given by*

$$\Theta(k) = \Theta(k-1) - \Phi^{\mathrm{T}}(k-d-1)H_d^{\mathrm{T}}\Psi^{-1}(k)\hat{y}(\Theta(k-1),k), \tag{3.25}$$

where

$$\Psi(k) \triangleq \mu I_{l_y} + H_d\Phi(k-d-1)\Phi^{\mathrm{T}}(k-d-1)H_d^{\mathrm{T}}. \tag{3.26}$$

Proof Substituting (3.23) into (3.24) and using (3.13) and (3.22) yields

$$\begin{aligned}
\Theta(k) &= \Gamma_1^{-1}(k)[\mu\Theta(k-1) - \Phi^{\mathrm{T}}(k-d-1)H_d^{\mathrm{T}}(y(k) - H_d u(k-d))] \\
&= \Gamma_1^{-1}(k)[\mu\Theta(k-1) - \Phi^{\mathrm{T}}(k-d-1)H_d^{\mathrm{T}}(y(k) - H_d u(k-d))] \\
&\quad + \Gamma_1^{-1}(k)[\Phi^{\mathrm{T}}(k-d-1)H_d^{\mathrm{T}}H_d\Phi(k-d-1)]\Theta(k-1) \\
&\quad - \Gamma_1^{-1}(k)[\Phi^{\mathrm{T}}(k-d-1)H_d^{\mathrm{T}}H_d\Phi(k-d-1)]\Theta(k-1) \\
&= \Gamma_1^{-1}(k)[\mu I + \Phi^{\mathrm{T}}(k-d-1)H_d^{\mathrm{T}}H_d\Phi(k-d-1)]\Theta(k-1) \\
&\quad - \Gamma_1^{-1}(k)[\Phi^{\mathrm{T}}(k-d-1)H_d^{\mathrm{T}}(y(k) - H_d u(k-d)) \\
&\quad + \Phi^{\mathrm{T}}(k-d-1)H_d^{\mathrm{T}}H_d\Phi(k-d-1)\Theta(k-1)] \\
&= \Theta(k-1) - \Gamma_1^{-1}(k)\Phi^{\mathrm{T}}(k-d-1)H_d^{\mathrm{T}}\hat{y}(\Theta(k-1),k).
\end{aligned} \tag{3.27}$$

Next, applying the matrix inversion lemma to (3.22) and using (3.26) yields

$$\Gamma_1^{-1}(k) = \frac{1}{\mu}[I - \Phi^{\mathrm{T}}(k-d-1)H_d^{\mathrm{T}}\Psi^{-1}(k)H_d\Phi(k-d-1)]. \tag{3.28}$$

Now, substituting (3.28) into (3.27) yields

$$\begin{aligned}\Theta(k) &= \Theta(k-1) - \frac{1}{\mu}\Phi^{\mathrm{T}}(k-d-1)H_d^{\mathrm{T}}\Psi^{-1}(k)\Psi(k)\hat{y}(\Theta(k-1),k)\\ &\quad + \frac{1}{\mu}\Phi^{\mathrm{T}}(k-d-1)H_d^{\mathrm{T}}\Psi^{-1}(k)H_d\Phi(k-d-1)\Phi^{\mathrm{T}}(k-d-1)H_d^{\mathrm{T}}\hat{y}(\Theta(k-1),k)\\ &= \Theta(k-1) - \frac{1}{\mu}\Phi^{\mathrm{T}}(k-d-1)H_d^{\mathrm{T}}\Psi^{-1}(k)[\mu\hat{y}(\Theta(k-1),k)\\ &\quad + H_d\Phi(k-d-1)\Phi^{\mathrm{T}}(k-d-1)H_d^{\mathrm{T}}\hat{y}(\Theta(k-1),k)\\ &\quad - H_d\Phi(k-d-1)\Phi^{\mathrm{T}}(k-d-1)H_d^{\mathrm{T}}\hat{y}(\Theta(k-1),k)]\\ &= \Theta(k-1) - \Phi^{\mathrm{T}}(k-d-1)H_d^{\mathrm{T}}\Psi^{-1}(k)\hat{y}(\Theta(k-1),k). \qquad \square\end{aligned}$$

3.3.3 Cumulative Update Law

For each $k \geq 1$, we define the *cumulative cost function*

$$J_{\mathrm{cum}}(\hat{\Theta},k) \triangleq \sum_{i=1}^{k}\hat{y}^{\mathrm{T}}(\hat{\Theta},i)\hat{y}(\hat{\Theta},i) + \hat{\Theta}^{\mathrm{T}}P_0^{-1}\hat{\Theta}, \tag{3.29}$$

where $P_0 \in \mathbb{R}^{l_u n_{\mathrm{c}}(l_u+l_y)\times l_u n_{\mathrm{c}}(l_u+l_y)}$. Throughout the chapter, we assume that $P_0 = \beta I$, where β is a positive constant. Substituting (3.17) into (3.29) yields

$$J_{\mathrm{cum}}(\hat{\Theta},k) = \hat{\Theta}^{\mathrm{T}}\mathcal{C}_1(k)\hat{\Theta} + \mathcal{C}_2^{\mathrm{T}}(k)\hat{\Theta} + \mathcal{C}_3(k), \tag{3.30}$$

where

$$\mathcal{C}_1(k) \triangleq \sum_{i=1}^{k}\Phi^{\mathrm{T}}(i-d-1)H_d^{\mathrm{T}}H_d\Phi(i-d-1) + P_0^{-1}, \tag{3.31}$$

$$\mathcal{C}_2(k) \triangleq \sum_{i=1}^{k}2\Phi^{\mathrm{T}}(i-d-1)H_d^{\mathrm{T}}[y(i) - H_d u(i-d)], \tag{3.32}$$

and $\mathcal{C}_3(k) \in \mathbb{R}$. Defining $\mathcal{C}_1(0) \triangleq P_0^{-1}$ and $\mathcal{C}_2(0) \triangleq 0$, we can rewrite (3.31), (3.32) in the recursive form

$$\mathcal{C}_1(k) = \mathcal{C}_1(k-1) + \Phi^{\mathrm{T}}(k-d-1)H_d^{\mathrm{T}}H_d\Phi(k-d-1), \tag{3.33}$$

$$\mathcal{C}_2(k) = \mathcal{C}_2(k-1) + 2\Phi^{\mathrm{T}}(k-d-1)H_d^{\mathrm{T}}[y(k) - H_d u(k-d)]. \tag{3.34}$$

Since $\mathcal{C}_1(k)$ is positive definite, $J_{\mathrm{cum}}(\hat{\Theta}, k)$ has the unique global minimizer

$$\Theta(k) = -\frac{1}{2}\mathcal{C}_1^{-1}(k)\mathcal{C}_2(k), \tag{3.35}$$

which is the cumulative RCAC update law. As in the case of the instantaneous controller update (3.24), the only modeling information required to implement (3.35) is knowledge of d and H_d. We write (3.35) in recursive form as follows. Recall that $\Theta(0) = 0$.

Lemma 3.3.2. *For all $k \geq 0$, define $P(k) \triangleq \mathcal{C}_1^{-1}(k)$. Then, for all $k \geq 1$, $P(k)$ satisfies*

$$P(k) = P(k-1) - P(k-1)\Phi^{\mathrm{T}}(k-d-1)H_d^{\mathrm{T}}\Lambda^{-1}(k)H_d\Phi(k-d-1)P(k-1), \tag{3.36}$$

where

$$\Lambda(k) \triangleq I_{l_y} + H_d\Phi(k-d-1)P(k-1)\Phi^{\mathrm{T}}(k-d-1)H_d^{\mathrm{T}}. \tag{3.37}$$

Furthermore, for each $k \geq 1$, let $\Theta(k)$ be the unique global minimizer of the cumulative cost function (3.29) *given by* (3.35)*. Then, for all $k \geq 1$,*

$$\Theta(k) = \Theta(k-1) - P(k-1)\Phi^{\mathrm{T}}(k-d-1)H_d^{\mathrm{T}}\Lambda^{-1}(k)\hat{y}(\Theta(k-1), k). \tag{3.38}$$

Proof It follows from (3.33) that

$$P^{-1}(k) = P^{-1}(k-1) + \Phi^{\mathrm{T}}(k-d-1)H_d^{\mathrm{T}}H_d\Phi(k-d-1). \tag{3.39}$$

Applying the matrix inversion lemma to (3.39) and using (3.37) yields

$$\begin{aligned}
P(k) &= P(k-1) - P(k-1)\Phi^{\mathrm{T}}(k-d-1)H_d^{\mathrm{T}}[I_{l_y} + H_d\Phi(k-d-1)P(k-1) \\
&\quad \cdot \Phi^{\mathrm{T}}(k-d-1)H_d^{\mathrm{T}}]^{-1}H_d\Phi(k-d-1)P(k-1) \\
&= P(k-1) - P(k-1)\Phi^{\mathrm{T}}(k-d-1)H_d^{\mathrm{T}}\Lambda^{-1}(k)H_d\Phi(k-d-1)P(k-1).
\end{aligned}$$

Hence, (3.36) holds. Next, since $P(k) = \mathcal{C}_1^{-1}(k)$, it follows from (3.34), (3.35), and (3.36) that

$$\begin{aligned}
\Theta(k) &= -\frac{1}{2}P(k)\mathcal{C}_2^{\mathrm{T}}(k) \\
&= -\frac{1}{2}P(k-1)\mathcal{C}_2^{\mathrm{T}}(k-1) - P(k-1)\Phi^{\mathrm{T}}(k-d-1)H_d^{\mathrm{T}}[y(k) - H_du(k-d)] \\
&\quad + \frac{1}{2}P(k-1)\Phi^{\mathrm{T}}(k-d-1)H_d^{\mathrm{T}}\Lambda^{-1}(k)H_d\Phi(k-d-1)P(k-1)\mathcal{C}_2^{\mathrm{T}}(k-1) \\
&\quad + P(k-1)\Phi^{\mathrm{T}}(k-d-1)H_d^{\mathrm{T}}\Lambda^{-1}(k)H_d\Phi(k-d-1)P(k-1)\Phi^{\mathrm{T}}(k-d-1) \\
&\quad \cdot H_d^{\mathrm{T}}[y(k) - H_du(k-d)] \\
&= \Theta(k-1) - P(k-1)\Phi^{\mathrm{T}}(k-d-1)H_d^{\mathrm{T}}\Lambda^{-1}(k)\Lambda(k)[y(k) - H_du(k-d)] \\
&\quad - P(k-1)\Phi^{\mathrm{T}}(k-d-1)H_d^{\mathrm{T}}\Lambda^{-1}(k)H_d\Phi(k-d-1)\Theta(k-1) \\
&\quad + P(k-1)\Phi^{\mathrm{T}}(k-d-1)H_d^{\mathrm{T}}\Lambda^{-1}(k)H_d\Phi(k-d-1)P(k-1)\Phi^{\mathrm{T}}(k-d-1) \\
&\quad \cdot H_d^{\mathrm{T}}[y(k) - H_du(k-d)] \\
&= \Theta(k-1) - P(k-1)\Phi^{\mathrm{T}}(k-d-1)H_d^{\mathrm{T}}\Lambda^{-1}(k)[H_d\Phi(k-d-1)\Theta(k-1) \\
&\quad + (I_{l_y} + H_d\Phi(k-d-1)P(k-1)\Phi^{\mathrm{T}}(k-d-1)H_d^{\mathrm{T}} - H_d\Phi(k-d-1)P(k-1) \\
&\quad \cdot \Phi^{\mathrm{T}}(k-d-1)H_d^{\mathrm{T}})[y(k) - H_du(k-d)]] \\
&= \Theta(k-1) - P(k-1)\Phi^{\mathrm{T}}(k-d-1)H_d^{\mathrm{T}}\Lambda^{-1}(k)\hat{y}(\Theta(k-1), k). \qquad \square
\end{aligned}$$

3.4 Adaptive Control of Nonsquare Plants: Motivating Examples

Under suitable assumptions on w and G_{yu}, it is shown in [43] for the instantaneous update law (3.25) that $\lim_{k\to\infty} y(k) = 0$, and u, Θ and x are bounded. In particular, it is assumed in [43] that G_{yu} is minimum phase and square, H_d is nonsingular, and w is a harmonic signal with unknown spectrum. These convergence results are extended to the cumulative update law (3.35) in [36]. We repeated these convergence results at the end of Chapter II for convenience. We now demonstrate that these properties may or may not hold if G_{yu} is nonsquare.

3.4.1 Examples with Wide Plants

Example 3.4.1 (2×3 wide plant, convergent output, bounded control)**.** Consider (3.1), (3.2) with

$$A = \begin{bmatrix} 0.5 & 0 & 0 & 0 \\ 0 & 0.7 & 0 & 0 \\ 0 & 0 & 0.4 & -0.4 \\ 0 & 0 & 0.4 & 0.4 \end{bmatrix}, \quad B = \begin{bmatrix} -0.8 & 1.35 & -0.85 \\ 1.02 & -0.22 & -1.12 \\ -0.13 & -0.59 & 2.53 \\ -0.71 & -0.29 & 1.66 \end{bmatrix}, \quad D_1 = \begin{bmatrix} 0 \\ 1 \\ 0 \\ 0 \end{bmatrix}, \tag{3.40}$$

$$C = \begin{bmatrix} 0.31 & -0.87 & 0.79 & -2.33 \\ -1.26 & -0.18 & -1.33 & -1.45 \end{bmatrix}, \quad D_2 = \begin{bmatrix} 0 \\ 0 \end{bmatrix}, \tag{3.41}$$

where (A, B, C) is minimal. We consider the harmonic disturbance $w(k) = \sin \frac{\pi}{5} k$. Since $\begin{bmatrix} D_1 & B \end{bmatrix}$ is nonsingular, it follows that D_1 is not an element of $\mathcal{R}(B)$, and thus w is unmatched. The plant G_{yu} has no transmission zeros. We let $n_c = 6$, and apply the cumulative update (3.35) with $P_0 = I$. As shown in Figure 3.1, y

approaches zero, u is bounded, and Θ is bounded. ■

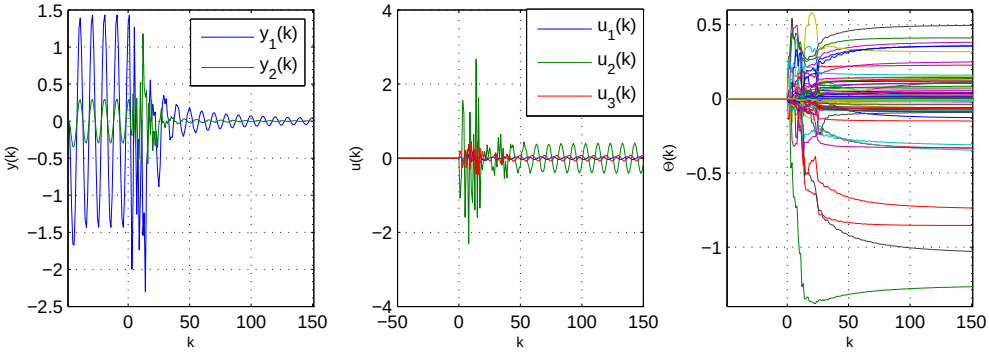

Figure 3.1: Example 3.4.1: Unmatched disturbance rejection for the minimum-phase, 2×3 wide plant (3.40), (3.41). The performance output y approaches zero, the control signal u is bounded, and the controller Θ converges.

Example 3.4.2 (2×3 wide plant, unbounded control)**.** Consider (3.1), (3.2), where the matrices A, B, D_1, C, and D_2 are as in (3.40), (3.41) except that $B_{(1,1)} = -1.8$. Note that (A, B, C) is minimal. We consider the same harmonic disturbance as in Example (3.4.1). Since $\begin{bmatrix} B & D_1 \end{bmatrix}$ is nonsingular, it follows that D_1 is not an element of $\mathcal{R}(B)$, and thus w is unmatched. The plant G_{yu} has no transmission zeros. We let $n_c = 6$ and apply the cumulative update (3.35) with $P_0 = I$. As shown in Figure 3.2, u grows without bound, while y approaches zero. ■

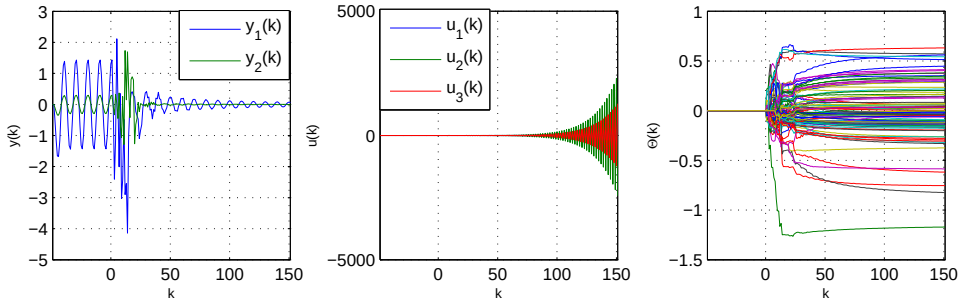

Figure 3.2: Example 3.4.2: Unmatched disturbance rejection for the 2×3 wide plant (3.40), (3.41) except that $B_{(1,1)} = -1.8$. Although G_{yu} is minimum phase, the control signal u grows without bound, while the performance output y approaches zero. The controller Θ converges.

We revisit Examples 3.4.1 and 3.4.2 in Section 3.7.3.1 to investigate the mechanics behind the instability observed in Example 3.4.2. These examples are further revisited in Section 3.9 to demonstrate a modified RCAC algorithm which does not exhibit the instability observed in Example 3.4.2.

3.4.2 Examples with Tall Plants

Example 3.4.3 (3×1 tall plant, matched disturbance, no instability observed)**.** Consider (3.1), (3.2) with

$$A = \begin{bmatrix} 0.3 & -0.16 & 0 \\ 0.125 & 0 & 0 \\ 0 & 0.125 & 0 \end{bmatrix}, \; B = \begin{bmatrix} 16 \\ 0 \\ 0 \end{bmatrix}, \; D_1 = B, \tag{3.42}$$

$$C = \begin{bmatrix} -0.0625 & -0.35 & -0.48 \\ 0.0625 & -1.5 & 9.16 \\ 0.1875 & -0.75 & -7.92 \end{bmatrix}, \quad D_2 = \begin{bmatrix} 0 \\ 0 \\ 0 \end{bmatrix}, \tag{3.43}$$

where (A, B, C) is minimal. In this example, we consider the special case of matched disturbance. Since u can be used to directly cancel w from (3.1), asymptotic disturbance rejection is achievable for tall plants in the case where w is matched with the input. We consider the two-tone harmonic disturbance $w(k) = \sin \frac{2\pi}{7}k + \sin \frac{\pi}{5}k$. The plant has no transmission zeros. We let $n_c = 7$ and apply the instantaneous update (3.24) with $\mu = 20$. As shown in Figure 3.3, all signals are bounded, Θ converges, and y approaches zero. Therefore, RCAC drives all three outputs to zero using only one control input, despite the sinusoidal disturbance. ■

Example 3.4.4 (3×1 tall plant, unmatched disturbance, no instability observed)**.** Consider (3.1), (3.2), where the matrices A, B, C, and D_2 are as in (3.42), (3.43),

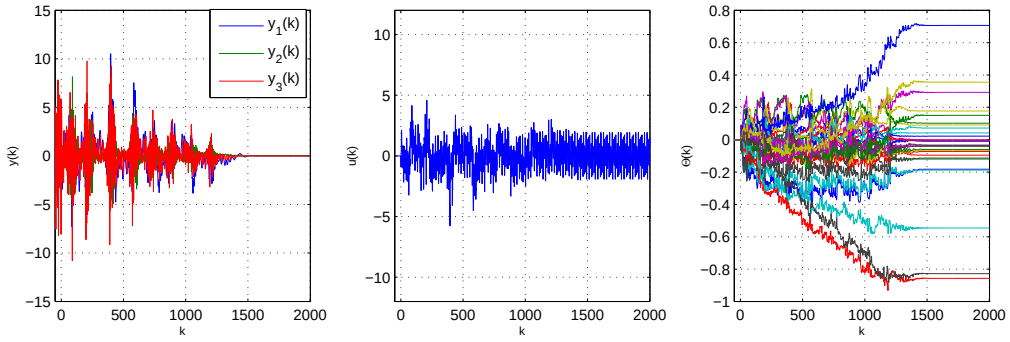

Figure 3.3: Example 3.4.3: Matched disturbance rejection for the minimum-phase, 3×1 tall plant (3.42), (3.43). The controller Θ converges, u is bounded, and y asymptotically approaches zero. RCAC cancels the matched sinusoidal disturbance from three outputs using only one actuator.

but D_1 is now given by $D_1 = \left[\begin{array}{ccc} 0 & 1 & 0 \end{array}\right]^{\mathrm{T}}$. We consider the same two-tone harmonic disturbance as in Example 3.4.3, however, since $\left[\begin{array}{cc} B & D_1 \end{array}\right]$ is nonsingular, it follows that D_1 is not an element of $\mathcal{R}(B)$, and thus w is now an unmatched disturbance. The plant G_{yu} has no transmission zeros. We let $n_{\mathrm{c}} = 7$ and apply the instantaneous update (3.24) with $\mu = 20$. As shown in Figure 3.4, all signals are bounded and Θ converges, but, since the plant is underactuated and the disturbance is unmatched, y does not converge to zero. ■

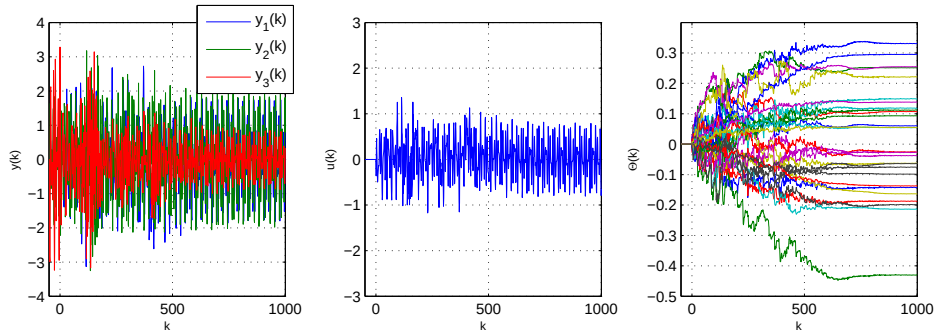

Figure 3.4: Example 3.4.5: Unmatched disturbance rejection for the minimum-phase, 3×1 tall plant of Example 3.4.3 with $D_1 = [0\ 1\ 0]^{\mathrm{T}}$. The controller Θ converges, and the signals u and y are bounded. The performance output y does not converge to zero due to the infeasibility of asymptotic rejection of an unmatched disturbance in the tall case.

Example 3.4.5 (3×1 tall plant, unmatched disturbance, input and output grow without bound)**.** Consider (3.1), (3.2) where the matrices A, B, C, D_1 and D_2 are as in Example 3.4.4, except that $C_{(1,2)} = 0.6$. Note that (A, B, C) is minimal. We consider the same unmatched harmonic disturbance as in Example 3.4.4. The plant G_{yu} has no transmission zeros. We let $n_c = 7$ and apply the instantaneous update (3.24) with $\mu = 20$. As shown in Figure 3.5, Θ converges, and both u and y grow without bound. ■

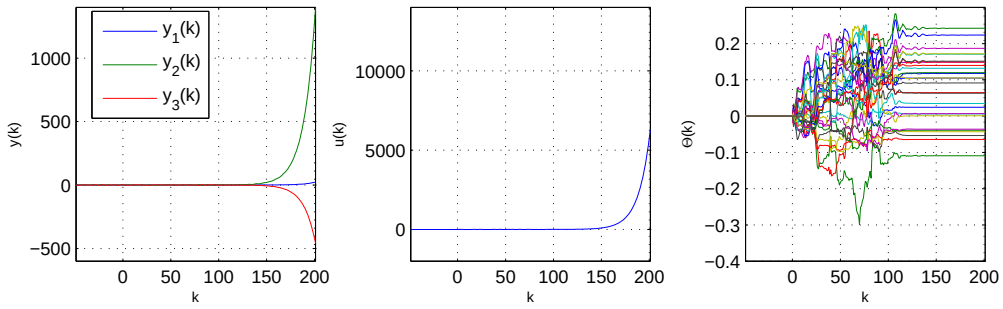

Figure 3.5: Example 3.4.5: Unmatched disturbance rejection for the 3×1 tall plant of Example 3.4.4 except that $C_{(1,2)} = 0.6$. Although G_{yu} is minimum phase, the signals u and y grow without bound. The controller Θ converges.

We revisit Examples 3.4.4 and 3.4.5 in Section 3.8.3.1 to investigate the mechanics behind the instability observed in Example 3.4.5. These examples are further revisited in Section 3.9 to demonstrate a modified RCAC algorithm which does not exhibit the instability observed in Example 3.4.5.

3.5 Input Subspace with Retrospective Cost Adaptive Control

We first consider the instantaneous update law (3.24), which is equivalent to (3.25), (3.26) as shown by Lemma 3.3.1. We require the following technical lemma.

Lemma 3.5.1. *Let $\Theta(k)$ be given by the instantaneous update law* (3.25), (3.26)*, let $\phi \in \mathbb{R}^{n_c(l_u+l_y)}$, and define $\Phi \triangleq I_{l_u} \otimes \phi^{\mathrm{T}}$. Then, for all $k \geq 1$,*

$$\Phi\Theta(k) \in \mathcal{R}(H_d^{\mathrm{T}}). \tag{3.44}$$

Proof Since $\Theta(0) = 0$, it follows from (3.25) that

$$\begin{aligned}
\Phi\Theta(1) &= -\Phi\Phi^{\mathrm{T}}(-d)H_d^{\mathrm{T}}\Psi^{-1}(1)\hat{y}(\Theta(0),1) \\
&= -(I_{l_u} \otimes \phi^{\mathrm{T}})(I_{l_u} \otimes \phi(-d))H_d^{\mathrm{T}}\Psi^{-1}(1)\hat{y}(\Theta(0),1) \\
&= -H_d^{\mathrm{T}}\phi^{\mathrm{T}}\phi(-d)\Psi^{-1}(1)\hat{y}(\Theta(0),1) \\
&\in \mathcal{R}(H_d^{\mathrm{T}}).
\end{aligned}$$

Hence, (3.44) holds for $k = 1$. Next, suppose that (3.44) holds for $k-1$. Then, there exists $v_\Phi(k-1) \in \mathbb{R}^{l_y}$ such that $\Phi\Theta(k-1) = H_d^{\mathrm{T}}v_\Phi(k-1)$. Multiplying (3.25) on the left by Φ yields

$$\begin{aligned}
\Phi\Theta(k) &= H_d^{\mathrm{T}}v_\Phi(k-1) - \Phi\Phi^{\mathrm{T}}(k-d-1)H_d^{\mathrm{T}}\Psi^{-1}(k)\hat{y}(\Theta(k-1),k) \\
&= H_d^{\mathrm{T}}v_\Phi(k-1) - H_d^{\mathrm{T}}\phi^{\mathrm{T}}\phi(k-d-1)\Psi^{-1}(k)\hat{y}(\Theta(k-1),k) \\
&= H_d^{\mathrm{T}}[v_\Phi(k-1) - \phi^{\mathrm{T}}\phi(k-d-1)\Psi^{-1}(k)\hat{y}(\Theta(k-1),k)] \\
&\in \mathcal{R}(H_d^{\mathrm{T}}).
\end{aligned}$$

By induction, (3.44) holds for all $k \geq 1$. □

We can now state the main result of this section for the instantaneous update law (3.24).

Theorem 3.5.1. *For all $k \geq 1$, let the control input $u(k)$ be given by the control law*

(3.13) *with the instantaneous update law* (3.25), (3.26). *Then, for all* $k \geq 1$,

$$u(k) \in \mathcal{R}(H_d^{\mathrm{T}}). \tag{3.45}$$

Proof For all $k \geq 1$, $\Phi(k-1) = I_{l_u} \otimes \phi^{\mathrm{T}}(k-1)$, where $\phi(k-1) \in \mathbb{R}^{n_{\mathrm{c}}(l_u+l_y)}$. Using Lemma 3.5.1, it follows from (3.13) and (3.44) that, for all $k \geq 1$, $u(k) \in \mathcal{R}(H_d^{\mathrm{T}})$. □

We now consider the cumulative update law (3.35), which is equivalent to (3.36)–(3.38) as shown by Lemma 3.3.2. The following technical lemma is needed.

Lemma 3.5.2. *For all* $k \geq 1$, *let* $P(k)$ *and* $\Theta(k)$ *be given by the cumulative update law* (3.36)–(3.38). *Then, for all* $k \geq 1$, *the following statements hold.*

(i) Let ϕ_1, $\phi_2 \in \mathbb{R}^{n_{\mathrm{c}}(l_u+l_y)}$, *and define* $\Phi_1 \triangleq I_{l_u} \otimes \phi_1^{\mathrm{T}}$, $\Phi_2 \triangleq I_{l_u} \otimes \phi_2^{\mathrm{T}}$. *Then, for all* $k \geq 1$, *there exists* $N_{\Phi_1,\Phi_2}(k) \in \mathbb{R}^{l_y \times l_y}$ *such that* $\Phi_1 P(k) \Phi_2^{\mathrm{T}} H_d^{\mathrm{T}} = H_d^{\mathrm{T}} N_{\Phi_1,\Phi_2}(k)$.

(ii) Let $\phi \in \mathbb{R}^{n_{\mathrm{c}}(l_u+l_y)}$, *and define* $\Phi \triangleq I_{l_u} \otimes \phi^{\mathrm{T}}$. *Then,* $\Phi\Theta(k) \in \mathcal{R}(H_d^{\mathrm{T}})$.

Proof To show (i), note that it follows from (3.36) that

$$\Phi_1 P(1) \Phi_2^{\mathrm{T}} H_d^{\mathrm{T}} = \Phi_1 P(0) \Phi_2 H_d^{\mathrm{T}} - \Phi_1 P(0) \Phi^{\mathrm{T}}(-d) H_d^{\mathrm{T}} \Lambda^{-1}(1) H_d \Phi(-d) P(0) \Phi_2^{\mathrm{T}} H_d^{\mathrm{T}},$$

and, since $P(0) = \beta I$,

$$\begin{aligned} \Phi_1 P(1) \Phi_2^{\mathrm{T}} H_d^{\mathrm{T}} &= \beta (I_{l_u} \otimes \phi_1^{\mathrm{T}})(I_{l_u} \otimes \phi_2) H_d^{\mathrm{T}} + \beta (I_{l_u} \otimes \phi_1^{\mathrm{T}})(I_{l_u} \otimes \phi(-d)) H_d^{\mathrm{T}} \Lambda^{-1}(1) H_d \\ &\quad \cdot \Phi(-d) \beta \Phi_2 H_d^{\mathrm{T}} \\ &= H_d^{\mathrm{T}} N_{\Phi_1,\Phi_2}(1), \end{aligned}$$

where $N_{\Phi_1,\Phi_2}(1) \triangleq \beta \phi_1^{\mathrm{T}} \phi_2 I_{l_y} + \beta^2 \phi_1^{\mathrm{T}} \phi(-d) \Lambda^{-1}(1) H_d \Phi(-d) \Phi_2^{\mathrm{T}} H_d^{\mathrm{T}} \in \mathbb{R}^{l_y \times l_y}$. Thus, (i) holds for $k = 1$. Now, suppose (i) holds for $k - 1 \geq 1$. Multiplying (3.36) on the left

by Φ_1 and on the right by $\Phi_2 H_d^{\mathrm{T}}$ yields

$$\begin{aligned}\Phi_1 P(k)\Phi_2 H_d^{\mathrm{T}} &= \Phi_1 P(k-1)\Phi_2 H_d^{\mathrm{T}} \\ &\quad - \Phi_1 P(k-1)\Phi^{\mathrm{T}}(k-d-1)H_d^{\mathrm{T}}\Lambda^{-1}(k)H_d\Phi(k-d-1)P(k-1)\Phi_2 H_d^{\mathrm{T}} \\ &= H_d^{\mathrm{T}} N_{\Phi_1,\Phi_2}(k-1) - H_d^{\mathrm{T}} N_{\Phi_1,\Phi(k-d-1)}(k-1)\Lambda^{-1}(k)H_d H_d^{\mathrm{T}} \\ &\quad \cdot N_{\Phi(k-d-1),\Phi_2}(k-1) \\ &= H_d^{\mathrm{T}} N_{\Phi_1,\Phi_2}(k),\end{aligned}$$

where

$$\begin{aligned}N_{\Phi_1,\Phi_2}(k) &\triangleq N_{\Phi_1,\Phi_2}(k-1) - N_{\Phi_1,\Phi(k-d-1)}(k-1)\Lambda^{-1}(k)H_d H_d^{\mathrm{T}} N_{\Phi(k-d-1),\Phi_2}(k-1) \\ &\in \mathbb{R}^{l_y \times l_y},\end{aligned}$$

and thus, if (i) holds with k replaced by $k-1$, then (i) holds for k. Therefore, by induction, (i) holds for all $k \geq 1$.

Next, note that, since $\Theta(0) = 0$ and $P(0) = \beta I$, it follows from (3.38) that $\Theta(1) = H_d^{\mathrm{T}} v_\Phi(1)$, where $v_\Phi(1) \triangleq -\beta\phi^{\mathrm{T}}\phi(-d)\Lambda^{-1}(1)\hat{y}(\Theta(0),1)$. Therefore, $\Phi\Theta(1) \in \mathcal{R}(H_d^{\mathrm{T}})$, and thus (ii) holds for $k = 1$. Next, suppose (ii) holds for $k-1 \geq 1$ so that $\Phi\Theta(k-1) \in \mathcal{R}(H_d^{\mathrm{T}})$. Then, there exists $v_\Phi(k-1) \in \mathbb{R}^{l_y}$ such that $\Phi\Theta(k-1) = H_d^{\mathrm{T}} v_\Phi(k-1)$. Multiplying (3.38) on the left by Φ and using (i) yields

$$\begin{aligned}\Phi\Theta(k) &= \Phi\Theta(k-1) - \Phi P(k-1)\Phi^{\mathrm{T}}(k-d-1)H_d^{\mathrm{T}}\Lambda^{-1}(k)\hat{y}(\Theta(k-1),k) \\ &= H_d^{\mathrm{T}} v_\Phi(k-1) - H_d^{\mathrm{T}} N_{\Phi,\Phi(k-d-1)}(k-1)\Lambda^{-1}(k)\hat{y}(\Theta(k-1),k) \\ &= H_d^{\mathrm{T}} v_\Phi(k),\end{aligned}$$

where

$$v_\Phi(k) = v_\Phi(k-1) - N_{\Phi,\Phi(k-d-1)}(k-1)\Lambda^{-1}(k)\hat{y}(\Theta(k-1),k).$$

Hence, if (ii) holds for $k-1$, then (ii) holds for k. Therefore, by induction, (ii) holds for all $k \geq 1$. □

We can now state the main result of this section for the cumulative update law (3.36)–(3.38).

Theorem 3.5.2. *For all $k \geq 1$, let the control input $u(k)$ be given by the control law* (3.13) *with the cumulative update law* (3.36)–(3.38)*. Then, for all $k \geq 1$,*

$$u(k) \in \mathcal{R}(H_d^{\mathrm{T}}). \tag{3.46}$$

Proof The result follows from statement (ii) of Lemma 3.5.2. □

3.6 Convergence of Θ

Examples 3.4.4 and 3.4.5 show that the controller Θ with the instantaneous update (3.24) may converge despite the fact that y does not converge and may be unbounded. In this section, we provide sufficient conditions under which Θ converges. These convergence results involve the *zero-update output subspace* $\mathcal{S} \subseteq \mathbb{R}^{l_y}$, which has the property that, if y approaches $\mathcal{S}$ exponentially, then Θ converges. For the case where G_{yu} is tall, we show that $\mathcal{S}$ is nonzero, and thus Θ may converge despite the fact that y does not converge. The discussion is limited to the instantaneous update law (3.25), but similar results apply to the cumulative update law (3.36), (3.38). Define the *controller update vector* $\Delta\Theta(k) \triangleq \Theta(k) - \Theta(k-1)$. Note that, since we assume that, for all $k \leq 0$, $\Theta(k) = 0$, it follows that, for all $k \leq 0$, $\Delta\Theta(k) = 0$.

3.6.1 Case 1: $d = 1$

Lemma 3.6.1. *Consider the instantaneous update law* (3.25)*, and assume that* $d = 1$*. Then,* $\Delta\Theta(k)$ *satisfies*

$$\Delta\Theta(k) = \mathcal{B}(k)H_1^{\mathrm{T}}y(k), \tag{3.47}$$

where

$$\mathcal{B}(k) \stackrel{\triangle}{=} -[\mu I_{l_u n_c(l_u+l_y)} + \Phi^{\mathrm{T}}(k-2)H_1^{\mathrm{T}}H_1\Phi(k-2)]^{-1}\Phi^{\mathrm{T}}(k-2). \tag{3.48}$$

Proof Subtracting $\Theta(k-1)$ from both sides of (3.25) and using the identity $Q(I + Q^{\mathrm{T}}Q)^{-1} = (I + QQ^{\mathrm{T}})^{-1}Q$ yields

$$\begin{aligned}\Delta\Theta(k) &= -\Phi^{\mathrm{T}}(k-2)H_1^{\mathrm{T}}[\mu I_{l_y} + H_1\Phi(k-2)\Phi^{\mathrm{T}}(k-2)H_1^{\mathrm{T}}]^{-1}\hat{y}(\Theta(k-1),k)\\ &= [\mu I_{l_u n_c(l_u+l_y)} + \Phi^{\mathrm{T}}(k-2)H_1^{\mathrm{T}}H_1\Phi(k-2)]^{-1}\Phi^{\mathrm{T}}(k-2)H_1^{\mathrm{T}}\hat{y}(\Theta(k-1),k).\end{aligned}$$

Since $d = 1$, it follows from (3.16) that $\hat{y}(\Theta(k-1),k) = y(k)$. Therefore,

$$\begin{aligned}\Delta\Theta(k) &= -[\mu I_{l_u n_c(l_u+l_y)} + \Phi^{\mathrm{T}}(k-2)H_1^{\mathrm{T}}H_1\Phi(k-2)]^{-1}\Phi^{\mathrm{T}}(k-2)H_1^{\mathrm{T}}y(k)\\ &= \mathcal{B}(k)H_1^{\mathrm{T}}y(k).\end{aligned}$$

□

It follows from Lemma 3.6.1 that, for $d = 1$, controller update (3.47) is a memoryless process driven by $H_1^{\mathrm{T}}y(k)$. Note that, if $y(k) \in \mathcal{N}(H_1^{\mathrm{T}})$, then $\Delta\Theta(k) = 0$. Furthermore, if G_{yu} is either square or wide, then $\mathcal{N}(H_1^{\mathrm{T}}) = \{0\}$, and thus $H_1^{\mathrm{T}}y(k) = 0$ if and only if $y(k) = 0$. However, if G_{yu} is tall, then $\mathcal{N}(H_1^{\mathrm{T}}) \neq \{0\}$, and thus $H_1^{\mathrm{T}}y(k)$ can be zero with nonzero $y(k)$. The next result shows that, if $H_1^{\mathrm{T}}y$ converges exponentially to zero, then Θ converges.

Theorem 3.6.1. *Consider the instantaneous update law* (3.25)*. Assume that* $\mathcal{B}$ *is*

bounded and there exist $\alpha > 0$ *and* $\gamma \in (0,1)$ *such that, for all* $k \geq 0$, $\|H_1^{\mathrm{T}} y(k)\| \leq \alpha\gamma^k$. *Then,* Θ *converges.*

Proof See Section 3.12.1. □

Assume that G_{yu} is tall or square. Then $H_1^{\mathrm{T}} H_1$ is positive definite, and it follows from (3.48) that $\mathcal{B}$ is bounded whether or not Φ is bounded. Therefore, if $H_1^{\mathrm{T}} y$ converges exponentially to zero, then Θ converges whether or not Φ is bounded.

Theorem 3.6.1 has a geometric interpretation. If G_{yu} is tall, and thus H_1^{T} has a nonzero null space, and if y converges to $\mathcal{N}(H_1^{\mathrm{T}}) \subset \mathbb{R}^{l_y}$ exponentially, then Θ converges. Thus, Θ may converge whether or not y is bounded as long as y remains in, or exponentially approaches, $\mathcal{N}(H_1^{\mathrm{T}})$. In Section 3.8.3.1, we show that this is what happens in Examples 3.4.4 and 3.4.5.

3.6.2 Case 2: $d = 2$

Lemma 3.6.2. *For all* $k \geq 1$, *let* $\Theta(k)$ *be given by the instantaneous update law* (3.25) *with* $d = 2$. *Then,* $\Delta\Theta(k)$ *satisfies*

$$\Delta\Theta(k) = \mathcal{A}(k)\Delta\Theta(k-1) + \mathcal{B}(k)H_2^{\mathrm{T}} y(k), \tag{3.49}$$

where

$$\mathcal{A}(k) \triangleq -\Phi^{\mathrm{T}}(k-3)H_2^{\mathrm{T}}[\mu I_{l_y} + H_2\Phi(k-3)\Phi^{\mathrm{T}}(k-3)H_2^{\mathrm{T}}]^{-1}H_2\Phi(k-3), \tag{3.50}$$

$$\mathcal{B}(k) \triangleq -[\mu I_{l_u n_c(l_u+l_y)} + \Phi^{\mathrm{T}}(k-3)H_2^{\mathrm{T}}H_2\Phi(k-3)]^{-1}\Phi^{\mathrm{T}}(k-3). \tag{3.51}$$

Proof Substituting $d = 2$ into (3.25) and using the matrix identity $Q(I+Q^{\mathrm{T}}Q)^{-1} = (I + QQ^{\mathrm{T}})^{-1}Q$ yields (3.49). □

As in the case $d = 1$, the controller update $\Delta\Theta(k)$ is driven by $H_d^{\mathrm{T}} y(k)$. However, unlike (3.47), which is memoryless, (3.49) is dynamic. Therefore, we need to consider

the stability of (3.49). In particular, for all $k \geq 1$, consider the free response of (3.49), which is given by

$$\Delta\Theta(k) = \mathcal{A}(k)\Delta\Theta(k-1). \tag{3.52}$$

Definition 3.6.3. *The zero solution of* (3.52) *is* globally exponentially stable *if, for all* $\Delta\Theta(0) \in \mathbb{R}^{l_u n_c(l_u+l_y)}$ *and* $k \geq 0$, *there exist* $\alpha \geq 1$ *and* $\gamma \in (0,1)$ *such that*

$$\|\Delta\Theta(k)\| \leq \alpha\|\Delta\Theta(0)\|\gamma^k. \tag{3.53}$$

Note that Definition 3.6.3 implies that the zero solution of (3.52) is Lyapunov stable. In particular, it follows from (3.53) that, for all $\varepsilon > 0$, if $\|\Delta\Theta(0)\| < \frac{\varepsilon}{\alpha}$, then, for all $k \geq 0$, $\|\Delta\Theta(k)\| < \varepsilon$.

Substituting the singular value decomposition $H_2\Phi(k-3) = U_k\Sigma_k V_k$ into (3.50) yields

$$\begin{aligned}\mathcal{A}(k) &= V_k^*\Sigma_k^* U_k^*[U_k\mu I U_k^* + U_k\Sigma_k V_k V_k^*\Sigma_k^* U_k^*]^{-1}U_k\Sigma_k V_k \\ &= V_k^*\Sigma_k^*[\mu I + \Sigma_k\Sigma_k^*]^{-1}\Sigma_k V_k,\end{aligned}$$

and thus,

$$\sigma_i(\mathcal{A}(k)) = \frac{\sigma_i^2(H_2\Phi(k-3))}{\mu + \sigma_i^2(H_2\Phi(k-3))}, \tag{3.54}$$

where $\sigma_i(\mathcal{A}(k))$ denotes the i^{th} singular value of $\mathcal{A}(k)$. Furthermore, define

$$\bar{\sigma}(\mathcal{A}) \stackrel{\triangle}{=} \sup_{k\geq 1} \sigma_{\max}(\mathcal{A}(k)),$$

where $\sigma_{\max}$ denotes the largest singular value. It follows from (3.54) that $\bar{\sigma}(\mathcal{A}) \in [0,1]$. Furthermore, if Φ is bounded, then $\bar{\sigma}(\mathcal{A}) \in [0,1)$.

Proposition 3.6.4. *Let $\Theta(k)$ be given by the instantaneous update* (3.25) *with $d = 2$, and assume that Φ is bounded. Then the zero solution of* (3.52) *is globally exponentially stable.*

Proof See Section 3.12.2. □

Proposition 3.6.4 is restrictive in the sense that it requires that the regressor Φ be bounded. We now relax this requirement by introducing a persistency condition. For $k \geq 1$ and $m \geq 2$, define

$$Q_m(k) \stackrel{\triangle}{=} \mathcal{A}(k) \cdots \mathcal{A}(k+m-1). \tag{3.55}$$

Proposition 3.6.5. *Let $\Theta(k)$ be given by the instantaneous update* (3.25) *with $d = 2$, and consider* (3.52)*. Assume that there exists $m \geq 2$ such that*

$$\bar{\sigma}(Q_m) < 1. \tag{3.56}$$

Then the zero solution of (3.52) *is globally exponentially stable.*

Proof See Section 3.12.3. □

The next result shows that (3.56) is satisfied if the regressor is sufficiently persistent, in particular, persistently exciting of order two. For nonzero ϕ_1, $\phi_2 \in \mathbb{R}^{l_u n_c (l_u + l_y)}$, let

$$\Omega(\phi_1, \phi_2) \stackrel{\triangle}{=} \cos^{-1} \frac{\phi_1^{\mathrm{T}} \phi_2}{\|\phi_1\| \|\phi_2\|} \in [0, \pi] \tag{3.57}$$

denote the angle between ϕ_1 and ϕ_2. We require the following technical lemma before stating the persistency condition.

Lemma 3.6.6. *For $r, k \geq 2$, let $\phi_1, \ldots, \phi_k \in \mathbb{R}^r$, assume that ϕ_1 and ϕ_k are not*

parallel, and let $\Omega_0 \in (0, \pi/2]$ *such that*

$$\Omega_0 \leq \Omega(\phi_1, \phi_k) \leq \pi - \Omega_0. \tag{3.58}$$

Then, there exists $l \in \{1, \ldots, k-1\}$ *such that*

$$\frac{1}{k-1}\Omega_0 \leq \Omega(\phi_l, \phi_{l+1}) \leq \pi - \frac{1}{k-1}\Omega_0. \tag{3.59}$$

Proposition 3.6.7. *Assume that* G_{yu} *is tall or square, and assume that there exist* $m \geq 2$ *and* $\Omega_0 \in (0, \pi/2]$ *such that, for all* $k \geq 1$*, there exist distinct* $k_1, k_2 \in \{k, \ldots, k+m-1\}$ *such that* $\Omega_0 \leq \Omega(\phi(k_1 - 3), \phi(k_2 - 3)) \leq \pi - \Omega_0$*. Then,* $\bar{\sigma}(Q_m) \leq \cos \frac{\Omega_0}{m-1} < 1$*.*

Proof See Section 3.12.4. □

It follows from Proposition 3.6.7 that, if there exist $m \geq 2$ and $\Omega_0 \in (0, \pi/2]$ such that, for all $k \geq 1$, the set $\{\phi(k-3), \ldots, \phi(k+m-4)\}$ contains at least two vectors the angle between which is at least Ω_0 radians and at most $\pi - \Omega_0$ radians, then (3.56) is satisfied. This condition implies that the regressor is persistently exciting of order two or more as defined in [34, 96].

Now that we have established global exponential stability for (3.52), we consider $\Theta(k)$ generated by (3.49). Since $\mathcal{N}(H_2^{\mathrm{T}}) \neq \{0\}$ if and only if G_{yu} is tall, we consider only the case where G_{yu} is tall.

Theorem 3.6.2. *Consider the instantaneous update law* (3.25) *with* $d = 2$*, let* G_{yu} *be tall, and assume that there exist* $\alpha > 0$ *and* $\gamma \in (0, 1)$ *such that, for all* $k \geq 0$*,* $\|H_2^{\mathrm{T}} y(k)\| \leq \alpha \gamma^k$*. Then, the following statements hold.*

(i) If Φ *is bounded, then* Θ *converges.*

(ii) If there exists $m \geq 2$ *such that* (3.56) *is satisfied, then* Θ *converges.*

Proof See Section 3.12.5. □

Theorem 3.6.1 has a geometric interpretation similar to the case $d = 1$ with $\mathcal{N}(H_1^{\mathrm{T}})$ replaced by $\mathcal{N}(H_2^{\mathrm{T}})$, that is, if y converges exponentially to $\mathcal{N}(H_2^{\mathrm{T}})$, then Θ converges.

3.6.3 Case 3: $d \geq 3$

We now briefly investigate the case $d \geq 3$. Consider the instantaneous update law (3.25) with arbitrary $d \geq 3$. First, from (3.16),

$$\begin{aligned}\hat{y}(\Theta(k-1),k) &= y(k) + H_d\Phi(k-d-1)[\Theta(k-1) - \Theta(k-d)]\\ &= y(k) + H_d\Phi(k-d-1)[\Theta(k-1) - \Theta(k-2) + \Theta(k-2)\\ &\quad - \cdots - \Theta(k-d+1) + \Theta(k-d+1) - \Theta(k-d)]\\ &= y(k) + H_d\Phi(k-d-1)\sum_{i=1}^{d-1}\Delta\Theta(k-i). \end{aligned} \tag{3.60}$$

Substituting (3.60) into (3.25), subtracting $\Theta(k-1)$ from (3.25) and using the identity $Q(I + Q^{\mathrm{T}}Q)^{-1} = (I + QQ^{\mathrm{T}})^{-1}Q$, we obtain

$$\Delta\Theta(k) = \mathcal{M}(k)\Delta\Theta(k-1) + \cdots + \mathcal{M}(k)\Delta\Theta(k-d+1) + \mathcal{N}(k)H_d^{\mathrm{T}}y(k), \tag{3.61}$$

where

$$\begin{aligned}\mathcal{M}(k) &\stackrel{\triangle}{=} -\Phi(k-d-1)^{\mathrm{T}}H_d^{\mathrm{T}}[\mu I_{l_y} + H_d\Phi(k-d-1)\Phi^{\mathrm{T}}(k-d-1)H_d^{\mathrm{T}}]^{-1}\\ &\quad \cdot H_d\Phi(k-d-1),\\ \mathcal{N}(k) &\stackrel{\triangle}{=} -[\mu I_{l_u n_{\mathrm{c}}(l_u+l_y)} + H_d\Phi(k-d-1)\Phi^{\mathrm{T}}(k-d-1)H_d^{\mathrm{T}}]\Phi(k-d-1).\end{aligned}$$

Now, letting

$$\mathcal{X}(k) \triangleq \begin{bmatrix} \Delta\Theta(k) \\ \vdots \\ \Delta\Theta(k-d+2) \end{bmatrix},$$

we rewrite (3.61) as

$$\mathcal{X}(k) = \mathcal{E}(k)\mathcal{X}(k-1) + \mathcal{F}(k)H_d^{\mathrm{T}}y(k), \tag{3.62}$$

$$\Delta\Theta(k) = \mathcal{C}\mathcal{X}(k), \tag{3.63}$$

where

$$\mathcal{E}(k) \triangleq \begin{bmatrix} \mathcal{M}(k) & \cdots & \mathcal{M}(k) & \mathcal{M}(k) \\ I & \cdots & 0 & 0 \\ \vdots & \ddots & \vdots & \vdots \\ 0 & \cdots & I & 0 \end{bmatrix}, \quad \mathcal{F}(k) \triangleq \begin{bmatrix} \mathcal{N}(k) \\ 0 \\ \vdots \\ 0 \end{bmatrix}, \tag{3.64}$$

$$\mathcal{C} \triangleq \begin{bmatrix} I & 0 & \cdots & 0 \end{bmatrix}. \tag{3.65}$$

Thus, as in the cases $d = 1$ and $d = 2$, the controller update (3.62), (3.63) is driven by $H_d^{\mathrm{T}}y(k)$. Furthermore, in addition to $H_d^{\mathrm{T}}y(k)$, $\Delta\Theta(k)$ also depends on $d-1$ past controller updates. It follows from (3.62) that, if, for all $k \geq 1$, $y(k) \in \mathcal{N}(H_d^{\mathrm{T}})$, then, for all $\mathcal{X}(0)$, $\mathcal{X}(k)$, and thus $\Delta\Theta(k)$, converges to zero if and only if the equilibrium $\mathcal{X} = 0$ of

$$\mathcal{X}(k) = \mathcal{E}(k)\mathcal{X}(k-1) \tag{3.66}$$

is globally attractive.

Since $\sigma_{\max}(\mathcal{E}(k))$ may be greater than 1, convergence results for $\Theta(k)$ in the case $d = 3$ are more complicated than in the cases $d = 1$ and $d = 2$. Numerical testing suggests that, if $y(k) \in \mathcal{N}(H_d)$ and (3.56) is satisfied, then $\{\mathcal{X}(k)\}_{k=1}^{\infty}$ and $\sum_{i=1}^{\infty} \Delta\Theta(k)$ converge, and thus Θ converges.

3.7 Input-Subspace Zeros

In this section, we build on the results of Section 3.5, and introduce the notion of input-subspace zeros, which arise due to the fact that the control input is contained in $\mathcal{R}(H_d^{\mathrm{T}})$, so that there exists $v \in \mathbb{R}^{l_y}$ such that $u = H_d^{\mathrm{T}} v$. If G_{yu} is square or tall, then $\mathcal{R}(H_d^{\mathrm{T}}) = \mathbb{R}^{l_u}$; in this case, we show that the input-subspace zeros of G_{yu} are equal to the transmission zeros of G_{yu}. However, in the case where G_{yu} is wide, $\mathcal{R}(H_d^{\mathrm{T}})$ is a proper subspace of $\mathbb{R}^{l_u}$. In this case, we show that G_{yu} may be minimum phase but have NMP input-subspace zeros. Finally, in light of input-subspace zeros, we revisit Examples 3.4.1 and 3.4.2 and demonstrate that the instability observed in Example 3.4.2 is caused by unstable cancellation of a NMP input-subspace zero that is not a transmission zero of G_{yu}.

3.7.1 Right-Squared Transfer Matrix from v to y

Consider $G_{yu} \overset{\min}{\sim} \left[\begin{array}{c|c} A & B \\ \hline C & 0 \end{array}\right]$, and define the right-squared transfer matrix

$$G_{yu}^{\mathrm{R}} \triangleq G_{yu} H_d^{\mathrm{T}} \sim \left[\begin{array}{c|c} A & BH_d^{\mathrm{T}} \\ \hline C & 0 \end{array}\right]. \tag{3.67}$$

Theorems 3.5.1 and 3.5.2 imply that, for all $k \geq 1$, the control input $u(k)$ generated by the instantaneous and cumulative update laws lies in the subspace $\mathcal{R}(H_d^{\mathrm{T}}) \subseteq \mathbb{R}^{l_y}$,

so that $u(k) = H_d^{\mathrm{T}} v(k)$, where $v(k) \in \mathbb{R}^{l_y}$. Hence, (3.6) becomes

$$y = G_{yu}^{\mathrm{R}} v + G_{yw} w. \tag{3.68}$$

Note that $G_{yu}^{\mathrm{R}} \in \mathbb{R}^{l_y \times l_y}(z)$. If the realization (3.67) is minimal, then the transmission zeros of G_{yu}^{R} are given by

$$\mathrm{tzeros}(G_{yu}^{\mathrm{R}}) = \{\zeta \in \mathbb{C} : \text{ rank } \Sigma^{\mathrm{R}}(\zeta) < \text{normal rank } \Sigma^{\mathrm{R}}\}, \tag{3.69}$$

where

$$\Sigma^{\mathrm{R}}(z) \triangleq \left[\begin{array}{cc} zI - A & BH_d^{\mathrm{T}} \\ C & 0 \end{array}\right] \in \mathbb{R}^{(n+l_y)\times(n+l_y)}[z]. \tag{3.70}$$

The transmission zeros of G_{yu}^{R} are the *input-subspace zeros* of G_{yu}. We consider the input-subspace zeros of tall, square, and wide plants separately.

3.7.2 Tall and Square Plants

The following result concerns minimality of (3.67) for tall and square G_{yu}.

Proposition 3.7.1. *If* $G_{yu} \overset{\min}{\sim} \left[\begin{array}{c|c} A & B \\ \hline C & 0 \end{array}\right]$ *is tall or square, then* $(A, BH_d^{\mathrm{T}}, C)$ *is minimal.*

Proof For all $\lambda \in \mathbb{C}$, we have

$$\left[\begin{array}{cc} \lambda I - A & BH_d^{\mathrm{T}} \end{array}\right] = \left[\begin{array}{cc} \lambda I - A & B \end{array}\right] \mathcal{Q}, \tag{3.71}$$

where

$$\mathcal{Q} \stackrel{\triangle}{=} \begin{bmatrix} I_n & 0_{n\times l_y} \\ 0_{l_u\times n} & H_d^{\mathrm{T}} \end{bmatrix} \in \mathbb{R}^{(n+l_u)\times(n+l_y)}. \tag{3.72}$$

Since G_{yu} is tall or square and H_d has full rank, we have rank $H_d = l_u$, and thus, rank $\mathcal{Q} = n + l_u$. Therefore, it follows from (3.71) that

$$\operatorname{rank} \begin{bmatrix} \lambda I - A & BH_d^{\mathrm{T}} \end{bmatrix} = \operatorname{rank} \begin{bmatrix} \lambda I - A & B \end{bmatrix}. \tag{3.73}$$

Since (A, B) is controllable, it follows from (3.73) that (A, BH_d^{T}) is controllable. Furthermore, since (A, C) is observable, (3.67) is minimal. □

Thus, if G_{yu} is tall or square, then the input-subspace zeros of G_{yu} are defined as in (3.69). We now show that, if G_{yu} is tall or square, then its input-subspace zeros and transmission zeros are identical.

Proposition 3.7.2. *If* $G_{yu} \stackrel{\min}{\sim} \left[\begin{array}{c|c} A & B \\ \hline C & 0 \end{array}\right]$ *is tall or square, then* $\operatorname{tzeros}(G_{yu}^{\mathrm{R}}) = \operatorname{tzeros}(G_{yu})$.

Proof It follows from (3.10) and (3.70) that $\Sigma^{\mathrm{R}}(z) = \Sigma(z)\mathcal{Q}$, where $\mathcal{Q}$ is given by (3.72). Since rank $\mathcal{Q} = n+l_u$, it follows that, for all $z \in \mathbb{C}$, rank $\Sigma(z) =$ rank $\Sigma^{\mathrm{R}}(z)$. It thus follows from (3.11), (3.69), and Proposition 3.7.1 that $\operatorname{tzeros}(G_{yu}^{\mathrm{R}}) = \operatorname{tzeros}(G_{yu})$. □

Therefore, for tall and square plants, the restriction $u(k) \in \mathcal{R}(H_d^{\mathrm{T}})$ has no effect on controllability, and does not alter the transmission zeros of the plant. This is expected because $\mathcal{R}(H_d^{\mathrm{T}}) = \mathbb{R}^{l_u}$ in the case where G_{yu} is tall or square.

3.7.3 Wide Plants

It is reasonable to expect that the properties of G_{yu}^{R} for wide plants are dual to those of tall plants. However, as we now show, this is not the case. For example, although the realization (3.67) is minimal for all tall plants G_{yu}, it turns out that (3.67) for a wide plant G_{yu} may or may not be minimal, as illustrated by the following example.

Example 3.7.3 (Minimality of (3.67))**.** Consider the 1×2 wide plant $G_{yu} \overset{\min}{\sim} \left[\begin{array}{c|c} A & B \\ \hline C & 0 \end{array}\right]$, where

$$A = \begin{bmatrix} 0 & 0 \\ 1 & 0 \end{bmatrix}, \; B = \begin{bmatrix} 0.5 & 0.5 \\ -0.5 & 0.5 \end{bmatrix}, \; C = \begin{bmatrix} 0 & 2 \end{bmatrix},$$

$n = 2$, $d = 1$, and $H_1 = \begin{bmatrix} -1 & 1 \end{bmatrix}$. Note that

$$\operatorname{rank} \begin{bmatrix} BH_1^{\mathrm{T}} & ABH_1^{\mathrm{T}} \end{bmatrix} = \operatorname{rank} \begin{bmatrix} 0 & 0 \\ 1 & 0 \end{bmatrix} < n,$$

which implies that (3.67) is not minimal. ■

Example 3.7.3 shows that minimality of (A, B, C) does not imply that (3.67) is minimal. However, throughout the rest of this section, we only consider plants for which (3.67) is minimal.

Since $(A, BH_d^{\mathrm{T}}, C)$ is minimal, the input-subspace zeros of G_{yu} are defined as in (3.69). The following example illustrates that the input-subspace zeros and the transmission zeros of a wide plant may be distinct.

Example 3.7.4 (Input-subspace zeros of a wide plant)**.** Consider $G_{yu} \overset{\min}{\sim} \left[\begin{array}{c|c} A & B \\ \hline C & 0 \end{array}\right]$ with

$$A = \begin{bmatrix} 0 & 0 \\ 1 & 0 \end{bmatrix},\ B = \begin{bmatrix} -0.8 & -0.3 \\ 0.5 & 0.5 \end{bmatrix},\ C = \begin{bmatrix} 0 & 2 \end{bmatrix},$$

$n = 2$, $d = 1$, $H_1 = \begin{bmatrix} 1 & 1 \end{bmatrix}$. For this example, (A, BH_1^{T}) is controllable. It can be shown that $\mathrm{tzeros}(G_{yu}) = \varnothing$ and $\mathrm{tzeros}(G_{yu}^{\mathrm{R}}) = \{1.1\}$. Hence, this example shows that the transmission zeros and the input-subspace zeros of a wide plant may be distinct. ■

It follows from [24, Theorem 5] that wide $G_{yu} \overset{\min}{\sim} \left[\begin{array}{c|c} A & B \\ \hline C & 0 \end{array}\right]$ generically has no transmission zeros, whereas, since $G_{yu}^{\mathrm{R}} \in \mathbb{R}^{l_y \times l_y}(z)$, G_{yu} generically has $n - l_y$ input-subspace zeros. In particular, in the case $d = 1$, since $\mathrm{rank}\, CB(CB)^{\mathrm{T}} = l_y$, it follows that G_{yu}^{R} has exactly $n - l_y$ zeros [71]. Therefore, G_{yu} typically has more input-subspace zeros than transmission zeros. Furthermore, if G_{yu} has NMP input-subspace zeros, then there exist infinitely many unbounded [70, 107, 108] *output-zeroing* input sequences $\{u(k)\}_{k=0}^{\infty} \subset \mathcal{R}(H_d^{\mathrm{T}})$, each of which is associated with an initial condition $x(0) \in \mathbb{R}^n$, such that, for all $k \geq 0$, the output $y(k)$ of G_{yu} due to $(x(0), \{u(k)\}_{k=0}^{\infty})$ is identically equal to zero. The next result characterizes pairs $(x(0), \{u(k)\}_{k=0}^{\infty})$ that produce identically zero output y.

Proposition 3.7.5. *Let* $G_{yu} \overset{\min}{\sim} \left[\begin{array}{c|c} A & B \\ \hline C & 0 \end{array}\right]$ *be wide with state* x *and output* y*, and let* ζ *be a nonzero input-subspace zero of* G_{yu}*. Then, the following statements hold.*

(i) There exist nonzero $\begin{bmatrix} x_0 \\ v_0 \end{bmatrix} \in \mathbb{C}^{n+l_y}$ *such that*

$$\Sigma^{\mathrm{R}}(\zeta) \begin{bmatrix} x_0 \\ v_0 \end{bmatrix} = 0. \tag{3.74}$$

(ii) Let $x(0) = -\mathrm{Re}(x_0)$*, and, for all* $k \geq 0$*, let*

$$u(k) = H_d^{\mathrm{T}}[\mathrm{Re}(\zeta^k)\mathrm{Re}(v_0) - \mathrm{Im}(\zeta^k)\mathrm{Im}(v_0)]. \tag{3.75}$$

Then, for all $k \geq 0$*,*

$$x(k) = -\mathrm{Re}(\zeta^k)\mathrm{Re}(x_0) + \mathrm{Im}(\zeta^k)\mathrm{Im}(x_0), \tag{3.76}$$

$$y(k) = 0. \tag{3.77}$$

(iii) Let $\alpha \in \mathbb{R}$*, let* $x(0) = -\alpha\mathrm{Re}(x_0)$*, and, for all* $k \geq 0$*, let*

$$u(k) = \alpha H_d^{\mathrm{T}}[\mathrm{Re}(\zeta^k)\mathrm{Re}(v_0) - \mathrm{Im}(\zeta^k)\mathrm{Im}(v_0)]. \tag{3.78}$$

Then, for all $k \geq 0$*,* $y(k) = 0$*.*

(iv) Let $\alpha \in \mathbb{R}$*, assume that* A *is discrete-time asymptotically stable, and let* $u(k)$ *be given by* (3.78)*. Then, for all* $x(0) \in \mathbb{R}^n$*,* $y(k) \to 0$ *as* $k \to \infty$ *with exponential convergence.*

Proof To show (i), suppose $\zeta \in \mathrm{tzeros}(G_{yu}^{\mathrm{R}})$. Then, it follows from (3.69), (3.70) that $\mathrm{rank}\ \Sigma^{\mathrm{R}}(\zeta) < \text{normal rank}\ \Sigma^{\mathrm{R}} \leq n + l_y$. Therefore, $\mathcal{N}(\Sigma^{\mathrm{R}}(\zeta)) \neq \{0\}$, and thus (i) is satisfied.

To show (ii), suppose that $x(0) = -\mathrm{Re}(x_0)$ and $u(k) = H_d^{\mathrm{T}}[\mathrm{Re}(\zeta^k)\mathrm{Re}(v_0) +$

$\mathrm{Im}(\zeta^k)\mathrm{Im}(v_0)]$. Since $\zeta^0 = 1$, (3.76) holds for $k = 0$, and, from (3.70) and (3.74), $y(0) = -C\mathrm{Re}(x_0) = 0$. Thus, (3.76), (3.77) hold for $k = 0$. Now, assume that (3.76), (3.77) hold for some $k > 0$. We thus have

$$\begin{aligned} x(k+1) &= Ax(k) + Bu(k) \\ &= -\mathrm{Re}(\zeta^k)A\mathrm{Re}(x_0) + \mathrm{Im}(\zeta^k)A\mathrm{Im}(x_0) + \mathrm{Re}(\zeta^k)BH_d^{\mathrm{T}}\mathrm{Re}(v_0) \\ &\quad - \mathrm{Im}(\zeta^k)BH_d^{\mathrm{T}}\mathrm{Im}(v_0). \end{aligned} \tag{3.79}$$

Next, it follows from (3.70) and (3.74) that

$$\zeta x_0 - Ax_0 + BH_d^{\mathrm{T}}v_0 = 0,$$

and thus,

$$BH_d^{\mathrm{T}}\mathrm{Re}(v_0) = A\mathrm{Re}(x_0) + \mathrm{Im}(\zeta)\mathrm{Im}(x_0) - \mathrm{Re}(\zeta)\mathrm{Re}(x_0) \tag{3.80}$$

and

$$BH_d^{\mathrm{T}}\mathrm{Im}(v_0) = A\mathrm{Im}(x_0) - \mathrm{Re}(\zeta)\mathrm{Im}(x_0) - \mathrm{Im}(\zeta)\mathrm{Re}(x_0). \tag{3.81}$$

Substituting (3.80) and (3.81) into (3.79), we obtain

$$\begin{aligned} x(k+1) &= -\mathrm{Re}(\zeta^k)A\mathrm{Re}(x_0) + \mathrm{Im}(\zeta^k)A\mathrm{Im}(x_0) + \mathrm{Re}(\zeta^k)[A\mathrm{Re}(x_0) + \mathrm{Im}(\zeta)\mathrm{Im}(x_0) \\ &\quad - \mathrm{Re}(\zeta)\mathrm{Re}(x_0)] - \mathrm{Im}(\zeta^k)[A\mathrm{Im}(x_0) - \mathrm{Re}(\zeta)\mathrm{Im}(x_0) - \mathrm{Im}(\zeta)\mathrm{Re}(x_0)] \\ &= [-\mathrm{Re}(\zeta^k)\mathrm{Re}(\zeta) + \mathrm{Im}(\zeta^k)\mathrm{Im}(\zeta)]\mathrm{Re}(x_0) \\ &\quad + [\mathrm{Re}(\zeta^k)\mathrm{Im}(\zeta) + \mathrm{Im}(\zeta^k)\mathrm{Re}(\zeta)]\mathrm{Im}(x_0) \\ &= -\mathrm{Re}(\zeta^{k+1})\mathrm{Re}(x_0) + \mathrm{Im}(\zeta^{k+1})\mathrm{Im}(x_0), \end{aligned} \tag{3.82}$$

which shows that (3.76) holds for $k+1$. Furthermore, since $Cx_0 = 0$ from (3.74), it follows from (3.82) that

$$y(k+1) = Cx(k+1) = 0.$$

Thus, (3.76), (3.77) hold for $k+1$ if they hold for k. By induction, it follows that (ii) holds. Statement (iii) follows from the homogeneity of linear systems.

Finally, to show (iv), consider

$$y(k) = CA^k x(0) + \sum_{i=1}^{k} H_i u(k-i), \tag{3.83}$$

where $u(k)$ is given by (3.78), and $x(0) \in \mathbb{R}^n$. Adding and subtracting $CA^k(-\alpha \mathrm{Re}(x_0))$ from (3.83) and using (iii), we have

$$\begin{aligned} y(k) &= CA^k[x(0) + \alpha \mathrm{Re}(x_0)] + CA^k[-\alpha \mathrm{Re}(x_0)] + \sum_{i=1}^{k} H_i u(k-i) \\ &= CA^k \tilde{x}(k), \end{aligned} \tag{3.84}$$

where $\tilde{x}(k) \triangleq x(0) + \alpha \mathrm{Re}(x_0) \in \mathbb{R}^n$. Since A is discrete-time asymptotically stable, it follows from (3.84) that $y(k) \to 0$ as $k \to \infty$ with exponential convergence. □

Note that, if the input-subspace zero ζ satisfies $|\zeta| > 1$, then the output-zeroing input sequence (3.78) with $\alpha \neq 0$ is unbounded. Hence, if G_{yu} has at least one NMP input-subspace zero, then there exist infinitely many unbounded output-zeroing input sequences that are contained in the subspace $\mathcal{R}(H_d^{\mathrm{T}})$, even though G_{yu} itself is minimum phase. Since the retrospective cost functions (3.20) and (3.29) do not contain a control penalty or a constraint on the amplitude of u, RCAC may converge to a controller that produces an unbounded output-zeroing input sequence, namely, an unstable controller with a pole (or poles) located at the NMP input-subspace zero(s)

of G_{yu}. In the next subsection, we show that this is the cause of the instability in Example 3.4.2. In Section 3.9, we remedy this behavior by modifying the retrospective cost (3.29).

3.7.3.1 Examples 3.4.1 and 3.4.2 Revisited

In Examples 3.4.1 and 3.4.2, which are identical except for $B_{(1,1)}$, the cumulative adaptive controller (3.35) is applied to 2×3 plants in order to reject an unmatched harmonic disturbance. Both plants have no transmission zeros, the given realizations are minimal, and the open-loop systems have the same eigenvalues. However, as shown in Figure 3.2, the control signal u for the adaptive system in Example 3.4.2 is unbounded. We now demonstrate that the unbounded control signal is caused by the NMP input-subspace zero of G_{yu}.

Example 3.7.6 (Example 3.4.2 revisited)**.** We first confirm that (3.46) holds. Note that $d = 1$ and

$$H_1 = \begin{bmatrix} 0.1062 & 0.8195 & -1.1582 \\ 3.2868 & -0.4562 & -4.4993 \end{bmatrix}.$$

Hence, $\mathcal{R}(H_1^{\mathrm{T}})$ is the plane described by $au_1 + bu_2 + cu_3 = 0$, where a, b, c satisfy

$$\begin{bmatrix} a \\ b \\ c \end{bmatrix} \in \mathcal{N}(H_1) = \operatorname{span}\left\{ \begin{bmatrix} 0.699 \\ 0.552 \\ 0.4547 \end{bmatrix} \right\}.$$

The phase portrait of $u(k)$ for $k \geq 1$ illustrated in Figure 3.6 shows that $u(k)$ is confined to the subspace $\mathcal{R}(H_1^{\mathrm{T}})$ for all $k \geq 1$.

We now investigate the input-subspace zeros of the plant. Since $(A, BH_d^{\mathrm{T}}, C)$ is minimal, (3.69) can be used to obtain the input-subspace zeros of G_{yu}, which are given

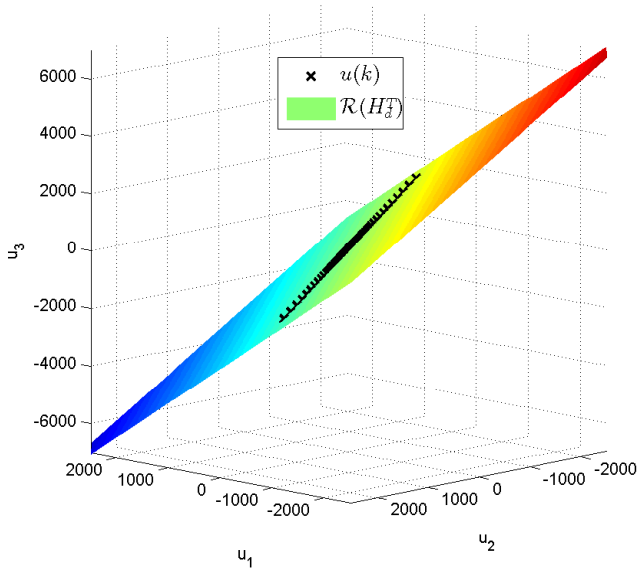

Figure 3.6: This figure illustrates the phase portrait of the unbounded control input u for Example 3.4.2 shown in Figure 3.5. For all $k \geq 1$, $u(k)$ is contained in the subspace $\mathcal{R}(H_d^{\mathrm{T}})$, which is the colored plane in this figure. The control input is unbounded due to the fact that the input-subspace zeros of G_{yu} are NMP.

by $\mathrm{tzeros}(G_{yu}^{\mathrm{R}}) = \{-1.0555,\ 0.7596\}$. Therefore, G_{yu} has a NMP input-subspace zero at -1.0555. Computing the controller poles at $k = 150$, Figure 3.7 shows that, as Θ converges, one controller pole is located near the NMP input-subspace zero location -1.0555. In effect, RCAC attempts to cancel the unmodeled NMP input-subspace zero. Thus, the results of Example 3.4.2 can be explained as follows: The unstable controller pole at the NMP input-subspace zero causes the control input to diverge, but the effect of the unbounded control input is blocked by the NMP input-subspace zero, and the performance output y converges to zero despite the fact that u is unbounded, as suggested by (iv) of Proposition 3.7.5. Furthermore, since G_{yu} is wide, $\mathcal{N}(H_d^{\mathrm{T}}) = \{0\}$, and thus Θ converges as y converges to zero. ■

Example 3.7.7 (Example 3.4.1 revisited)**.** We now revisit Example 3.4.1, where the control input u is bounded. The phase portrait of $u(k)$ for $k \geq 1$ illustrated in Figure 3.8 shows that $u(k)$ is contained in the subspace $\mathcal{R}(H_1^{\mathrm{T}})$ for all $k \geq 1$.

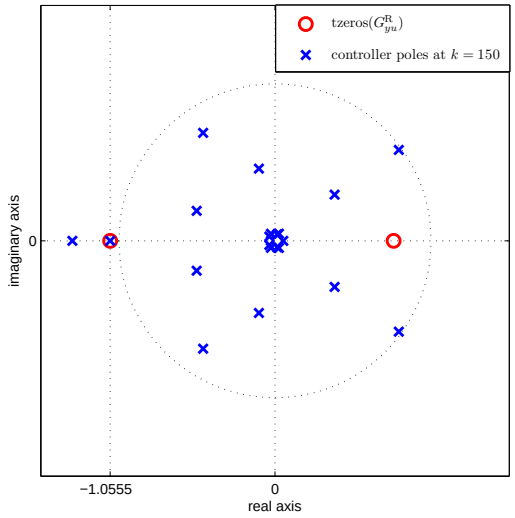

Figure 3.7: This figure illustrates the input-subspace zeros of the plant in Example 3.4.2 along with the poles of the adaptive controller at $k = 150$, whose time evolution is shown in Figure 3.2. The adaptive controller places a pole near the NMP input-subspace zero of G_{yu}, which is located at -1.0555. This unstable pole-zero cancellation is the cause of the unbounded control input shown in Figure 3.2. Note that the NMP input-subspace zero is not a transmission zero of G_{yu}.

The input-subspace zeros of the plant (3.40), (3.41) are given by $\mathrm{tzeros}(G_{yu}^{\mathrm{R}}) = \{-0.7334,\ 0.7679\}$. The input-subspace zeros for Example 3.4.1 are thus minimum phase, and, as shown in Figure 3.1, the control input u is bounded. Furthermore, Θ converges as y converges to zero. ■

3.8 Output-Subspace Zeros

In this section we build on the convergence results of Section 3.6 and introduce the notion of output-subspace zeros, which are the zeros from the control input to the scaled performance variable $H_d^{\mathrm{T}} y$, which drives the update of Θ, as shown in Section 3.6. If G_{yu} is square or wide, then, since $\mathcal{N}(H_d^{\mathrm{T}}) = \{0\}$, $H_d^{\mathrm{T}} y = 0$ if and only if $y = 0$. In this case, it is reasonable to expect that the zeros from u to y and zeros from u to $H_d^{\mathrm{T}} y$ are identical, which we show by proving that the output-subspace zeros and

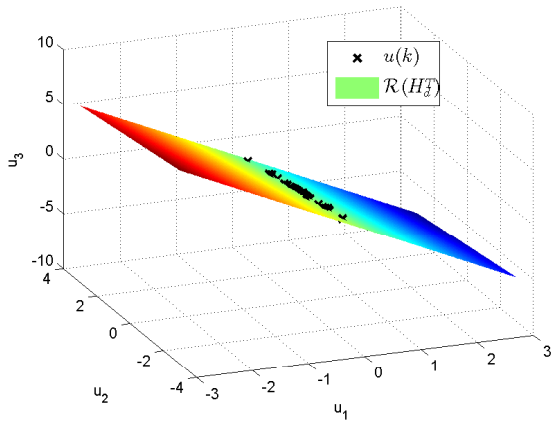

Figure 3.8: This figure illustrates the phase portrait of the bounded control input u for Example 3.4.1 shown in Figure 3.1. For all $k \geq 1$, $u(k)$ is contained in the subspace $\mathcal{R}(H_d^{\mathrm{T}})$, which is the colored plane in this figure. The control input is bounded due to the fact that the input-subspace zeros of G_{yu} are minimum phase.

the transmission zeros of square and wide plants are identical. However, in the case where G_{yu} is tall, $\mathcal{N}(H_d^{\mathrm{T}})$ is a proper subspace of $\mathbb{R}^{l_y}$, and thus $H_d^{\mathrm{T}} y$ may be zero with nonzero y. In this case, we show that the output-subspace zeros and the transmission zeros of G_{yu} may be distinct. In particular, we show that G_{yu} may be minimum phase, but have NMP output-subspace zeros, and, in this case, we show that the control input may be unbounded despite the fact that $H_d^{\mathrm{T}} y$ is exponentially decaying, which in turn leads to converging Θ. At the end of the section, we revisit Examples 3.4.4 and 3.4.5 in light of output-subspace zeros, and demonstrate that the instability observed in 3.4.5 is caused by unstable cancellation of a NMP output-subspace zero, which leads to an unbounded control input and performance output, although the unbounded control input does not affect $H_d^{\mathrm{T}} y$ because of the NMP output-subspace zero.

3.8.1 Left-Squared Transfer Matrix from u to $H_d^{\mathrm{T}} y$

Consider $G_{yu} \overset{\min}{\sim} \left[\begin{array}{c|c} A & B \\ \hline C & 0 \end{array}\right]$, and define the left-squared transfer matrix

$$G_{yu}^{\mathrm{L}} \triangleq H_d^{\mathrm{T}} G_{yu} \sim \left[\begin{array}{c|c} A & B \\ \hline H_d^{\mathrm{T}} C & 0 \end{array}\right]. \tag{3.85}$$

For plants with $d = 1$ or $d = 2$, Theorems 3.6.1 and 3.6.2 imply that, if $H_d^{\mathrm{T}} y$ converges to zero, then Θ converges. For tall plants, $\mathcal{N}(H_d^{\mathrm{T}}) \neq \{0\}$, and thus $H_d^{\mathrm{T}} y$ may converge to zero with possibly unbounded y. It follows from (3.47) and (3.49) that $H_d^{\mathrm{T}} y$ drives the controller update $\Delta\Theta$. To investigate the zeros from u to $H_d^{\mathrm{T}} y$, we multiply (3.6) by H_d^{T}, and consider

$$H_d^{\mathrm{T}} y = G_{yu}^{\mathrm{L}} u + H_d^{\mathrm{T}} G_{yw} w. \tag{3.86}$$

Note that $G_{yu}^{\mathrm{L}} \in \mathbb{R}^{l_u \times l_u}(z)$. If (3.85) is minimal, then the transmission zeros of G_{yu}^{L} are given by

$$\mathrm{tzeros}(G_{yu}^{\mathrm{L}}) = \{\zeta \in \mathbb{C} : \text{ rank } \Sigma^{\mathrm{L}}(\zeta) < \text{normal rank } \Sigma^{\mathrm{L}}\}, \tag{3.87}$$

where

$$\Sigma^{\mathrm{L}}(z) \triangleq \left[\begin{array}{cc} zI - A & B \\ H_d^{\mathrm{T}} C & 0 \end{array}\right]. \tag{3.88}$$

The transmission zeros of G_{yu}^{L} are the *output-subspace zeros* of G_{yu}. We consider the output-subspace zeros of wide, square and tall plants separately. Unlike Section 3.7, where we consider tall and square plants before wide plants, in this section, we

consider wide and square plants before tall plants. As it turns out, there exists a duality between output-subspace zeros of wide and square (tall) plants and input-subspace zeros of tall and square (wide) plants.

3.8.2 Wide and Square Plants

First, as pointed out in Section 3.6, if G_{yu} is wide or square, then $\mathcal{N}(H_d^{\mathrm{T}}) = \{0\}$, and thus, $H_d^{\mathrm{T}} y(k) = 0$ if and only if $y(k) = 0$. It is therefore intuitive to expect that the output-subspace zeros of G_{yu} are equal to the transmission zeros of G_{yu}, that is, $\mathrm{tzeros}(G_{yu}^{\mathrm{L}}) = \mathrm{tzeros}(G_{yu})$. We now show that this is indeed the case.

First, we show that (3.85) is minimal for all wide and square plants G_{yu}.

Proposition 3.8.1. *If* $G_{yu} \overset{\min}{\sim} \left[\begin{array}{c|c} A & B \\ \hline C & 0 \end{array}\right]$ *is wide or square, then* $(A, B, H_d^{\mathrm{T}} C)$ *is minimal.*

Proof Since G_{yu} is wide or square and H_d has full rank, we have rank $H_d = l_y$, and thus, rank $\mathcal{Q} = n + l_y$, where $\mathcal{Q}$ is given by (3.72). Therefore, for all $\lambda \in \mathbb{C}$, we have

$$\mathrm{rank} \begin{bmatrix} \lambda I - A \\ H_d^{\mathrm{T}} C \end{bmatrix} = \mathrm{rank} \left(\mathcal{Q} \begin{bmatrix} \lambda I - A \\ C \end{bmatrix} \right) = \mathrm{rank} \begin{bmatrix} \lambda I - A \\ C \end{bmatrix}. \tag{3.89}$$

Since (A, C) is observable, it follows from (3.89) that $(A, H_d^{\mathrm{T}} C)$ is observable. Furthermore, since (A, B) is controllable, (3.85) is minimal.

Since (3.85) is minimal, the output-subspace zeros of G_{yu} are defined as in (3.87). We now show that if G_{yu} is wide or square, then its output-subspace zeros and transmission zeros are identical.

Proposition 3.8.2. *If* $G_{yu} \overset{\min}{\sim} \left[\begin{array}{c|c} A & B \\ \hline C & 0 \end{array}\right]$ *is wide or square, then* $\mathrm{tzeros}(G_{yu}^{\mathrm{L}}) =$

tzeros(G_{yu}).

Proof It follows from (3.10) and (3.88) that $\Sigma^{\mathrm{L}}(z) = \mathcal{Q}\Sigma(z)$, where $\mathcal{Q}$ is defined as in (3.72). Since G_{yu} is wide or square and H_d has full rank, rank $\mathcal{Q} = n + l_y$. Therefore, for all $z \in \mathbb{C}$, rank $\Sigma(z) =$ rank $\Sigma^{\mathrm{L}}(z)$. It thus follows from (3.11), (3.87) and Proposition 3.8.1 that tzeros(G^{L}_{yu}) = tzeros(G_{yu}).

Therefore, for wide and square plants, G^{L}_{yu} is NMP if and only if G_{yu} is NMP. Therefore, if G_{yu} is minimum phase, then y cannot converge to $\mathcal{N}(H_d^{\mathrm{T}}) = \{0\}$ with an unbounded input sequence, and thus Θ cannot converge to a controller that generates an unbounded input sequence.

3.8.3 Tall Plants

We first investigate the minimality of the realization (3.85) for tall plants. The following example illustrates that the minimality of (A, B, C) does not imply that (3.85) is minimal.

Example 3.8.3 (Minimality of (3.85))**.** Consider the 2×1 plant $G_{yu} \overset{\min}{\sim} \left[\begin{array}{c|c} A & B \\ \hline C & 0 \end{array}\right]$, where

$$A = \begin{bmatrix} 0 & 1 \\ 0 & 0 \end{bmatrix}, \ B = \begin{bmatrix} 0 \\ 2 \end{bmatrix}, \ C = \begin{bmatrix} 0.5 & -0.5 \\ 0.5 & 0.5 \end{bmatrix}, \tag{3.90}$$

$n = 2$, $d = 1$, and $H_1 = \begin{bmatrix} -1 & 1 \end{bmatrix}^{\mathrm{T}}$. Note that

$$\operatorname{rank} \begin{bmatrix} H_1^{\mathrm{T}} C \\ H_1^{\mathrm{T}} CA \end{bmatrix} = \operatorname{rank} \begin{bmatrix} 0 & 1 \\ 0 & 0 \end{bmatrix} < n,$$

which implies that (3.85) is not minimal. ■

Example 3.8.3 shows that minimality of (A, B, C) does not imply that (3.85) is minimal. However, throughout the rest of this section, we only consider plants for which (3.85) is minimal.

Since (3.85) is minimal, the output-subspace zeros of G_{yu} are defined as in (3.87). The following example illustrates that the output-subspace zeros and the transmission zeros of G_{yu} may be distinct.

Example 3.8.4 (Output-subspace zeros of a tall plant)**.** Consider the 3×2 plant $G_{yu} \overset{\min}{\sim} \left[\begin{array}{c|c} A & B \\ \hline C & 0 \end{array}\right]$, where

$$A = \begin{bmatrix} 0.5 & 0.3 & 2.5 & 0.7 \\ 1.8 & -1.3 & 1.2 & 0 \\ -2.2 & -0.4 & -1.3 & 0.7 \\ 0.8 & 0.3 & 2 & -0.2 \end{bmatrix}, \; B = \begin{bmatrix} -0.1 & 0.6 \\ 1.5 & -1.2 \\ 1.4 & 0.7 \\ 1.4 & 1.6 \end{bmatrix}, \tag{3.91}$$

$$C = \begin{bmatrix} 0.4 & -0.3 & 0.8 & -0.8 \\ 1 & 0.3 & -1.1 & -1.9 \\ 0.7 & -0.8 & -1 & 1.4 \end{bmatrix}, \tag{3.92}$$

$n = 4$, $d = 1$, and $H_1 = \begin{bmatrix} -0.49 & -0.12 \\ -3.85 & -3.57 \\ -0.71 & 2.92 \end{bmatrix}$. For this example, $(A, H_1^{\mathrm{T}} C)$ is observable so that $(A, B, H_1^{\mathrm{T}} C)$ is minimal. It can be shown that $\mathrm{tzeros}(G_{yu}) = \varnothing$ and $\mathrm{tzeros}(G_{yu}^{\mathrm{L}}) = \{0.0969 + \jmath 0.8774, 0.0969 - \jmath 0.8774\}$. Hence, this example shows that the transmission zeros and the output-subspace zeros of a tall plant may be distinct.

■

It turns out that the properties of G_{yu}^{L} for tall plants are dual to those of G_{yu}^{R} for wide plants. In particular, for almost all tall $G_{yu} \overset{\min}{\sim} \left[\begin{array}{c|c} A & B \\ \hline C & 0 \end{array}\right]$, it follows from [24, Theorem 5] that $\mathrm{tzeros}(G_{yu}) = \varnothing$, whereas, since $G_{yu}^{\mathrm{L}} \in \mathbb{R}^{l_u \times l_u}(z)$, G_{yu} generically has $n - l_u$ output-subspace zeros. Furthermore, in the case $d = 1$, it follows that G_{yu} has exactly $n - l_u$ output-subspace zeros. Therefore, tall G_{yu} typically has more output-subspace zeros than transmission zeros. Furthermore, if G_{yu} has NMP output-subspace zeros, then there exist infinitely many unbounded input sequences $\{u(k)\}_{k=0}^{\infty}$, each of which associated with an initial condition $x(0) \in \mathbb{R}^n$, such that, for all $k \geq 0$, the scaled performance output $H_d^{\mathrm{T}} y(k)$ due to $(x(0), \{u(k)\}_{k=0}^{\infty})$ is identically equal to zero. The following result, which is the dual of Proposition 3.7.5, characterizes pairs $(x(0), u(k))$ that produce identically zero $H_d^{\mathrm{T}} y$. The proof is similar to the proof of Proposition 3.7.5 and is omitted.

Proposition 3.8.5. *Let* $G_{yu} \overset{\min}{\sim} \left[\begin{array}{c|c} A & B \\ \hline C & 0 \end{array}\right]$ *be tall with state* $x(k)$ *and output* $y(k)$, *and let* ζ *be a nonzero output-subspace zero of* G_{yu}. *Then, the following statements hold.*

(i) There exist nonzero $\left[\begin{array}{c} x_0 \\ \\ u_0 \end{array}\right] \in \mathbb{C}^{n+l_u}$ *such that*

$$\Sigma^{\mathrm{L}}(z) \left[\begin{array}{c} x_0 \\ \\ u_0 \end{array}\right] = 0. \tag{3.93}$$

(ii) Let $x(0) = -\mathrm{Re}(x_0)$, *and, for all* $k \geq 0$, *let the control input be given by*

$$u(k) = \mathrm{Re}(\zeta^k)\mathrm{Re}(u_0) - \mathrm{Im}(\zeta^k)\mathrm{Im}(u_0). \tag{3.94}$$

Then, for all $k \geq 0$, $x(k)$ and $H_d^{\mathrm{T}} y(k)$ satisfy

$$x(k) = -\mathrm{Re}(\zeta^k)\mathrm{Re}(x_0) + \mathrm{Im}(\zeta^k)\mathrm{Im}(x_0), \tag{3.95}$$

$$H_d^{\mathrm{T}} y(k) = 0. \tag{3.96}$$

(iii) Let $\alpha \in \mathbb{R}$, let $x(0) = -\alpha \mathrm{Re}(x_0)$, and, for all $k \geq 0$, assume that the control input is given by

$$u(k) = \alpha[\mathrm{Re}(\zeta^k)\mathrm{Re}(u_0) - \mathrm{Im}(\zeta^k)\mathrm{Im}(u_0)]. \tag{3.97}$$

Then, for all $k \geq 0$, $H_d^{\mathrm{T}} y(k) = 0$.

(iv) Let $\alpha \in \mathbb{R}$, assume that A is discrete-time asymptotically stable, and let $u(k)$ be given by (3.97)*. Then, for all $x(0) \in \mathbb{R}^n$, $H_d^{\mathrm{T}} y(k) \to 0$ as $k \to \infty$ with exponential convergence.*

It follows from Proposition 3.8.5 that, if G_{yu} has at least one NMP output-direction zero, then there exist infinitely many unbounded input sequences such that $y(k) \in \mathcal{N}(H_d^{\mathrm{T}})$ for all $k \geq 0$. It is shown in Section 3.6 that, if $y(k) \in \mathcal{N}(H_d^{\mathrm{T}})$, then Θ converges independently of y. Therefore, if G_{yu} has NMP output-direction zeros, then Θ may converge to a controller producing an unbounded input sequence which drives $y(k)$ to $\mathcal{N}(H_d^{\mathrm{T}})$, namely, an unstable controller with a pole (or poles) located at the NMP output-subspace zero(s) of G_{yu}. In this case, unless G_{yu} and G_{yu}^{L} have the same NMP transmission zeros, since the control input is unbounded, the performance output y is also unbounded. In the next subsection, we verify that these heuristic arguments explain the closed-loop responses shown in Examples 3.4.4 and 3.4.5.

3.8.3.1 Examples 3.4.4 and 3.4.5 Revisited

In Examples 3.4.4 and 3.4.5, the instantaneous adaptive controller (3.24) is applied to a 3×1 plant in order to reject the unmatched harmonic disturbance $w(k) = \sin \frac{2\pi}{7}k + \sin \frac{\pi}{5}k$. In both cases, the plant G_{yu} has no transmission zeros, the realization (A, B, C) is minimal, and the eigenvalues of the open-loop system are equal. The only difference between Examples 3.4.4 and 3.4.5 is the entry $C_{(1,2)}$. In Example 3.4.4, Θ converges, and u and y are bounded. In Example 3.4.5, Θ converges, but u and y are unbounded. We now demonstrate that, in both cases, as k increases, $y(k)$ approaches $\mathcal{N}(H_d^{\mathrm{T}})$. Furthermore, we show that, in Example 3.4.5, the instability is due to the presence of a NMP output-direction zero. Note that, since G_{yu} is tall in Examples 3.4.4 and 3.4.5, $\mathcal{R}(H_d^{\mathrm{T}}) = \mathbb{R}^{l_u}$, which, since G_{yu} has no transmission zeros, implies that G_{yu} has no input-subspace zeros.

Example 3.8.6 (Example 3.4.5 revisited)**.** We first verify that $y(k)$ approaches $\mathcal{N}(H_d^{\mathrm{T}})$ as Θ converges. First, note that $d = 1$ and $H_1 = \begin{bmatrix} -1 & 1 & 3 \end{bmatrix}^{\mathrm{T}}$. Hence, $\mathcal{N}(H_1^{\mathrm{T}})$ is the plane described by $ay_1 + by_2 + cy_3 = 0$, where a, b, c satisfy

$$\begin{bmatrix} a \\ b \\ c \end{bmatrix} \in \mathcal{R}(H_1) = \operatorname{span}\left\{ \begin{bmatrix} -1 \\ 1 \\ 3 \end{bmatrix} \right\}.$$

The phase portrait of $y(k)$ for $k \in [100, 200]$ illustrated in Figure 3.9 shows that, as the controller converges, y grows without bound on the surface $\mathcal{N}(H_1^{\mathrm{T}})$, which is the colored surface in the figure. Therefore, even though y grows without bound in Figure 3.5, since $y \in \mathcal{N}(H_1^{\mathrm{T}})$, Θ converges.

We now investigate the output-subspace zeros of the plant. It is easy to verify that $(A, B, H_1^{\mathrm{T}}C)$ is minimal. Therefore, (3.87) can be used to solve for the output-subspace zeros of G_{yu}, which are given by $\operatorname{tzeros}(G_{yu}^{\mathrm{L}}) = \{-0.2954, 1.0863\}$. There-

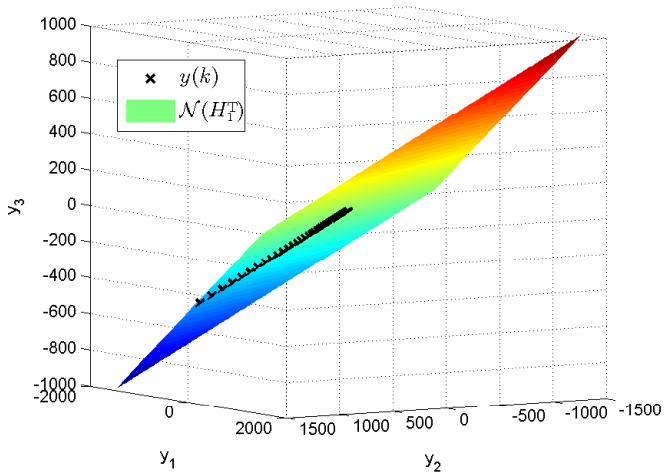

Figure 3.9: This figure illustrates the phase portrait for $k \in [100, 200]$ of the unbounded performance output y for Example 3.4.5 shown in Figure 3.5. Since the output-subspace zeros of G_{yu} are NMP, the unbounded output y grows without bound on the surface $\mathcal{N}(H_1^{\mathrm{T}})$. Since y is contained in $\mathcal{N}(H_1^{\mathrm{T}})$, the controller Θ in Figure 3.5 converges despite the fact that y is unbounded.

fore, G_{yu} has a NMP output-subspace zero at 1.0863. Computing the controller poles at $k = 200$, Figure 3.10 shows that, as Θ converges, one controller pole is located near the NMP output-subspace zero location 1.0863. Thus, the results of Example 3.4.5 can be evaluated as follows. The unstable controller pole at the NMP output-subspace zero location causes the input signal u to diverge. Since G_{yu} is minimum phase, the performance output y also diverges due to the unbounded input. However, since G_{yu} has a NMP output-subspace zero near the unstable controller pole location, it follows from Proposition 3.8.5 that y approaches $\mathcal{N}(H_1^{\mathrm{T}})$. Therefore, it follows from the results of Section 3.6 that Θ converges. ■

Example 3.8.7 (Example 3.4.4 revisited)**.** We now revisit Example 3.4.4, where u and y are bounded, y does not converge, and Θ converges. Figure 3.11 shows the phase portrait of $y(k)$ in $\mathbb{R}^3$ for $k \in [800, 1000]$. As shown in Figure 3.11, y oscillates on the surface $\mathcal{N}(H_1^{\mathrm{T}})$, which drives $\Delta\Theta$ to zero as k increases, as shown in Figure 3.4.

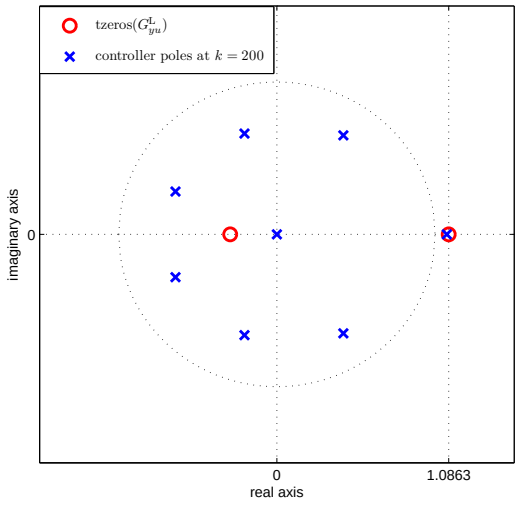

Figure 3.10: This figure illustrates the output-subspace zeros of the plant in Example 3.4.5 along with the poles of the adaptive controller at $k = 200$, whose time evolution is shown in Figure 3.5. The adaptive controller places a pole near the NMP output-subspace zero of G_{yu}, which is located at 1.0863. This unstable pole-zero cancellation is the cause of the unbounded control input shown in Figure 3.5. Note that the NMP output-subspace zero is not a transmission zero of G_{yu}, and thus the performance output shown in Figure 3.5 is also unbounded.

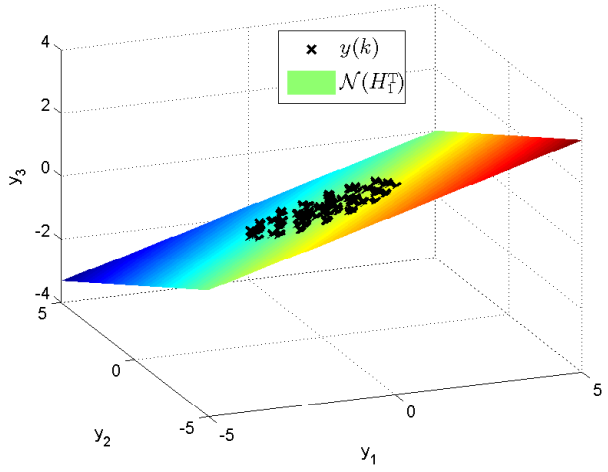

Figure 3.11: This figure illustrates the phase portrait for $k \in [800, 1000]$ of the output y for Example 3.4.4 shown in Figure 3.5. Since the output-subspace zeros of G_{yu} are minimum phase, the performance output y is bounded, and oscillates on the surface $\mathcal{N}(H_1^{\mathrm{T}})$. Since y is contained in $\mathcal{N}(H_1^{\mathrm{T}})$, the controller Θ converges.

We now investigate the output-subspace zeros of G_{yu}. Since $(A, B, H_1^{\mathrm{T}}C)$ is minimal, we use (3.87) to obtain $\mathrm{tzeros}(G_{yu}^{\mathrm{L}}) = \{-0.3362, 0.9544\}$. Note that the output-subspace zeros for Example (3.4.4) are minimum phase, and, as shown in Figure 3.4, both u and y are bounded. ■

3.9 Robustness Modification for NMP Subspace Zeros

As shown in Examples 3.4.2 and 3.4.5, the update laws of Section 3.3 may converge to a controller that cancels NMP subspace zeros, leading to an unbounded control input and possibly unbounded performance output. We now modify the update laws of Section 3.3 in order to prevent the controller from generating an unbounded control input. This is done by extending the retrospective cost function to include a performance-dependent control penalty term. This approach is related to the leakage modification for robust adaptive control [4, 50, 79]. We apply the modified RCAC update laws to Examples 3.4.2 and 3.4.5 to demonstrate this approach.

3.9.1 Instantaneous Update Law with η-Modification

For each $k \geq 1$, we define the *modified instantaneous cost function*

$$\tilde{J}_{\mathrm{ins}}(\hat{\Theta}, k) \triangleq \hat{y}^{\mathrm{T}}(\hat{\Theta}, k)\hat{y}(\hat{\Theta}, k) + \mu[\hat{\Theta} - \Theta(k-1)]^{\mathrm{T}}[\hat{\Theta} - \Theta(k-1)] + \eta(k)\hat{\Theta}^{\mathrm{T}}\Phi^{\mathrm{T}}(k-d-1)\Phi(k-d-1)\hat{\Theta}, \tag{3.98}$$

where

$$\eta(k) \triangleq \eta_1 + \eta_0\|y(k)\|^2, \tag{3.99}$$

$\eta_1 \geq 0$, and $\eta_0 \geq 0$. Substituting (3.17) into (3.98), we have

$$\tilde{J}_{\text{ins}}(\hat{\Theta}, k) = \hat{\Theta}^{\mathrm{T}} \tilde{\Gamma}_1(k) \hat{\Theta} + \Gamma_2^{\mathrm{T}}(k) \hat{\Theta} + \Gamma_3(k), \tag{3.100}$$

where

$$\begin{aligned} \tilde{\Gamma}_1(k) &\triangleq \Gamma_1(k) + \eta(k) \Phi^{\mathrm{T}}(k-d-1) \Phi(k-d-1) \\ &= \Phi^{\mathrm{T}}(k-d-1)[H_d^{\mathrm{T}} H_d + \eta(k) I_{l_u}] \Phi(k-d-1) + \mu I_{l_u n_{\mathrm{c}}(l_u+l_y)}. \end{aligned} \tag{3.101}$$

The terms $\Gamma_2(k)$ and $\Gamma_3(k)$ in (3.100) are identical to those in (3.21). Since $\tilde{\Gamma}_1(k)$ is positive definite, $\tilde{J}_{\text{ins}}(\hat{\Theta}, k)$ has the unique global minimizer

$$\Theta(k) = -\frac{1}{2} \tilde{\Gamma}_1(k) \Gamma_2(k), \tag{3.102}$$

which is the instantaneous RCAC update law with η-modification.

The modified cost function (3.98) includes an additional term with the weighting $\eta(k)$, which penalizes $\|\Phi(k-d-1)\hat{\Theta}\|$. This term tends to push the unique global minimizer of (3.98) toward $\mathcal{N}(\Phi(k-d-1))$, which drives Θ toward a controller that would have generated $u(k-d) = 0$ if it had been used in place of $\Theta(k-d)$. The modified cost (3.98) thus indirectly penalizes the control effort. Furthermore, note that if $\eta_0 > 0$, then $\eta(k)$ is an increasing function of $\|y\|$. Therefore, if y diverges, then $\eta(k)\hat{\Theta}^{\mathrm{T}}\Phi^{\mathrm{T}}(k-d-1)\Phi(k-d-1)\hat{\Theta}$ dominates (3.98), and the optimization problem is approximately $\min_{\hat{\Theta}} \|\Phi(k-d-1)\hat{\Theta}\|$. Choosing $\eta_0 > 0$ can thus prevent the situation in Example 3.4.5, where the adaptive controller destabilizes an open-loop plant and leads to an unbounded performance variable y.

3.9.2 Cumulative Update Law with η-Modification

For each $k \geq 1$, we define the *modified cumulative cost function*

$$\tilde{J}_{\mathrm{cum}}(\hat{\Theta}, k) \triangleq \sum_{i=1}^{k} \hat{y}^{\mathrm{T}}(\hat{\Theta}, i)\hat{y}(\hat{\Theta}, i) + \eta(i)\hat{\Theta}^{\mathrm{T}}\Phi^{\mathrm{T}}(i-d-1)\Phi(i-d-1)\hat{\Theta} + \hat{\Theta}^{\mathrm{T}}P_0^{-1}\hat{\Theta}, \tag{3.103}$$

where $\eta(i)$ is as in (3.99). Substituting (3.17) into (3.103), we have

$$J_{\mathrm{cum}}(\hat{\Theta}, k) = \hat{\Theta}^{\mathrm{T}}\tilde{\mathcal{C}}_1(k)\hat{\Theta} + \mathcal{C}_2^{\mathrm{T}}(k)\hat{\Theta} + \mathcal{C}_3(k), \tag{3.104}$$

where

$$\begin{aligned}\tilde{\mathcal{C}}_1(k) &\triangleq \mathcal{C}_1(k) + \sum_{i=1}^{k} \eta(i)\Phi^{\mathrm{T}}(i-d-1)\Phi(i-d-1) \\ &= \sum_{i=1}^{k} \Phi^{\mathrm{T}}(i-d-1)[H_d^{\mathrm{T}}H_d + \eta(i)I_{l_u}]\Phi(i-d-1) + P_0^{-1}.\end{aligned} \tag{3.105}$$

The terms $\mathcal{C}_2(k)$ and $\mathcal{C}_3(k)$ in (3.104) are identical to those in (3.30). Furthermore, defining $\tilde{\mathcal{C}}_1(0) \triangleq P_0^{-1}$, we can rewrite (3.105) in the recursive form

$$\tilde{\mathcal{C}}_1(k) = \tilde{\mathcal{C}}_1(k-1) + \Phi^{\mathrm{T}}(k-d-1)[H_d^{\mathrm{T}}H_d + \mu I_{l_u}]\Phi(k-d-1). \tag{3.106}$$

Since $\tilde{\mathcal{C}}_1(k)$ is positive definite, $\tilde{J}_{\mathrm{cum}}(\hat{\Theta}, k)$ has the unique global minimizer

$$\Theta(k) = -\frac{1}{2}\tilde{\mathcal{C}}_1^{-1}(k)\mathcal{C}_2(k), \tag{3.107}$$

which is the cumulative RCAC update law with η-modification. The rationale for the η-modification is the same as for the instantaneous cost stated at the end of Section 3.9.1.

3.9.3 Examples 3.4.2 and 3.4.5 Revisited with η-Modification

In this section, we apply the RCAC update laws with η-modification to Examples 3.4.2 and 3.4.5.

Example 3.9.1 (Example 3.4.2, cumulative RCAC with η-modification)**.** We consider the plant and unmatched harmonic disturbance in Example 3.4.2. We use the same tuning parameters $n_c = 6$, $P_0 = I$, let $\eta_1 = 0.1$, $\eta_0 = 0.05$, and apply the cumulative update law with η-modification. Figure 3.12 shows that η-modification does not alter the input subspace, that is, u is still contained in $\mathcal{R}(H_d^{\mathrm{T}})$. Although the plant has an unmodeled NMP input-subspace zero near -1.0555, the control penalty prevents the control input from growing without bound, as shown in Figure 3.12.

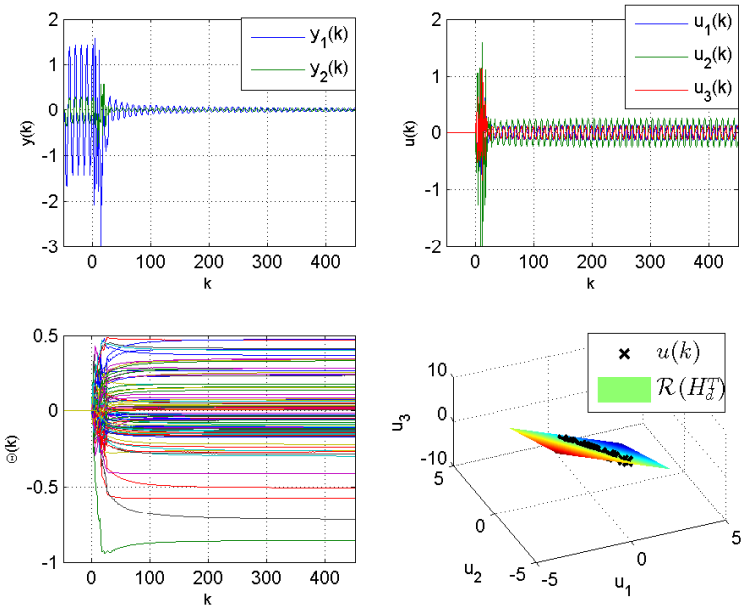

Figure 3.12: Example 3.4.2, RCAC with η-modification: We consider the same plant and disturbance as in Example 3.4.2, and apply the cumulative update law with η-modification. We use $n_c = 6$, $P_0 = I$, $\eta_1 = 0.1$, and $\eta_0 = 0.05$. Despite the unmodeled NMP input-subspace zero, Θ converges, y is driven toward zero, and u is bounded.

As shown in Section 3.9.2, the modified cost function (3.103) has the additional control weighting $\eta(k)$. The term $\eta_0\|y(k)\|^2$ in (3.99) vanishes as y approaches zero,

but the constant term η_1 does not vanish. Therefore, for $\eta_1 > 0$, we expect a tradeoff between control effort and closed-loop performance. To demonstrate this tradeoff, we keep n_c and P_0 the same, but increase η_1 to 1. Figure 3.13 shows the closed-loop response with $\eta_1 = 1$. Comparing Figure 3.13 to Figure 3.12, we observe that, as η_1 increases, the control effort is reduced during transients as well as in steady state, but with a degradation in the steady-state performance level. ■

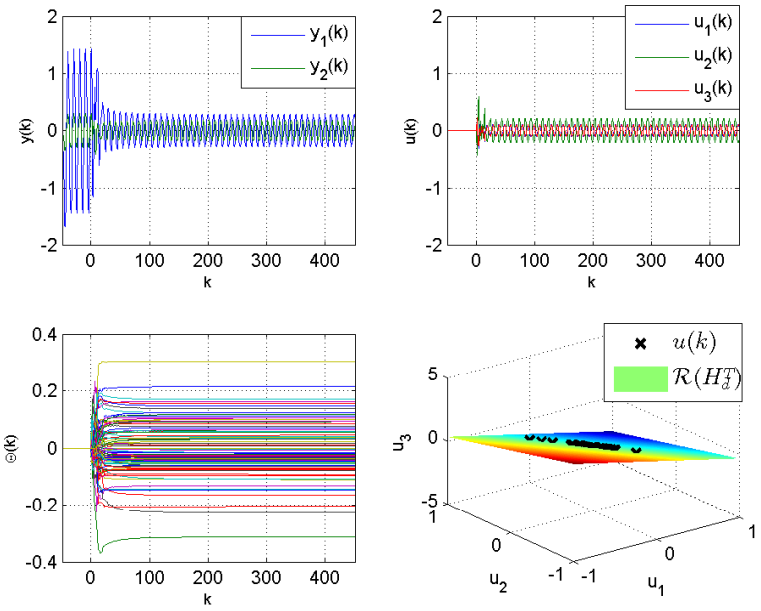

Figure 3.13: Example 3.4.2, RCAC with η-modification: We now increase the constant penalty term η_1 to 1. This leads to a reduction in the control effort as well as a degradation in the steady-state performance level. Thus, η-modification introduces a tradeoff between control effort and steady-state performance.

Example 3.9.2 (Example 3.4.5, instantaneous RCAC with η-modification)**.** We consider the plant and unmatched disturbance in Example 3.4.5. We use the same tuning parameters $n_c = 7$, $\mu = 20$, let $\eta_1 = 0$, $\eta_0 = 0.01$, and apply the instantaneous update law with η-modification. Although the plant has an unmodeled NMP output-subspace zero near 1.0863, the control penalty prevents the control input u and the performance output y from growing without bound, as shown in Figure 3.14. ■

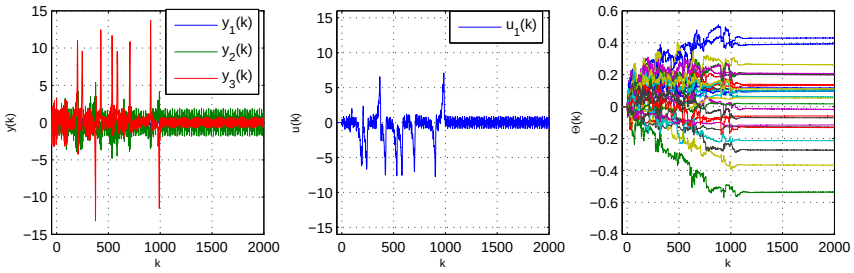

Figure 3.14: Example 3.4.5, RCAC with η-modification: We consider the same plant and disturbance as in Example 3.4.5, and apply the instantaneous update law with η-modification. We use $n_c = 7$, $\mu = 20$, $\eta_1 = 0$, and $\eta_0 = 0.01$. Despite the unmodeled NMP output-subspace zero, Θ converges, and u and y are bounded.

3.10 Numerical Example: Boeing 747 Longitudinal Dynamics

Consider the longitudinal dynamics of a Boeing 747 aircraft, linearized about steady flight at 40000 ft and 774 ft/sec. The control inputs to the longitudinal dynamics are taken to be elevator deflection and thrust. The linearized equations of motion are thus given by

$$\begin{bmatrix} \dot{u} \\ \dot{w} \\ \dot{q} \\ \dot{\theta} \end{bmatrix} = \begin{bmatrix} -0.003 & 0.039 & 0 & -0.322 \\ -0.065 & -0.319 & 7.74 & 0 \\ 0.02 & -0.101 & -0.429 & 0 \\ 0 & 0 & 1 & 0 \end{bmatrix} \begin{bmatrix} u \\ w \\ q \\ \theta \end{bmatrix} + \begin{bmatrix} 0.01 & 1 \\ -0.18 & -0.04 \\ -1.16 & 0.598 \\ 0 & 0 \end{bmatrix} \begin{bmatrix} \delta_e \\ \delta_T \end{bmatrix}, \tag{3.108}$$

where the state variables u, w, q and θ are forward speed, vertical speed, pitch rate, and pitch perturbations respectively. Furthermore, the control input variables δ_e and δ_T represent elevator deflection (deg) and thrust (ft/sec^2) perturbations respectively. The control objective is to have the pitch perturbation follow the output θ_m of the

reference model

$$G_{\rm m}(s) = \frac{0.0131}{s^2 + 0.16s + 0.0131}, \tag{3.109}$$

whose input is the exogenous model reference command r.

We discretize (3.108) using a zero-order hold and a sampler with sampling period $h = 0.1$ sec/sample. We assume that the samples of θ and r are measured. We thus have

$$y(k) = \begin{bmatrix} 0 & 0 & 0 & 1 \\ 0 & 0 & 0 & 0 \end{bmatrix} \begin{bmatrix} u(k) \\ w(k) \\ q(k) \\ \theta(k) \end{bmatrix} + \begin{bmatrix} 0 \\ 1 \end{bmatrix} r(k), \tag{3.110}$$

$$z(k) = \begin{bmatrix} 0 & 0 & 0 & 1 \end{bmatrix} \begin{bmatrix} u(k) \\ w(k) \\ q(k) \\ \theta(k) \end{bmatrix} - \theta_{\rm m}(k). \tag{3.111}$$

Therefore, we consider the 1×2 discretized plant G_{zu} with poles $\{0.9999\pm\jmath0.0067, 0.9594\pm\jmath0.0848\}$, and input-subspace zeros $\{-0.9857, 0.9714, 0.9972\}$. Throughout this example, the only modeling information used in controller synthesis is the first nonzero Markov parameter $H_1 = \begin{bmatrix} -0.0057 & 0.0029 \end{bmatrix}$ of G_{zu}.

We take the model reference command to be a 1 deg step command in pitch angle, let $n_{\rm c} = 5$, and apply the cumulative update law (3.36)–(3.38) with $P_0 = 10^{10}I$, $\eta_0 = 0$, $\eta_1 = 0$. The closed-loop response is shown in Figure 3.15. The command-following error reduces to zero within 10 seconds, but elevator deflection and thrust inputs oscillate during transients. In fact, elevator deflection has the peak magnitude

71 deg, and thrust has the peak magnitude 36 ft/sec^2. Because of saturation limits, these peak transient values may be unacceptable in practice. The large transients in control input are caused by the cancellation of the input-subspace zero -0.9857, as shown in Figure 3.16.

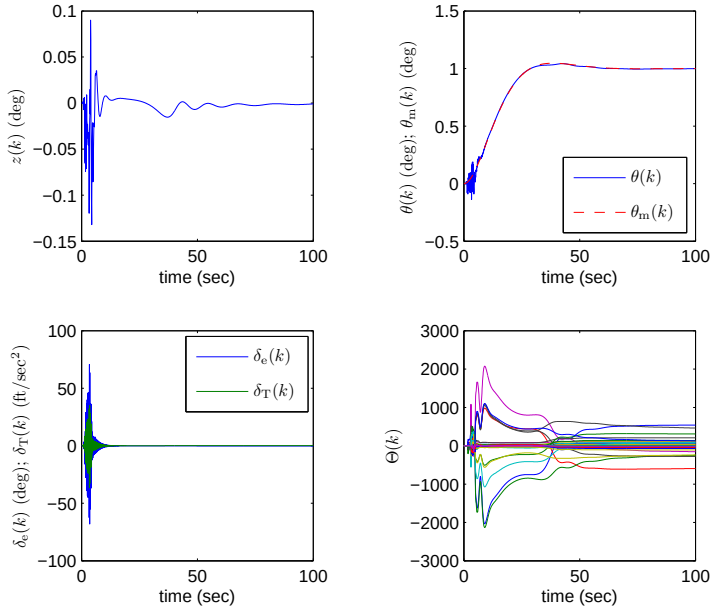

Figure 3.15: Boeing 747 longitudinal dynamics: We apply RCAC without η-modification. The pitch angle follows the output of the reference model, but elevator deflection and thrust oscillate during transients with peak magnitudes 71 deg and 36 ft/sec^2, respectively.

We now consider the same step reference command, keep $n_{\rm c}$ and P_0 the same, but introduce η-modification with $\eta_0 = 2000$, $\eta_1 = 1$. The closed-loop response is shown in Figure 3.17. The command-following error $z(k)$ does not exceed 0.015 deg throughout the simulation. Furthermore, peak elevator deflection magnitude is less than 0.9 deg, and peak thrust magnitude is less than 0.5 ft/sec^2.

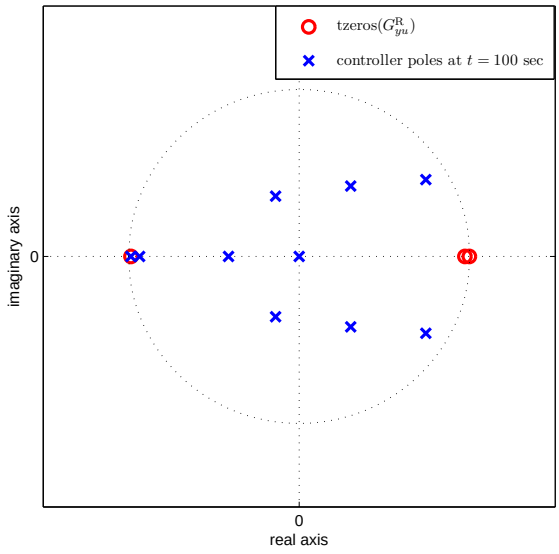

Figure 3.16: This figure illustrates the input-subspace zeros of Boeing 747 longitudinal dynamics along with the poles of the adaptive controller at $t = 100$ sec. The adaptive controller places a pole near the input-subspace zero -0.9857. This pole-zero cancellation near the unit circle causes large transient peaks in elevator deflection and thrust inputs, as illustrated in Figure 3.15.

3.11 Conclusion

In this chapter, we provided a detailed analysis of RCAC for nonsquare plants. We have shown that for nonsquare plants that the fact that the plant is minimum phase does not guarantee closed-loop stability and signal boundedness properties, unlike the square case. Specifically, we have shown that, due to the nature of the RCAC update law, retrospective cost adaptive control involves two implicit squaring operations; one performed by pre-compensating the plant, the other performed by post-compensating the plant. In the wide case, pre-compensation leads to squaring-down, which incorporates additional zeros due to squaring, which we call input-subspace zeros. Similarly, in the tall case, post-compensation changes the zero structure and incorporates additional zeros, which we call output-subspace zeros. We have shown that if the nonsquare plant has NMP subspace zeros, then RCAC attempts to cancel these zeros,

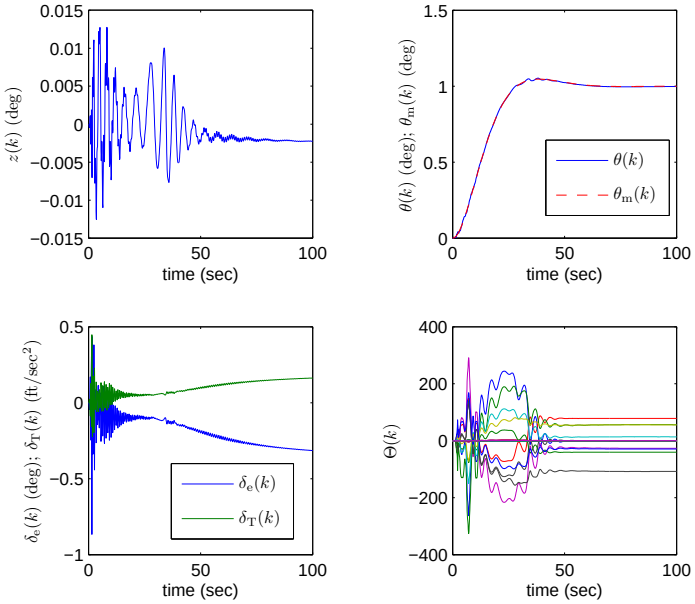

Figure 3.17: Boeing 747 longitudinal dynamics: We apply RCAC with η-modification. The pitch angle follows the output of the reference model, peak elevator deflection magnitude is less than 0.9 deg, and peak thrust magnitude is less than 0.5 ft/sec^2. The command-following error $z(k)$ is less than 0.015 deg throughout the simulation.

and leads to unbounded control input in the wide case, and unbounded control input and performance output in the tall case. Finally, in light of these findings, we extend the retrospective cost function to include a performance-dependent control penalty in order to prevent the controller from generating an unbounded control input.

3.12 Appendix: Proofs

3.12.1 Proof of Theorem 3.6.1

We show that $\{\Theta(k)\}_{k=0}^{\infty}$ is a Cauchy sequence. Let N, m_1, m_2 be positive integers such that $m_2 > m_1 > N$. Then, it follows from Lemma 3.6.1 that

$$\begin{aligned}\|\Theta(m_1) - \Theta(m_2)\| &= \left\|\Theta(0) + \sum_{i=1}^{m_1}\Delta\Theta(i) - \sum_{i=1}^{m_2}\Delta\Theta(i) - \Theta(0)\right\| = \left\|\sum_{i=m_1+1}^{m_2}\Delta\Theta(i)\right\| \\ &\leq \sum_{i=m_1+1}^{m_2}\|\Delta\Theta(i)\| \leq \sum_{i=m_1+1}^{m_2}\sigma_{\max}(\mathcal{B}(i))\left\|H_1^{\mathrm{T}}y(i)\right\|.\end{aligned}$$

Since $\mathcal{B}$ is bounded, it follows that $\bar{\sigma}(\mathcal{B}) \stackrel{\triangle}{=} \sup_{k\geq 1}\sigma_{\max}(\mathcal{B}(k)) \in [0,\infty)$. Note that, if $\bar{\sigma}(\mathcal{B}) = 0$, then, for all $k \geq 1$, $\Delta\Theta(k) = 0$, and thus $\lim_{k\to\infty}\Theta(k) = \Theta(0)$. Now, assume that $\bar{\sigma}(\mathcal{B}) > 0$. Then,

$$\begin{aligned}\|\Theta(m_1) - \Theta(m_2)\| &\leq \bar{\sigma}(\mathcal{B})\sum_{i=m_1+1}^{m_2}\left\|H_1^{\mathrm{T}}y(i)\right\| \leq \bar{\sigma}(\mathcal{B})\sum_{i=m_1+1}^{m_2}\alpha\gamma^i \leq \bar{\sigma}(\mathcal{B})\sum_{i=N}^{\infty}\alpha\gamma^i \\ &= \bar{\sigma}(\mathcal{B})\gamma^N\sum_{i=0}^{\infty}\alpha\gamma^i = \bar{\sigma}(\mathcal{B})\gamma^N\frac{\alpha}{1-\gamma}. \qquad (3.112)\end{aligned}$$

Hence, since $0 < \gamma < 1$, it follows from (3.112) that, for all $\varepsilon > 0$, there exists N such that, for all $m_1, m_2 > N$, $\|\Theta(m_1) - \Theta(m_2)\| < \varepsilon$. Therefore, $\{\Theta(k)\}_{k=0}^{\infty}$ is a Cauchy sequence and thus Θ converges. □

3.12.2 Proof of Proposition 3.6.4

For all $k \geq 0$, it follows from (3.52) that

$$\|\Delta\Theta(k)\| = \|\mathcal{A}(k)\cdots\mathcal{A}(1)\Delta\Theta(0)\| \leq \sigma_{\max}(\mathcal{A}(k))\cdots\sigma_{\max}(\mathcal{A}(1))\|\Delta\Theta(0)\|. \quad (3.113)$$

Since Φ is bounded, it follows that $\sigma_{\max}(H_2\Phi)$ is bounded, and thus, it follows from (3.54) that $\bar{\sigma}(\mathcal{A}) < 1$. Therefore, it follows from (3.113) that

$$\|\Delta\Theta(k)\| \leq \|\Delta\Theta(0)\|\gamma^k, \tag{3.114}$$

where $\gamma \stackrel{\triangle}{=} \bar{\sigma}(\mathcal{A}) < 1$. Therefore, the zero solution of (3.52) is globally exponentially stable.

3.12.3 Proof of Proposition 3.6.5

For all $k \geq 0$, define

$$V(\Delta\Theta(k)) \stackrel{\triangle}{=} \|\Delta\Theta(k)\|^2. \tag{3.115}$$

It follows from (3.52) that

$$V(\Delta\Theta(k+m)) = \Delta\Theta^{\mathrm{T}}(k)Q_m(k+1)Q_m^{\mathrm{T}}(k+1)\Delta\Theta(k). \tag{3.116}$$

Subtracting (3.115) from (3.116) yields

$$V(\Delta\Theta(k+m)) - V(\Delta\Theta(k)) = \Delta\Theta^{\mathrm{T}}(k)[Q_m(k+1)Q_m^{\mathrm{T}}(k+1) - I]\Delta\Theta(k).$$

Now, from (3.56), we have

$$V(\Delta\Theta(k+m)) - V(\Delta\Theta(k)) \leq [\bar{\sigma}^2(Q_m) - 1]\Delta\Theta^{\mathrm{T}}(k)\Delta\Theta(k),$$

and thus, for all $k \geq 0$,

$$V(\Delta\Theta(k+m)) \leq \bar{\sigma}^2(Q_m)V(\Delta\Theta(k)).$$

Hence, it follows that there exists a nonnegative integer N such that, for all $k \geq 0$,

$$\|\Delta\Theta(k+mN)\| \leq \bar{\sigma}^N(Q_m)\|\Delta\Theta(k)\|. \tag{3.117}$$

Rewriting $k = mN + r$, where $0 \leq r \leq m-1$, it follows from (3.117) that, for all $k \geq 0$,

$$\begin{aligned}\|\Delta\Theta(k)\| = \|\Delta\Theta(mN+r)\| &\leq \bar{\sigma}^N(Q_m)\|\Delta\Theta(r)\| \leq \bar{\sigma}^N(Q_m) \max_{0\leq i\leq m-1} \|\Delta\Theta(i)\| \\ &\leq \bar{\sigma}^{k/m}(Q_m) \max_{0\leq i\leq m-1} \|\Delta\Theta(i)\| = (\bar{\sigma}^{1/m})^k(Q_m) \max_{0\leq i\leq m-1} \|\Delta\Theta(i)\|.\end{aligned}$$

Since $\bar{\sigma}(\mathcal{A}) \leq 1$, it follows from (3.52) that $\max_{0\leq i\leq m-1} \|\Delta\Theta(i)\| = \|\Delta\Theta(0)\|$. Therefore, for all $k \geq 0$,

$$\|\Delta\Theta(k)\| \leq \|\Delta\Theta(0)\|\gamma^k,$$

where $\gamma \stackrel{\triangle}{=} \bar{\sigma}^{1/m}(Q_m)$. Since $\bar{\sigma}(Q_m) \in (0,1)$ it follows that $\gamma < 1$, which implies that the zero solution of (3.52) is globally exponentially stable. □

3.12.4 Proof of Proposition 3.6.7

Let $r \stackrel{\triangle}{=} l_u n_c(l_u + l_y)$, and, without loss of generality, assume that $k_1 < k_2$. Since $\bar{\sigma}(\mathcal{A}) \in [0,1]$, it follows from (3.55) that

$$\begin{aligned}\sigma_{\max}(Q_m(k)) &= \sigma_{\max}(\mathcal{A}(k)\cdots\mathcal{A}(k_1)\cdots\mathcal{A}(k_2)\cdots\mathcal{A}(k+m-1)) \\ &\leq \sigma_{\max}(\mathcal{A}(k_1)\cdots\mathcal{A}(k_2)).\end{aligned} \tag{3.118}$$

Since $\Omega_0 \leq \Omega(\phi(k_1-3), \phi(k_2-3) \leq \pi - \Omega_0$, it follows from Lemma 3.6.6 that there exists $l \in \{k_1, \ldots, k_2 - 1\}$ such that

$$\tilde{\Omega}_0 \leq \Omega(\phi(l-3), \phi(l-2)) \leq \pi - \tilde{\Omega}_0, \tag{3.119}$$

where

$$\tilde{\Omega}_0 \triangleq \frac{1}{k_2 - k_1}\Omega_0.$$

Since $k_1, k_2 \in \{k, \ldots, k+m-1\}$, it follows that $\tilde{\Omega}_0 \geq \frac{\Omega_0}{m-1} > 0$. Furthermore, since $\Omega_0 \leq \pi/2$ and $m \geq 2$, it follows that $\tilde{\Omega}_0 \leq \pi/2$. Therefore, $\tilde{\Omega}_0 \in [\frac{\Omega_0}{m-1}, \pi/2]$.

Now, it follows from (3.118) that

$$\begin{aligned}\sigma_{\max}(Q_m(k)) &\leq \sigma_{\max}(\mathcal{A}(k_1)\cdots\mathcal{A}(l)\mathcal{A}(l+1)\cdots\mathcal{A}(k_2)) \\ &\leq \sigma_{\max}(\mathcal{A}(l)\mathcal{A}(l+1)),\end{aligned}$$

and thus,

$$\sigma_{\max}(Q_m(k)) = \max_{v\in\mathbb{R}^r\setminus\{0\}} \frac{\|Q_m(k)v\|}{\|v\|} \leq \max_{v\in\mathbb{R}^r\setminus\{0\}} \frac{\|\mathcal{A}(l)\mathcal{A}(l+1)v\|}{\|v\|}. \tag{3.120}$$

Next, it follows from [5, Fact 3.9.5] that there exists an orthogonal matrix $R \in \mathbb{R}^{n_{\mathrm{c}}(l_u+l_y)\times n_{\mathrm{c}}(l_u+l_y)}$ such that

$$\phi(l-3) = \alpha R\phi(l-2), \tag{3.121}$$

where $\alpha \stackrel{\triangle}{=} \frac{\|\phi(l-3)\|}{\|\phi(l-2)\|}$. It follows from (3.14), (3.50), and (3.121) that

$$\begin{aligned}
\mathcal{A}(l) &= (I_{l_u} \otimes \alpha R\phi(l-2))H_2^{\mathrm{T}}[\mu I + H_2(I_{l_u} \otimes \alpha\phi^{\mathrm{T}}(l-2)R^{\mathrm{T}}) \\
&\quad \cdot (I_{l_u} \otimes \alpha R\phi(l-2))]^{-1}H_2(I_{l_u} \otimes \alpha\phi^{\mathrm{T}}(l-2)R^{\mathrm{T}}) \\
&= \alpha^2(I_{l_u} \otimes R)(I_{l_u} \otimes \phi(l-2))H_2^{\mathrm{T}}[\mu I + \alpha^2 H_2(I_{l_u} \otimes \phi^{\mathrm{T}}(l-2))(I_{l_u} \otimes R^{\mathrm{T}}) \\
&\quad \cdot (I_{l_u} \otimes R)(I_{l_u} \otimes \phi(l-2))]^{-1}H_2(I_{l_u} \otimes \phi^{\mathrm{T}}(l-2))(I_{l_u} \otimes R^{\mathrm{T}}) \\
&= (I_{l_u} \otimes R)\Phi^{\mathrm{T}}(l-2)H_2^{\mathrm{T}}[\frac{\mu}{\alpha^2}I + H_2\Phi(l-2)\Phi^{\mathrm{T}}(l-2)H_2^{\mathrm{T}}]^{-1} \qquad (3.122) \\
&\quad \cdot H_2\Phi(l-2)(I_{l_u} \otimes R^{\mathrm{T}}) \\
&= (I_{l_u} \otimes R)\tilde{\mathcal{A}}(l+1)(I_{l_u} \otimes R^{\mathrm{T}}), \qquad (3.123)
\end{aligned}$$

where $\tilde{\mathcal{A}}(l+1)$ is given by (3.50) with μ replaced by μ/α^2. Note that $\mathcal{R}(\tilde{\mathcal{A}}(l+1)) = \mathcal{R}(\mathcal{A}(l+1))$, $\mathcal{N}(\tilde{\mathcal{A}}(l+1)) = \mathcal{N}(\mathcal{A}(l+1))$, and $\mathcal{N}^{\perp}(\tilde{\mathcal{A}}(l+1)) = \mathcal{R}(\tilde{\mathcal{A}}(l+1))$. In particular, since G_{yu} is tall or square, H_2^{T} is right invertible. It thus follows from (3.50) that

$$\begin{aligned}
\mathcal{R}(\mathcal{A}(l+1)) &= \mathcal{R}(\tilde{\mathcal{A}}(l+1)) = \mathcal{R}(\Phi^{\mathrm{T}}(l-2)) \\
&= \mathrm{span}\left\{ \begin{bmatrix} \phi(l-2) \\ 0 \\ \vdots \\ 0 \end{bmatrix}, \ldots, \begin{bmatrix} 0 \\ \vdots \\ 0 \\ \phi(l-2) \end{bmatrix} \right\},
\end{aligned}$$

and thus, for all $v \in \mathbb{R}^r$,

$$\mathcal{A}(l+1)v = \sum_{i=1}^{l_u} \alpha_i \begin{bmatrix} 0_{(i-1)n_{\mathrm{C}}(l_u+l_y)\times 1} \\ \phi(l-2) \\ 0_{(l_u-i)n_{\mathrm{C}}(l_u+l_y)\times 1} \end{bmatrix}. \qquad (3.124)$$

Therefore, it follows from (3.123) and (3.124) that, for all nonzero $v \in \mathbb{R}^r$,

$$\begin{aligned}
\frac{\|\mathcal{A}(l)\mathcal{A}(l+1)v\|_2}{\|v\|} &= \frac{1}{\|v\|}\left\|(I_{l_u}\otimes R)\tilde{\mathcal{A}}(l+1)\sum_{i=1}^{l_u}\alpha_i\begin{bmatrix}0_{(i-1)n_{\mathrm{c}}(l_u+l_y)\times 1}\\ R^{\mathrm{T}}\phi(l-2)\\ 0_{(l_u-i)n_{\mathrm{c}}(l_u+l_y)\times 1}\end{bmatrix}\right\| \\
&= \frac{1}{\|v\|}\left\|\tilde{\mathcal{A}}(l+1)\sum_{i=1}^{l_u}\alpha_i\begin{bmatrix}0_{(i-1)n_{\mathrm{c}}(l_u+l_y)\times 1}\\ R^{\mathrm{T}}\phi(l-2)\\ 0_{(l_u-i)n_{\mathrm{c}}(l_u+l_y)\times 1}\end{bmatrix}\right\| \\
&= \frac{1}{\|v\|}\left\|\tilde{\mathcal{A}}(l+1)\left(\sum_{i=1}^{l_u}\cos(\Omega(\phi(l-3),\phi(l-2)))\alpha_i\begin{bmatrix}0_{(i-1)n_{\mathrm{c}}(l_u+l_y)\times 1}\\ \phi(l-2)\\ 0_{(l_u-i)n_{\mathrm{c}}(l_u+l_y)\times 1}\end{bmatrix}\right.\right. \\
&\quad \left.\left. + \sum_{i=1}^{l_u}\sin(\Omega(\phi(l-3),\phi(l-2)))\alpha_i\begin{bmatrix}0_{(i-1)n_{\mathrm{c}}(l_u+l_y)\times 1}\\ \phi_{\mathrm{perp}}(l-2)\\ 0_{(l_u-i)n_{\mathrm{c}}(l_u+l_y)\times 1}\end{bmatrix}\right)\right\|, \quad (3.125)
\end{aligned}$$

where $\phi_{\mathrm{perp}}(l-2) \in \mathbb{R}^{n_{\mathrm{c}}(l_u+l_y)}$ is orthogonal to $\phi(l-2)$. Since $\phi_{\mathrm{perp}}(l-2)$ is orthogonal to $\phi(l-2)$, it follows that

$$\sum_{i=1}^{l_u}\sin(\Omega(\phi(l-3),\phi(l-2)))\alpha_i\begin{bmatrix}0_{(i-1)n_{\mathrm{c}}(l_u+l_y)\times 1}\\ \phi_{\mathrm{perp}}(l-2)\\ 0_{(l_u-i)n_{\mathrm{c}}(l_u+l_y)\times 1}\end{bmatrix} \in \mathcal{N}(\tilde{\mathcal{A}}(l+1)), \quad (3.126)$$

and thus, it follows from (3.119), (3.124), (3.125), and (3.126) that

$$\begin{aligned}
\frac{\|\mathcal{A}(l)\mathcal{A}(l+1)v\|}{\|v\|} &= \frac{1}{\|v\|}\left\|\cos\Omega(\phi(l-3),\phi(l-2))\tilde{\mathcal{A}}(l+1)\mathcal{A}(l+1)v\right\| \\
&\le \frac{|\cos\Omega(\phi(l-3),\phi(l-2))|}{\|v\|}\left\|\tilde{\mathcal{A}}(l+1)\mathcal{A}(l+1)v\right\| \\
&\le |\cos\Omega(\phi(l-3),\phi(l-2))|\,\sigma_{\max}(\tilde{\mathcal{A}}(l+1))\sigma_{\max}(\mathcal{A}(l+1)) \\
&\le \cos\tilde{\Omega}_0.
\end{aligned}$$

Since $\tilde{\Omega}_0 \in [\frac{\Omega_0}{m-1}, \pi/2]$, it follows from (3.120) that $\sigma_{\max}(Q_m(k)) \le \cos\frac{\Omega_0}{m-1}$, and it thus follows that $\bar{\sigma}(Q_m) \le \cos\frac{\Omega_0}{m-1} < 1$. □

3.12.5 Proof of Theorem 3.6.2

Let N, k_1, k_2 be positive integers such that $k_2 > k_1 > N$. Then,

$$\|\Theta(k_1) - \Theta(k_2)\| = \left\|\Theta(0) + \sum_{i=1}^{k_1} \Delta\Theta(i) - \Theta(0) - \sum_{i=1}^{k_2} \Delta\Theta(i)\right\| = \left\|\sum_{i=k_1+1}^{k_2} \Delta\Theta(i)\right\|. \tag{3.127}$$

For all $k \geq 2$, it follows from Lemma 3.6.2 that

$$\Delta\Theta(k) = \sum_{i=1}^{k-1} \mathcal{A}(k)\cdots\mathcal{A}(i+1)\mathcal{B}(i)H_d^{\mathrm{T}}y(i) + \mathcal{B}(k)H_d^{\mathrm{T}}y(k). \tag{3.128}$$

Substituting (3.128) into (3.127) and using (3.112) yields

$$\begin{aligned}
\|\Theta(k_1) - \Theta(k_2)\| &= \left\|\sum_{i=k_1+1}^{k_2}\left(\sum_{j=1}^{i-1} \mathcal{A}(i)\cdots\mathcal{A}(j+1)\mathcal{B}(j)H_d^{\mathrm{T}}y(j) + \mathcal{B}(i)H_d^{\mathrm{T}}y(i)\right)\right\| \\
&= \left\|\sum_{i=k_1+1}^{k_2}\sum_{j=1}^{i-1} \mathcal{A}(i)\cdots\mathcal{A}(j+1)\mathcal{B}(j)H_d^{\mathrm{T}}y(j) + \sum_{i=k_1+1}^{k_2} \mathcal{B}(i)H_d^{\mathrm{T}}y(i)\right\| \\
&\leq \left\|\sum_{i=k_1+1}^{k_2}\sum_{j=1}^{i-1} \mathcal{A}(i)\cdots\mathcal{A}(j+1)\mathcal{B}(j)H_d^{\mathrm{T}}y(j)\right\| + \left\|\sum_{i=k_1+1}^{k_2} \mathcal{B}(i)H_d^{\mathrm{T}}y(i)\right\| \\
&\leq \alpha \sum_{i=k_1+1}^{k_2}\sum_{j=1}^{i-1} \|\mathcal{A}(i)\cdots\mathcal{A}(j+1)\mathcal{B}(j)\|\,\gamma^j + \frac{\alpha\bar{\sigma}(\mathcal{B})}{1-\gamma}\gamma^N,
\end{aligned} \tag{3.129}$$

where the second term in (3.129) can be obtained by the same procedure that is used to obtain (3.112). Note that, since G_{yu} is tall, $H_2^{\mathrm{T}}H_2$ is positive definite. Therefore, it follows from (3.51) that $\mathcal{B}$ is bounded and thus $\bar{\sigma}(\mathcal{B})$ is finite.

Assume that Φ is bounded so that $\bar{\sigma}(\mathcal{A}) < 1$. Defining $\tilde{\gamma} \stackrel{\triangle}{=} \gamma/\bar{\sigma}(\mathcal{A})$ and applying

Cauchy-Schwarz inequality to (3.129) yields

$$\begin{aligned}\|\Theta(k_1) - \Theta(k_2)\| &\leq \alpha \sum_{i=k_1}^{k_2} \sum_{j=1}^{i-1} \bar{\sigma}^{i-j}(\mathcal{A})\bar{\sigma}(\mathcal{B})\gamma^j + \frac{\alpha\bar{\sigma}(\mathcal{B})}{1-\gamma}\gamma^N \\ &\leq \alpha \sum_{i=N}^{\infty} \sum_{j=1}^{i-1} \bar{\sigma}^{i-j}(\mathcal{A})\bar{\sigma}(\mathcal{B})\gamma^j + \frac{\alpha\bar{\sigma}(\mathcal{B})}{1-\gamma}\gamma^N \\ &= \alpha\bar{\sigma}(\mathcal{B}) \sum_{i=N}^{\infty} \bar{\sigma}^{i}(\mathcal{A}) \sum_{j=1}^{i-1} \tilde{\gamma}^j + \frac{\alpha\bar{\sigma}(\mathcal{B})}{1-\gamma}\gamma^N. \end{aligned} \tag{3.130}$$

First, consider (3.130) with $\tilde{\gamma} = 1$. In this case, we have

$$\begin{aligned}\|\Theta(k_1) - \Theta(k_2)\| &\leq \alpha\bar{\sigma}(\mathcal{B}) \sum_{i=N}^{\infty} (i-1)\bar{\sigma}^{i}(\mathcal{A}) + \frac{\alpha\bar{\sigma}(\mathcal{B})}{1-\gamma}\gamma^N \\ &\leq \alpha\bar{\sigma}(\mathcal{B}) \sum_{i=N}^{\infty} i\bar{\sigma}^{i}(\mathcal{A}) + \frac{\alpha\bar{\sigma}(\mathcal{B})}{1-\gamma}\gamma^N \\ &= \alpha\bar{\sigma}(\mathcal{B})\bar{\sigma}^N(\mathcal{A}) \sum_{i=0}^{\infty} (i+N)\bar{\sigma}^{i}(\mathcal{A}) + \frac{\alpha\bar{\sigma}(\mathcal{B})}{1-\gamma}\gamma^N \\ &= \alpha\bar{\sigma}(\mathcal{B})\bar{\sigma}^N(\mathcal{A}) \left[\frac{\bar{\sigma}(\mathcal{A})}{(1-\bar{\sigma}(\mathcal{A}))^2} + \frac{N}{1-\bar{\sigma}(\mathcal{A})}\right] + \frac{\alpha\bar{\sigma}(\mathcal{B})}{1-\gamma}\gamma^N. \end{aligned} \tag{3.131}$$

Since $\bar{\sigma}(\mathcal{A}) \in (0,1)$ and $\gamma \in (0,1)$, it follows from (3.131) that, in the case $\tilde{\gamma} = 1$, for all $\varepsilon > 0$, there exists N such that, for each $k_1, k_2 > N$, $\|\Theta(k_1) - \Theta(k_2)\| < \varepsilon$. Therefore, in the case $\tilde{\gamma} = 1$, $\{\Theta(k)\}_{k=0}^{\infty}$ is Cauchy, and thus Θ converges. Next, consider (3.130) with $\tilde{\gamma} \neq 1$. In this case, we have

$$\begin{aligned}\|\Theta(k_1) - \Theta(k_2)\| &\leq \frac{\alpha\bar{\sigma}(\mathcal{B})}{1-\tilde{\gamma}} \sum_{i=N}^{\infty} \bar{\sigma}^{i}(\mathcal{A})(\tilde{\gamma} - \tilde{\gamma}^i) + \frac{\alpha\bar{\sigma}(\mathcal{B})}{1-\gamma}\gamma^N \\ &= \frac{\alpha\bar{\sigma}(\mathcal{B})}{1-\tilde{\gamma}} \left(\sum_{i=N}^{\infty} \tilde{\gamma}\bar{\sigma}^{i}(\mathcal{A}) - \sum_{i=N}^{\infty} \gamma^i\right) + \frac{\alpha\bar{\sigma}(\mathcal{B})}{1-\gamma}\gamma^N \\ &= \frac{\alpha\bar{\sigma}(\mathcal{B})}{1-\tilde{\gamma}} \left(\frac{\tilde{\gamma}}{1-\bar{\sigma}(\mathcal{A})}\bar{\sigma}^N(\mathcal{A}) - \frac{1}{1-\gamma}\gamma^N\right). \end{aligned} \tag{3.132}$$

Since $\bar{\sigma}(\mathcal{A}) < 1$ and $\gamma < 1$, it follows from (3.132) that, in the case $\tilde{\gamma} \neq 1$, for all

$\varepsilon > 0$, there exists N such that $\|\Theta(k_1) - \Theta(k_2)\|_2 < \varepsilon$, and thus Θ converges. Thus we have verified (i).

Now, assume that there exists $m \geq 2$ such that (3.56) is satisfied. Define $\kappa \triangleq \bar{\sigma}(Q_m)$ and $\tilde{\kappa} \triangleq \kappa^{1/m} \in (0,1)$. For $N > m$, it follows from (3.129) that

$$\begin{aligned}
&\|\Theta(k_1) - \Theta(k_2)\| \\
&\leq \alpha \sum_{i=k_1+1}^{k_2} \sum_{j=i-m+1}^{i-1} \|\mathcal{A}(i)\cdots\mathcal{A}(j+1)\mathcal{B}(j)\|\,\gamma^j + \sum_{j=1}^{i-m} \|\mathcal{A}(i)\cdots\mathcal{A}(j+1)\mathcal{B}(j)\|\,\gamma^j + \\
&\quad + \frac{\alpha\bar{\sigma}(\mathcal{B})}{1-\gamma}\gamma^N \\
&\leq \alpha \sum_{i=N}^{\infty} \sum_{j=i-m+1}^{i-1} \|\mathcal{A}(i)\cdots\mathcal{A}(j+1)\mathcal{B}(j)\|\,\gamma^j + \sum_{j=1}^{i-m} \|\mathcal{A}(i)\cdots\mathcal{A}(j+1)\mathcal{B}(j)\|\,\gamma^j \\
&\quad + \frac{\alpha\bar{\sigma}(\mathcal{B})}{1-\gamma}\gamma^N \\
&\leq \alpha \sum_{i=N}^{\infty} \sum_{j=i-m+1}^{i-1} \bar{\sigma}(\mathcal{B})\gamma^j + \sum_{j=1}^{i-m} \kappa^{\frac{i-j}{m}-1}\bar{\sigma}(\mathcal{B})\gamma^j + \frac{\alpha\bar{\sigma}(\mathcal{B})}{1-\gamma}\gamma^N \\
&= \alpha\bar{\sigma}(\mathcal{B}) \sum_{i=N}^{\infty} \gamma^{i-m+1} \sum_{j=0}^{m-1} \gamma^j + \gamma\kappa^{-1}\tilde{\kappa}^{-1} \sum_{j=0}^{i-m-1} \left(\frac{\gamma}{\tilde{\kappa}}\right)^j + \frac{\alpha\bar{\sigma}(\mathcal{B})}{1-\gamma}\gamma^N \\
&= \alpha\bar{\sigma}(\mathcal{B}) \sum_{i=N}^{\infty} \frac{1-\gamma^{m+1}}{1-\gamma}\gamma^{1-m}\gamma^i + \alpha\bar{\sigma}(\mathcal{B})\gamma\kappa^{-1}\tilde{\kappa}^{-1} \sum_{i=N}^{\infty} \tilde{\kappa}^i \frac{1-\left(\frac{\gamma}{\tilde{\kappa}}\right)^{i-m}}{1-\frac{\gamma}{\tilde{\kappa}}} + \frac{\alpha\bar{\sigma}(\mathcal{B})}{1-\gamma}\gamma^N.
\end{aligned} \tag{3.133}$$

Define $c_1 \triangleq \frac{\gamma^{1-m}-\gamma^2}{(1-\gamma)^2}$, $c_2 \triangleq \frac{\alpha\bar{\sigma}(\mathcal{B})\gamma}{\kappa\tilde{\kappa}\left(1-\frac{\gamma}{\tilde{\kappa}}\right)}$. It follows from (3.133) that

$$\begin{aligned}
\|\Theta(k_1) - \Theta(k_2)\| &\leq \alpha\bar{\sigma}(\mathcal{B})c_1\gamma^N + c_2\left(\sum_{i=N}^{\infty}\tilde{\kappa}^i - \sum_{i=N}^{\infty}\left(\frac{\tilde{\kappa}}{\gamma}\right)^m\tilde{\kappa}^i\left(\frac{\gamma}{\tilde{\kappa}}\right)^i\right) + \frac{\alpha\bar{\sigma}(\mathcal{B})}{1-\gamma}\gamma^N \\
&= \alpha\bar{\sigma}(\mathcal{B})c_1\gamma^N + \frac{c_2}{1-\tilde{\kappa}}\tilde{\kappa}^N - \frac{c_2\tilde{\kappa}^m}{\gamma^m(1-\gamma)}\gamma^N + \frac{\alpha\bar{\sigma}(\mathcal{B})}{1-\gamma}\gamma^N.
\end{aligned} \tag{3.134}$$

Since $\gamma \in (0,1)$ and $\tilde{\kappa} \in (0,1)$, it follows from (3.134) that $\{\Theta(k)\}_{k=0}^{\infty}$ is Cauchy, and thus Θ converges. Thus we have verified (ii). $\square$

CHAPTER IV

η-Modification for Robust RCAC

4.1 Introduction

The history of adaptive control is marked by two key events. The first was the tragic accident in 1967 involving the X-15. The second was the publication in 1985 of [84], which presented two counterexamples showing the fragility of MRAC schemes. These counterexamples considered plants with high-frequency unmodeled dynamics that can induce a large, unknown phase shift in the plant's open-loop response leading to unbounded response. These events motivated the development of robust adaptive control schemes, and adaptive control continued to be developed and applied to a vast range of applications [4, 34, 50].

The purpose of the present chapter is to extend the RCAC update laws of Chapter II to remove the need to know the NMP zeros by incorporating a robustness modification into the update law. We use the same performance-dependent control penalty approach that is used for nonsquare plants at the end of Chapter III. However, unlike the algorithms presented in Chapter III, we now allow filtering of the data that is used in retrospective-cost optimization as in Chapter II. Furthermore, rather than penalizing the amplitude of the control input as in Chapter III, we now penalize the distance between the control input and the output of an a priori known stabilizing controller, which allows adaptive control of unstable, NMP plants, assuming that a stabilizing

output-feedback controller is known. The effectiveness of the approach is illustrated on SISO and MIMO plants with unknown NMP zeros. At the final section of this chapter, we revisit the celebrated Rohrs counterexamples using robust RCAC. From a sampled-data point of view, the challenging aspect of these problems for RCAC is not the unmodeled dynamics per se, but rather the sampling zeros, which may be NMP under fast sampling. Since the Rohrs counterexamples are open-loop asymptotically stable, there is no need to know the parameters of a stabilizing controller, and RCAC is able to provide reliable performance without knowledge of either the unmodeled high-frequency dynamics or the NMP sampling zeros.

4.2 Problem Formulation

Consider the MIMO discrete-time system

$$x(k+1) = Ax(k) + Bu(k) + D_1 w(k), \tag{4.1}$$

$$y(k) = Cx(k) + D_2 w(k), \tag{4.2}$$

$$z(k) = E_1 x(k) + E_0 w(k), \tag{4.3}$$

where $k \geq 0$, $x(k) \in \mathbb{R}^n$, $z(k) \in \mathbb{R}^{l_z}$ is the measured performance variable to be minimized, $y(k) \in \mathbb{R}^{l_y}$ contains additional measurements that are available for control, $u(k) \in \mathbb{R}^{l_u}$ is the input signal, $w(k) \in \mathbb{R}^{l_w}$ is the exogenous signal that can represent either a reference command, an external disturbance, or both. The system (4.1)–(4.3) can represent a sampled-data application arising from a continuous-time system with sample and hold operations with the sampling period h, where $y(k)$ represents $y(kh)$, $z(k)$ represents $z(kh)$, and so on. The operator matrix from u to z is thus given by

$$G_{zu}(\mathbf{q}) \triangleq E_1(\mathbf{q}I - A)^{-1}B, \tag{4.4}$$

where $\mathbf{q}$ is the shift operator which accounts for possibly nonzero initial conditions. Furthermore, for a positive integer i, $H_i \triangleq E_1 A^{i-1} B$ is the i^{th} Markov parameter of G_{zu}.

Now, consider the output-feedback controller

$$x_{\mathrm{c}}(k+1) = A_{\mathrm{c}}(k)x_{\mathrm{c}}(k) + B_{\mathrm{c}}(k)y(k), \tag{4.5}$$

$$u(k) = C_{\mathrm{c}}(k)x_{\mathrm{c}}(k), \tag{4.6}$$

where $x_{\mathrm{c}} \in \mathbb{R}^{n_{\mathrm{c}}}$. The closed-loop system with output feedback (4.5), (4.6) is thus given by

$$\tilde{x}(k+1) = \tilde{A}(k)\tilde{x}(k) + \tilde{D}_1(k)w(k), \tag{4.7}$$

$$y(k) = \tilde{C}\tilde{x}(k) + D_2 w(k), \tag{4.8}$$

$$z(k) = \tilde{E}_1\tilde{x}(k) + E_0 w(k), \tag{4.9}$$

where $\tilde{x} \triangleq \begin{bmatrix} x^{\mathrm{T}} & x_c^{\mathrm{T}} \end{bmatrix}^{\mathrm{T}}$,

$$\tilde{A}(k) = \begin{bmatrix} A & BC_{\mathrm{c}}(k) \\ B_{\mathrm{c}}(k)C & A_{\mathrm{c}}(k) \end{bmatrix}, \tilde{D}_1(k) = \begin{bmatrix} D_1 \\ B_{\mathrm{c}}(k)D_2 \end{bmatrix},$$

$$\tilde{C} = \begin{bmatrix} C & 0_{l_y \times n_{\mathrm{c}}} \end{bmatrix}, \quad \tilde{E}_1 = \begin{bmatrix} E_1 & 0_{l_z \times n_{\mathrm{c}}} \end{bmatrix}.$$

The goal is to develop a robust adaptive output feedback controller to minimize the performance measure $z^{\mathrm{T}}z$ in the presence of the unknown exogenous signal w with no modeling information about the plant zeros and dynamics.

For the adaptive controller (4.5), (4.6), the closed-loop state matrix $\tilde{A}(k)$ may be time-varying. To monitor the ability of the adaptive controller to stabilize the plant, we compute the spectral radius $\mathrm{spr}(\tilde{A}(k))$ at each time step. If the controller

converges, and $\mathrm{spr}(\tilde{A}(k))$ converges to a number less than 1, then the asymptotic closed-loop system is internally stable.

4.3 RCAC with η-Modification

In this section, we modify the instantaneous and cumulative update laws of Chapter II to include a performance-dependent control penalty. The modification is made in the cost function and thus does not change the control law and the definition of retrospective performance. However, before introducing the modified update laws, we briefly summarize the control law and the retrospective performance below for convenience to reader.

We represent (4.5), (4.6) by

$$u(k) = \theta^{\mathrm{T}}(k)\phi(k-1), \tag{4.10}$$

where $\phi(k-1) = \begin{bmatrix} y^{\mathrm{T}}(k-1) & \cdots & y^{\mathrm{T}}(k-n_{\mathrm{c}}) & u^{\mathrm{T}}(k-1) & \cdots & u^{\mathrm{T}}(k-n_{\mathrm{c}}) \end{bmatrix}^{\mathrm{T}}$, $\theta(k) = \begin{bmatrix} N_1^{\mathrm{T}}(k) & \cdots & N_{n_{\mathrm{c}}}^{\mathrm{T}}(k) & M_1^{\mathrm{T}}(k) & \cdots & M_{n_{\mathrm{c}}}^{\mathrm{T}}(k) \end{bmatrix}^{\mathrm{T}}$, and, for all $1 \le i \le n_{\mathrm{c}}$, $N_i(k) \in \mathbb{R}^{l_y \times l_u}$, $M_i(k) \in \mathbb{R}^{l_u \times l_u}$. The control law (4.10) can be reformulated as

$$u(k) = \Phi(k-1)\Theta(k), \tag{4.11}$$

where $\Phi(k-1) \triangleq I_{l_u} \otimes \phi^{\mathrm{T}}(k-1) \in \mathbb{R}^{l_u \times l_u n_{\mathrm{c}}(l_u+l_y)}$, and $\Theta(k) \triangleq \mathrm{vec}(\theta(k)) \in \mathbb{R}^{l_u n_{\mathrm{c}}(l_u+l_y)}$.

Now, for a positive integer r, we define the finite-impulse-response (FIR) transfer matrix

$$G_{\mathrm{f}}(\mathbf{q}^{-1}) \triangleq K_1\mathbf{q}^{-1} + K_2\mathbf{q}^{-2} + \cdots + K_r\mathbf{q}^{-r}, \tag{4.12}$$

where $K_i \in \mathbb{R}^{l_z \times l_u}$ for $1 \le i \le r$. Next, for $k \ge 1$, we define the *retrospective*

performance variable

$$\hat{z}(\hat{\Theta}, k) \triangleq z(k) + \Phi_{\mathrm{f}}(k-1)\hat{\Theta} - u_{\mathrm{f}}(k), \tag{4.13}$$

with

$$\Phi_{\mathrm{f}}(k-1) \triangleq G_{\mathrm{f}}(\mathbf{q}^{-1})\Phi(k-1) \in \mathbb{R}^{l_z \times l_u n_{\mathrm{c}}(l_u+l_y)}, \tag{4.14}$$

$$u_{\mathrm{f}}(k) \triangleq G_{\mathrm{f}}(\mathbf{q}^{-1})u(k) \in \mathbb{R}^{l_z}, \tag{4.15}$$

where $\hat{\Theta}(k)$ will be determined by optimization below.

4.3.1 Instantaneous Update Law with η-Modification

For $k \geq 1$, we define the modified instantaneous cost function

$$\begin{aligned} J_{\mathrm{ins}}(\hat{\Theta}, k) \triangleq{}& \hat{z}^{\mathrm{T}}(\hat{\Theta}, k)R_1(k)\hat{z}(\hat{\Theta}, k) + \alpha(k)(\hat{\Theta} - \Theta(k-1))^{\mathrm{T}}R_2(k)(\hat{\Theta}(k) - \Theta(k-1)) \\ &+ \eta(k)(\hat{\Theta} - \Theta^*)^{\mathrm{T}}\Phi_{\mathrm{f}}^{\mathrm{T}}(k-1)R_3(k)\Phi_{\mathrm{f}}(k-1)(\hat{\Theta} - \Theta^*), \end{aligned} \tag{4.16}$$

where, for all $k \geq 0$, $\alpha(k) > 0$ and $\eta(k) \geq 0$ are scalars, $R_1(k) \in \mathbb{R}^{l_z \times l_z}$ is positive definite, $R_2(k) \in \mathbb{R}^{l_u n_{\mathrm{c}}(l_u+l_y) \times l_u n_{\mathrm{c}}(l_u+l_y)}$ is positive definite, $R_3(k) \in \mathbb{R}^{l_z \times l_z}$ is positive definite, and Θ^* is a stabilizing output-feedback controller of the form (4.11). Note that if the open-loop plant is not unstable, then a rather obvious choice of Θ^* is $\Theta^* = 0$. Furthermore, we choose the weighting $\eta(k)$ as

$$\eta(k) = \eta_1 + \eta_0 \sum_{i=0}^{p_c-1} z^{\mathrm{T}}(k-i)z(k-i), \tag{4.17}$$

where $\eta_1 \geq 0$, $\eta_0 \geq 0$ and p_c is a positive integer. Unless stated otherwise, we take $\eta_1 = 0$ throughout this dissertation.

Comparing to (2.26), the modified instantaneous cost function given in (4.16) has

the additional term with the weighting $\eta(k)$ which penalizes the distance between the updated controller $\Theta(k)$ and the stabilizing controller Θ^* on the regressor directions. It follows from (4.17) that the penalty becomes larger as z gets larger, and vanishes as z approaches zero. Therefore, when z is small, (4.16) approaches (2.26), which has the provable convergence properties given in Chapter II in the ideal case. On the other hand, when z is large, the penalty term dominates (4.16) and tends to push Θ toward Θ^*, thus discouraging the update law from destabilizing the closed-loop system.

Now, substituting (4.13) into (4.16) yields

$$J_{\rm ins}(\hat{\Theta}, k) = \hat{\Theta}^{\rm T}\Gamma_1(k)\hat{\Theta} + \Gamma_2^{\rm T}(k)\hat{\Theta} + \Gamma_3(k), \tag{4.18}$$

where

$$\Gamma_1(k) \triangleq \Phi_{\rm f}^{\rm T}(k-1)\left[R_1(k) + \eta(k)R_3(k)\right]\Phi_{\rm f}(k-1) + \alpha(k)R_2(k) \in \mathbb{R}^{l_u n_{\rm c}(l_u+l_y)\times l_u n_{\rm c}(l_u+l_y)}, \tag{4.19}$$

$$\begin{aligned}\Gamma_2(k) \triangleq\ & 2[\Phi_{\rm f}^{\rm T}(k-1)R_1(k)\left(z(k) - u_{\rm f}(k)\right) - \eta(k)\Phi_{\rm f}^{\rm T}(k-1)R_3(k)\Phi_{\rm f}(k-1)\Theta^* \\ & - \alpha(k)R_2(k)\Theta(k-1)] \in \mathbb{R}^{l_u n_{\rm c}(l_u+l_y)}.\end{aligned} \tag{4.20}$$

Since $\Gamma_1(k)$ is positive definite, $J_{\rm ins}(\hat{\Theta}, k)$ has the unique global minimizer

$$\Theta(k) = -\frac{1}{2}\Gamma_1^{-1}(k)\Gamma_2(k). \tag{4.21}$$

Note that (4.21) involves the on-line inversion of a positive definite matrix of size $l_u n_{\rm c}(l_u + l_y)$. The following result provides a recursive computation for (4.21) that involves the on-line inversion of a positive definite matrix of size l_z.

Proposition 4.3.1. *Let $R_1(k) \equiv R_3(k) \equiv I_{l_z}$, $R_2(k) \equiv I_{l_u n_{\rm c}(l_u+l_y)}$, and $\Theta^* = 0$. Then, for each $k \geq 1$, the unique global minimizer of the modified instantaneous cost*

function (4.16) *is given by*

$$\Theta(k) = \Theta(k-1) - \gamma(k)\Phi_{\mathrm{f}}^{\mathrm{T}}(k-1)\left(\mu(k)I_{l_z} + \Phi_{\mathrm{f}}(k-1)\Phi_{\mathrm{f}}^{\mathrm{T}}(k-1)\right)^{-1}\epsilon(k), \quad (4.22)$$

where

$$\gamma(k) \triangleq \frac{1}{1+\eta(k)}, \quad (4.23)$$

$$\mu(k) \triangleq \alpha(k)\gamma(k), \quad (4.24)$$

$$\epsilon(k) \triangleq z(k) - u_{\mathrm{f}}(k) + (1+\eta(k))\hat{u}_{\mathrm{f}}(k), \quad (4.25)$$

and

$$\hat{u}_{\mathrm{f}}(k) \triangleq \Phi_{\mathrm{f}}(k-1)\Theta(k-1). \quad (4.26)$$

Proof Substituting (4.20) into (4.21) and using (4.19), we obtain

$$\begin{aligned}\Theta(k) &= \Gamma_1^{-1}(k)\left(\alpha(k)\Theta(k-1) - \Phi_{\mathrm{f}}^{\mathrm{T}}(k-1)(z(k)-u_{\mathrm{f}}(k))\right)\\ &= \Gamma_1^{-1}(k)\left(\alpha(k)I_{l_u n_{\mathrm{c}}(l_u+l_y)} + (1+\eta(k))\Phi_{\mathrm{f}}^{\mathrm{T}}(k-1)\Phi_{\mathrm{f}}(k-1)\right)\Theta(k-1)\\ &\quad - \Gamma_1^{-1}(k)\left(\Phi_{\mathrm{f}}^{\mathrm{T}}(k-1)(z(k)-u_{\mathrm{f}}(k)) + (1+\eta(k))\Phi_{\mathrm{f}}^{\mathrm{T}}(k-1)\Phi_{\mathrm{f}}(k-1)\Theta(k-1)\right)\\ &= \Theta(k-1) - \Gamma_1^{-1}(k)\Phi_{\mathrm{f}}^{\mathrm{T}}(k-1)\epsilon(k). \end{aligned} \quad (4.27)$$

Now, applying the matrix inversion lemma to (4.19) yields

$$\Gamma_1^{-1}(k) = \frac{1}{\alpha(k)}\left(I_{l_u n_{\mathrm{c}}(l_u+l_y)} - (1+\eta(k))\Phi_{\mathrm{f}}^{\mathrm{T}}(k-1)\Psi^{-1}(k)\Phi_{\mathrm{f}}(k-1)\right), \quad (4.28)$$

where

$$\Psi(k) \triangleq \alpha(k)I_{l_z} + (1+\eta(k))\Phi_{\mathrm{f}}(k-1)\Phi_{\mathrm{f}}^{\mathrm{T}}(k-1).$$

Finally, substituting (4.28) into (4.27) yields

$$\begin{aligned}\Theta(k) &= \Theta(k-1) - \frac{1}{\alpha(k)}\Phi_{\mathrm{f}}^{\mathrm{T}}(k-1)\Psi^{-1}(k)\Psi(k)\epsilon(k)\\ &\quad + \frac{1+\eta(k)}{\mu(k)}\Phi_{\mathrm{f}}^{\mathrm{T}}(k-1)\Psi^{-1}(k)\Phi_{\mathrm{f}}(k-1)\Phi_{\mathrm{f}}^{\mathrm{T}}(k-1)\epsilon(k)\\ &= \Theta(k-1) - \frac{1}{\alpha(k)}\Phi_{\mathrm{f}}^{\mathrm{T}}(k-1)\Psi^{-1}(k)[\alpha(k)\epsilon(k) + (1+\eta(k))\Phi_{\mathrm{f}}(k-1)\Phi^{\mathrm{T}}(k-1)\epsilon(k)\\ &\quad - (1+\eta(k))\Phi_{\mathrm{f}}(k-1)\Phi_{\mathrm{f}}^{\mathrm{T}}(k-1)\epsilon(k)],\end{aligned}$$

and thus, we have

$$\Theta(k) = \Theta(k-1) - \gamma(k)\Phi_{\mathrm{f}}^{\mathrm{T}}(k-1)\left(\mu(k)I_{l_z} + \Phi_{\mathrm{f}}(k-1)\Phi_{\mathrm{f}}^{\mathrm{T}}(k-1)\right)^{-1}\epsilon(k). \qquad \square$$

4.3.2 Cumulative Update Law with η-Modification

For $k \geq 1$, we define the modified cumulative cost function

$$\begin{aligned}J_{\mathrm{cum}}(\hat{\Theta}, k) \triangleq \sum_{i=1}^{k} &\lambda^{k-i}\hat{z}^{\mathrm{T}}(\hat{\Theta}, i)R_1(i)\hat{z}(\hat{\Theta}, i)\\ &+ \sum_{i=1}^{k}\lambda^{k-i}\eta(i)(\hat{\Theta}-\Theta^*)^{\mathrm{T}}\Phi_{\mathrm{f}}^{\mathrm{T}}(i-1)R_2(i)\Phi_{\mathrm{f}}(i-1)(\hat{\Theta}-\Theta^*)\\ &+ \lambda^k(\hat{\Theta}-\Theta(0))^{\mathrm{T}}P_0^{-1}(\hat{\Theta}-\Theta(0)),\end{aligned} \tag{4.29}$$

where $\lambda \in (0,1]$, $R_1(i) \in \mathbb{R}^{l_z \times l_z}$ is positive definite, $R_2(i) \in \mathbb{R}^{l_z \times l_z}$ is positive semidefinite, and $P_0 \in \mathbb{R}^{l_u n_{\mathrm{c}}(l_u+l_y)\times l_u n_{\mathrm{c}}(l_u+l_y)}$ is positive definite. Substituting (4.13) into (4.29) yields

$$J_{\mathrm{cum}}(\hat{\Theta}(k), k) = \hat{\Theta}^{\mathrm{T}}(k)\mathcal{C}_1(k)\hat{\Theta}(k) + \mathcal{C}_2^{\mathrm{T}}(k)\hat{\Theta}(k) + \mathcal{C}_3(k), \tag{4.30}$$

where $\mathcal{C}_1(0) = P_0^{-1}$, $\mathcal{C}_2(0) = -2P_0^{-1}\Theta(0)$, and, for all $k \geq 1$,

$$\mathcal{C}_1(k) \triangleq \sum_{i=1}^{k} \lambda^{k-i} \Phi_{\mathrm{f}}^{\mathrm{T}}(i-1) \left[R_1(i) + \eta(i) R_2(i) \right] \Phi_{\mathrm{f}}(i-1) + \lambda^k P_0^{-1}, \tag{4.31}$$

$$\begin{aligned} \mathcal{C}_2(k) \triangleq & \sum_{i=1}^{k} 2\lambda^{k-i} \Phi_{\mathrm{f}}^{\mathrm{T}}(i-1) [R_1(i)(z(i) - u_{\mathrm{f}}(i)) - \eta(i) R_2(i) \Phi_{\mathrm{f}}(i-1) \Theta^*] \\ & - 2\lambda^k P_0^{-1} \Theta(0). \end{aligned} \tag{4.32}$$

Since $\mathcal{C}_1(k)$ is positive definite, the modified cumulative cost function (4.29) has the unique global minimizer

$$\Theta(k) = -\frac{1}{2} \mathcal{C}_1^{-1}(k) \mathcal{C}_2(k). \tag{4.33}$$

To reduce memory usage, $\mathcal{C}_1(k)$ and $\mathcal{C}_2(k)$ can be computed recursively using

$$\mathcal{C}_1(k) = \lambda \mathcal{C}_1(k-1) + \Phi_{\mathrm{f}}^{\mathrm{T}}(k-1) \left[R_1(k) + \eta(k) R_2(k) \right] \Phi_{\mathrm{f}}(k-1), \tag{4.34}$$

$$\mathcal{C}_2(k) = \lambda \mathcal{C}_2(k-1) + 2\Phi_{\mathrm{f}}^{\mathrm{T}}(k-1) [R_1(k)(z(k) - u_{\mathrm{f}}(k)) - \eta(i) R_2(i) \Phi_{\mathrm{f}}(i-1) \Theta^*]. \tag{4.35}$$

Furthermore, (4.33) requires the on-line inversion of a positive definite matrix of size $l_u n_{\mathrm{c}}(l_u + l_y) \times l_u n_{\mathrm{c}}(l_u + l_y)$. The following result reformulates (4.33) as an RLS update law that requires inversion of a matrix of size $l_z \times l_z$.

Proposition 4.3.2. *For all $k \geq 0$, define $P(k) \triangleq \mathcal{C}_1^{-1}(k)$, and let $R_1(k) \equiv R_2(k) \equiv I_{l_z}$ and $\Theta^* = 0$. Then, for all $k \geq 1$, $P(k)$ satisfies*

$$P(k) = \frac{1}{\lambda} \left[P(k-1) - P(k-1) \Phi_{\mathrm{f}}^{\mathrm{T}}(k-1) \Lambda^{-1}(k) \Phi_{\mathrm{f}}(k-1) P(k-1) \right], \tag{4.36}$$

where

$$\Lambda(k) \stackrel{\triangle}{=} \frac{\lambda}{1+\eta(k)} I_{l_z} + \Phi_{\mathrm{f}}(k-1)P(k-1)\Phi_{\mathrm{f}}^{\mathrm{T}}(k-1). \tag{4.37}$$

Furthermore, for all $k \geq 1$, *let* $\Theta(k)$ *be the unique global minimizer of the modified cumulative cost function* (4.29) *given by* (4.33). *Then, for all* $k \geq 1$,

$$\Theta(k) = \Theta(k-1) - \frac{1}{1+\eta(k)} P(k-1)\Phi_{\mathrm{f}}^{\mathrm{T}}(k-1)\Lambda^{-1}(k)\epsilon(k), \tag{4.38}$$

where $\epsilon(k)$ *is as defined in* (4.25).

Proof From (4.34),

$$P^{-1}(k) = \lambda P^{-1}(k-1) + (1+\eta(k))\Phi_{\mathrm{f}}^{\mathrm{T}}(k-1)\Phi_{\mathrm{f}}(k-1). \tag{4.39}$$

Applying the matrix inversion lemma to (4.39) yields

$$\begin{aligned} P(k) &= \frac{1}{\lambda}P(k-1) - \frac{1}{\lambda}P(k-1)\Phi_{\mathrm{f}}^{\mathrm{T}}(k-1) \\ &\quad \cdot \left[\frac{\lambda}{1+\eta(k)} I_{l_z} + \Phi_{\mathrm{f}}(k-1)P(k-1)\Phi_{\mathrm{f}}^{\mathrm{T}}(k-1)\right]^{-1} \Phi_{\mathrm{f}}(k-1)P(k-1) \\ &= \frac{1}{\lambda}\left[P(k-1) - P(k-1)\Phi_{\mathrm{f}}^{\mathrm{T}}(k-1)\Lambda^{-1}(k)\Phi_{\mathrm{f}}(k-1)P(k-1)\right]. \end{aligned}$$

Hence, (4.36) holds. Next, since $P(k) = \mathcal{C}_1^{-1}(k)$, it follows from (4.33), (4.35) and (4.36) that

$$\begin{aligned}
\Theta(k) &= -\frac{1}{2}P(k)\mathcal{C}_2^{\mathrm{T}}(k) \\
&= -\frac{1}{2}P(k-1)\mathcal{C}_2^{\mathrm{T}}(k-1) - \frac{1}{\lambda}P(k-1)\Phi_{\mathrm{f}}^{\mathrm{T}}(k-1)(z(k)-u_{\mathrm{f}}(k)) \\
&\quad + \frac{1}{2}P(k-1)\Phi_{\mathrm{f}}^{\mathrm{T}}(k-1)\Lambda^{-1}(k)\Phi_{\mathrm{f}}(k-1)P(k-1)\mathcal{C}_2^{\mathrm{T}}(k-1) \\
&\quad + \frac{1}{\lambda}P(k-1)\Phi_{\mathrm{f}}^{\mathrm{T}}(k-1)\Lambda^{-1}(k)\Phi_{\mathrm{f}}(k-1)P(k-1)\Phi_{\mathrm{f}}^{\mathrm{T}}(k-1)(z(k)-u_{\mathrm{f}}(k)) \\
&= \Theta(k-1) - \frac{1}{\lambda}P(k-1)\Phi_{\mathrm{f}}^{\mathrm{T}}(k-1)\Lambda^{-1}(k)\Lambda(k)(z(k)-u_{\mathrm{f}}(k)) \\
&\quad - P(k-1)\Phi_{\mathrm{f}}^{\mathrm{T}}(k-1)\Lambda^{-1}(k)\hat{u}_{\mathrm{f}}(k) \\
&\quad + \frac{1}{\lambda}P(k-1)\Phi_{\mathrm{f}}^{\mathrm{T}}(k-1)\Lambda^{-1}(k)\Phi_{\mathrm{f}}(k-1)P(k-1)\Phi_{\mathrm{f}}^{\mathrm{T}}(k-1)(z(k)-u_{\mathrm{f}}(k)) \\
&= \Theta(k-1) - P(k-1)\Phi_{\mathrm{f}}^{\mathrm{T}}(k-1)\Lambda^{-1}(k)[\hat{u}_{\mathrm{f}}(k) + (\frac{1}{1+\eta(k)}I_{l_z} + \frac{1}{\lambda}\Phi_{\mathrm{f}}(k-1) \\
&\quad \cdot P(k-1)\Phi_{\mathrm{f}}^{\mathrm{T}}(k-1) - \frac{1}{\lambda}\Phi_{\mathrm{f}}(k-1)P(k-1)\Phi_{\mathrm{f}}^{\mathrm{T}}(k-1))(z(k)-u_{\mathrm{f}}(k))] \\
&= \Theta(k-1) - \frac{1}{1+\eta(k)}P(k-1)\Phi_{\mathrm{f}}^{\mathrm{T}}(k-1)\Lambda^{-1}(k)\epsilon(k). \qquad \square
\end{aligned}$$

4.4 Numerical Examples

We now present numerical examples to illustrate the response of RCAC with η-modification. In each example, the modified cumulative update law (4.33) is used with $\lambda = 1$, $R_1(k) \equiv R_2(k) \equiv I_{l_z}$. For the examples with asymptotically stable plants, we use $\Theta^* = 0$ and apply the RLS update (4.36), (4.38), which yields the same solution as (4.33), as shown in Proposition 4.3.2. All examples assume $y = z$ and, unless stated otherwise, $\Theta(k)$ is initialized to zero. Furthermore, in all examples, the state is initialized to a random vector with norm $\|x(0)\|_2 = 1$.

Example 4.4.1 (SISO, NMP, Asymptotically Stable Plant)**.** Consider the 3$^{\mathrm{rd}}$-order

plant

$$A = \begin{bmatrix} 1.9 & -1.4 & 0.45 \\ 1 & 0 & 0 \\ 0 & 1 & 0 \end{bmatrix}, \quad B = \begin{bmatrix} 1 \\ 0 \\ 0 \end{bmatrix}, \quad D_1 = \begin{bmatrix} 0 \\ 1 \\ 0 \end{bmatrix},$$

$$E_1 = \begin{bmatrix} 1 & -1.8 & 2.77 \end{bmatrix}, \quad E_0 = 0.$$

Therefore, the plant has the poles $\{0.5 \pm \jmath 0.5, 0.9\}$ and the NMP zeros $\{0.9 \pm \jmath 1.4\}$. We consider the unmatched disturbance $w(k) = \sin \omega k$ with $\omega = \pi/10$ rad/sample. Assuming $H_1 = 1$ is known, we take $G_{\mathrm{f}}(\mathbf{q}^{-1}) = H_1 \mathbf{q}^{-1}$, $n_{\mathrm{c}} = 5$, $P_0 = I$, $\eta_0 = 0.05$, and $p_c = 1$. The control is turned on at $k = 100$, and, after a slight transient, the performance variable reduces to zero, the controller converges, and, after convergence, the closed-loop system is asymptotically stable with spectral radius 0.92, as shown in Figure 4.1. ■

Example 4.4.2 (SISO, NMP, Not Strongly Stabilizable Plant)**.** Consider the 2nd-order plant

$$A = \begin{bmatrix} 1.7 & -0.6 \\ 1 & 0 \end{bmatrix}, \quad B = \begin{bmatrix} 1 \\ 0 \end{bmatrix}, \quad D_1 = \begin{bmatrix} 0 \\ 1 \end{bmatrix}, \tag{4.40}$$

$$E_1 = \begin{bmatrix} 1 & -1.1 \end{bmatrix}, \quad E_0 = 0. \tag{4.41}$$

Therefore, the plant has the poles $\{0.5, 1.2\}$, and the NMP zero $\{1.1\}$. Using basic root locus rules, it can be shown that this plant is not strongly stabilizable, that is, there does not exist a stable controller output feedback controller G_{c} that stabilizes this plant. We consider the unmatched disturbance $w(k) = \sin \omega k$, where $\omega = \pi/10$ rad/sample. We assume that the first Markov parameter $H_1 = 1$ is known. Further-

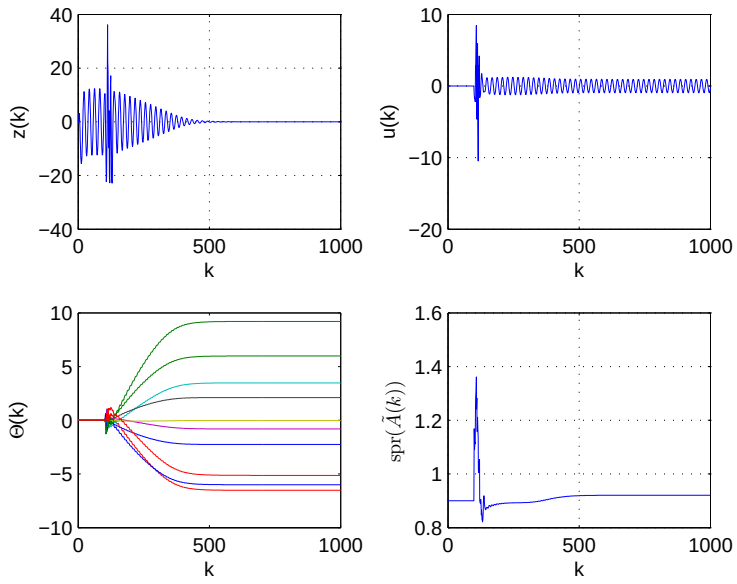

Figure 4.1: Example 4.4.1: Unmatched disturbance rejection for the asymptotically stable, SISO plant with NMP zeros $\{0.9 \pm \jmath 1.4\}$. The performance output y approaches zero, the control signal u is bounded, the controller Θ converges, and, after convergence, the closed-loop dynamics matrix has the spectral radius 0.92.

more, we assume that the stabilizing control law

$$(1 - 0.9667\mathbf{q}^{-1} - 0.5724\mathbf{q}^{-2})u(k) = (-0.9401\mathbf{q}^{-1} + 0.47\mathbf{q}^{-2})y(k) \tag{4.42}$$

is known. Note that the control law (4.42) is the low-authority discrete-time LQG controller for plant (4.40), (4.41). Choosing $n_{\mathrm{c}} = 5$, we rewrite (4.42) in regressor form

$$u(k) = \Theta^{*}\phi(k-1),$$

where

$$\Theta^{*} \triangleq \left[\begin{array}{cccccccccc} -0.9401 & 0.47 & 0 & 0 & 0 & 0.9667 & 0.5724 & 0 & 0 & 0 \end{array}\right],$$

and $\phi(k-1)$ is as in (2.18). We initialize $\Theta(k)$ to Θ^*, and take $G_{\mathrm{f}}(\mathbf{q}^{-1}) = H_1\mathbf{q}^{-1}$, $P_0 = I$, $\eta_0 = 0.2$, and $p_c = 1$. The modified cumulative update law (4.33) is turned on at $k = 500$, and, after a slight transient, the performance variable reduces to zero, as shown in Figure 4.2. In order to reject the unmatched disturbance, the controller gains adapt, and converge to different values than the gains of Θ^* without destabilizing the closed-loop system. ■

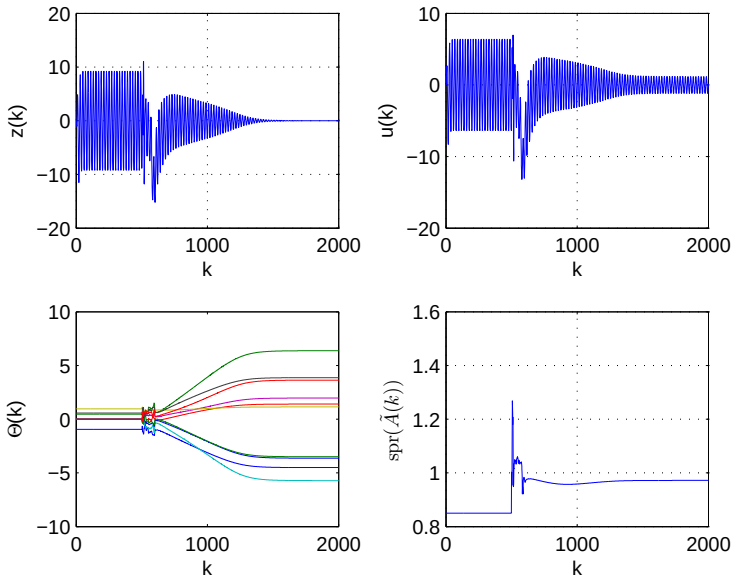

Figure 4.2: Example 4.4.2: Unmatched disturbance rejection for the SISO, NMP, not strongly stabilizable plant. The controller is initialized to the low-authority discrete-time LQG controller Θ^*. The update is turned on at $k = 500$. After a slight transient, the performance output y is reduced to zero, the control signal u is bounded, the controller Θ converges to a different controller than Θ^*, and, after convergence, the closed-loop dynamics matrix has the spectral radius 0.97.

Example 4.4.3 (MIMO, NMP, Asymptotically Stable Plant)**.** Consider the two

input, two output, 4^{th}-order plant

$$A = \begin{bmatrix} 0.66 & 0.1 & 0.07 & 0.31 \\ 0.18 & 0.58 & -0.14 & 0.32 \\ 0.61 & -1.38 & 0.93 & -2.08 \\ -0.12 & -0.34 & 0.38 & -0.28 \end{bmatrix}, \quad B = \begin{bmatrix} 0.81 & -0.75 \\ 0.55 & 1.52 \\ -1.05 & -0.03 \\ 0.4 & 1.64 \end{bmatrix}, \quad D_1 = 0,$$

$$E_1 = \begin{bmatrix} 0.6 & -2.19 & -1.44 & 1.47 \\ 0.59 & -1.33 & 0.4 & -0.33 \end{bmatrix}, \quad E_0 = I_2.$$

Therefore, the plant has the poles $\{0.297 \pm \jmath 0.596, 0.797, 0.499\}$ and the transmission zeros $\{-0.35, 1.342\}$. We consider the sinusoidal command $w(k) = \begin{bmatrix} \sin \omega_1 k & 2 \sin \omega_2 k \end{bmatrix}^{\mathrm{T}}$ with $\omega_1 = \pi/9$ rad/sample and $\omega_2 = \pi/2$ rad/sample. Assuming H_1 is known, we take $G_{\mathrm{f}}(\mathbf{q}^{-1}) = H_1 \mathbf{q}^{-1}$, $n_{\mathrm{c}} = 10$, $P_0 = I$, $\eta_0 = 0.1$, and $p_c = 1$. The control is turned on at $k = 100$, and, after a slight transient, the performance variable reduces to zero, and the controller converges, as shown in Figure 4.3. ■

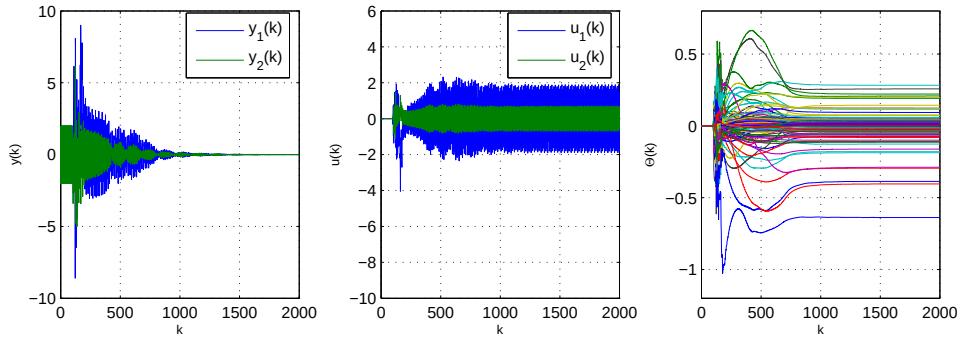

Figure 4.3: Example 4.4.3: Sinusoidal-command following for the asymptotically stable, 2×2 MIMO plant with NMP transmission zero 1.342. The performance output y approaches zero, the control signal u is bounded, and the controller Θ converges.

4.5 Robust Sampled-Data Adaptive Control of Rohrs Counterexamples

In [84], the authors presented two counterexamples showing the fragility of model reference adaptive control (MRAC) schemes. These counterexamples considered plants with high-frequency unmodeled dynamics that can induce a large, unknown phase shift in the plant's open-loop response leading to an unbounded response. These examples are commonly referred to as the "Rohrs counterexamples".

The purpose of this section is to revisit both Rohrs counterexamples using RCAC. From a sampled-data point of view, the challenging aspect of these problems for RCAC is not the unmodeled dynamics per se, but rather the sampling zeros, which may be NMP under fast sampling. The goal of this section is thus to apply the robust RCAC update laws developed in this chapter to Rohrs counterexamples, and compare the effectiveness of the robustness modification with the unmodified RCAC update laws presented in Chapter II in the case where the plant contains unmodeled dynamics and unknown NMP sampling zeros.

4.5.1 Rohrs Counterexamples: Problem Formulation

We consider the first-order transfer function $T_0(s) \triangleq \frac{2}{s+1}$ cascaded with the unmodeled high-frequency dynamics

$$\Lambda(s) \triangleq \frac{229}{(s-15-\jmath 2)(s-15+\jmath 2)}.$$

The plant is given by $T_{zu}(s) \triangleq T_0(s)\Lambda(s)$, which is minimum phase. Although the phase of $T_0(\jmath\omega)$ is in $[0,\ 90]$ deg for all ω, $T_{zu}(\jmath\omega)$ has a phase crossover frequency of $\omega_{pc} = 16.1$ rad/sec. The goal is to have the output z of the cascade plant T_{zu} follow the output of the reference model $G_m(s) = \frac{3}{s+3}$.

In [84], the authors formulated two counterexamples demonstrating the fragility of

MRAC in the presence of the unknown dynamics $\Lambda(s)$. In the first counterexample, the input to the reference model is a biased sinusoidal signal. In particular, two sinusoidal reference inputs are considered: $r_1(t) \triangleq 0.3 + 2\sin(8t)$, and $r_2(t) \triangleq 0.3 + 1.8\sin(16.1t)$. It is shown in [84] that, if the reference signal is chosen to be $r_2(t)$, whose frequency content includes the phase crossover frequency of the cascade plant, then MRAC destabilizes the closed-loop system.

In the second counterexample, the output measurements are corrupted by an unknown sensor noise, and, it is shown that, if the unknown sensor noise has higher order of persistency than the reference input, then MRAC destabilizes the system. Specifically, the second counterexample involved the reference input $r(t) \triangleq 2\mathbf{1}(t)$, which is persistently exciting of order one, and the sinusoidal sensor noise $d(t) \triangleq 0.5\sin(8t)$, which is persistently exciting of order two.

4.5.2 Sampling Zeros of the Rohrs Plant

Consider a discrete-time sampled-data system consisting of a zero-order hold, a continuous-time transfer function $T_{zu}(s)$, and a sampler with sampling period h, connected in series. The resulting discrete-time system is characterized by the *pulse transfer function* $G_{zu}(z)$ given by [61]

$$G_{zu}(z) = (1 - z^{-1})\mathcal{Z}\{T_{zu}(s)/s\}. \tag{4.43}$$

If the relative degree of $T_{zu}(s)$ is at least 2, then $G_{zu}(z)$ typically has more zeros than $T_{zu}(s)$. The additional zeros are called *sampling zeros* [3].

Proposition 4.5.1. *Let $T_{zu}(s)$ be the n^{th}-order rational transfer function*

$$T_{zu}(s) = H\frac{(s - z_1)\dots(s - z_m)}{(s - p_1)\dots(s - p_n)} \tag{4.44}$$

with relative degree $d = n - m \geq 2$, and let $G_{zu}(z)$ be the corresponding pulse transfer

function. Then, as the sampling period h approaches 0, $n-d$ zeros of $G_{zu}(z)$ approach 1, and the remaining $d-1$ zeros of $G_{zu}(z)$ approach the roots of $B_d(z)$, where

$$B_d(z) \triangleq \beta_{d,1} z^{d-1} + \beta_{d,2} z^{d-2} + \cdots + \beta_{d,d}, \tag{4.45}$$

and for $k \in \{1, \ldots, d\}$,

$$\beta_{d,k} \triangleq \sum_{i=1}^{k} (-1)^{k-j} i^d \left(\begin{array}{c} d+1 \\ k-i \end{array} \right). \tag{4.46}$$

Proof. See Theorem 1 of [3]. □

All of the zeros of $B_d(z)$ are negative, and $B_d(z)$ has at least one zero that is on or outside the unit circle [112]. For $d \geq 3$, $B_d(z)$ has at least one zero outside the unit circle.

As a consequence of Proposition 4.5.1, sampled-data systems are typically NMP. In particular, for sufficiently small h, the pulse transfer function corresponding to a continuous-time system with relative degree 3 or more is NMP.

We now discuss the complications that arise in sampled-data control of the Rohrs counterexamples due to unmodeled high-frequency dynamics. In Chapter II, the NMP-zero-based construction of G_{f} requires knowledge of the NMP zeros of $G_{zu}(z)$, rather than the NMP zeros of $T_{zu}(s)$. Therefore, we consider the pulse transfer function $G_{zu}(z)$.

Since the relative degree of $T_0(s)$ is 1, the pulse transfer function $G_0(z)$ has no sampling zeros for every sampling period h, and thus, $G_0(z)$ is minimum phase. However, due to the unmodeled dynamics $\Lambda(s)$, the relative degree of the plant $T_{zu}(s)$ is 3. Therefore, in accordance with Proposition 4.5.1, $G_{zu}(z)$ is NMP for all sufficiently small h.

Applying (4.43) into $T_0(s)$ and $T_{zu}(s)$, the numerator polynomial corresponding

to the pulse transfer functions $G_0(z) = N_0(z)/D_0(z)$ and $G_{zu}(z) = N_{zu}(z)/D_{zu}(z)$ are

$$N_0(z) = 2(1 - e^{-h}), \tag{4.47}$$

$$N_{zu}(z) = \beta_2 z^2 + \beta_1 z + \beta_0, \tag{4.48}$$

where

$$\begin{aligned}\beta_0 &= -2e^{-31h} + 2.29e^{-30h} + 1.03e^{-16h}\sin 2h \\ &\quad - 0.29e^{-16h}\cos 2h, \end{aligned} \tag{4.49}$$

$$\begin{aligned}\beta_1 &= -0.29e^{-30h} + 4.29(e^{-16h} - e^{-15h})\cos 2h \\ &\quad + 0.29e^{-h} - 1.03e^{-15h}\sin 2h, \end{aligned} \tag{4.50}$$

$$\begin{aligned}\beta_2 &= 0.29e^{-15h}\cos 2h - 2.29e^{-h} + 2 \\ &\quad + 1.03e^{-15h}\sin 2h. \end{aligned} \tag{4.51}$$

Figure 4.4 illustrates the zeros of (4.48). We observe that for all $h \lesssim 0.2$, one of the sampling zeros is outside the unit circle and thus $G_{zu}(z)$ has an unknown NMP zero, which is caused by the high-frequency dynamics $\Lambda(s)$. Neither the presence nor the location of this NMP zero can be assumed to be known, because $\Lambda(s)$ is assumed to be unmodeled.

4.5.3 Robustness of RCAC for the Rohrs Counterexamples

For $h > 0.2$ sec, the Rohrs sampled-data plant $G_{zu}(z)$ is minimum phase. In this case, as a consequence of Assumption (A11) in Section 2.5, the only modeling information required for implementing RCAC is the first nonzero Markov parameter. Therefore, in the case where $h > 0.2$ sec, robustness of unmodified RCAC update laws is determined by the ratio of the first Markov parameters of $G_0(z)$ and $G_{zu}(z)$. In

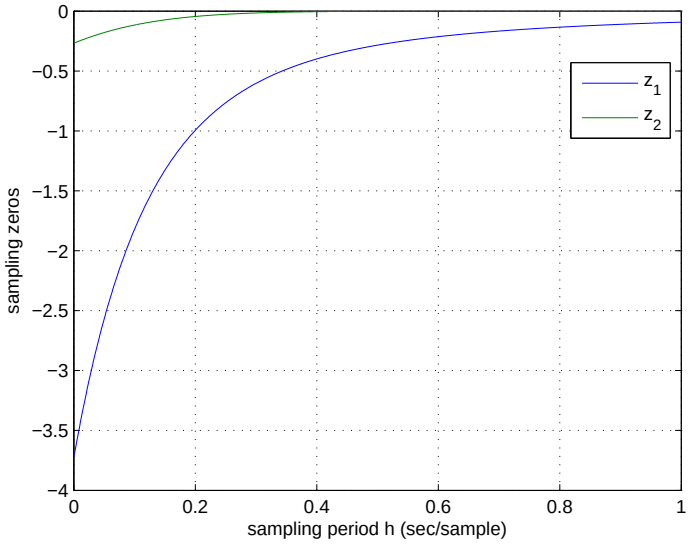

Figure 4.4: Sampling Zeros of $G_{zu}(z)$ as a function of h.

Figure 4.5, we illustrate the first Markov parameters $H_{0,1} = 2(1-e^{-h})$ and $H_{zu,1} = \beta_2$ of $G_0(z)$ and $G_{zu}(z)$ for $h \in [0, 5]$. As $h \to \infty$, it follows from (4.47) and (4.51) that both Markov parameters approach 2. Therefore, $\frac{H_{0,1}}{H_{zu,1}} \geq 0.5$ for all h. Hence, Markov parameter uncertainty is not a robustness issue for RCAC in Rohrs counterexamples. However, for $h \lesssim 0.2$, the available model $G_0(z)$ does not capture the NMP sampling zeros, and therefore, unmodified RCAC update laws of Chapter II will not work in this case.

On the other hand, using RCAC with η-modification ensures robustness and closed-loop stability, whether $G_{zu}(z)$ is NMP or not. Intuitively, closed-loop stability is expected with $\eta_0 > 0$. Indeed, suppose that the closed-loop system becomes unstable, and $z(k)$ diverges to infinity. In this case, the term $\sum_{i=1}^{k} \lambda^{k-i} \eta(i) \hat{\Theta}^{\mathrm{T}} \Phi_{\mathrm{f}}^{\mathrm{T}}(i-1) \Phi_{\mathrm{f}}(i-1) \hat{\Theta}$ in (4.29) starts dominating other terms. Therefore, assuming $\sum_{i=1}^{k} \Phi_{\mathrm{f}}^{\mathrm{T}}(i-1) \Phi_{\mathrm{f}}(i-1) \geq \alpha I > 0$, the optimization problem reduces to $\min_{\hat{\Theta}} \|\hat{\Theta}\|$, which gives $\hat{\Theta} = 0$. Thus, the closed-loop system reverts back to open-loop. Since the open-loop plant is asymptotically stable, $z(k)$ cannot diverge to infinity, which contradicts the

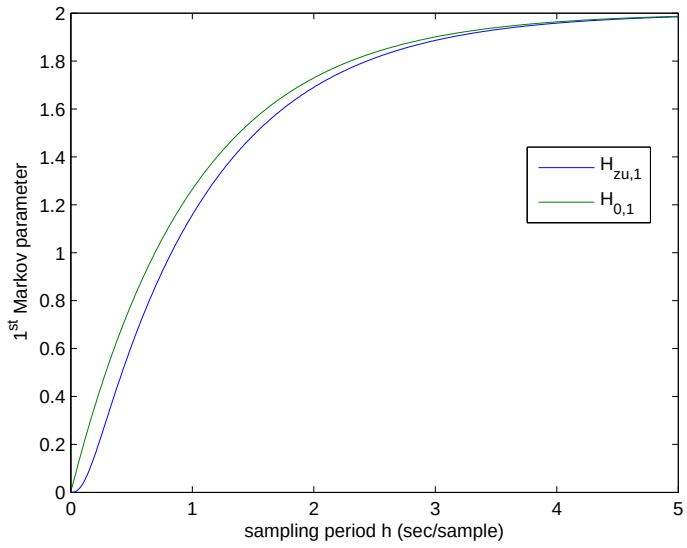

Figure 4.5: First Markov parameters of $G_0(z)$ and $G_{zu}(z)$.

assumption that the closed-loop system is unstable.

It should be noted that, since closed-loop stability does not imply zero asymptotic performance, the use of η-modification does not guarantee zero asymptotic performance. In the next chapter, we present numerical evidence suggesting that a phase condition is required for zero asymptotic performance when η-modification is used. Nevertheless, for Rohrs counterexamples, the following section illustrates that η-modification not only results in closed-loop stability, but also provides asymptotic command following for the reference inputs considered in [84].

4.5.4 Sampled-Data Adaptive Control of the Rohrs Counterexamples with RCAC

We now apply RCAC to the Rohrs counterexamples. In each example, the goal is to follow the output of the reference model $G_{\rm m}(s) = \frac{3}{s+3}$. Each simulation is initialized with the controller gain vector $\Theta(0)$ set to zero, and RCAC is turned on at $k = 5$. We use $\lambda = 1$ in all simulations. For consistency with the MRAC architecture, we use the

measurements of the plant output y_0 and the reference signal r so that $y = \begin{bmatrix} y_0 & r \end{bmatrix}^{\mathrm{T}}$. All modeling information we use is based on $G_0(z)$ rather than $G_{zu}(z)$. In each case, we illustrate the time traces of $z(k)$, $u(k)$, $\Theta(k)$, and the closed-loop spectral radius $\mathrm{spr}(\tilde{A}(k))$.

4.5.4.1 First Rohrs Counterexample: Sinusoidal Reference Inputs

In this section, we provide simulation results that illustrate the effectiveness of η-modification in preserving the closed-loop stability as predicted in Section 4.5.3 regardless of the frequency content of the reference signal. We first examine the unmodified RCAC cumulative update law with NMP-based construction of G_{f} as in Chapter II, and show that the method exhibits instability when the sampling rate is small enough to cause the sampling zeros to become NMP. We illustrate that the NMP sampling zero is the only cause of instability, and when the sampling period is large, RCAC does not suffer instability nor any parameter drift, regardless of the frequency spectrum of the reference input. Next, we introduce η-modification by letting $\eta_0 > 0$, and show that the closed-loop system remains stable even in the presence of the unknown NMP sampling zero independently of the frequency content of the reference signal.

RCAC without η-modification We first consider the reference input $r_1(t) = 0.3 + 2\sin(8.0t)$. We sample the continuous-time plant with $h = 0.25$ sec/sample, so that the Nyquist frequency $\omega_{\mathrm{N}} = 4\pi$ rad/sec is larger than the largest reference frequency 8 rad/sec. For this sampling period, the sampling zeros are minimum-phase. The first Markov parameters corresponding to the pulse transfer functions $G_{zu}(z)$ and $G_0(z)$ are $H_{zu,1} = 0.2341$ and $H_{0,1} = 0.4424$, respectively. We let $G_{\mathrm{f}} = H_{0,1}\mathbf{q}^{-1}$, and choose $P_0 = 10I$, $n_{\mathrm{c}} = 10$. As shown in Figure 4.6, z converges to zero, u remains bounded, Θ converges, and $\mathrm{spr}(\tilde{A})(k)$ converges below 1.

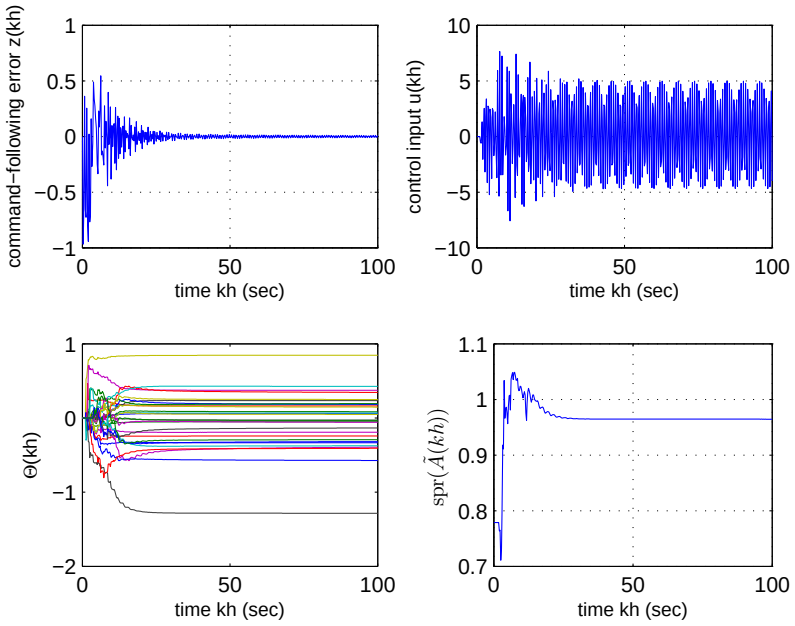

Figure 4.6: Response of RCAC without η-modification. The reference input is $r_1(t) = 0.3 + 2\sin(8.0t)$, and the sampling period is $h = 0.25$ sec/sample. Under this sampling rate, the sampling zeros contributed by the unmodeled dynamics are minimum phase, the asymptotic closed-loop system is asymptotically stable, and z converges to zero.

Keeping h the same, we now consider the reference input $r_2(t) = 0.3+1.8\sin(16.1t)$, which causes parameter drift and instability in traditional adaptive methods [84]. Note that the frequency of the reference signal is selected at the point where $T_{zu}(s)$ has a 180-deg phase lag. Furthermore, note that the Nyquist rate $\omega_{\rm N}$ is smaller than the largest reference frequency 16.1 rad/sec. However, the goal here is to show that closed-loop stability is maintained independently of the frequency of the reference command, as long as the sampling zeros arising from the unknown dynamics are minimum phase. Choosing the same controller and tuning parameters, the parameters converge, and the closed-loop system is stable after convergence, as shown in Figure 4.7. Of course, since h is not small enough to reconstruct $r_2(t)$ from the sampled data, the performance $z(t)$ is not equal to zero between consecutive sampling instants due to disturbance aliasing, as shown in Figure 4.8.

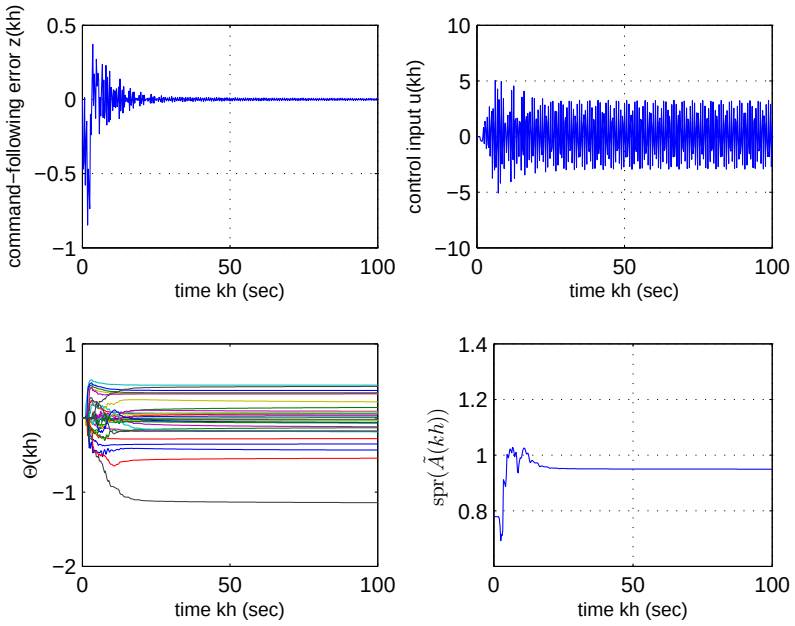

Figure 4.7: Response of RCAC without η-modification. The reference input is $r_2(t) = 0.3+1.8\sin(16.1t)$ and the sampling period is $h = 0.25$ sec/sample. Under this sampling rate, the sampling zeros contributed by the unmodeled dynamics are minimum phase, the asymptotic closed-loop system is asymptotically stable, the samples of z converge to zero, but the continuous-time signal $z(t)$ is not zero between consecutive sampling instants as shown in Figure 4.8.

Finally, to improve the intersample behavior, we reduce h to 0.1 sec/sample, and consider $r_2(t)$ again. We have shown in Section 4.5.3 that $G_{zu}(z)$ is NMP for this sampling rate, and predicted that the choice $G_{\mathrm{f}} = H_{0,1}\mathbf{q}^{-1}$ without η-modification would lead to instability, since G_{f} does not capture the NMP zeros of G_{zu}. The first Markov parameters are now $H_{zu,1} = 0.037$, $H_{0,1} = 0.1903$, and we choose $G_{\mathrm{f}} = H_{0,1}\mathbf{q}^{-1}$, $P_0 = 10I$, and $n_{\mathrm{c}} = 10$. RCAC destabilizes the closed-loop system as shown in Figure 4.9. Similar behavior is obtained with $r_1(t)$ and other reference signals, which confirms that the only cause of instability is the unknown NMP sampling zero.

RCAC with η-modification We now introduce η-modification, and reconsider the plant sampled at $h = 0.1$ sec/sample. We let $G_{\mathrm{f}} = H_{0,1}\mathbf{q}^{-1}$. Note that the NMP

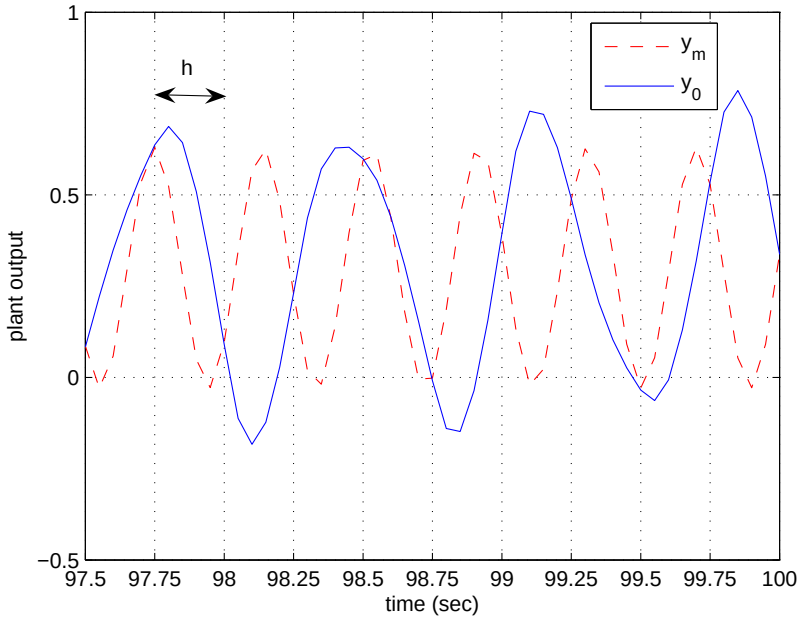

Figure 4.8: Since the Nyquist rate $\omega_{\mathrm{N}} = 4\pi$ rad/sec is smaller than the reference frequency 16.1 rad/sec, the intersample command following error is not zero due to aliasing.

sampling zero -1.82 of G_{zu} is not captured by G_{f}.

We first consider $r_1(t)$. Choosing $\eta_0 = 0.2$, $p_c = 10$, $P_0 = 10I$, and $n_{\mathrm{c}} = 10$, z converges to zero, and the asymptotic closed-loop system is stable with no parameter drift as shown in Figure 4.10.

Keeping the same tuning and controller parameters G_{f}, η_0, P_0, and n_{c}, we now consider $r_2(t) = 0.3 + 1.8\sin(16.1t)$. In order to ensure that no parameter drift occurs, we simulate the adaptive system for 1000 seconds. The performance converges to zero, and the asymptotic closed-loop system is stable with no parameter drift as shown in Figure 4.11. Furthermore, since h is now sufficiently small to avoid aliasing, the command-following error is zero between consecutive sampling instants, as shown in Figure 4.12.

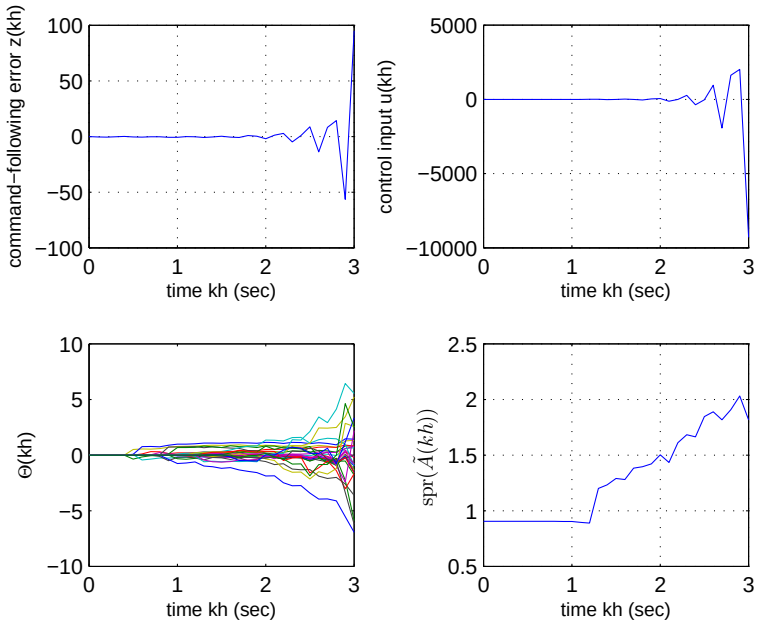

Figure 4.9: Response of RCAC without η-modification. The reference input is $r_2(t) = 0.3 + 1.8\sin(16.1t)$ and the sampling period is $h = 0.1$ sec/sample. Under this sampling rate, the sampling zeros contributed by the unmodeled dynamics are NMP. Since the sampling zeros are unmodeled and are not captured by G_{f}, RCAC without η-modification destabilizes the closed-loop system.

4.5.4.2 Second Rohrs Counterexample: Sensor Noise and Lack of Persistent Excitation

Unknown additive sensor noise is pointed out as the second main robustness challenge for common adaptive methods [84]. In this section, we show that RCAC is unconditionally robust to sensor noise with either construction method.

We consider the unknown additive sensor noise $d(t)$, and modify the measurement vectors y and z to have

$$y(k) \triangleq \begin{bmatrix} y_0(k) + d(k) & r(k) \end{bmatrix}^{\mathrm{T}},$$

$$z(k) \triangleq \begin{bmatrix} y_0(k) + d(k) - y_{\mathrm{M}}(k) \end{bmatrix}.$$

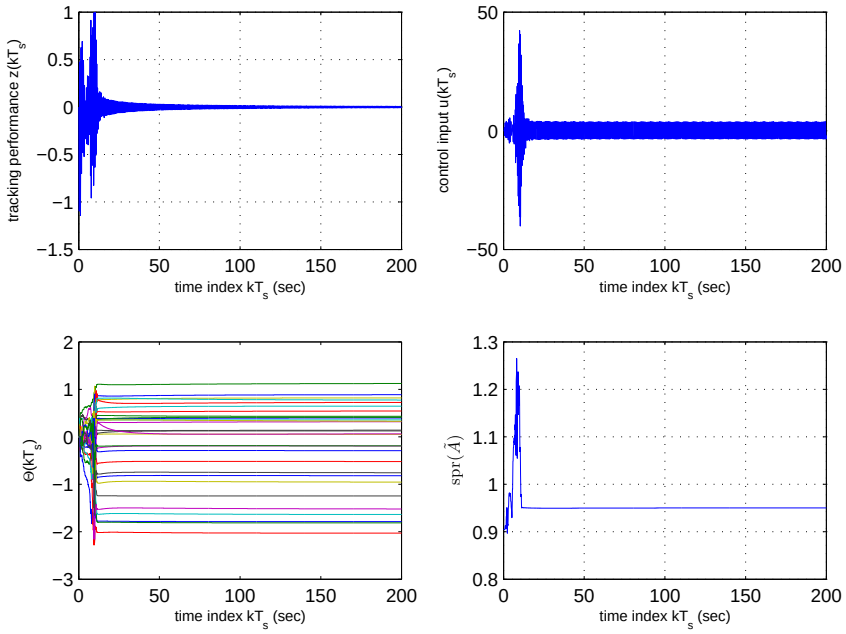

Figure 4.10: Response of RCAC with η-modification. The reference input is $r_1(t) = 0.3+2\sin(8t)$ and the sampling period is $h = 0.1$ sec/sample. Under this sampling rate, the sampling zeros contributed by the unmodeled dynamics are NMP. However, η-modification prevents the adaptive controller from destabilizing the plant, controller gains converge, and z converges to zero, and the asymptotic closed-loop system is stable.

Hence, RCAC interprets the sensor noise as an additional component of the command that needs to be followed. Hence, the performance measurement z is not equal to the command-following error $y_0 - y_{\rm M}$. For illustration, we consider the step reference input $r(t) = 2$, which is persistently exciting of order one, with the unknown sensor noise $d(t) = 0.5\sin 8t$, which is persistently exciting of order two.

RCAC without η-modification We sample the continuous-time plant $h = 0.25$ sec/sample, and thus the sampling zeros are minimum-phase. Choosing $G_{\rm f} = H_{0,1}\mathbf{q}^{-1}$, $n_{\rm c} = 10$, and $P_0 = 10I$, we apply cumulative RCAC without η-modification. The performance measurement (not the command-following error) is driven to zero, the parameters converge, and the asymptotic closed-loop system is stable as shown in

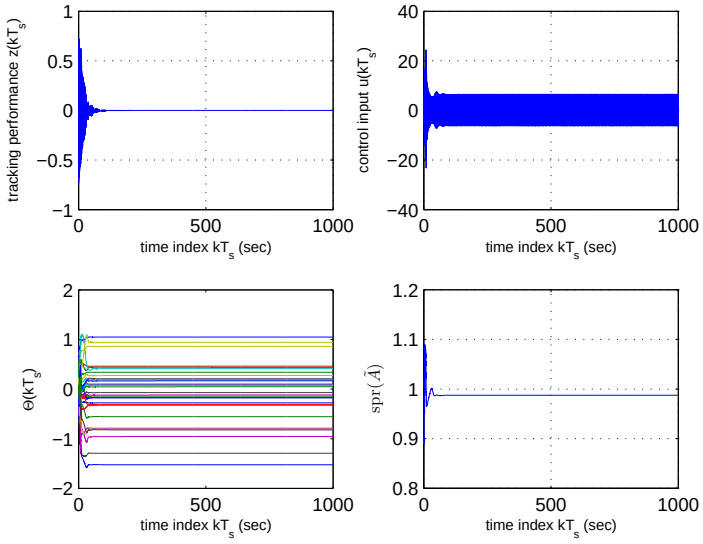

Figure 4.11: Response of RCAC with η-modification. The reference input is $r_2(t) = 0.3 + 1.8\sin(8t)$ and the sampling period is $h = 0.1$ sec/sample. Under this sampling rate, the sampling zeros contributed by the unmodeled dynamics are NMP. However, η-modification prevents the adaptive controller from destabilizing the plant, controller gains converge, and z converges to zero, and the asymptotic closed-loop system is stable.

Figure 4.13.

RCAC with η-modification We now sample the continuous-time plant with $h = 0.1$ sec/sample, and thus one of the sampling zeros is NMP. Choosing $G_{\rm f}(\mathbf{q}^{-1}) = H_{0,1}\mathbf{q}^{-1}$, $\eta_0 = 0.2$, $p_c = 10$, $P_0 = I$, and $n_{\rm c} = 10$, we apply cumulative RCAC with η-modification. The performance measurement reduces to zero, the parameters converge, and the closed-loop system is stable as shown in Figure 4.14.

4.6 Conclusion

In this chapter, we modified the RCAC update laws of Chapter II by incorporating a performance-dependent control penalty into the retrospective cost function. This modification, which we call the η-modification, penalizes the distance between

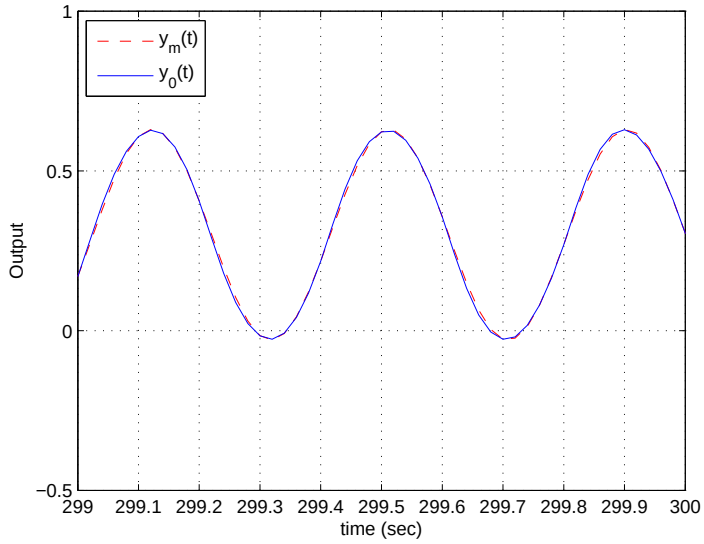

Figure 4.12: Since the Nyquist rate $\omega_{\rm N} = 10\pi$ rad/sec is larger than the reference frequency 16.1 rad/sec, there is no aliasing of exogenous signal aliasing, and the command-following error is zero between consecutive sampling instants.

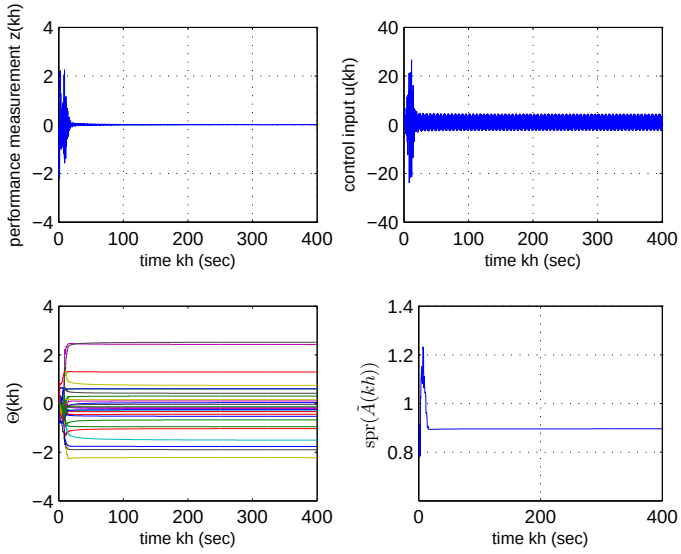

Figure 4.13: RCAC without η-modification: Response to the reference input $r(t) = 2$ and sensor noise $d(t) = 0.5 \sin 8t$ with $h = 0.25$ sec/sample. The performance measurement reduces to zero, the control gains converge, and the asymptotic closed-loop system is stable.

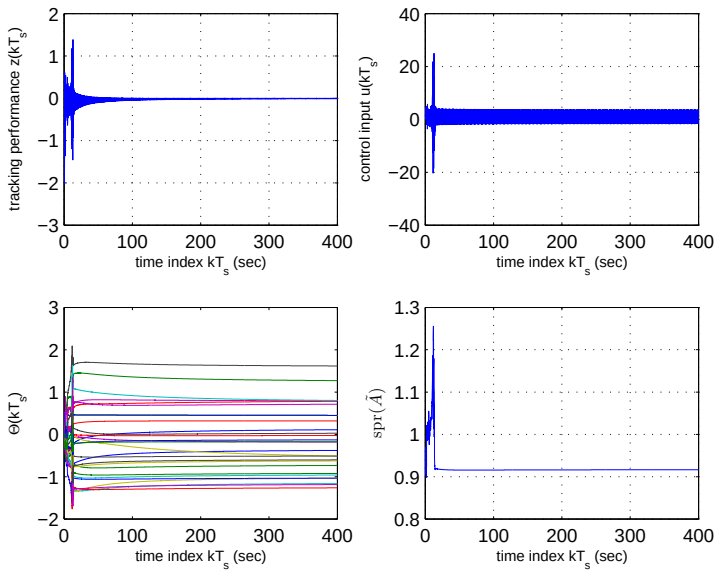

Figure 4.14: RCAC with η-modification: Response to the reference input $r(t) = 2$ and sensor noise $d(t) = 0.5 \sin 8t$ with $h = 0.1$ sec/sample. The performance measurement reduces to zero, the control gains converge, and the asymptotic closed-loop system is stable, despite the unknown NMP sampling zero.

the adaptive controller and an a priori known stabilizing controller on the regressor directions. Therefore, η-modification pushes the control input toward the input signal that would have been generated by the stabilizing controller. In the open-loop stable case, a simple choice for the stabilizing controller is the zero controller, that is, $\Theta = 0$. In this case, the the robustness modification prevents the control input from growing without bound. We presented numerical examples demonstrating RCAC with η-modification for both SISO and MIMO plants. Finally, we applied robust RCAC to Rohrs counterexamples. We demonstrated that the unmodified RCAC update laws of Chapter II exhibit instability when the unknown sampling zero is NMP. However, we showed that the robust RCAC update law with η-modification is able to follow the sinusoidal command despite the unmodeled modes, the unknown sinusoidal disturbance, and the unknown NMP sampling zero.

CHAPTER V

FIR-Based Phase Matching for Robust RCAC

5.1 Introduction

One of the motivations for adaptive control is the desire to minimize the amount of required modeling information [4, 34, 50, 105]. Since an adaptive controller tunes itself to the actual plant, the main benefit of adaptive control is thus the reduced need to model the system for controller tuning without sacrificing performance.

Although model-free adaptive control allows arbitrary plant uncertainty, model-free control may entail large learning transients and may be subject to restrictions on zero locations [46]. Therefore, adaptive controllers typically rely on some plant modeling data, which is obtained through either prior modeling and identification or on-line identification.

In the present chapter we focus on the robust RCAC developed in Chapter V. In Chapter V, the retrospective cost function is modified to include a performance dependent control penalty to remove the need to know the NMP zeros, as well as to reduce the number of required Markov parameters. In particular, it is shown in [102, 97, 98] that in many cases, a single nonzero Markov parameter suffices to achieve convergence of the adaptive controller. However, in this chapter, we present counterexamples in which using a single nonzero Markov parameter does not lead to perfect asymptotic performance. In addition, we conduct a large-scale simulation

with random plants and random controller tuning parameters, and demonstrate that the mismatch between the plant and the finite-impulse-response (FIR) approximation constructed from the chosen set of Markov parameters is highly correlated with the asymptotic performance of the robust RCAC.

The main purpose of this chapter is thus to develop system identification algorithms to match the phase of an IIR transfer function with FIR transfer functions. The underlying goal is to use the FIR transfer function to minimize the phase mismatch, and improve the performance of the robust RCAC. Therefore, we develop FIR fitting methods, both based on least-squares minimization. These system identification methods rely on the frequency response estimates of the IIR transfer function. We present numerical examples illustrating the use of the fit methods developed in this chapter. These identification methods lead to a new phase-matching-based controller construction technique in addition to the Markov-parameter, NMP-zero, and time-series-based construction methods given in Chapter II. We demonstrate the phase-matching-based construction on mass-spring-dashpot systems in the presence of multi-tone sinusoidal disturbances.

5.2 Phase Mismatch

For scalar transfer functions G_{f} and G_{zu}, consider the *phase mismatch* function $\Delta(\Omega)$ defined by

$$\begin{aligned} \Delta : [0, \pi] &\to [0, 180], \\ \Omega &\to \cos^{-1} \frac{\mathrm{Re}\left[G_{zu}(e^{\jmath\Omega})\overline{G_{\mathrm{f}}(e^{\jmath\Omega})}\right]}{|G_{zu}(e^{\jmath\Omega})|\,|G_{\mathrm{f}}(e^{\jmath\Omega})|}. \end{aligned} \tag{5.1}$$

Note that $\Delta(\Omega)$ represents the angle between $G_{zu}(e^{\jmath\Omega})$ and $G_{\mathrm{f}}(e^{\jmath\Omega})$ in the complex plane as illustrated in Figure 5.1. For convenience, we express the phase mismatch

in degrees rather than radians.

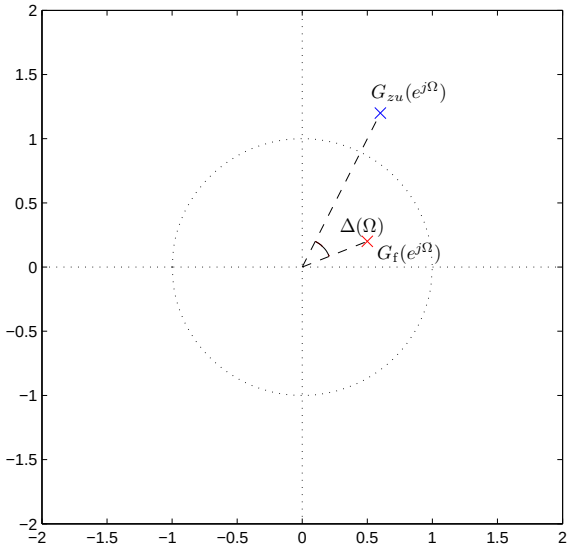

Figure 5.1: Phase mismatch $\Delta(\Omega)$ is the angle between $G_{zu}(e^{\jmath\Omega})$ and $G_{\rm f}(e^{\jmath\Omega})$ in the complex plane.

5.3 Motivating Examples

In this section, we present numerical evidence suggesting that the phase mismatch (5.1) plays a critical role for asymptotic performance of robust RCAC with η-modification.

5.3.1 Example 1: Step Command Following

Consider the NMP plant G_{zu} with $d = 1$, $H_1 = 1$, poles $\{0.7, 0.5, 0.4 \pm \jmath 0.5\}$, and zeros $\{1.2, 1.1 \pm \jmath 0.7\}$. We consider the step command $w(k) = \mathbf{1}(k)$. Assuming that the NMP zeros are unknown, we take $G_{\rm f}(\mathbf{q}^{-1}) = H_1\mathbf{q}^{-1}$, and apply cumulative RCAC with η-modification using the parameters $\eta_0 = 0.1$, $p_c = 10$, $\lambda = 1$, and $P_0 = 10I$. The phase mismatch $\Delta(\Omega)$ and the closed-loop response are illustrated in Figure 5.2.

Note that $\Delta(0) = 180$ deg. The asymptotic closed-loop system is stable, but the performance z does not reduce to zero.

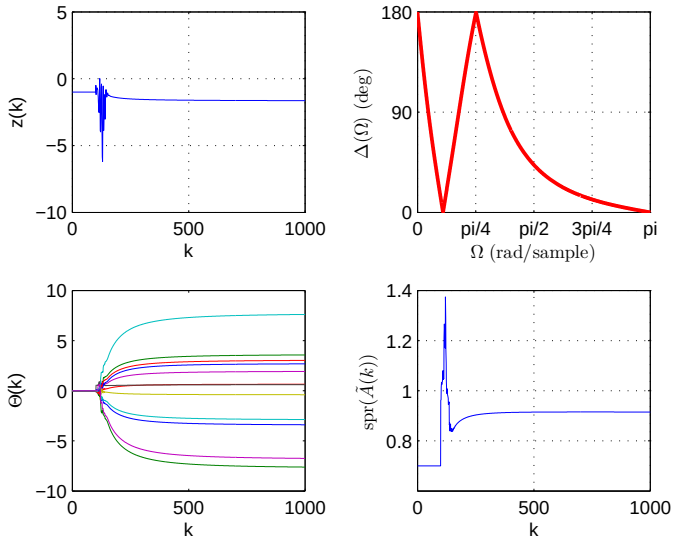

Figure 5.2: Example 1: Step command following, NMP plant, $G_{\rm f}(\mathbf{q}^{-1})$ is constructed using H_1. With this choice of $G_{\rm f}$, the phase mismatch $\Delta(\Omega)$ is 180 deg at the command frequency 0 rad/sample. The controller converges, and the asymptotic closed-loop system is asymptotically stable, but the performance z does not converge to zero. In fact, RCAC drives z to the opposite direction, and the closed-loop performance is worse than the open-loop performance.

We now consider the same plant and the same step command, but, assuming the knowledge of H_1 and H_2 is available, we now take $G_{\rm f}(\mathbf{q}^{-1}) = H_1\mathbf{q}^{-1} + H_2\mathbf{q}^{-2}$. Therefore, we use the Markov-parameter-based construction (2.48) with $r = 2$. Note that $G_{\rm f}(\mathbf{q}^{-1})$ still does not capture the NMP zeros of G_{zu}, therefore, we apply cumulative RCAC with η-modification using the same tuning parameters as above. The phase mismatch $\Delta(\Omega)$ and the closed-loop response are illustrated in Figure 5.3. Note that $\Delta(0) = 0$ deg. The asymptotic closed-loop system is stable, and the performance z now reduces to zero after learning transients.

We now consider the same plant and the same step command, but now take $G_{\rm f}(\mathbf{q}^{-1}) = -0.1\mathbf{q}^{-1}$. Note that -0.1 is not a Markov parameter or a time-series

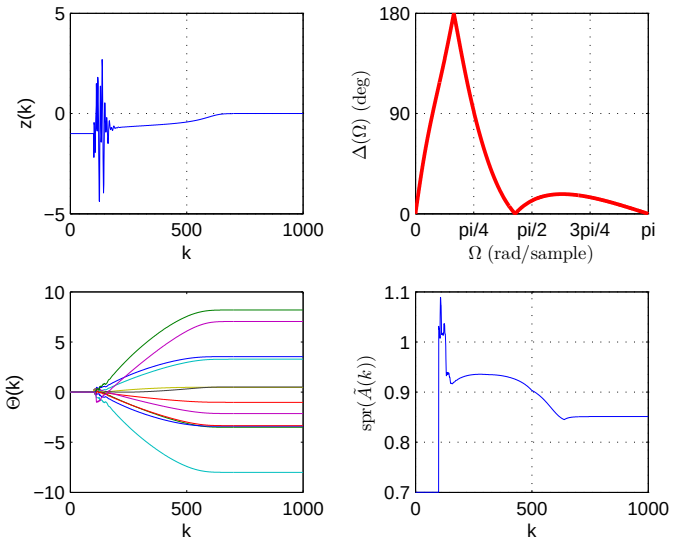

Figure 5.3: Example 1: Step command following, NMP plant, G_{f} is constructed using H_1 and H_2. With this choice of G_{f}, we have $\Delta(0) = 0$ deg. The controller converges, the asymptotic closed-loop system is asymptotically stable, and the performance z now reduces to zero.

coefficient of G_{zu}, and it has the opposite sign of $H_1 = 1$. We choose $\eta_0 = 1$, $p_c = 10$, $P_0 = 100I$, and apply cumulative RCAC with η-modification. The phase mismatch $\Delta(\Omega)$ and the closed-loop response are illustrated in Figure 5.4. Note that $\Delta(0) = 0$ deg. The asymptotic closed-loop system is stable, and the performance z reduces to zero after learning transients.

5.3.2 Example 2: Sinusoidal Command Following

We consider the same plant as in Section 5.3.1, but now consider the sinusoidal command $w(k) = \sin \omega k$, where $\omega = 0.52$ rad/sample. We first take $G_{\mathrm{f}}(\mathbf{q}^{-1}) = H_1\mathbf{q}^{-1} + H_2\mathbf{q}^{-2}$, which led to zero asymptotic command-following-performance for step command. However, with this choice of G_{f}, the phase mismatch at the command frequency ω is $\Delta(0.52) = 179.3$ deg. We choose $\eta_0 = 1$, $p_c = 1$, $P_0 = 10I$, and apply cumulative RCAC with η-modification. The closed-loop response is illustrated in Figure 5.5. The asymptotic closed-loop system is stable, but the performance z does

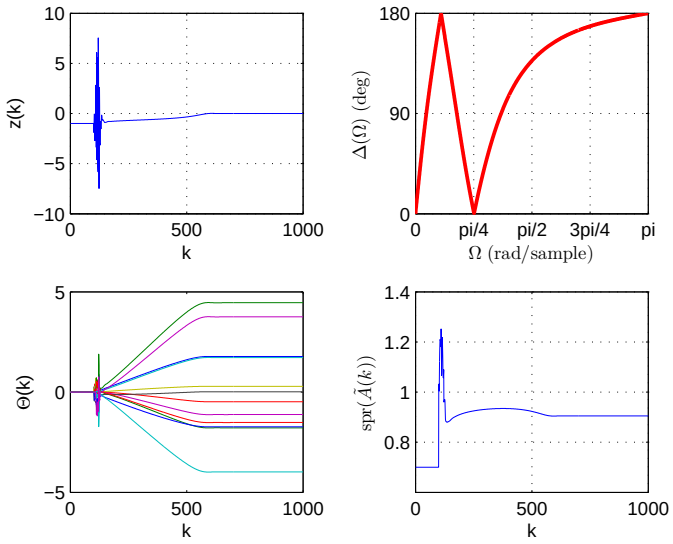

Figure 5.4: Example 1: Step command following, NMP plant, we take $G_{\rm f}(\mathbf{q}^{-1}) = -0.1\mathbf{q}^{-1}$. With this choice of $G_{\rm f}$, we have $\Delta(0) = 0$ deg. The controller converges, the asymptotic closed-loop system is asymptotically stable, and the performance z reduces to zero.

not reduce to zero.

We now consider the same plant and the same sinusoidal command, but now take $G_{\rm f}(\mathbf{q}^{-1}) = H_1\mathbf{q}^{-1}$ and thus use less modeling information. However, with this choice of $G_{\rm f}$, we now have $\Delta(0.52) = 73.6$ deg. We choose $\eta_0 = 1$, $p_c = 1$, $P_0 = 10I$, and apply cumulative RCAC with η-modification. The closed-loop response is illustrated in Figure 5.6. The asymptotic closed-loop system is stable, and the performance z now reduces to zero after learning transients.

5.3.3 Large-Scale Monte Carlo Simulations

In this section, we present a numerical investigation of the closed-loop stability and performance characteristics of RCAC with η-modification for open-loop stable plants.

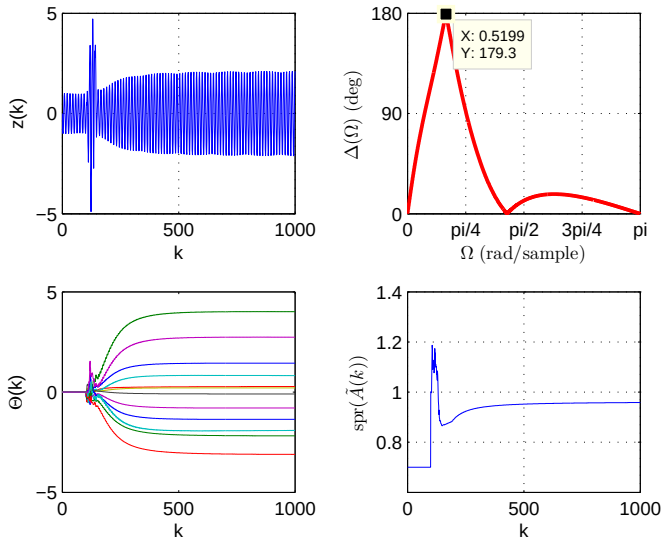

Figure 5.5: Example 2: Sinusoidal command following, NMP plant, $G_{\mathrm{f}}(\mathbf{q}^{-1})$ is constructed using H_1 and H_2. With this choice of G_{f}, we have $\Delta(\omega) = 179.3$ deg at the command frequency $\omega = 0.52$ rad/sample. The controller converges, and the asymptotic closed-loop system is asymptotically stable, but the performance z does not converge to zero. In fact, the closed-loop performance is worse than the open-loop performance.

5.3.3.1 Simulation Setup

The large-scale simulation parameters are set up as follows. In each simulation, we turn on the robust cumulative update law at $k = 100$, and simulate the adaptive system for 2000 time steps. In this study, we only consider sinusoidal command following with $E_0 = -1$, where the frequency of the sinusoid is chosen randomly from the uniform distribution on the interval $\omega \in [0.01, \pi/2]$ rad/sample, and the peak amplitude of the sinusoid is fixed at one in each case. In each simulation, the plant is SISO, $y = z$, and the plant parameters are chosen randomly. Specifically, the order n takes values from the uniform distribution on the set $\{2, \ldots, 10\}$, and the matrices A, B, E_1 are matrices of appropriate sizes, generated randomly using "randn" command in MATLAB. In this study, we set $\Theta^* = 0$, which limits out consideration to Lyapunov stable plants. Therefore, in each simulation, we ensure

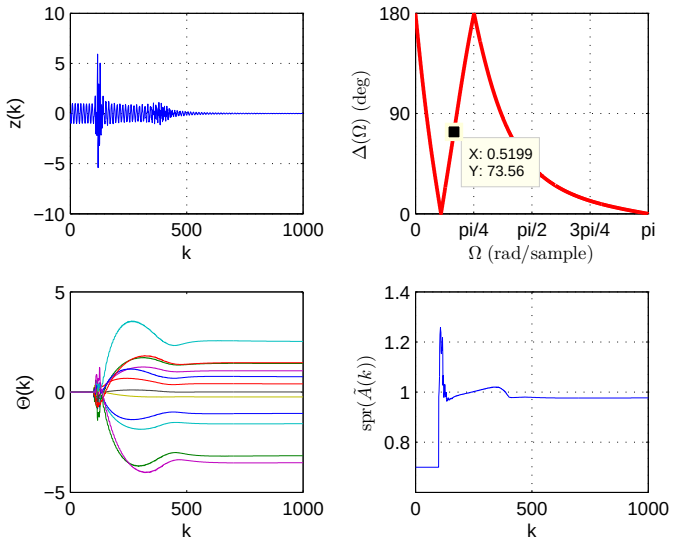

Figure 5.6: Example 2: Sinusoidal command following, NMP plant, $G_{\mathrm{f}}(\mathbf{q}^{-1})$ is constructed using H_1. With this choice of G_{f}, we have $\Delta(\omega) = 73.6$ deg at the command frequency $\omega = 0.52$ rad/sample. The controller converges, the asymptotic closed-loop system is asymptotically stable, and the performance z now reduces to zero.

that the open-loop plant is Lyapunov stable by multiplying A with $c\rho(A)$, where c takes values from the uniform distribution on the interval $[0, 1]$, and $\rho(A)$ is the spectral radius of A. After the state space matrices are generated, the state x is initialized to a random unit vector of appropriate size. In each simulation, we choose the tuning and controller parameters $n_{\mathrm{c}} = n + 2$, $\lambda = 1$, $p_{\mathrm{c}} = 1$, $P_0 = I$, $G_{\mathrm{f}}(\mathbf{q}^{-1}) = H_1\mathbf{q}^{-1}$, $\eta_1 = 0.005$, and, we choose η_0 from the uniform distribution on the interval $[0.5, 2]$. It should be stressed that, in a practical application, the control parameters may require a moderate amount of tuning effort in order to improve transient and steady-state performance. For the subsequent discussion, let z_{rms} denote the RMS value of the closed-loop performance calculated for $k \in [1901, 2000]$, and let $\|\Delta\Theta\|_{\mathrm{rms}}$ denote the RMS value of $\|\Delta\Theta(k)\| = \|\Theta(k) - \Theta(k-1)\|$. We use these values to compare the closed-loop RMS performance to the open-loop RMS performance and numerically assess the convergence of the controller Θ.

5.3.3.2 Simulation Results

We ran a total of 10000 simulations with the simulation setup described above. In 3240 cases, G_{zu} was NMP, and in the remaining cases, G_{zu} was minimum phase. In 3337 cases, we had $2 \leq n \leq 4$, in 3288 cases, we had $5 \leq n \leq 7$, and in the remaining 3375 cases, we had $8 \leq n \leq 10$. In 4953 cases, the normalized open-loop spectral radius $\rho(A)$ satisfied $0 \leq \rho(A) \leq 0.5$, in 3979 cases, we had $0.5 < \rho(A) \leq 0.9$, and, in the remaining 1068 cases, we had $0.9 < \rho(A) \leq 1$. Finally, we had 7713 cases with $\Delta(\omega) \leq 45$ deg, 1300 cases with $45 < \Delta(\omega) \leq 90$ deg, 575 cases with $90 < \Delta(\omega) \leq 135$, and 412 cases with $135 < \Delta(\omega) \leq 180$ deg, where ω is the command frequency. The distribution of these plant parameters is shown in Table 5.3.3.2. It should be noted that, as expected, the parameters n and $\rho(A)$ are uniformly distributed as expected from simulation setup. However, the number of minimum phase plants was about two times more than the number of NMP plants. This suggests that the random construction of A, B and E_1 using the MATLAB "randn" command is more likely to lead to a minimum phase plant G_{zu}. Furthermore, note that the phase mismatch $\Delta(\omega)$ was less than 45 deg in most cases. This outcome may be correlated with the bias in favor of minimum phase cases.

In order to evaluate the closed-loop performance at each sample, we calculate $\|\Delta\Theta\|_{\text{rms}}$, z_{rms}, and $\rho(\tilde{A}(2000))$ at the end of each simulation. For evaluating the improvement in the closed-loop performance, we compare z_{rms} with the open-loop RMS performance. If $z_{\text{rms}} < \%100$, then the closed-loop RMS performance is smaller than the open-loop RMS performance. For evaluating the convergence of Θ, we calculate the normalized RMS controller update $\|\Delta\Theta\|_{norm} \stackrel{\triangle}{=} \frac{\|\Delta\Theta\|_{\text{rms}}}{\|\Theta(2000)\|}$, which is a measure of total adaptation that took place in the final 100 steps of each simulation. Distribution of these performance measures is shown in Table 5.3.3.2. Note that in more than 99% of the simulations, the normalized RMS controller update is less than 10^{-3}, which suggests that the controller converged in almost all cases. Furthermore,

Plant Parameter		Number of Samples	Percentage
Zeros	MP	6760	68%
	NMP	3240	32%
Order	$2 \leq n \leq 4$	3337	33%
	$5 \leq n \leq 7$	3288	33%
	$8 \leq n \leq 10$	3375	34%
Spectral radius	$0 \leq \rho(A) \leq 0.5$	4953	50%
	$0.5 < \rho(A) \leq 0.9$	3979	40%
	$0.9 < \rho(A) < 1$	1068	11%
Phase mismatch	$0 \leq \Delta(\omega) \leq 45$	7713	77%
	$45 < \Delta(\omega) \leq 90$	1300	13%
	$90 < \Delta(\omega) \leq 135$	575	6%
	$135 < \Delta(\omega) \leq 180$	412	4%

Table 5.1: Distribution of plant parameters for the large-scale simulation with 10000 samples.

97% of the simulations resulted in an asymptotic closed-loop system with spectral radius less than 1. Furthermore, in 94% of the simulations, the closed-loop RMS performance was smaller than the open-loop RMS performance. It should be noted that all simulations resulted in bounded closed-loop performance.

Finally, we investigate the correlations between the open-loop plant parameters and the closed-loop RMS performance level. Figure 5.7 shows the correlation between z_{rms} and the order of the open-loop plant, Figure 5.8 shows the correlation between z_{rms} and the spectral radius of the open-loop system, and, finally, Figure 5.9 shows the correlation between z_{rms} and the phase mismatch $\Delta(\omega)$ between the open-loop plant and G_{f} at the command frequency ω. Figure 5.7 suggests that the plant order does not have a significant effect on z_{rms}. Figure 5.8 shows that there is a moderate amount of correlation between the open-loop spectral radius and z_{rms}. Specifically, as the open-loop spectral radius increases, z_{rms} increases. However, Figure 5.9 shows that the phase mismatch $\Delta(\omega)$ is the most important factor in closed-loop RMS performance. Specifically, almost all the simulations with $\Delta(\omega) \leq 45$ deg led to improved closed-loop

Performance measure		Number of Samples	Percentage
Convergence of Θ	$0 \leq \|\Delta\Theta\|_{\text{norm}} \leq 10^{-6}$	8390	84%
	$10^{-6} < \|\Delta\Theta\|_{\text{norm}} \leq 10^{-3}$	1607	16%
	$\|\Delta\Theta\|_{\text{norm}} > 10^{-3}$	3	<1%
Closed-loop stability	$0 \leq \rho(\tilde{A}) < 1$	9710	97%
	$1 \leq \rho(\tilde{A}) < 1.01$	207	2%
	$1.01 \leq \rho(\tilde{A}) < 1.1$	81	1%
	$\rho(\tilde{A}) \geq 1.1$	2	<1%
Closed-loop performance	$0 \leq z_{\text{rms}} \leq 10\%$	8808	88%
	$10\% < z_{\text{rms}} \leq 100\%$	567	6%
	$100\% < z_{\text{rms}} \leq 1000\%$	572	6%
	$1000\% < z_{\text{rms}} \leq 10000\%$	53	1%

Table 5.2: Distribution of closed-loop performance metrics for the large-scale simulation with 10000 samples.

performance compared to open-loop, whereas, in 88% of the cases with $\Delta(\omega) \geq 135$ deg, the closed-loop performance was worse than the open-loop performance. In fact, the most intriguing part of this numerical study is that, although $\Delta(\omega) > 90\%$ took place in only about 10% of simulations, it accounted for 81% of the cases where z_{rms} was larger than the open-loop RMS performance. Therefore, these results suggest that phase matching is a significant factor influencing the asymptotic closed-loop performance of RCAC with η-modification.

5.4 FIR Fitting Methods for Minimizing Phase Mismatch

The numerical results of the previous section suggest that the closed-loop performance of RCAC with η-modification is highly correlated with the phase mismatch. Specifically, numerical results suggest that the closed-loop performance gets progressively better as the phase mismatch at the exogenous frequency is reduced. In this section, we formulate two least-squares-based methods to fit an IIR transfer function with an FIR transfer function to minimize the phase mismatch at a predefined set of frequencies. The underlying goal is to increase the closed-loop performance obtained

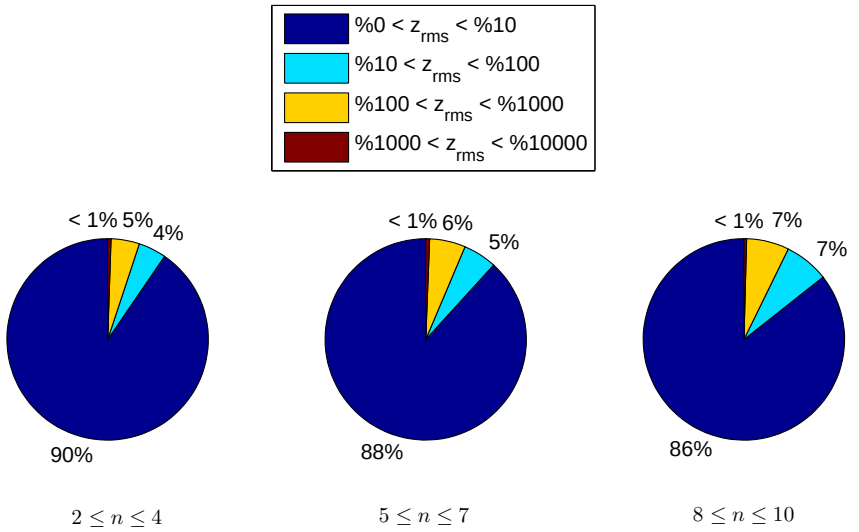

Figure 5.7: The plant order has a marginal effect on closed-loop RMS performance.

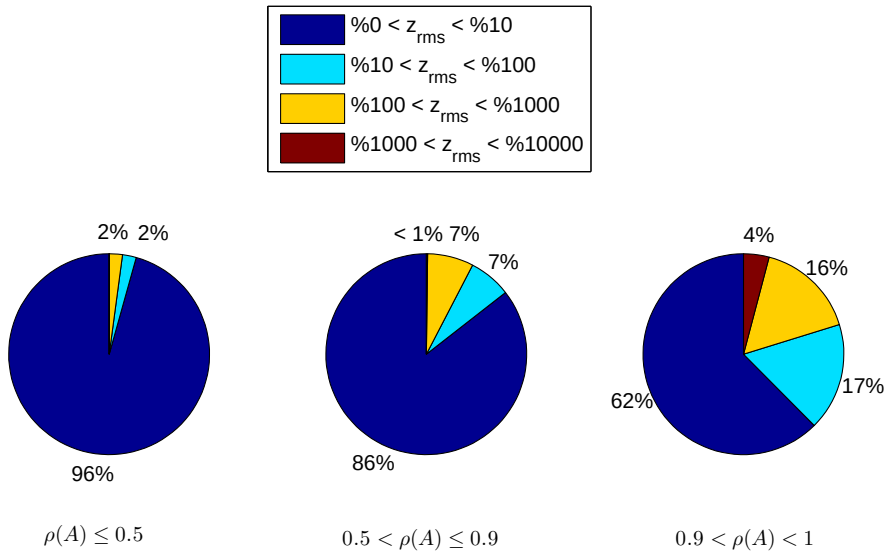

Figure 5.8: Open-loop spectral radius has a moderate effect on closed-loop RMS performance. As $\rho(A)$ increases, the closed-loop performance becomes poorer. This figure suggests that RCAC with η-modification may lead to better performance on plants with smaller spectral radius.

with RCAC when η-modification is employed.

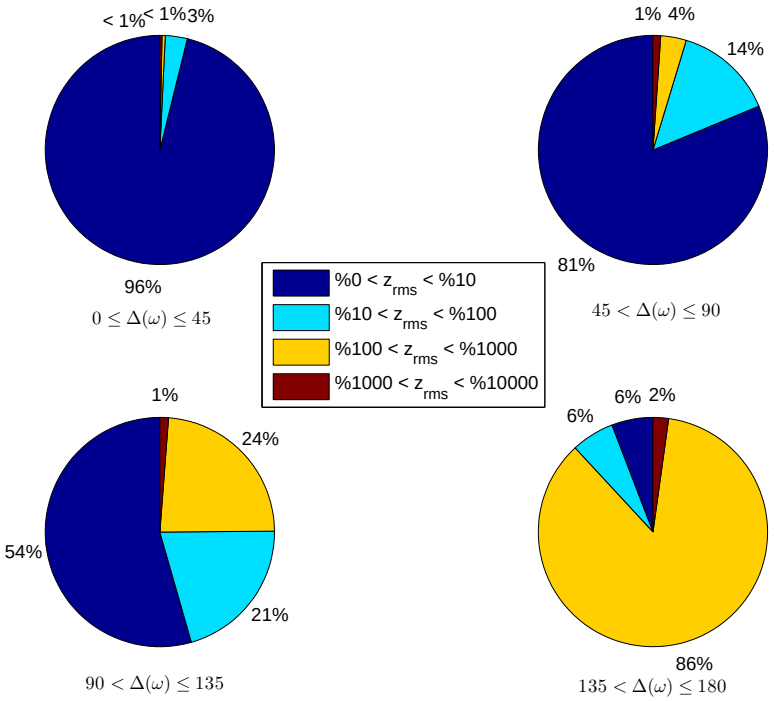

Figure 5.9: This figure illustrates that the closed-loop performance of RCAC with η-modification is highly correlated with the phase mismatch $\Delta(\omega)$ at the command frequency ω. The likelihood of obtaining improved closed-loop performance progressively drops as the phase mismatch increases. For the case $\Delta(\omega) \le 45$ deg, almost all simulations lead to improved performance compared to open-loop. For the case $\Delta(\omega) > 135$ deg, 88% of simulations resulted in poorer closed-loop performance compared to open-loop. These results suggest that the phase mismatch is critical for obtaining acceptable closed-loop performance with RCAC when η-modification is employed.

5.4.1 Linear FIR Fitting Method

In this section, we formulate a constrained linear least squares method that fits the frequency response of G_{zu} with an FIR transfer function G_{f}. We assume that an estimate of the frequency response of the plant $G_{zu}(e^{\jmath\theta})$ is available at a finite number of frequencies. This knowledge can be obtained through either modeling or frequency-domain identification. We constrain the least squares solution to bound the phase mismatch $\Delta(\theta)$ over a chosen frequency interval $[\theta_l, \theta_h]$, where $0 \le \theta_l < \theta_h \le \pi$.

The phase mismatch bound does not need to be uniform over $[\theta_l, \theta_h]$. Furthermore, the largest bound that we allow is 90 deg. Finally, we show that the numerator coefficients of G_{f} obtained by using the unconstrained least squares solution are Markov parameters of G_{zu}. However, this is not the case when phase constraints are imposed.

5.4.1.1 Linear Least Squares Parametric Model

For $1 \leq i \leq N$, consider the frequency response estimates

$$\hat{G}_{zu}(e^{\jmath\theta_i}) = \alpha_i + \jmath\beta_i, \tag{5.2}$$

at the frequencies θ_i, where $\alpha_i \in \mathbb{R}$, $\beta_i \in \mathbb{R}$. The goal is to fit the above estimates with the FIR transfer function

$$G_{\mathrm{f}}(z) \triangleq \frac{\kappa_1 z^{s-1} + \cdots + \kappa_{s-1} z + \kappa_s}{z^s}, \tag{5.3}$$

where s is the order of the FIR model, and $\kappa_i \in \mathbb{R}$ are the corresponding numerator coefficients that will be determined. We now expand (5.3) into the Laurent series

$$G_{\mathrm{f}}(z) = \kappa_1 z^{-1} + \cdots + \kappa_s z^s, \tag{5.4}$$

which is finite since G_{f} is an FIR transfer function. We now evaluate (5.4) at $e^{\jmath\theta_i}$ for $i = 1, \ldots, N$, and separate the unknown parameters κ_i to obtain the linear parametric model

$$\begin{aligned} G_{\mathrm{f}}(z)\big|_{e^{\jmath\theta_i}} &= \kappa_1 e^{-\jmath\theta_i} + \cdots + \kappa_s e^{-\jmath s\theta_i} \\ &= \begin{bmatrix} \kappa_1 & \cdots & \kappa_s \end{bmatrix} \Big(\begin{bmatrix} \cos\theta_i & \cdots & \cos(s\theta_i) \end{bmatrix}^{\mathrm{T}} \\ &\quad + \jmath \begin{bmatrix} -\sin\theta_i & \cdots & -\sin(s\theta_i) \end{bmatrix}^{\mathrm{T}} \Big). \end{aligned} \tag{5.5}$$

Then, the linear least squares fit of (5.2) with the FIR parametric model (5.5) is obtained by minimizing

$$\min_X \|Y - \Phi^{\mathrm{T}} X\|, \tag{5.6}$$

where

$$Y = \begin{bmatrix} \alpha_1 & \cdots & \alpha_N & \beta_1 & \cdots & \beta_N \end{bmatrix}^{\mathrm{T}}, \tag{5.7}$$

$$\Phi = \begin{bmatrix} \cos\theta_1 & \cdots & \cos\theta_N & -\sin\theta_1 & \cdots & -\sin\theta_N \\ \vdots & & \vdots & \vdots & & \vdots \\ \cos(s\theta_1) & \cdots & \cos(s\theta_N) & -\sin(s\theta_1) & \cdots & -\sin(s\theta_N) \end{bmatrix}, \tag{5.8}$$

$$X = \begin{bmatrix} \kappa_1 & \cdots & \kappa_s \end{bmatrix}^{\mathrm{T}}. \tag{5.9}$$

5.4.1.2 Phase Mismatch Constraints

To impose phase mismatch bounds on the solution X of (5.6), we consider the constrained linear least squares problem

$$\min_X \|Y - \Phi^{\mathrm{T}} X\|, \quad \text{subject to} \quad \mathcal{C}X \leq 0, \tag{5.10}$$

where $\mathcal{C}$ is constructed based on the phase information of each $\hat{G}_{zu}(e^{\jmath\theta_i})$ and the desired phase mismatch bounds at each frequency.

For example, consider the frequency-response estimate $\hat{G}_{zu}(e^{\jmath\theta_m}) = \alpha_m + \jmath\beta_m$, and the phase mismatch bound $\bar{\Delta}_m \in (0, 90)$ deg imposed on $\Delta(\theta)$ at the frequency θ_m. Then, the linear phase mismatch bounds $\mathrm{Im}(x) = u_m \mathrm{Re}(x)$ and $\mathrm{Im}(x) = l_m \mathrm{Re}(x)$ are determined by $\bar{\Delta}_m$ as shown in Figure 5.10. The slopes u_m and l_m are given by

$$u_m \stackrel{\triangle}{=} \tan(\angle(\alpha_m + \jmath\beta_m) + \bar{\Delta}_m), \tag{5.11}$$

$$l_m \stackrel{\triangle}{=} \tan(\angle(\alpha_m + \jmath\beta_m) - \bar{\Delta}_m). \tag{5.12}$$

Since $u_m \geq \frac{\beta_m}{\alpha_m} \geq l_m$, and $\alpha_m > 0$, we have the inequality constraints $\beta_m - u_m\alpha_m \leq 0$ and $l_m\alpha_m - \beta_m \leq 0$. Then, the linear constraint that needs to be imposed on X to bound $\Delta(\theta_m)$ by $\bar{\Delta}_m$ is given by

$$\mathcal{C}_m X \leq 0, \quad \mathcal{C}_m = \begin{bmatrix} l_m\Phi^{\mathrm{T}}(m,:) - \Phi^{\mathrm{T}}(N+m,:) \\ \Phi^{\mathrm{T}}(N+m,:) - u_m\Phi^{\mathrm{T}}(m,:) \end{bmatrix},$$

and $\Phi^{\mathrm{T}}(m,:)$ represents the m^{th} row of Φ^{T}.

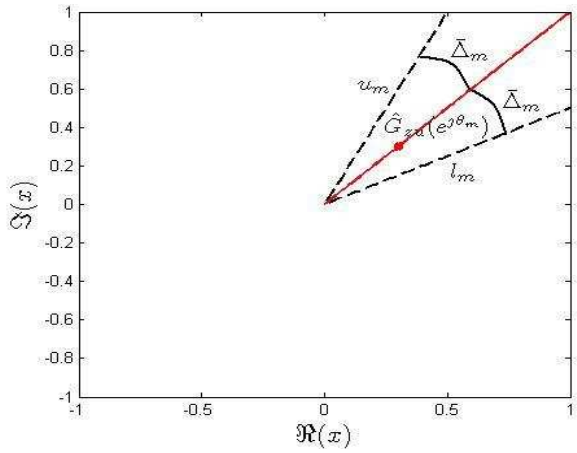

Figure 5.10: $\hat{G}_{zu}(e^{j\theta_m})$, the linear upper bound u_m and the linear lower bound l_m. Note that u_m and l_m are the slopes of the dashed black lines, and are given by (5.11), (5.12) respectively.

The above procedure is carried out for each frequency $\theta_1, \ldots, \theta_N$ to construct the constraint matrix

$$\mathcal{C} = \begin{bmatrix} \mathcal{C}_1 & \cdots & \mathcal{C}_N \end{bmatrix}^{\mathrm{T}} \in \mathbb{R}^{2N \times s}.$$

Note that there are 4 possible constraint inequality conditions corresponding to 12 possible configurations of u_m and l_m, all of which are illustrated in Figure 5.11.

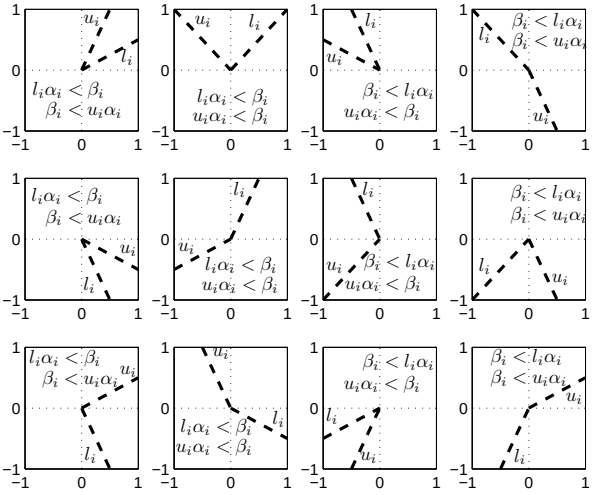

Figure 5.11: Possible bound configurations and associated linear constraints.

5.4.1.3 Special Case: Unconstrained Least Squares Solution

We now illustrate the unconstrained least squares solution of (5.6) with exact frequency response estimates (5.2) of G_{zu}. Consider

$$G_{zu}(z) = 12\frac{(z-1.4)(z-0.6)(z-0.4)}{(z-0.85)(z-0.5)(z-0.3+0.8\jmath)(z-0.3-0.8\jmath)}.$$

We apply unconstrained least squares fitting using exact frequency response estimates $\hat{G}_{zu}(e^{\jmath\theta_i}) = G_{zu}(e^{\jmath\theta_i})$, where θ_i are equally placed between 0 and π. We let the order of G_{f} be $s = 10$. Figure 5.12 shows that the estimated coefficients $\kappa_1, \ldots, \kappa_{10}$ converge to the Markov parameters $H_1, \ldots, H_{10}$ as the number of data points used in the estimation is increased.

5.4.2 Nonlinear FIR Fitting Method

We now develop a nonlinear parameterization to fit the phase plot of G_{zu} with the phase of an FIR transfer function. This nonlinear formulation requires only an estimate of the phase plot of G_{zu} in $[\theta_l, \theta_h]$, and thus it requires less modeling information than the linear method presented in the previous section.

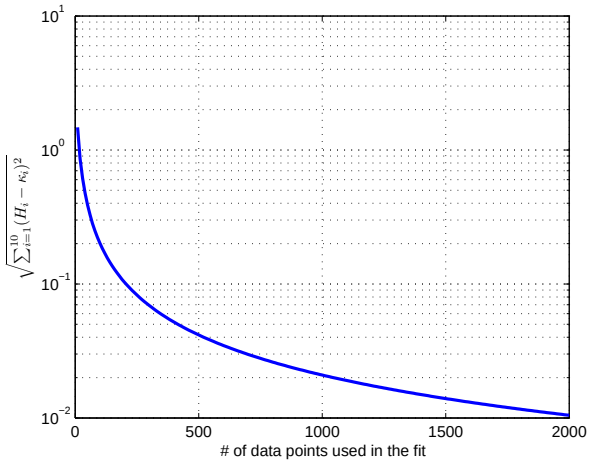

Figure 5.12: Unconstrained linear least squares solution converges to Markov parameters of G_{zu}.

For $1 \leq i \leq N$, let

$$\phi(\theta_i) \stackrel{\triangle}{=} \angle \hat{G}_{zu}(e^{\jmath\theta_i}) \in [0, 360), \tag{5.13}$$

be the estimates of the phase of G_{zu} at frequencies $0 \leq \theta_1 \leq \ldots \leq \theta_N \leq \pi$. The goal is to fit the above phase estimates using the phase plot of the FIR model (5.3). Let $g(\theta_i)$ denote the phase $\angle G_{\text{FIR}}(e^{\jmath\theta})$ of the FIR model evaluated at the frequency θ_i. Then, it follows from (5.5) that

$$\begin{aligned} g(\theta_i) &= \angle \left(\kappa_1 e^{-\jmath\theta_i} + \cdots + \kappa_s e^{\jmath s\theta_i} \right) \\ &= \angle \sigma_i + \jmath \omega_i \\ &= \text{atan2}(\omega_i, \sigma_i) \end{aligned}$$

where

$$\sigma_i = \sum_{l=1}^{s} \kappa_l \cos(l\theta_i), \quad \omega_i = -\sum_{l=1}^{s} \kappa_l \sin(l\theta_i),$$

and atan2 is the four-quadrant inverse of the tangent function mapped to $[0, 360)$.

Then, the phase mismatch $\Delta(\theta_i)$ is

$$\Delta(\theta_i) = \min\left(\phi(\theta_i) - g(\theta_i) \mod 360,\right.$$
$$\left. 360 - (\phi(\theta_i) - g(\theta_i) \mod 360)\right). \tag{5.14}$$

Now, solving the minimization problem

$$\min_{\kappa_i} \sum_{l=1}^{N} \|\Delta(\theta_l)\| \tag{5.15}$$

yields the numerator coefficients κ_i of the FIR approximation G_{FIR} that provides the best phase matching with the estimated phase plot (5.13) of G_{zu}.

5.5 FIR Fitting Examples

We now present numerical examples illustrating the use of linear and nonlinear fitting methods for minimizing $\Delta(\theta)$. We use numerical optimization tools for both linear and nonlinear fitting; we use the MATLAB functions *lsqlin* for minimizing (5.10), and *lsqnonlin* for minimizing (5.15).

The constrained minimization problem (5.10) may not have a solution if the chosen order of the FIR fit is too small to satisfy the constraints. If that is the case, we increase the order of the FIR fit until the minimization problem is feasible.

Since we are using only the phase information (5.13) in the nonlinear method, scaling each coefficient κ_i by a positive constant γ results in the same cost value (5.15). In order to avoid numerical problems that can arise, we first fix $\kappa_1 = 1$, and solve for κ_i, $2 \leq i \leq s$. Next, we fix $\kappa_1 = -1$, and repeat the process. Finally, we compare the residuals and take the solution with the smaller residual norm.

Example 5.5.1. Consider the plant $G_{zu}(z)$ with $H_1 = 1$, poles 0.1, 0.5 ± 0.3, 0.85, 0, minimum-phase zero 0.45, and NMP zeros 1.5, 1.2 ± 0.5. We first assume we

have the exact knowledge of the frequency response $G_{zu}(e^{\jmath\theta_i})$ at 1001 equally spaced frequencies in $[0, \pi]$. With this knowledge, we apply linear fitting to uniformly bound the phase mismatch $\Delta(\theta)$ by $\bar{\Delta}_1 = 80$ deg, $\bar{\Delta}_2 = 40$ deg, and $\bar{\Delta}_3 = 10$ deg. Figure 5.13 shows the phase mismatch functions of the resulting FIR approximations. Note that the order of the FIR fit increases as the phase mismatch bound becomes tighter.

We now assume that we do not have complete frequency response information of G_{zu}, but we do have exact knowledge of the phase plot at the above specified frequencies. With this knowledge, we apply nonlinear fitting to minimize $\Delta(\theta)$ over $[0, \pi]$. Figure 5.14 shows the phase mismatch functions of the resulting FIR approximations with orders $s = 4$, 5, and 7.

We now assume we have no frequency domain knowledge of G_{zu}, but we have exact knowledge of Markov parameters. With this knowledge, we construct 4^{th}, 5^{th} and 7^{th}-order FIR plants, the phase mismatch functions of which are illustrated in Figure 5.15. Note that $\Delta(0) = 180$ deg in each case. ■

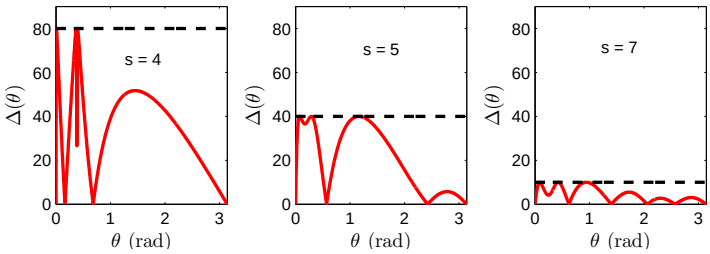

Figure 5.13: Ex1: Lin Fit.

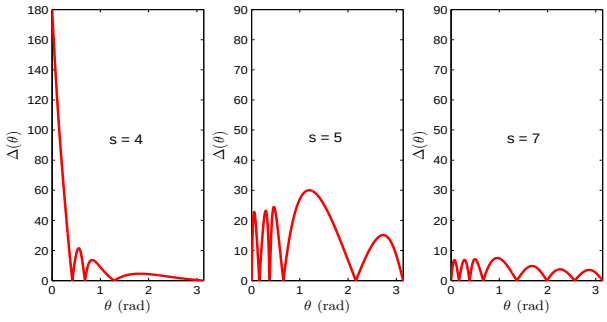

Figure 5.14: Ex1: NonLin Fit.

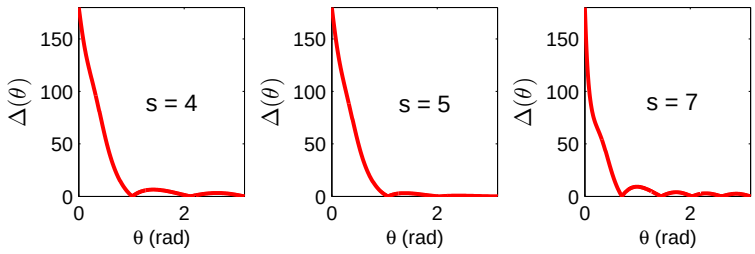

Figure 5.15: Ex1: MP Fit.

Example 5.5.2. Consider the same plant G_{zu} as in Example 5.5.1, and assume we have the exact knowledge of the frequency response $G_{zu}(e^{\jmath\theta_i})$ at 1001 equally spaced frequencies in $[0, \pi]$. Suppose we are interested in tracking sinusoids at a particular frequency range with RCAC. Therefore, the objective is to impose nonuniform bounds that are tighter at the frequencies of interest. In particular, we consider three cases: smaller mismatch at low frequencies, smaller mismatch at high frequencies, and smaller mismatch at intermediate frequencies. Furthermore, to have robustness at all frequencies, we want $\Delta(\theta) < 90$ deg for all $\theta \in [0, \pi]$. We apply linear fitting with nonuniform bounds to obtain the phase mismatch functions illustrated in Figure 5.16. The order of the FIR fit is $s = 5$ in each case, which is smaller than the order $s = 7$ we obtain when we impose a uniform 10 deg bound at every frequency. ■

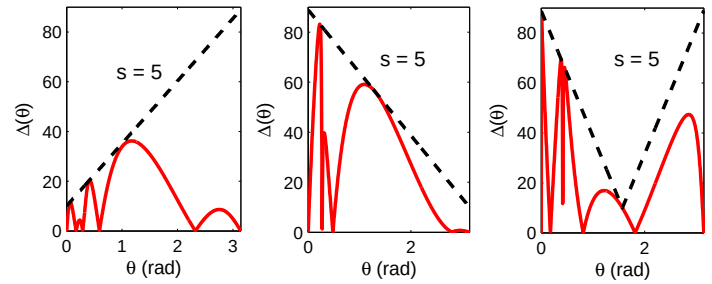

Figure 5.16: Ex2: Lin Fit.

Example 5.5.3. Consider the same plant G_{zu} as above. We now assume that the plant model is unknown. With the plant realized in controllable canonical form, we excite the unknown plant with a white noise sequence and collect output mea-

surements for 2500 time steps with the unknown nonzero initial condition $x(0) = \begin{bmatrix} 0.8644 & 0.0942 & -0.8519 & 0.8735 & -0.4380 \end{bmatrix}^{\mathrm{T}}$. We then take the ratio of the fast fourier transforms of the output and input signals to obtain frequency response estimates $\hat{G}_{zu}(e^{\jmath\theta})$ over $\theta \in [0, \pi]$. The Bode plot of G_{zu} and the estimated frequency response are shown in Figure 5.17.

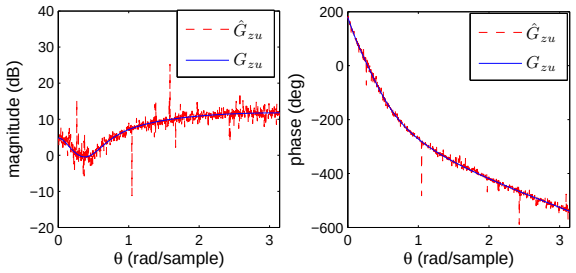

Figure 5.17: Ex2: Lin Fit.

Using the noisy frequency response estimates, we first apply the linear fitting method with a uniform phase mismatch bound $\bar{\Delta} = 80$ deg. Figure 5.18 shows the phase plot of the resulting FIR transfer function G_{f} and the phase mismatch function $\Delta(\theta)$ between the actual plant G_{zu} and G_{f}. Although the phase of G_{f} is within a ± 80 deg envelope of the estimated phase plot $\angle \hat{G}_{zu}$, the phase mismatch with G_{zu} gets above 80 deg near $\theta = 1$ rad/sample. Furthermore, the order of G_{f} is now $s = 11$, which is larger than the order $s = 4$ we obtain if the frequency response estimates are exact.

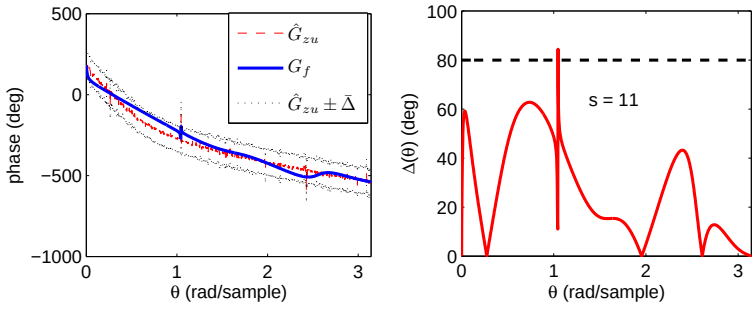

Figure 5.18: Ex2: Lin Fit.

Using the estimated phase plot, we now apply the nonlinear fitting method to

minimize $\bar{\Delta}$. Figure 5.19 shows the phase plot of the resulting FIR transfer function G_{f} and the phase mismatch function $\Delta(\theta)$ between the actual plant G_{zu} and G_{f}. Since the nonlinear method directly minimizes the phase difference between the estimated phase plot and the G_{f} model in a least squares sense, the effect of noise is less significant than the linear method, and G_{f} matches the actual plant with less than 30 deg phase mismatch for all $\theta \in [0, \pi]$. Furthermore, the order of G_{f} $s = 8$ is lower than the order $s = 11$ we obtain with the linear method. ■.

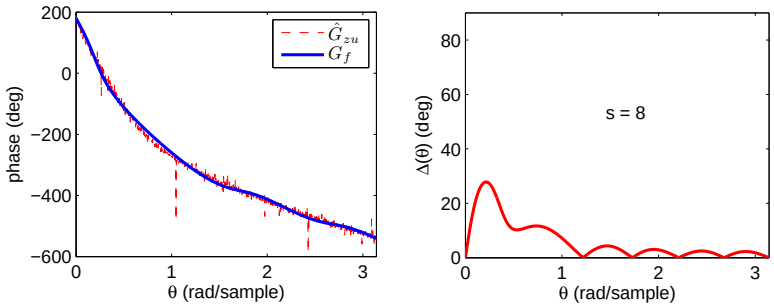

Figure 5.19: Ex: NonLin Fit.

5.6 Example: Adaptive Control of Flexible Structures

5.6.1 Problem Formulation

We consider the generic structural model

$$M\ddot{q} + C_{\mathrm{d}}\dot{q} + Kq = B_0 f + D_w \bar{w}, \tag{5.16}$$

where $q \in \mathbb{R}^r$ is a vector of generalized displacements, and M, C_{d}, and K are the mass, damping, and stiffness matrices, respectively. Throughout this section, we assume that M is positive definite, and C_{d} and K are positive semidefinite. Positive-definite and positive-semidefinite matrices are assumed to be symmetric. The control input to this system is the force $f \in \mathbb{R}^m$, and the disturbance force is given by $\bar{w} \in \mathbb{R}^{l_w}$.

Measurements are given by

$$\bar{y} = \begin{bmatrix} C_0 & C_1 & C_2 \end{bmatrix} \begin{bmatrix} q \\ \dot{q} \\ \ddot{q} \end{bmatrix} + \bar{D}_2 \bar{v}, \tag{5.17}$$

$$\bar{z} = \begin{bmatrix} E_{\mathrm{p}} & E_{\mathrm{v}} & E_{\mathrm{a}} \end{bmatrix} \begin{bmatrix} q \\ \dot{q} \\ \ddot{q} \end{bmatrix} + \bar{E}_3 \bar{v}, \tag{5.18}$$

where $\bar{v}$ denotes sensor noise. The measurements $\bar{z}$ are the performance variables. We assume that $\bar{w}$ and $\bar{v}$ are uncorrelated. We can write (5.16), (5.17), (5.18) in state space form as

$$\dot{\xi}(t) = \bar{A}\xi(t) + \bar{B}\bar{u}(t) + \bar{D}_1 \bar{w}(t), \tag{5.19}$$

$$\bar{y}(t) = \bar{C}\xi(t) + \bar{D}\bar{u}(t) + \bar{D}_2 \bar{v}(t) + \bar{D}_3 \bar{w}(t), \tag{5.20}$$

$$\bar{z}(t) = \bar{E}_1 \xi(t) + \bar{E}_2 \bar{u}(t) + \bar{E}_3 \bar{v}(t) + \bar{E}_0 \bar{w}(t) \tag{5.21}$$

where

$$\bar{A} \triangleq \begin{bmatrix} 0 & I_r \\ -M^{-1}K & -M^{-1}C_{\mathrm{d}} \end{bmatrix},\ \bar{B} \triangleq \begin{bmatrix} 0_{r\times m} \\ M^{-1}B_0 \end{bmatrix},\ \bar{D}_1 \triangleq \begin{bmatrix} 0_{r\times l_w} \\ M^{-1}D_w \end{bmatrix}, \tag{5.22}$$

$$\bar{C} \triangleq \begin{bmatrix} C_0 - C_2M^{-1}K & C_1 - C_2M^{-1}C_{\mathrm{d}} \end{bmatrix},\ \bar{D} \triangleq C_2M^{-1}B_0,\ \bar{D}_3 \triangleq C_2M^{-1}D_w, \tag{5.23}$$

$$\bar{E}_1 \triangleq \begin{bmatrix} E_p - E_aM^{-1}K & E_v - E_aM^{-1}C_{\mathrm{d}} \end{bmatrix},\ \bar{E}_2 \triangleq E_aM^{-1}B_0,\ \bar{E}_0 \triangleq E_aM^{-1}D_w, \tag{5.24}$$

$$\xi(t) \triangleq \begin{bmatrix} q(t) \\ \dot{q}(t) \end{bmatrix} \in \mathbb{R}^{2r},\ \bar{u}(t) \triangleq f(t). \tag{5.25}$$

We consider four special cases of (5.16) when it is unforced, namely,

$$M\ddot{q} + C_{\mathrm{d}}\dot{q} + Kq = 0. \tag{5.26}$$

These cases are distinguished by the stability of (5.26). For details, see [6].

In state space form, (5.26) can be written as

$$\dot{\xi} = \bar{A}\xi. \tag{5.27}$$

5.6.1.1 Case 1: Lyapunov-Stable Case

The unforced structure (5.27) is *Lyapunov stable* if every eigenvalue of $\bar{A}$ lies in the closed left-half plane and is semisimple on the imaginary axis. In this case the response of (5.27) is bounded for all initial conditions.

Fact 5.6.1. *(5.27) is Lyapunov stable if and only if*

$$\operatorname{rank} \begin{bmatrix} K \\ \\ C_{\mathrm{d}} \end{bmatrix} = r. \tag{5.28}$$

5.6.1.2 Case 2: Semistable Case

The unforced structure (5.27) is semistable if every eigenvalue of $\bar{A}$ lies in the open left-half plane or is zero and the zero eigenvalue (if present) is semisimple. In this case, the free response of such a structure is bounded and the state q converges, but not necessarily to $q = 0$.

Fact 5.6.2. *(5.27) is semistable if and only if* $(M^{-1}K, C_{\mathrm{d}})$ *is observable.*

The observability condition in Fact 5.6.2 is known as *pervasive damping*.

The presence of a semisimple eigenvalue at zero signifies the presence of a damped rigid body mode.

5.6.1.3 Case 3: Asymptotically Stable Case

The unforced structure (5.27) is *asymptotically stable* if every eigenvalue of $\bar{A}$ lies in the open left-half plane. In this case the free response of (5.27) converges to $q = 0$, $\dot{q} = 0$ for all initial conditions.

Fact 5.6.3. *(5.27) is asymptotically stable if and only if A is semistable and K is positive definite.*

5.6.1.4 Case 4: Unstable Case

If (5.27) is not Lyapunov stable, then we say that (5.27) is *unstable*. The following result shows that an unstable structure must have at least one rigid body mode and that this is precisely the nature of the instability.

Fact 5.6.4. *Assume that (5.27) is not Lyapunov stable. Then $\bar{A}$ has a repeated zero eigenvalue that appears in a 2×2 block in the Jordan canonical form of $\bar{A}$, and no zero eigenvalue of $\bar{A}$ appears in a Jordan block of size greater than 2×2.*

5.6.2 Numerical Examples

We now apply cumulative RCAC with η-modification to structural models. We consider disturbance rejection problems for SISO plants. In all cases, the adaptive controller gain matrix is initialized to be zero, that is, $\Theta(0) = 0$, and the forgetting factor $\lambda = 1$ in all examples.

Each example is constructed using the multiple degrees-of-freedom (MDOF) lumped parameter structure shown in Figure 5.20, and the output measurement is sampled with zero-order hold. The equations of motion for this system can be written in the form (5.16) with $M = \mathrm{diag}(m_1, \ldots, m_r)$,

$$C_d = \begin{bmatrix} c_1 + c_2 & -c_2 & 0 & \cdots & & 0 \\ -c_2 & c_2 + c_3 & -c_3 & 0 & \cdots & 0 \\ & \ddots & \ddots & \ddots & \ddots & \vdots \\ 0 & \cdots & -c_{r-1} & c_{r-1} + c_r & -c_r & 0 \\ 0 & \cdots & & 0 & -c_r & c_r + c_{r+1} \end{bmatrix}$$

$$K = \begin{bmatrix} k_1 + k_2 & -k_2 & 0 & \cdots & & 0 \\ -k_2 & k_2 + k_3 & -k_3 & 0 & \cdots & 0 \\ & \ddots & \ddots & \ddots & \ddots & \vdots \\ 0 & \cdots & -k_{r-1} & k_{r-1} + k_r & -k_r & 0 \\ 0 & \cdots & & 0 & -k_r & k_r + k_{r+1} \end{bmatrix}.$$

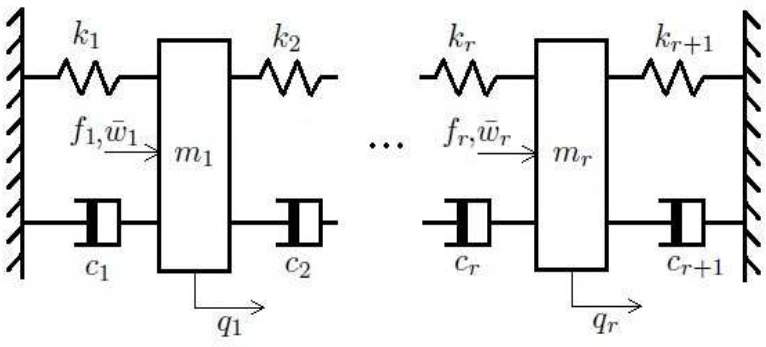

Figure 5.20: An r-mass lumped parameter structure.

Example 5.6.5 (Adaptive control of a 2DOF asymptotically stable lumped parameter structure)**.**

Consider a two-mass lumped parameter structure with the masses $m_1 = 1$, $m_2 = 1$; the spring constants $k_1 = 5$ kg/sec^2, $k_2 = 0$ kg/sec^2, $k_3 = 2$ kg/sec^2; and the damping coefficients $c_1 = 2$ kg/sec, $c_2 = 1$ kg/sec, and $c_3 = 0$ kg/sec. With these parameters, every eigenvalue of $\bar{A}$ lies in the open left-half plane, thus the structure is asymptotically stable. The continuous-time plant $T_{zu}(s) = \bar{E}_1(sI - \bar{A})^{-1}\bar{B}$ is sampled at 4 Hz so that $T_s = 0.25$ sec/sample. The sampled-data system $G_{zu}(\mathbf{q})$ has the sampling zeros -0.211 and -2.8758, one of which is NMP.

The control objective is to keep q_2 near zero in the presence of the disturbance forces $\bar{w}_1$ and $\bar{w}_2$, using the control force f_1. Therefore, we consider a SISO disturbance rejection problem with $z = q_2$, $B_0 = \begin{bmatrix} 1 & 0 \end{bmatrix}^{\mathrm{T}}$, $D_w = I_2$. We assume that q_2 is the only measurement, therefore, $y = z$. Furthermore, we assume that the measurements are noise-free.

We first consider an unknown sinusoidal disturbance $\bar{w}_2(t)$ with frequency $\omega_2 = \frac{1}{7}$ Hz, that is, $w(k) = \begin{bmatrix} 0 & 100 \sin \Theta_2 k \end{bmatrix}^{\mathrm{T}}$ N, where $\Theta_2 = 2\pi\omega_2 T_s = 2\pi/28$ rad/sample. The open-loop system is given the initial conditions $q(0) = \begin{bmatrix} 4 & -1 \end{bmatrix}^{\mathrm{T}}$ m, and

$\dot{q}(0) = \begin{bmatrix} -2 & -0.5 \end{bmatrix}^{\mathrm{T}}$ m/sec. The plant is simulated in open-loop for 25 seconds, and at $t = 25$ sec, RCAC is turned on with tuning parameters $n_{\mathrm{c}} = 10$, $\eta_0 = 0.5$, $P_0 = 10I$, $p_c = 1$, and $G_{\mathrm{f}}(\mathbf{q}^{-1}) = H_1\mathbf{q}^{-1} = 0.002\mathbf{q}^{-1}$. The performance converges to zero, the asymptotic closed-loop system is stable, and RCAC converges to an internal model controller with high-gain at the disturbance frequency Θ_2 as shown in Figure 5.21.

We now consider the unknown sinusoidal disturbances $\bar{w}_1(t)$ and $\bar{w}_2(t)$ with frequencies $\omega_1 = 0.5$ Hz and $\omega_2 = \frac{2}{9}$ Hz, that is, $w(k) = \begin{bmatrix} w_1(k) & w_2(k) \end{bmatrix}^{\mathrm{T}} = \begin{bmatrix} 100\sin\Theta_1 k & 10\sin\Theta_2 k \end{bmatrix}^{\mathrm{T}}$ N, where $\Theta_1 = 2\pi/8$ rad/sample and $\Theta_2 = 2\pi/18$ rad/sample. We use the nonlinear FIR fitting method to obtain the 8^{th}-order FIR fit

$$G_{\mathrm{f}}(\mathbf{q}^{-1}) = K_1\mathbf{q}^{-1} + \cdots + K_8\mathbf{q}^{-8}, \tag{5.29}$$

with

$$\begin{bmatrix} K_1 & \cdots & K_8 \end{bmatrix} = 10^{-3}\begin{bmatrix} -2.1 & 0.3 & 1.4 & 1.6 & 1.2 & 0.2 & -0.7 & -1.8 \end{bmatrix}, \tag{5.30}$$

which results in $\Delta(\theta) < 90$ for all $\theta \in [0, \pi]$ rad/sample. Note that the NMP sampling zero -2.8758 is not a zero of G_{f}. The open-loop system is given the same initial conditions as above. The plant is simulated in open-loop for 100 seconds, and at $t = 100$ sec, RCAC is turned on with tuning parameters $n_{\mathrm{c}} = 15$, $\eta_0 = 0.1$, $P_0 = 0.1I$, and $p_c = 5$. The closed-loop response is shown in Figure 5.22. After convergence, the disturbance frequencies $\pi/9$ rad/sample and $\pi/4$ rad/sample are attenuated as shown in Figure 5.23. ■

Example 5.6.6 (3DOF asymptotically stable lumped parameter structure with uncertain dynamics and measurement noise)**.**

Consider a 3DOF lumped parameter structure with the masses $m_1 = 4.6$ kg,

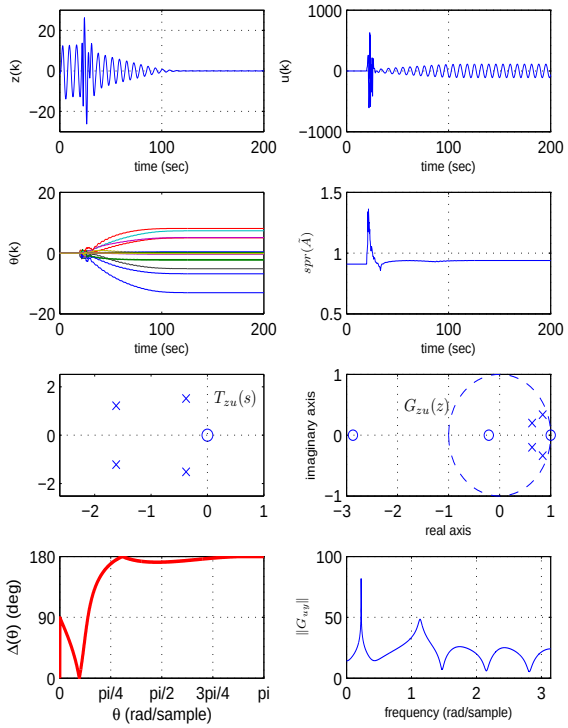

Figure 5.21: Example 5.6.5: 2DOF, asymptotically stable structure, sampled with $T_s = 0.25$ sec/sample. The sampled-data system has a NMP sampling zero. The control objective is to keep $q_2(t)$ near zero in the presence of the disturbance force $\bar{w}_2(t) = 100\sin(2\pi t/7)$ N using the control force f_1. RCAC is turned on at $t = 25$ sec with the tuning parameters $n_c = 10$, $\eta_0 = 0.5$, $P_0 = 10I$, $p_c = 1$, and $G_f(\mathbf{q}^{-1}) = H_1\mathbf{q}^{-1}$. With this choice of G_f, the phase mismatch is smaller than 90 deg at the disturbance frequency $\Theta_1 = \pi/14$ rad/sample. The controller gain vector $\Theta(k)$ converges, and q_2 converges to zero in about 70 seconds (280 time steps). RCAC converges to an internal model controller with high-gain at the disturbance frequency. After convergence, the spectral radius $\text{spr}(\tilde{A})$ of the closed-loop system is 0.94.

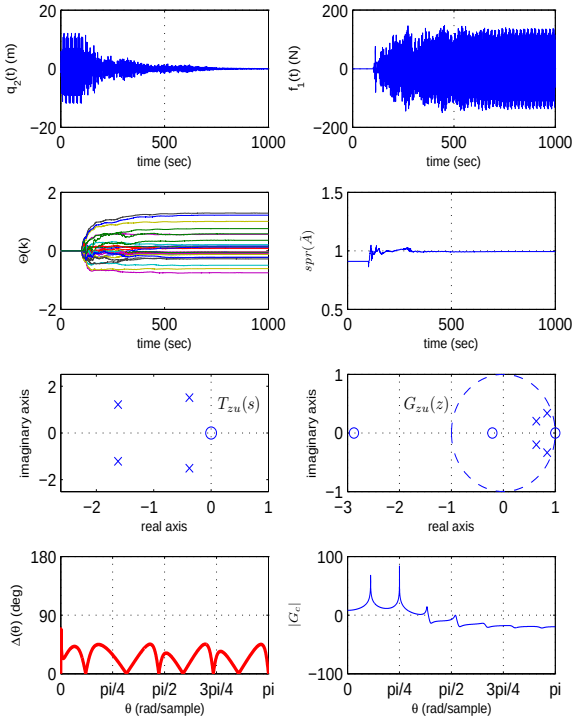

Figure 5.22: Example 5.6.5: 2DOF, asymptotically stable structure sampled with $T_s = 0.25$ sec/sample. The sampled-data system has a NMP sampling zero. The control objective is to keep $q_2(t)$ near zero in the presence of the disturbance forces $\bar{w}_1(t) = 100\sin(2\pi t/2)$ N and $\bar{w}_2(t) = 10\sin(2\pi\frac{2}{9}t)$ N using the control force f_1. RCAC is turned on at $t = 100$ sec with the tuning parameters $n_c = 15$, $\eta_0 = 0.1$, $P_0 = 0.1I$, and $p_c = 5$. G_f is constructed using the nonlinear FIR fitting method to obtain $\Delta(\theta) \leq 90$ deg for all $\theta \in [0, \pi]$ rad/sample. The controller gain vector $\Theta(k)$ converges, and q_2 converges to zero in about 400 seconds (2000 time steps). The performance variable does not exceed the open-loop during the transient period. After convergence, the spectral radius $\text{spr}(\tilde{A})$ of the closed-loop system is 0.99.

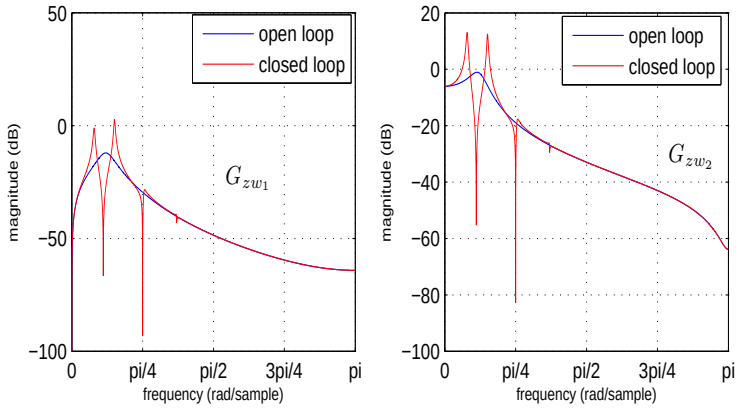

Figure 5.23: Example 5.6.5: 2DOF asymptotically stable structure with NMP sampling zeros, two-tone disturbance rejection problem. The Bode plots show the attenuation at the disturbance frequencies $\pi/9$ and $\pi/4$ rad/sample after controller convergence.

$m_2 = 4.7$ kg, $m_3 = 5.2$ kg; the spring constants $k_1 = 9.9$ kg/sec^2, $k_2 = 5.8$ kg/sec^2, $k_3 = 8$ kg/sec^2, $k_4 = 8.5$ kg/sec; and the damping coefficients $c_1 = 2.8$ kg/sec, $c_2 = 2.7$ kg/sec, $c_3 = 2.42$ kg/sec, and $c_4 = 2.65$ kg/sec. With these parameters, every eigenvalue of $\bar{A}$ lies in the open left-half plane, therefore, the structure is asymptotically stable. The continuous-time plant $T_{zu}(s)$ is sampled at 1 Hz so that $T_s = 1$ sec/sample. The sampled-data system $G_{zu}(z)$ has two sampling zeros, one of which is NMP.

In this example, we assume that the structure parameters, including the Markov parameters, are completely unknown, that is, no prior modeling information is available. Therefore, we first apply an off-line frequency-domain identification to construct G_{f}. In particular, with the unknown nonzero initial conditions $q(0) = \begin{bmatrix} 0.04 & 0.1 & -0.02 \end{bmatrix}^{\mathrm{T}}$ m and $\dot{q}(0) = \begin{bmatrix} 0.02 & -0.03 & 0.01 \end{bmatrix}^{\mathrm{T}}$ m/sec, we excite the uncertain plant with a white noise sequence and collect output measurements for 1500 time steps. We then take the ratio of the fast fourier transforms of the output and input signals to obtain frequency response estimates $\hat{G}_{zu}(e^{\jmath\theta})$ of G_{zu} in 750 equally spaced points in $\theta \in [0, \pi]$ rad/sample. The Bode plot of the estimated frequency response is shown in Figure 5.24. Next, using the frequency response estimates, we apply the constrained linear least squares

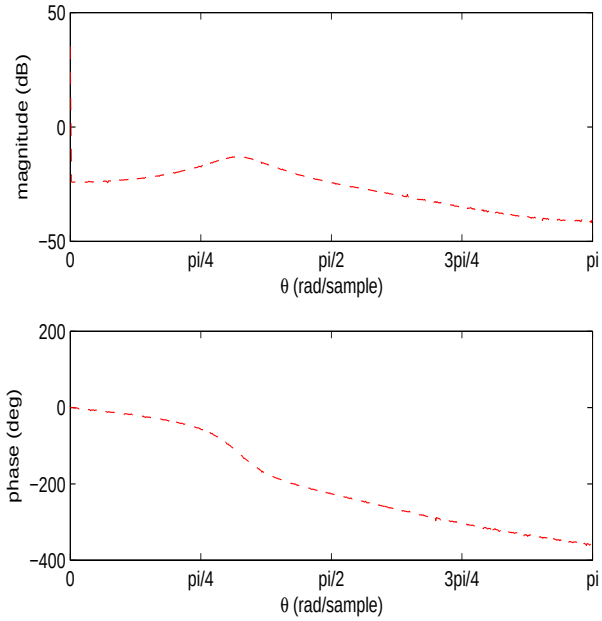

Figure 5.24: Example 5.6.6: Frequency response estimate of G_{zu}, obtained through frequency domain system identification using a gaussian white noise sequence.

method to fit $\hat{G}_{zu}(e^{j\theta})$ with an FIR plant using a uniform phase mismatch bound $\Delta(\theta) \leq 80$ deg. The resulting FIR fit is

$$G_{\mathrm{f}}(\mathbf{q}^{-1}) = 0.041\mathbf{q}^{-1} + 0.0709\mathbf{q}^{-2},$$

Note that the coefficients of G_{f} are not the Markov parameters $H_1 = 0.0155$ and $H_2 = 0.0578$ of G_{zu}.

The control objective is to keep q_2 near zero in the presence of the disturbance forces $\bar{w}_1$, $\bar{w}_2$ and $\bar{w}_3$ using the control force f_3. Furthermore, we assume that the measurements y and z are corrupted by a zero-mean gaussian white noise $v(k)$ with standard deviation $\sigma_v = 0.32$ m, so that $y(k) = z(k) = q_2(kT_s) + v(k)$. We consider the unknown sinusoidal disturbances $\bar{w}_1$, $\bar{w}_2$ and $\bar{w}_3$ with frequencies $\omega_1 = 0.1429$ Hz, $\omega_2 = \frac{1}{3}$ Hz, $\omega_3 = 0.0588$ Hz, that is, $w(k) = \begin{bmatrix} w_1(k) & w_2(k) & w_3(k) \end{bmatrix}^{\mathrm{T}} =$

$\begin{bmatrix} 75\sin\Theta_1 k & 30\sin\Theta_2 k & 70\sin\Theta_3 k \end{bmatrix}^{\mathrm{T}}$ N, where $\Theta_1 = 2\pi/7$ rad/sample, $\Theta_2 = 2\pi/3$ rad/sample, and $\Theta_3 = 2\pi/17$ rad/sample. The open-loop system is given the initial conditions $q(0) = \begin{bmatrix} -0.7 & 0.65 & -0.35 \end{bmatrix}^{\mathrm{T}}$ m, and $\dot{q} = \begin{bmatrix} 0.5 & 0.1 & 0.3 \end{bmatrix}^{\mathrm{T}}$ m/sec. The plant is simulated in open-loop for 100 seconds, and at $t = 100$ sec, RCAC is turned on with tuning parameters $n_{\mathrm{c}} = 15$, $\eta_0 = 0.005$, $p_c = 1$, $P_0 = I$, and G_{f} as given above. The closed-loop response is shown in Figure 5.25. After convergence, the disturbance frequencies $\pi/7$ rad/sample, $2\pi/3$ rad/sample and $2\pi/17$ are attenuated as shown in Figure 5.26. ■

5.7 Conclusion

In this chapter, we defined the phase mismatch, and numerically demonstrated that it is highly correlated with the asymptotic performance of RCAC with η-modification. This numerical evidence motivated the development of two system identification methods to fit IIR transfer functions with FIR transfer functions to minimize the phase mismatch. These identification methods led to a new phase-matching-based controller construction technique in addition to the Markov-parameter, NMP-zero, and time-series-based construction methods given in Chapter II. We demonstrated the phase-matching-based construction on mass-spring-dashpot systems in the presence of multi-tone sinusoidal disturbances.

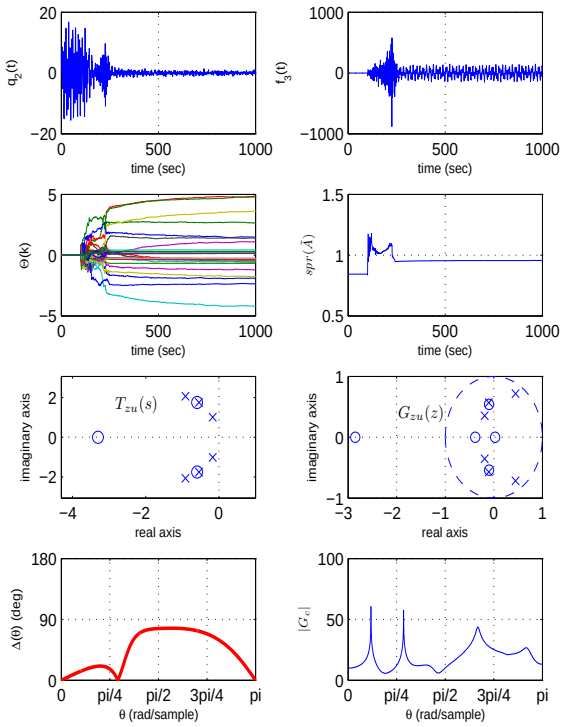

Figure 5.25: Example 5.6.6: 3DOF, asymptotically stable structure, sampled with $T_s = 1$ sec/sample. The sampled-data system has a NMP sampling zero. The plant parameters are assumed to be completely unknown, and $G_{\rm f}$ is constructed using the constrained linear least squares method developed in Section 5.4.1. The frequency response estimates are obtained with frequency domain system identification using a white-noise input sequence. The control objective is to keep q_2 near zero in the presence of the disturbance forces $\bar{w}_1(t) = 75\sin(2\pi t/7)$ N, $\bar{w}_2(t) = 30\sin(2\pi t/3)$ N and $\bar{w}_3(t) = 70\sin(2\pi t/17)$ N, using the control force f_3. Furthermore, the measurements are corrupted by a gaussian white-noise with standard deviation 0.32 m. RCAC is turned on at $t = 100$ sec with the tuning parameters $n_{\rm c} = 15$, $\eta_0 = 0.005$, $p_c = 1$ and $P_0 = I$. The performance variable q_2 converges near zero in about 100 seconds (100 time steps), and the transient performance does not exceed the open-loop performance. The spectral radius $\mathrm{spr}(\tilde{A})$ of the closed-loop system is 0.96 at $t = 1000$ sec.

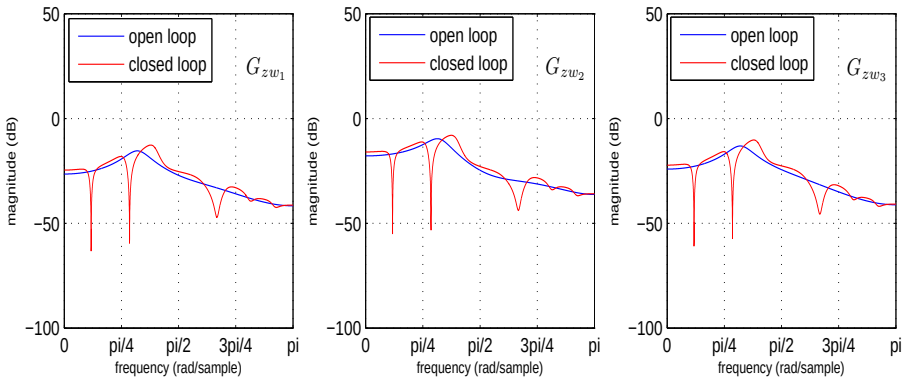

Figure 5.26: Example 5.6.6: 3DOF asymptotically stable uncertain structure. The Bode plots show the attenuation at the disturbance frequencies $2\pi/7$, $2\pi/3$ and $2\pi/17$ rad/sample after controller convergence.

CHAPTER VI

Aliasing Effects in Retrospective Cost Adaptive Control of Plants with High-Frequency Dynamics and Disturbances

6.1 Introduction

Because of the ability to implement nonlinear and logical operators in embedded code, as well as the ability to easily modify that code, even remotely, the vast majority of modern control systems are implemented digitally. Digital controllers possess one drawback relative to analog controllers, however, namely, aliasing effects, which arise when the sampled signal possesses frequency content above the Nyquist frequency, which is half of the sampling frequency. Aliasing implies that frequency content above the Nyquist frequency is "folded" down to a lower frequency by mirror imaging its spectral content about the Nyquist frequency. The aliased harmonics of the folded signal thus constitute harmonics that are not present in the original, analog signal. Consequently, the controller may be forced to operate on an error signal that is not a true representation of the error signal that it was designed to operate on. The aliased signal thus acts as a disturbance that is injected into the system due to sampling.

There are two strategies for addressing the effects of aliasing. First, the sampling rate can be chosen to be significantly above the highest frequency content of the

sampled signal, including both the dynamic response of the system and exogenous signals. This approach may require a sampling rate that is far beyond the required bandwidth of the system, thus entailing an undue burden on the digital hardware. For example, if the goal is to control rigid body motion but the system has a high-frequency flexible mode, then a fast sampling rate is needed in order to avoid aliasing the contribution of the flexible mode. Thus, the flexible mode may be inadvertently excited by the feedback controller. Furthermore, fast sampling may be undesirable because of the sampling zeros, which are typically NMP for sufficiently fast sampling rates [3].

The second approach to addressing the effects of aliasing is to employ an anti-aliasing filter. An anti-aliasing filter is a filter that is designed to roll off at a chosen frequency and thus to attenuate the frequency content of the signal above the Nyquist frequency. Anti-aliasing filters are almost always analog; a digital filter cannot reliably remove the effects of aliasing once the signal has been sampled, except perhaps as a notch filter when the aliased frequencies are known. Consequently, the analog anti-aliasing filter is a fixed component that must be engineered into the system along with the choice of sampling rate and controller bandwidth.

In summary, aliasing can be addressed by either fast sampling or analog anti-aliasing. Both approaches have drawbacks and both may be imperfect. For virtually all digital control systems, the question thus remains as to whether the effects of aliasing can degrade the performance of the closed-loop system. The goal of this chapter is thus to investigate the effects of aliasing without assuming the benefits of either sufficiently fast sampling or sufficiently effective analog anti-aliasing filters.

Control under arbitrarily slow sampling is considered in [81], where it is shown that, under perfect modeling, the effects of aliasing can be addressed by sampled-data LQG control, except at sampling rates at which controllability is lost [57]. A general approach to H_2-optimal sampled-data control is considered in [16, 17]. The present

chapter, however, focuses on the more realistic case of model uncertainty, especially at high frequencies. Within the context of adaptive control, unmodeled high-frequency dynamics are known to present difficulties, as demonstrated by the celebrated Rohrs counterexample [84]. Recently, this issue was revisited in [100] within the context of sampled-data adaptive control. Specifically, retrospective cost adaptive control (RCAC) was applied to this problem in order to determine its ability to address the effects of unmodeled high-frequency dynamics. As shown in [100], RCAC was able to follow the command despite the unmodeled modes, the unknown sinusoidal disturbance, and the unknown nonminimum-phase sampling zero contributed by the unmodeled high-frequency dynamics.

The results of [100], however, assumed that the sampling rate was sufficiently high as to avoid aliasing. Therefore, the goal of the present chapter is to consider adaptive control in the presence of aliasing, due to either the high-frequency free response of the plant or the high-frequency content in the disturbances. To investigate this question, we present a numerical investigation of RCAC applied to sampled-data command-following and disturbance-rejection problems, and we investigate the performance of RCAC in the presence of aliasing, that is, the case in which the continuous-time plant is sampled at a rate slower than the Nyquist rate corresponding to the frequency content of the free response of the plant and exogenous signals. We are especially interested in the intersample behavior of the plant and performance variables as a consequence of sampling and aliasing. Within the context of fixed-gain control, intersample behavior is examined in [8, 17, 35].

6.2 Problem Formulation

Consider the MIMO plant

$$\dot{\bar{x}}(t) = \bar{A}\bar{x}(t) + \bar{B}\bar{u}(t) + \bar{D}_1\bar{w}(t), \tag{6.1}$$

$$\bar{z}(t) = E_1\bar{x}(t) - \bar{r}(t), \tag{6.2}$$

where $(\bar{A}, \bar{B}, \bar{E}_1)$ is minimal, $\bar{x}(t) \in \mathbb{R}^n$ is the state variable, $\bar{z}(t) \in \mathbb{R}^{l_z}$ is the performance output, $\bar{u}(t) \in \mathbb{R}^{l_u}$ is the control input, $\bar{w}(t) \in \mathbb{R}^{l_w}$ is the disturbance signal, $\bar{r}(t) \in \mathbb{R}^{l_r}$ is the reference command, and $t \geq 0$. In this chapter, we assume that $w(t)$ and $r(t)$ are harmonic signals with bandwidth $\omega_{\mathrm{B},w}$ and $\omega_{\mathrm{B},r}$ respectively. Furthermore, we define $\omega_{\mathrm{N},w} = 2\omega_{\mathrm{B},w}$ and $\omega_{\mathrm{N},r} = 2\omega_{\mathrm{B},r}$ as the Nyquist rate corresponding to w and r respectively. The plant (6.1), (6.2) can be discretized for sampled-data control using sample and hold operators, as illustrated for the SISO case in Figure 6.1. For a zero-order-hold operator and a sampler with sampling period h sec/sample and sampling rate $\omega_{\mathrm{s}} = 2\pi/h$ rad/sample, the sampled-data system is described by

$$x(k+1) = Ax(k) + Bu(k) + f(w, k, h), \tag{6.3}$$

$$z(k) = E_1x(k) - r(k), \tag{6.4}$$

where

$$A = e^{\bar{A}h}, \quad B = \int_{kh}^{(k+1)h} e^{\bar{A}((k+1)h-\tau)}d\tau\bar{B}, \tag{6.5}$$

$f(w, k, h) = \int_{kh}^{(k+1)h} e^{\bar{A}((k+1)h-\tau)}\bar{D}_1\bar{w}(\tau)d\tau$, and $x(k)$, $u(k)$, $r(k)$ and $z(k)$ represent $\bar{x}(kh)$, $\bar{u}(kh)$, $\bar{r}(kh)$ and $\bar{z}(kh)$, respectively.

For the sampled-data system (6.3), a sufficient condition for controllability is given by the following proposition [57].

Proposition 6.2.1. *A sufficient condition for complete controllability of* (A, B) *is to have*

$$\mathrm{Im}\{\lambda_i(\bar{A}) - \lambda_j(\bar{A})\} \neq 2\pi l/h, \tag{6.6}$$

for all eigenvalues $\lambda_i(\bar{A})$, $\lambda_j(\bar{A})$ *of* $\bar{A}$ *such that*

$$\mathrm{Re}\{\lambda_i(\bar{A}) - \lambda_j(\bar{A})\} = 0, \tag{6.7}$$

for all nonzero integers l. *Furthermore, condition* (6.6), (6.7) *is necessary as well if* $l_u = 1$.

A weaker condition suffices for (A, E_1) to be observable [67]. Thus, (A, B, E_1) is minimal if (6.6), (6.7) is satisfied.

The input-output relationship from u to z is described by the operator matrix

$$G_{zu}(\mathbf{q}) \stackrel{\triangle}{=} E_1(\mathbf{q}I - A)^{-1}B, \tag{6.8}$$

where $\mathbf{q}$ is the forward shift operator. Unlike the z-transform, (6.8) accounts for possibly nonzero initial conditions. Furthermore, for each positive integer i,

$$H_i \stackrel{\triangle}{=} E_1 A^{i-1} B$$

is the i^{th} Markov parameter of G_{zu}.

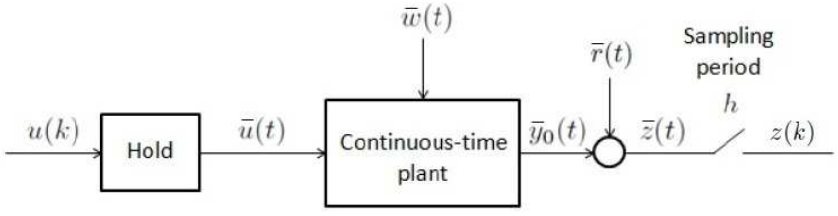

Figure 6.1: Typical sampled-data system.

Now, consider the $n_{\mathrm{c}}^{\mathrm{th}}$-order strictly proper output feedback controller

$$x_{\mathrm{c}}(k+1) = A_{\mathrm{c}}(k)x_{\mathrm{c}}(k) + B_{\mathrm{c}}(k)z(k), \tag{6.9}$$

$$u(k) = C_{\mathrm{c}}(k)x_{\mathrm{c}}(k), \tag{6.10}$$

where $x_{\mathrm{c}} \in \mathbb{R}^{n_{\mathrm{c}}}$. The feedback control (6.9), (6.10) is represented by $u = G_{\mathrm{c}}(\mathbf{q}, k)z$, where

$$G_{\mathrm{c}}(\mathbf{q}, k) \triangleq C_{\mathrm{c}}(k)(\mathbf{q}I - A_{\mathrm{c}}(k))^{-1}B_{\mathrm{c}}(k). \tag{6.11}$$

The closed-loop system with output feedback (6.9), (6.10) is thus given by

$$\tilde{x}(k+1) = \tilde{A}\tilde{x}(k) + \tilde{f}(w, k, h), \tag{6.12}$$

$$z(k) = \tilde{E}_1\tilde{x}(k) + E_0 r(k), \tag{6.13}$$

where

$$\tilde{A} \triangleq \begin{bmatrix} A & BC_{\mathrm{c}} \\ B_{\mathrm{c}}E_1 & A_{\mathrm{c}} \end{bmatrix}, \quad \tilde{f}(w, k, h) \triangleq \begin{bmatrix} f(w, k, h) \\ 0 \end{bmatrix},$$

$$\tilde{E}_1 \triangleq \begin{bmatrix} E_1 & 0_{l_z \times n_{\mathrm{c}}} \end{bmatrix}, \tag{6.14}$$

and $\tilde{x}(k) = \begin{bmatrix} x^{\mathrm{T}}(k) & x_{\mathrm{c}}^{\mathrm{T}}(k) \end{bmatrix}^{\mathrm{T}} \in \mathbb{R}^{n+n_{\mathrm{c}}}$.

From a sampled-data point of view, the objective is to develop an adaptive output feedback controller to minimize $z^{\mathrm{T}}(k)z(k)$ in the presence of the disturbance signal $\bar{w}(t)$ and the reference command $\bar{r}(t)$ with limited modeling information about the dynamics, disturbance signal, and command signal. We assume that the measurement of the performance variable $z(k)$ is available for feedback. However, having $z(k)$ near zero at every sample k does not guarantee that $\bar{z}(t)$ is small for all t. Therefore, in

practice, the objective is to design a sampled-data adaptive controller to minimize $\bar{z}(t)$ not only at the sampling instants $t = kh$, but for all t.

In practice, the effects of aliasing may be mitigated by filtering the performance output $\bar{z}(t)$ with an anti-aliasing filter to decrease the bandwidth of the cascade continuous-time plant. Indeed, this would facilitate the problem for the adaptive controller since the high-frequency components due to $\bar{w}(t)$ and internal dynamics would be filtered out from the performance measurement. But this would go against the goal of this chapter, which is to study the effects of aliasing in digital adaptive control. Thus, we apply adaptive control using the sampled measurements of $z(k)$ directly, with no intermediate anti-aliasing filters acting on $\bar{z}(t)$.

For the adaptive controller (6.9), (6.10), the closed-loop state matrix $\tilde{A}(k)$ may be time-dependent. To monitor the ability of the adaptive controller to stabilize the plant, we compute the spectral radius $\mathrm{spr}(\tilde{A}(k))$ at each time step. If the controller converges, and $\mathrm{spr}(\tilde{A}(k))$ converges to a number less than 1, then the asymptotic closed-loop system is internally stable.

6.3 Numerical Examples with Disturbance Aliasing

We now investigate the performance of RCAC with undersampling of disturbances, that is, the continuous-time plant is sampled at a rate slower than the Nyquist rate corresponding to the disturbance $\bar{w}(t)$ so that $\omega_{\mathrm{s}} < \omega_{\mathrm{N},w}$. In each example, the controller gain matrix $\Theta(k)$ is initialized to be zero, and the cumulative update law (2.42)–(2.44) is used with $\lambda = 1$.

Example 6.3.1 (Undersampled disturbances.)**.** Consider the third-order continuous-time plant $T_{zu}(s) = T_0(s)\Lambda(s)$ with $T_0(s) = \frac{2}{s+1}$ and $\Lambda(s) = \frac{229}{(s-15-\jmath 2)(s-15+\jmath 2)}$. This plant is used in [84] to show that if the fast poles contributing by $\Lambda(s)$ are unmodeled or ignored, traditional continuous-time MRAC may lead to an unstable closed-loop

system. Sampled-data adaptive control of Rohrs counterexamples with RCAC is extensively covered in [100], where it is shown that the pulse transfer function $G_{zu}(z)$ corresponding to $T_{zu}(s)$ has a NMP sampling zero for sampling frequencies larger than 10π rad/sample. In this example, we consider a problem where the sampling rate is chosen so that the sampled-data plant is minimum-phase. Furthermore, the control objective is to follow the reference command $\bar{r}(t) = 2 + \sin t$, and the only modeling information available is the first Markov parameter H_1 of G_{zu}.

First, we consider the case with no disturbances. Choosing $n_c = 10$ and $P_0 = 10^8 I$, RCAC drives the sampled error signal $z(k)$ to zero by converging to an internal model controller with high gain at the command frequencies $\Omega_1 = 0$ rad/sample and $\Omega_2 = 0.25$ rad/sample $= 1$ rad/sec. Furthermore, after convergence, the command-following error $\bar{z}(t)$ is small between consecutive sampling instants, as shown in Figure 6.2.

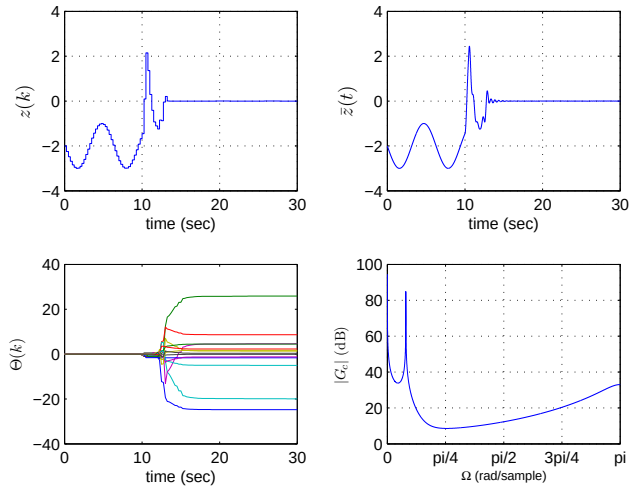

Figure 6.2: Example 6.3.1: Undersampled disturbances. This figure illustrates the closed-loop response with no disturbances. Both the samples $z(k)$ and the actual continuous-time command-following error $\bar{z}(t)$ converge to zero, the controller gains converge, and RCAC converges to an internal model controller with high gain at the command frequencies 0 rad/sample and 0.25 rad/sample.

Now, we consider the same problem in the presence of the matched disturbance

$\bar{w}(t) = 2.5 \sin 5\pi t$. Unlike $\omega_{\mathrm{N},r}$, the Nyquist rate $\omega_{\mathrm{N},w} = 10\pi$ rad/sec corresponding to $\bar{w}(t)$ is larger than the sampling rate $\omega_{\mathrm{s}} = 8\pi$ rad/sec and thus $\bar{z}(t)$ is undersampled at this sampling rate. Choosing the same control parameters, RCAC drives the sampled error signal $z(k)$ to zero in about 15 samples by converging to an internal model controller with high gain at the command frequencies, as well as the disturbance aliasing frequency $2\pi - 1.25\pi = 0.75\pi$ rad/sample. Thus the actual command-following error $\bar{z}(t)$ does not converge to zero due to aliasing, as shown in Figure 6.3. ■

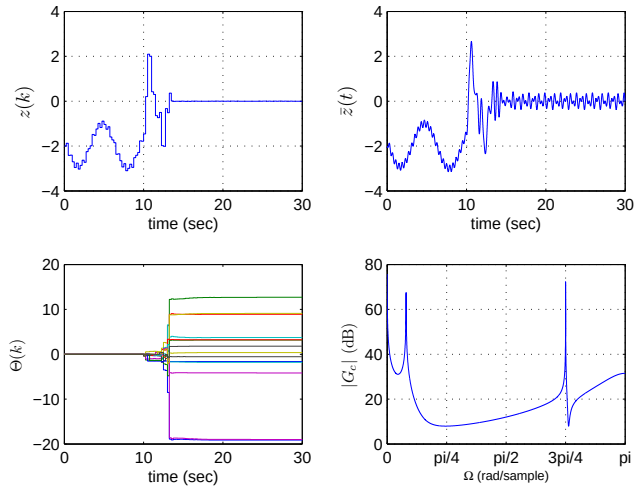

Figure 6.3: Example 6.3.1: Undersampled disturbances. This figure illustrates the closed-loop response with the matched disturbance $\bar{w}(t) = 2.5 \sin 5\pi t$. The disturbance frequency is larger than the Nyquist frequency 4π rad/sample. RCAC drives the sampled performance $z(k)$ to zero, but the actual command-following error $\bar{z}(t)$ is nonzero between consecutive samples, due to disturbance aliasing. In addition to the command frequency, RCAC places an internal model into the disturbance aliasing frequency 0.75π rad/sample.

6.4 Numerical Examples with High-Frequency Dynamics

We now apply RCAC to sampled-data stabilization, command following, and disturbance rejection problems. We consider plants with lightly-damped, undamped, or unstable high-frequency dynamics, and, to investigate the performance of RCAC

with aliasing of plant dynamics, we choose the sampling rate below the Nyquist rate corresponding to the free response of the plant. In each example, the controller gain matrix $\Theta(k)$ is initialized to be zero, and the cumulative update law (2.42)–(2.44) is used with $\lambda = 1$.

Example 6.4.1 (Undersampled asymptotically stable lightly-damped modes.)**.** Consider the 4$^{\text{th}}$-order Lyapunov stable plant $T_{zu}(s) = 50\frac{(s+0.2+\jmath 3)(s+0.2-\jmath 3)}{(s+\jmath 1.5)(s-\jmath 1.5)(s+0.5+\jmath 10)(s+0.5-\jmath 10)}$. The goal is to have the output of the plant follow the reference command $\bar{r}(t) = \sin 0.5t$ while rendering the closed-loop system asymptotically stable. The plant is initialized with nonzero initial conditions so that the free response is nonzero.

First, we choose the sampling rate to be $\omega_{\text{s}} = 4\pi$ rad/sec. Notice that the Nyquist frequency $\omega_{\text{s}}/2$ is smaller than 10 rad/sec and thus the plant is undersampled due to the high-frequency component of the free response contributed by the lightly-damped modes. Choosing $n_{\text{c}} = 6$, $P_0 = 10^5 I$ and $G_{\text{f}}(\mathbf{q}^{-1}) = H_1\mathbf{q}^{-1}$, RCAC is turned on at $t = 5$ sec. RCAC drives the sampled command-following error $z(k)$ to zero, and the actual command-following error $\bar{z}(t)$ is small between consecutive sampling instants, as shown in Figure 6.4.

We now investigate the performance of RCAC when the lightly-damped modes of T_{zu} become uncontrollable due to sampling in accordance with Proposition 6.2.1. For this, it follows from (6.6) that the sampling rate should be chosen so that $l\omega_{\text{s}} = 20$ rad/sec, where l is a positive integer. We consider $l = 1$, that is, $\omega_{\text{s}} = 20$ rad/sec, and thus $h = \pi/10$ sec/sample. As shown in Figure 6.5, this causes the sampled-data plant to have a stable pole-zero cancellation near -0.62. Choosing the same control parameters, RCAC is turned on at $t = 5$ sec. RCAC stabilizes the system and drives the sampled-command-following error to zero, and the command following error remains small between consecutive sampling instants. This examples suggests that undersampling of asymptotically stable dynamics does not harm the asymptotic performance of RCAC, even when these modes are uncontrollable due to sampling in

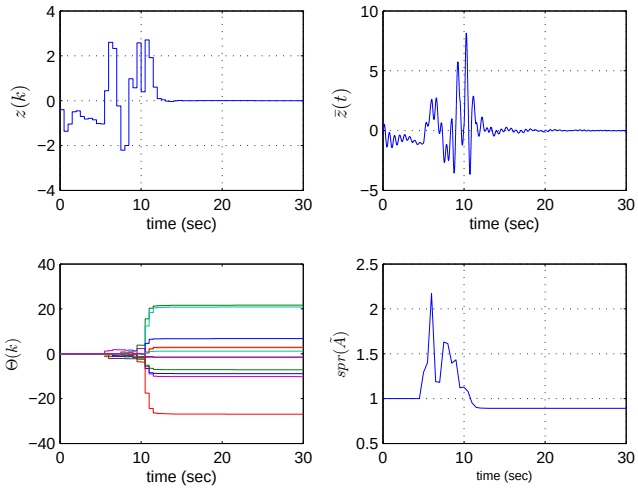

Figure 6.4: Example 6.4.1: Undersampled asymptotically stable modes. This figure illustrates the closed-loop response with the command $\bar{r}(t) = \sin 0.5t$. The Nyquist frequency 2π rad/sec is smaller than the damped frequency 10 rad/sec corresponding to the lightly-damped modes. RCAC is turned on at $t = 5$ sec, drives both $z(k)$ and $\bar{z}(t)$ to zero, and stabilizes the closed-loop system.

accordance with Proposition 6.2.1. ■

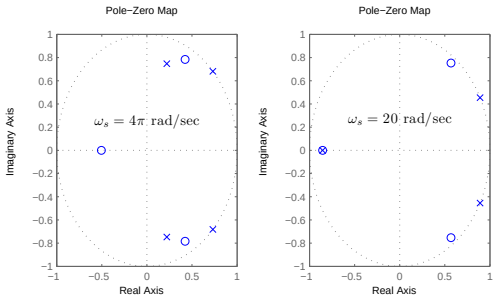

Figure 6.5: Example 6.4.1: Pole-zero maps corresponding to G_{zu} with $\omega_s = 4\pi$ rad/sec (left) and $\omega_s = 20$ rad/sec (right). With $\omega_s = 20$ rad/sec, modes $-0.5 \pm \jmath 10$ of the continuous-time plant are uncontrollable due to sampling.

Example 6.4.2 (Undersampled undamped modes)**.** Consider the 4^{th}-order Lyapunov stable plant $T_{zu}(s) = 50\frac{(s+0.2+\jmath 3)(s+0.2-\jmath 3)}{(s+\jmath 10)(s-\jmath 10)(s+0.5+\jmath 1.5)(s+0.5-\jmath 1.5)}$. The plant is initialized with the nonzero initial condition $x(0) = \begin{bmatrix} 0.0846 & -0.0229 & -0.0474 & -0.0083 \end{bmatrix}^{\mathrm{T}}$ in controllable canonical form. Due to the nonzero initial conditions, $\bar{z}(t)$ oscillates in

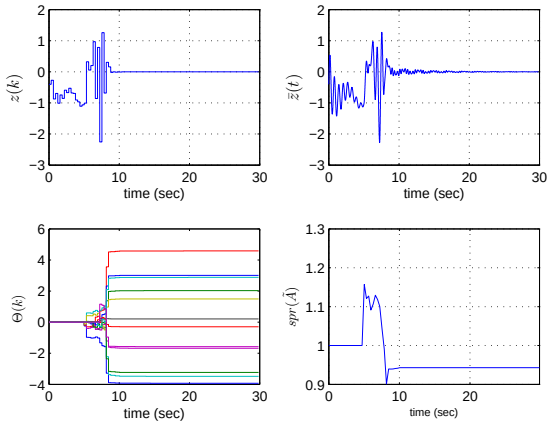

Figure 6.6: Example 6.4.1: Undersampled asymptotically stable modes. This figure illustrates the closed-loop response with lightly-damped modes that are uncontrollable due to sampling. Nevertheless, RCAC drives both $z(k)$ and $\bar{z}(t)$ to zero, and the closed-loop sampled-data system is stable after convergence.

open-loop, and the control objective is to drive $\bar{z}(t)$ to zero. Furthermore, at $t = 50$ sec, the matched sinusoidal disturbance $\bar{w}(t) = \mathbf{1}(t - 50)25\sin(t)$ starts exciting the system. Therefore, the objective is to first regulate the output $\bar{z}(t)$ and then reject the disturbance $\bar{w}(t)$ from $\bar{z}(t)$. Note that the disturbance frequency is $\omega = 1$ rad/sec $= 0.16$ Hz.

We first sample the plant with $\omega_{\mathrm{s}} = 20\pi$ rad/sec $= 10$ Hz, which is faster than the Nyquist rate 20 rad/sec associated with the undamped modes. RCAC is turned on at $t = 20$ sec, and choosing $n_{\mathrm{c}} = 6$, $P_0 = 10^4 I$ and $G_{\mathrm{f}}(\mathbf{q}^{-1}) = H_1\mathbf{q}^{-1} = 0.23\mathbf{q}^{-1}$, both $z(k)$ and $\bar{z}(t)$ are driven to zero, and the closed-loop sampled-data system is asymptotically stable after convergence, as shown in Figure 6.7. Note that the controller readapts at $t = 50$ sec in order to reject the disturbance $\bar{w}(t)$.

Now, we sample the plant with $\omega_{\mathrm{s}} = 20$ rad/sample $= 10/\pi$ Hz. The sampled-data plant is uncontrollable at this sampling rate, and the uncontrollable modes correspond to the undamped modes of the continuous-time plant. Choosing $n_{\mathrm{c}} = 6$, $P_0 = 10^4 I$, and $G_{\mathrm{f}}(\mathbf{q}^{-1}) = H_1\mathbf{q}^{-1} = \mathbf{q}^{-1}$, the closed-loop response is shown in Figure 6.8. The first observation is the inability of the adaptive controller to reduce the spectral

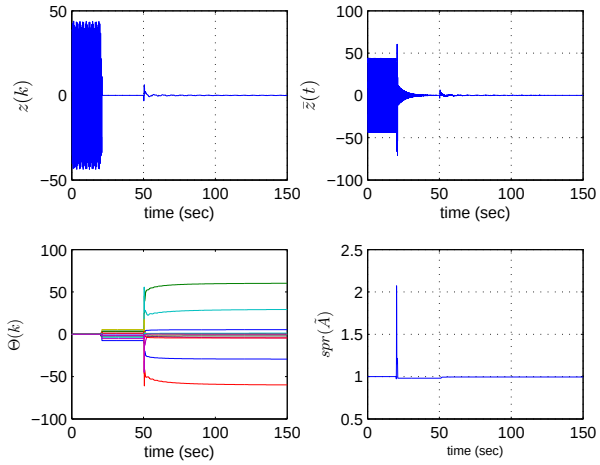

Figure 6.7: Example 6.4.2: Undersampled undamped modes. This figure illustrates the closed-loop response with sufficiently fast sampling, that is, the sampling rate 20π rad/sec is faster than the Nyquist rate corresponding to the disturbance and the dynamics. RCAC first stabilizes the system and then readapts at $t = 50$ sec to reject the disturbance. The spectral radius of the closed-loop system is 0.99 after convergence.

radius of the closed-loop sampled-data system below 1. This is expected, because the undamped modes are uncontrollable due to sampling. The second observation is that, despite the fact that $z(k)$ converges to zero, the intersample values of $\bar{z}(t)$ are large, in fact, in steady-state, $\bar{z}(t)$ has a peak magnitude of about 22. To study the cause of large intersample behavior, we perform a spectral analysis of $\bar{z}(t)$ after convergence. Figure 6.9 shows the power spectral density of $\bar{z}(t)$ for $t > 100$. In particular, we notice spikes near frequencies $\omega_1 = 0.16$ Hz, $\omega_2 = 1.59$ Hz, $\omega_3 = 3.04$ Hz and $\omega_4 = 3.34$ Hz. Note that ω_1 is exactly the frequency ω of the disturbance signal $\bar{w}(t)$. Furthermore, $\omega_3 = \omega_s - \omega_1$, and $\omega_4 = \omega_s + \omega_1$ are alias frequencies associated with the disturbance frequency ω and sampling rate ω_s. However, the spike with the largest magnitude corresponds to ω_2, which is exactly the frequency of the undamped modes. Note that ω_2 is also the Nyquist frequency of the sampled-data system. The large intersample oscillations in $\bar{z}(t)$ are therefore caused by the aliasing effects associated with the undamped, uncontrollable modes of the continuous-time

plant.

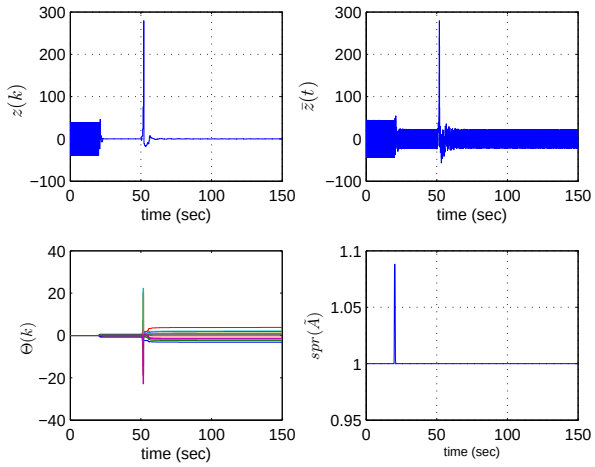

Figure 6.8: Example 6.4.2: Undersampled undamped modes. This figure illustrates the closed-loop response with undamped modes that are uncontrollable due to sampling. Although RCAC drives the sampled output $z(k)$ to zero, the actual continuous-time signal $\bar{z}(t)$ is not equal to zero between sampling instants. Since the undamped modes are uncontrollable, RCAC cannot decrease the closed-loop spectral radius below 1.

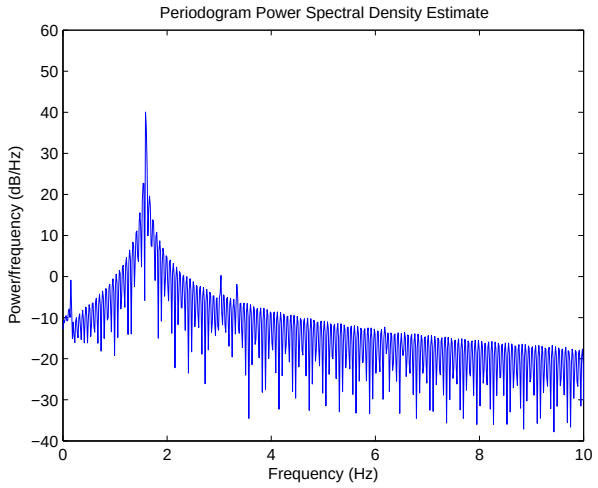

Figure 6.9: Example 6.4.2: Undersampled undamped modes. This figure illustrates the power spectral density of the closed-loop performance $\bar{z}(t)$ shown in Figure 6.8 in steady-state. The largest peak in the spectral content is near 1.59 Hz, which is the frequency of the uncontrollable, undamped modes.

Finally, we reconsider the same problem with $\omega_s = 4\pi$ rad/sample $= 2$ Hz, which is

slower than the Nyquist rate corresponding to the undamped modes. The continuous-time plant is thus undersampled, however, the sampled-data plant does not lose controllability due to sampling. Furthermore, the sampled-data plant now has a NMP sampling zero near -1.34. Choosing $n_{\rm c} = 6$, $P_0 = 10^4 I$, and $G_{\rm f}(\mathbf{q}) = H_1 \frac{(\mathbf{q}+1.34)}{\mathbf{q}^2}$, the closed-loop response is shown in Figure 6.10. We observe that before the disturbance is introduced, both $z(k)$ and $\bar{z}(t)$ are driven to zero, and then, after the disturbance is introduced, $z(k)$ converges to zero after a transient period, although $\bar{z}(t)$ exhibits intersample oscillations. This suggests that the intersample oscillations are caused by the aliasing effects associated with the disturbance, rather than the undamped modes. The power spectral density of $\bar{z}(t)$ shown in Figure 6.11 confirms this view, as the spikes in the spectral density are near ω, and the alias frequencies $l\omega_{\rm s} \pm \omega$, where l is a positive integer. In conclusion, aliasing of the undamped dynamics causes trouble only if these modes are uncontrollable due to sampling. Otherwise, RCAC moves these modes inside the unit circle so that the natural response of the closed-loop plant converges to zero as t increases.

Example 6.4.3 (Undersampled unstable modes)**.** Consider the $4^{\rm th}$-order unstable plant $T_{zu}(s) = 20\frac{(s+0.6)(s+1.5)}{(s-1+\jmath 10)(s-1-\jmath 10)(s+0.5+\jmath 1.5)(s+0.5-\jmath 1.5)}$. The plant is initialized with the nonzero initial conditions $x(0) = \begin{bmatrix} -0.09 & 0.03 & -0.02 & -0.005 \end{bmatrix}^{\rm T}$ in controllable canonical form. The control objective is to stabilize the closed-loop system and drive the output $\bar{z}(t)$ to zero.

It follows from (6.6) that if the sampling rate is chosen to be $\omega_{\rm s} = 20/l$, where l is a positive integer, sampled-data control of T_{zu} becomes impractical, since the unstable modes are uncontrollable due to sampling.

Now, to investigate the effects of undersampling of unstable (but controllable) modes, we sample $T_{zu}(s)$ with $\omega_{\rm s} = 2\pi$ rad/sample $= 1$ Hz. Note that $\omega_{\rm s}$ is slower than the Nyquist rate 20 rad/sample corresponding to the unstable modes. Furthermore, the sampled-data system has a NMP sampling zero near -2.91. RCAC is turned on at

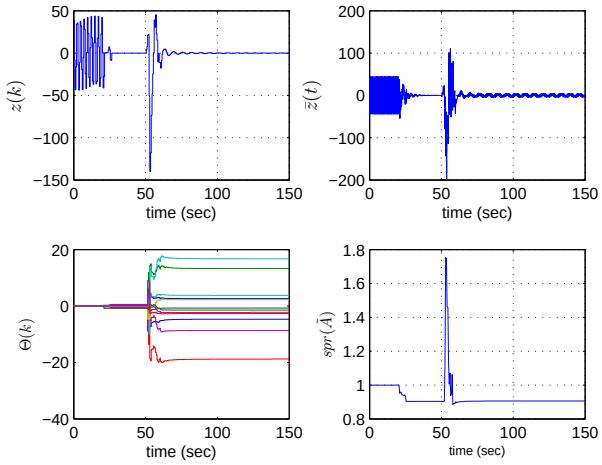

Figure 6.10: Example 6.4.2: Undersampled undamped modes. Sampling rate 4π rad/sec is now lower than the Nyquist rate corresponding to the undamped modes, however, these modes are now controllable after sampling. The output first oscillates due to nonzero initial conditions, and then, RCAC is turned on at $t = 20$ sec, and drives both $z(k)$ and $\bar{z}(t)$ to zero. Then, at $t = 50$ sec, the disturbance starts exciting the system, RCAC readapts, and rejects the disturbance from $z(k)$. However, $\bar{z}(t)$ is nonzero between sampling instants due to disturbance aliasing.

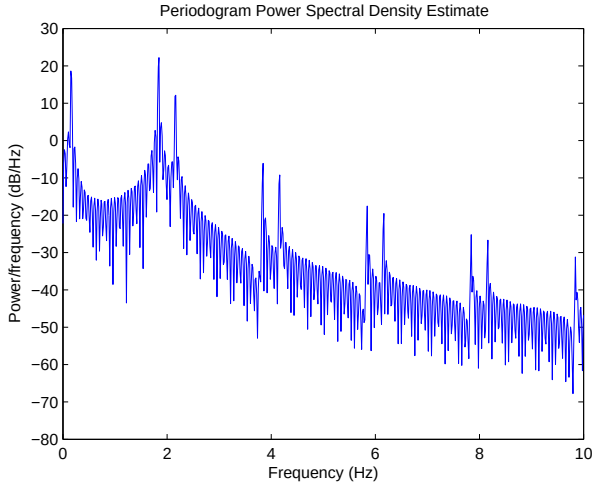

Figure 6.11: Example 6.4.2: Undersampled undamped modes. This figure illustrates the power spectral density of the closed-loop performance $\bar{z}(t)$ shown in Figure 6.8 in steady-state. The power spectral density does not have a peak near the frequency of the undamped modes. Rather, the peaks are near the disturbance frequency ω and aliased frequencies $l\omega_s \pm \omega$, where l is a positive integer.

$t = 2$ sec with $n_c = 4$, $P_0 = 1000I$, and $G_f(\mathbf{q}) = H_1 \frac{(\mathbf{q}+2.91)}{\mathbf{q}^2}$. Since the sampling rate is chosen to be slow, the output $\bar{z}(t)$ undergoes large transients, but nevertheless, RCAC stabilizes the plant, and both $z(k)$ and $\bar{z}(t)$ converge to zero in about 30 seconds, which is 30 time steps, as shown in 6.12.

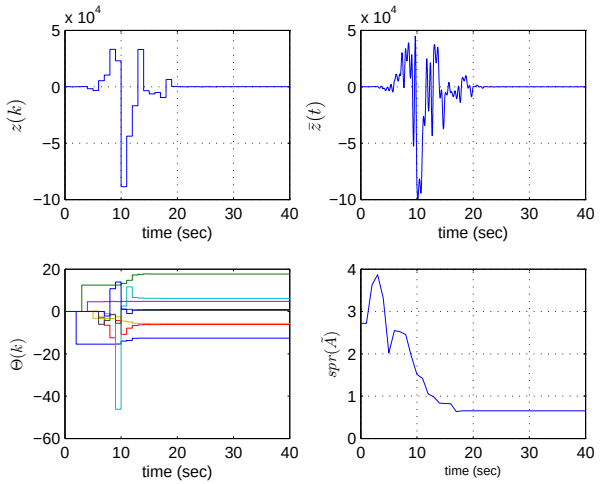

Figure 6.12: Example 6.4.3: Undersampled unstable modes. This figure illustrates the closed-loop response with the sampling rate 2π rad/sample, which is slower than the Nyquist rate 20 rad/sample corresponding to the unstable modes. The plant is initialized with nonzero initial conditions, and therefore, the output $\bar{z}(t)$ first diverging away from zero. Then, at $t = 2$, RCAC is turned on. Since the sampling rate and therefore the sampled-data controller is slow, the output $\bar{z}(t)$ undergoes large transients before controller convergence, but eventually, RCAC stabilizes the plant, and drives both $z(k)$ and $\bar{z}(t)$ to zero.

Indeed, transient performance and convergence time can be improved by sampling faster. For example, choosing $\omega_s = 20\pi$ rad/sample $= 10$ Hz, $n_c = 4$, $P_0 = 1000I$, and $G_f(\mathbf{q}) = H_1 \frac{\mathbf{q}^{-1}+1.1}{\mathbf{q}^2}$, RCAC is turned on at $t = 2$ sec. Now, $\bar{z}(t)$ converges to zero in about 30 time steps, which is the same as in the previous case, but since a time step is equal to 0.1 sec, convergence occurs in only 3 sec, and the transient performance is much better compared to Figure 6.12 as shown in Figure 6.13.

In conclusion, the adaptive controller is able to stabilize the unstable plant even if the unstable modes are undersampled, however, if the sampling rate and therefore the

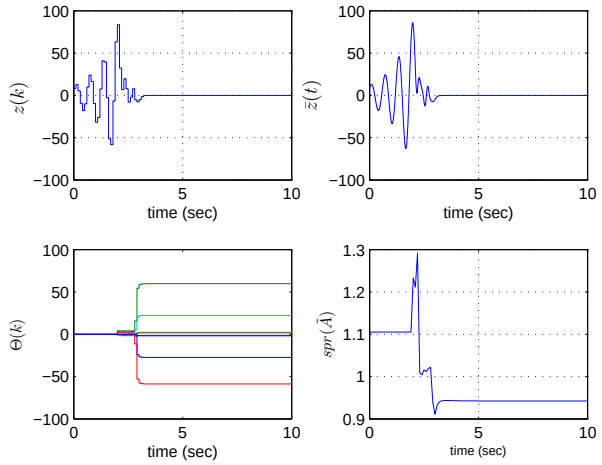

Figure 6.13: Example 6.4.3: Undersampling of unstable modes. This figure illustrates the closed-loop response with the sampling rate 20π rad/sample, which is ten times faster than the sampling rate of Figure 6.12. The convergence is faster, and the transient performance is better compared to Figure 6.12.

controller is too slow, the output may become too large before it can be regulated by the controller, and therefore, undersampling the unstable modes may be undesirable in practice. Obviously, the sampling rate should be chosen so that the unstable modes of the system are controllable.

6.5 Conclusion

In this chapter, we presented a numerical investigation of retrospective cost adaptive control (RCAC) applied to sampled-data control in the presence of aliasing of dynamics and disturbances. It is shown that RCAC stabilizes plant even if the high-frequency unstable modes are undersampled. However, even if the samples of the performance variable converge to zero, intersample command following error may be nonzero due to aliasing of disturbances. If the disturbance frequency is larger than the Nyquist frequency, RCAC converges to an internal model controller with high gain at the aliased disturbance frequency. Controllability loss due to sampling is also considered, and it is shown that the performance of RCAC is not degraded as long

as the uncontrollable modes are stable.

6.6 Appendix: Undersampling and Aliasing

In this appendix section, we provide a review of several major results concerning sampling and reconstruction theory [9, 61, 90]. The goal here is not to provide a thorough analysis of the sampling theory, rather, the goal here is to provide a quick overview of certain terminology and results in sampling theory for the sake of clarity in upcoming sections.

Consider the continuous-time harmonic signal $\bar{z}(t)$ and a sampler with sampling period h sec/sample as shown in Figure 6.1. The sampler thus has the frequency $\nu_{\rm s} = \frac{1}{h}$ Hz, or $\omega_{\rm s} = \frac{2\pi}{h}$ rad/sec. Notice that the units of $\nu_{\rm s}$ and $\omega_{\rm s}$ are different, but they both represent the same sampling frequency. The sampling operator maps the continuous-time signal $\bar{z}(t)$ to a discrete-time signal that we call the *sampled signal*. The sampled signal is denoted by $z(k)$, which represents $\bar{z}(kh)$, where k is an integer. Unlike $\bar{z}(t)$, the sampled signal $z(k)$ is a discrete sequence whose domain is the set of integers. For example, $z(3)$, $z(5)$ and $z(17)$ are well-defined, but $z(1.7)$, $z(\pi)$ or $z(0.01)$ are not defined, whereas $\bar{z}(1.7)$, $\bar{z}(\pi)$ or $\bar{z}(0.01)$ are well-defined. Furthermore, in general, $z(k) \neq \bar{z}(t)$. This is why we use a bar symbol to distinguish the continuous-time signal from the sampled signal.

The (almost) inverse of the sampling operator is referred to as the *reconstruction operator*. The reconstruction operator maps the discrete-time signal $z(k)$ to a continuous-time signal $\tilde{z}(t)$. The typical reconstruction method is the *Whittaker-Shannon (W-S) interpolation formula* [113, 93], which passes $z(k)$ through an ideal low-pass filter with the cutoff frequency $\frac{\omega_{\rm s}}{2}$ to obtain $\tilde{z}(t)$. Thus, sampling and reconstruction are, in certain conditions, exact inverses of each other. However, in general, sampling is not one-to-one, that is, sampling two continuous-time signals $\bar{z}_1(t)$ and $\bar{z}_2(t)$ may yield the same sampled signal $z(k)$, even when $\bar{z}_1(t) \neq \bar{z}_2(t)$. Therefore,

the continuous-time signal $\bar{z}(t)$ may not be equal to the reconstructed signal $\tilde{z}(t)$. This relates to the famous sampling theorem [93], which provides the necessary and sufficient condition to have $\bar{z}(t) = \tilde{z}(t)$.

Theorem 6.6.1. *A function $\bar{z}(t)$ is completely determined by giving its ordinates at a series of points spaced $\frac{1}{2\nu_{\mathrm{B}}}$ seconds apart if and only if $\bar{z}(t)$ contains no frequencies higher than ν_{B} Hz.*

In essence, it follows from Theorem 6.6.1 that if the sampling rate ν_{s} (or ω_{s}) is at least twice as large as the highest frequency (or bandwidth) ν_{B} (or ω_{B}) of $\bar{z}(t)$, then $\tilde{z}(t) = \bar{z}(t)$, that is, the continuous-time signal $\bar{z}(t)$ can be reconstructed from the sampled signal $z(k)$ by the means of W-S interpolation.

Notice that the frequency $2\nu_{\mathrm{B}}$ is a threshold for the sampling rate ν_{s}, determining whether or not the sampling rate is sufficiently fast for reconstructing the signal $\bar{z}(t)$ from its samples. Conversely, $\frac{\nu_{\mathrm{s}}}{2}$ is a threshold for the bandwidth of the signal $\bar{z}(t)$, and, if $\nu_{\mathrm{B}} < \frac{\nu_{\mathrm{s}}}{2}$, then $\bar{z}(t)$ can be reconstructed from the samples $z(k)$. The former threshold $2\nu_{\mathrm{B}}$ is referred to as the *Nyquist rate* corresponding to $\bar{z}(t)$, whereas the latter threshold $\frac{\nu_{\mathrm{s}}}{2}$ is defined as the *Nyquist frequency* corresponding to the sampler. Nyquist rate and Nyquist frequency are not to be confused; Nyquist rate is a property of the signal, whereas Nyquist frequency is a property of the sampler.

When $\bar{z}(t)$ is sampled at a rate slower than the Nyquist rate, we say that the signal is *undersampled*. Conversely, $\bar{z}(t)$ is undersampled if the Nyquist frequency is slower than the bandwidth of $\bar{z}(t)$. If $\bar{z}(t)$ is undersampled, it follows from Theorem 6.6.1 that the signal $\bar{z}(t)$ cannot be recovered from the sampled signal $z(k)$ by the means of W-S interpolaation. For instance, for the harmonic signal $\bar{z}(t)$ with a frequency component at ω_0, the sampled signal $z(k)$ will have replicate frequency components or *aliases* at $\omega_0 + l\omega_{\mathrm{s}}$ and $-\omega_0 + l\omega_{\mathrm{s}}$, where l is an integer. Thus, if $\omega_0 > \omega_{\mathrm{N}}$, where ω_{N} is the Nyquist frequency, then $z(k)$ will have an alias frequency component between 0 rad/sec and ω_{N} rad/sec. In particular, the alias frequency component $\omega_{0\mathrm{a}} \in [0, \omega_{\mathrm{N}}]$

is given by

$$\omega_{0\mathrm{a}} = \min(\omega_0[\omega_\mathrm{s}], \omega_\mathrm{N} - \omega_0[\omega_\mathrm{N}]), \tag{6.15}$$

and, once the sampled signal $z(k)$ is reconstructed by passing it through a low-pass filter with the cutoff frequency ω_N, the reconstructed signal $\tilde{z}(t)$ contains the alias frequency $\omega_{0\mathrm{a}}$, but does not contain the actual frequency component ω_0 since it is filtered out during the interpolation.

As an example, consider the sinusoidal signal $\bar{z}_1(t) = \sin(1.3\pi t)$. To illustrate aliasing due to sampling, we choose $h = 1$ sec/sample and thus $\omega_\mathrm{s} = 2\pi$ rad/sec, which is smaller than the Nyquist rate 2.6π rad/sec corresponding to $\bar{z}_1(t)$. The sampled signal is thus $z_1(k) = \sin(1.3\pi k)$. We claim that this signal is indistinguishable from the sampled signal $z_2(k) = -\sin(0.7\pi k)$ corresponding to the continuous-time signal $\bar{z}_2(t) = -\sin(0.7\pi t)$, and, interpolating $z_1(k)$ by the means of W-S generates $\bar{z}_2(t)$ rather than $\bar{z}_1(t)$. Indeed, since $e^{\jmath x}$ is a periodic function with the period $X = 2\pi$, we have

$$\begin{aligned} z_1(k) = \sin(1.3\pi k) &= \frac{1}{2\jmath}\left(e^{\jmath 1.3\pi k} - e^{-\jmath 1.3\pi k}\right) \\ &= \frac{1}{2\jmath}\left(e^{\jmath 1.3\pi k - 2\pi k} - e^{-\jmath 1.3\pi k + 2\pi k}\right) \\ &= -\frac{1}{2\jmath}\left(e^{\jmath 0.7\pi k} - e^{-\jmath 0.7\pi k}\right) \\ &= -\sin(0.7\pi k). \end{aligned}$$

Now, if this signal is passed through an ideal low-pass filter with the cutoff frequency $\frac{\omega_\mathrm{s}}{2}$, the resulting signal $\tilde{z}_1(t)$ is given by $-\sin(0.7\pi t) = \bar{z}_2(t)$.

CHAPTER VII

Conclusion and Future Work

This dissertation presented the latest advances and extensions in retrospective cost adaptive control. The main topics of this dissertation included theory and analysis for retrospective cost adaptive control of nonsquare systems, and development of a modified RCAC update law for maintaining stability and convergence in the presence of unmodeled NMP zeros. Other contributions of this work included: a stability analysis for the RCAC update equations and derivation of sufficient conditions for convergence of RCAC, sampled-data analysis and adaptive control of Rohrs counterexamples using robust RCAC, numerical investigation of the role of phase mismatch between an FIR filter involved in the retrospective cost optimization and the open-loop plant, development of least-squares based fitting algorithms to match the phase of an IIR transfer function with an FIR transfer function, and an investigation of RCAC in the presence of aliasing of high-frequency dynamics and disturbances.

In Chapter II, we reviewed the instantaneous and cumulative RCAC update laws developed in [88, 36]. We reformulated the instantaneous update law given in [88] as a recursive gradient update. We also reformulated the cumulative update law given in [36] using the quadratic minimization lemma [5] as in [88], and then derived the RLS update equations presented in [36]. Next, we provided a summary of the Markov-parameter-based, time-series-coefficients-based, and NMP-zero-based

controller construction techniques that have been developed in [110, 88, 36]. We presented a summary of closed-loop stability and convergence properties of the instantaneous and cumulative RCAC update laws. The most notable assumption required for these properties is that the NMP zeros of the plant, if any, are known. Finally, we presented an application of the algorithm to road-following preview control problem.

In Chapter III, we investigated RCAC for nonsquare plants, which generically have no transmission zeros. Except for the limited investigation of RCAC for SIMO and MISO plants provided in [97], RCAC for nonsquare plants has not been studied before. We started the main discussion by providing motivating examples which show that RCAC may lead to unbounded control input and unbounded plant response, even when the nonsquare plant has no transmission zeros. Next, we provided an analysis which shows that, in the wide case, the control signal generated by RCAC lies inside a subspace that is contained within the input space, which we call the "input subspace". Next, we analyzed the stability of the controller update. We demonstrated that, in the case where $d = 1$, the controller update is static, and therefore stability is irrelevant, and, in the case where $d = 2$, the controller update is globally exponentially stable under a weak persistency assumption. We also provide sufficient conditions for convergence of the adaptive controller, which shows that, if the performance output lies inside an output subspace which depends on the first nonzero Markov parameter, then the controller converges. These results point out the existence of two implicit squaring operations performed on the nonsquare plant: one performed by pre-compensating the plant, the other performed by post-compensating the plant. In the wide case, pre-compensation leads to squaring-down, which incorporates additional zeros due to squaring, which we call "input-subspace zeros". Similarly, in the tall case, post-compensation changes the zero structure and incorporates additional zeros, which we call "output-subspace zeros". We showed that if the nonsquare plant has NMP subspace zeros, then RCAC attempts to cancel these zeros, which leads to

unbounded control input in the wide case, and unbounded control input and performance output in the tall case. In light of these findings, we extended the retrospective cost function to include a performance-dependent control penalty in order to prevent the controller from generating an unbounded control input.

With regard to retrospective cost adaptive control of nonsquare plants, future work should focus on a proof of stability and convergence for the adaptive system. In this dissertation, we analyzed the mechanics behind the instability observed in nonsquare plants, and showed that the presence of NMP subspace zeros may cause RCAC to converge to a destabilizing controller. However, we did not provide a rigorous stability and convergence analysis for the case when the subspace zeros are minimum phase. Future research might focus on extending the stability proof in [43] to nonsquare plants with minimum phase subspace zeros. Furthermore, the analysis presented in Chapter III is confined to the case $G_{\mathrm{f}}(\mathbf{q}^{-1}) = H_d\mathbf{q}^{-1}$, where H_d is assumed to have full rank. Future work might focus on extending the results developed in this dissertation to higher-order G_{f}, and to the case where H_d may have less than full rank. It should be noted that, in the case where H_d has less than full rank, input and subspaces do play a role in square plants as well as nonsquare plants. Specifically, assume that the plant is square, and that H_d has less than full rank. Then, $\dim \mathcal{R}(H_d^{\mathrm{T}}) < l_u$ and thus u is contained inside a proper subspace of the input space. Furthermore, since $\dim \mathcal{N}(H_d^{\mathrm{T}}) \geq 1$, the controller may converge with nonzero performance output. Therefore, square, minimum-phase plants that have rank-deficient H_d may have NMP subspace zeros, which may lead to the same instability that was demonstrated for nonsquare plants in Chapter III.

In Chapter IV, we modified the RCAC update laws of [36, 88] to include a performance dependent control penalty. This modification is called "η-modification" because of the similarities of the technique with the ϵ-modification developed in [78]. This modification penalizes the distance between the adaptive controller and an a

priori known stabilizing controller on the regressor directions. Therefore, this modification pushes the control input toward the input signal that would have been generated by the stabilizing controller. In the open-loop stable case, a simple choice for the stabilizing controller is the zero-gain controller. In this case, the η-modification prevents the control input from growing without bound. We presented numerical examples demonstrating RCAC with η-modification for both SISO and MIMO plants. Finally, we applied robust RCAC to Rohrs counterexamples in order to determine its ability to address the effects of unmodeled dynamics and unknown NMP sampling zeros. We showed that the RCAC update laws of Chapter II without η-modification exhibit instability when the unknown sampling zero is NMP. However, we showed that the robust RCAC update law with η-modification is able to follow the sinusoidal command despite the unmodeled modes, the unknown sinusoidal disturbance, and the unknown NMP sampling zero contributed by the unmodeled dynamics.

With regard to η-modification, future work might focus on extending the heuristic stability arguments and developing a rigorous stability proof for the adaptive system with η-modification. Because of the similarities of the approach with ϵ-modification in continuous-time adaptive control, the proof may be carried out by extending the stability proofs of ϵ-modification to discrete-time adaptive control. Furthermore, a proof-by-contradiction may be possible for open-loop stable plants with the assumption that the adaptive controller does not involve an asymptotic pole-zero cancellation. This can be done by showing that, if the closed-loop system becomes unstable and observability is preserved, then the performance output must diverge to infinity, which would cause Θ to converge to the nullspace of the regressor, which would then revert the closed-loop system back to open-loop, which is asymptotically stable.

In Chapter V, we provided a numerical investigation of the asymptotic command following and disturbance rejection capabilities of RCAC with η-modification. This numerical investigation included a large-scale simulation with random plants and ran-

dom tuning parameters. The results of this numerical study suggested that the phase mismatch between an FIR filter G_{f} involved in the retrospective cost optimization and the open-loop plant G_{zu} plays critical role in the asymptotic convergence of the performance output to zero. This numerical evidence motivated the development of two system identification methods to fit IIR transfer functions with FIR transfer functions to minimize the phase mismatch. These identification methods lead to a new phase-matching-based controller construction technique in addition to the Markov-parameter, NMP-zero, and time-series-based construction methods given in Chapter II. We demonstrated the effectiveness of the phase-matching-based construction on mass-spring-dashpot systems in the presence of multi-tone sinusoidal disturbances. Future work includes a more in-depth analysis of the effects of phase mismatch on the asymptotic convergence of performance to zero. In particular, phase mismatch may be linked to positive realness of the plant transfer function G_{zu} divided by the FIR transfer function G_{f}. It should be noted that passivity of G_{zu}/G_{f} is a sufficient condition for having less than 90 deg phase mismatch at the frequency interval $[0, \pi]$ rad/sample.

Finally, in Chapter VI, we considered RCAC in the presence of aliasing, due to either the high frequency free response of the plant, or the high-frequency content in the disturbances. We showed that the intersample command-following performance may be nonzero due to aliasing of disturbances. We demonstrated that if the disturbance frequency is larger than the Nyquist frequency, then RCAC converges to an internal model controller with high gain at the aliased disturbance frequency. Therefore, the samples of the performance output converge to zero, but the actual continuous-time performance output is not zero between two consecutive sampling instants. Nevertheless, the numerical examples suggest that RCAC is able to stabilize the plant despite the high-frequency dynamics, and does not destabilize the closed-loop system because of disturbance aliasing, unless the controllability of unstable modes is lost

due to sampling.

BIBLIOGRAPHY

BIBLIOGRAPHY

[1] S. Akhtar and D. S. Bernstein, "Optimal Adaptive Feedback Disturbance Rejection," in *Proc. ACTIVE 04,* Williamsburg, VA, September 2004.

[2] S. Akhtar and D. S. Bernstein, "Lyapunov-stable Discrete-time Model Reference Adaptive Control," *Int. J. Adaptive Contr. Signal Proc.,* Vol. 19, pp. 745767, 2005.

[3] K. J. Astrom, P. Hagander, and J. Sternby, "Zeros of Sampled Systems," *IEEE Trans. Autom. Contr.*, Vol. 20, No. 1, pp. 31–38, 1984.

[4] K. J. Astrom and B. Wittenmark, *Adaptive Control,* 2^{nd} *ed.,* Addison-Wesley, 1995.

[5] D. S. Bernstein, *Matrix Mathematics,* Princeton University Press, 2009.

[6] D. S. Bernstein and S. P. Bhat, "Lyapunov Stability, Semistability, and Asymptotic Stability of Matrix Second-Order Systems," *ASME J. Mechanical Design*, Vol. 117, Issue B, pp. 145–153, 1995.

[7] R. R. Bitmead, M. Gevers, and V. Wertz, *A*daptive Optimal Control: The Thinking Mans GPC, Prentice Hall, 1990.

[8] M. J. Blachuta, "Continuous-time Design of Discrete-time Control Systems," *Proc. 1997 Europ. Contr. Conf.,* Brussels, Belgium, 1997.

[9] H. S. Black, *Modulation Theory*, Princeton, N.J.: Van Nostrant, 1953.

[10] M. Bodson, and S. C. Douglas, "Adaptive Algorithms for the Rejection of Sinusoidal Disturbances with Unknown Frequency," *Automatica,* Vol. 33, pp. 2213–2221, 1997.

[11] M. Bodson, J. S. Jensen, and S. C. Douglas, "Active Noise Control for Periodic Disturbances," *IEEE Trans. Contr. Sys. Tech.,* Vol. 9, pp. 200–205, 2001.

[12] L. Chai, J. Zhang, C. Zhang, and E. Mosca , "From IIR to FIR Digital MIMO Models: A Constructive Hankel Norm Approximation Method," *Proc. Conf. Dec. Contr.*, pp. 5893–5898, Seville, Spain, December 2005.

[13] C. T. Chen, *Linear System Theory and Design: Third Edition,* Oxford University Press, 1998.

[14] J. Chen, "Multivariable Gain-Phase and Sensitivity Integral Relations and Design Tradeoffs," *IEEE Trans. on Autom. Contr.,* Vol. 43, No. 3, pp. 373–385, March 1998.

[15] J. Chen, "On Logarithmic Complementary Sensitivity Integrals for MIMO Systems," in *Proceedings of American Control Conference,* Philadelphia, PA, pp. 3529–3530, June 1998.

[16] T. Chen and B. A. Francis, "H_2-Optimal Sampled-Data Control," *IEEE Trans. Autom. Contr.*, Vol. 36, No. 4, pp. 387–397, April 1991.

[17] T. Chen and B. A. Francis, *Optimal Sampled-Data Control Systems*, Springer, 1996.

[18] J. Daams, and J. W. Polderman, "Almost Optimal Adaptive LQ Control: SISO Case," *Math. Contr. Sig. Sys.,* Vol. 15, pp. 71–100, 2002.

[19] A. M. DAmato, E. D. Sumer, K. S. Mitchell, A. V. Morozov, J. B. Hoagg, and D. S. Bernstein, "Adaptive Output Feedback Control of the NASA GTM

Model with Unknown Nonminimum-Phase Zeros," *AIAA Guid. Nav. Contr. Conf.,* Portland, OR, August 2011, AIAA-2011-6204.

[20] A. M. D'Amato, E. D. Sumer, and D. S. Bernstein, "Frequency-Domain Stability Analysis of Retrospective Cost Adaptive Control for Systems with Unknown Nonminimum-Phase Zeros," *Proc. Conf. Dec. Contr.*, Orlando, FL, December 2011.

[21] A. Datta, *Adaptive Internal Model Control,* Springer-Verlag, 1998.

[22] E. J. Davison, "Some Properties of Minimum Phase and Squared-down Systems," *IEEE Trans. Autom. Contr.,* Vol. 28, No. 2, pp. 221-222, February 1983.

[23] E. J. Davison and H. W. Smith, "Pole Assignment in Linear Time-Invariant Multivariable Systems with Constant Disturbances," *Automatica,* Vol. 7, pp. 489498, 1971.

[24] E. J. Davison and S. H. Wang, "Properties and Calculation of Transmission Zeros of Linear Multivariable Systems," *Automatica*, Vol. 10, pp. 643–658, 1974.

[25] J. C. Doyle, B. A. Francis, and A. R. Tannenbaum, *Feedback Control Theory,* Macmillan, 1992.

[26] S. J. Elliott, and P. A. Nelson, "Active Noise Control," *IEEE Signal Processing Magazine,* Vol. 10, No. 4, pp. 12–35, October 1993.

[27] M. S. Fledderjohn, M. S. Holzel, H. Palanthandalam-Madapusi, R. J. Fuentes and D. S. Bernstein, "A Comparison of Least Squares Algorithms for Estimating Markov Parameters", *Proc. Amer. Contr. Conf.*, pp. 3735–3740, Baltimore, MD, June 2010.

[28] G. D. Forney, "Minimal Bases of Rational Vector Spaces, with Applications to Multivariable Linear Systems," *SIAM Journal on Control,* Vol. 13, No. 3, pp. 493–520, 1975.

[29] B. A. Francis, "Internal Model Principle of Control Theory," *Automatica*, Vol. 12, No. 5, pp. 457–465, September 1976.

[30] B. A. Francis, A. Sebakhy, and W. M. Wonham, "Synthesis of Multivariable Regulators: The Internal Model Principle," *J. Appl. Math. Optim.,* Vol. 1, pp. 64-86, 1974.

[31] B. A. Francis and W. M. Wonham, "The internal model principle for linear multivariable regulators," *J. Appl. Math. Optim.,* Vol. 2, pp. 170-194, 1975.

[32] G. F. Franklin, J. D. Powell, A. Emami-Naein, *Feedback Control of Dynamic Systems*, Sixth Edition, Prentice Hall, 2009.

[33] J. S. Freudenberg and D. P. Looze, "Right Half Plane Poles and Zeros and Design Tradeoffs in Feedback Systems," *IEEE Trans. Autom. Contr.,* Vol. 30, No. 6, pp. 555–565, June 1985.

[34] G. C. Goodwin and K. S. Sin, *Adaptive Filtering Prediction and Control,* Prentice-Hall, 1984.

[35] A. Feuer and G. C. Goodwin, "Generalized Sample Hold Functions–Frequency Domain Analysis of Robustness, Sensitivity, and Intersample Difficulties," *IEEE Trans. Autom. Contr.,* Vol. 39, No. 5, May 1994.

[36] J. B. Hoagg, "Retrospective Cost Adaptive Control for Nonminimum-Phase Discrete-Time Systems, Part 1: The Ideal Controller and Error System, Part 2: The Adaptive Controller and Stability Analysis," *Proceedings of the 49th Conference on Decision and Control,* pp. 893–904, Atlanta, GA, December 2010.

[37] J. B. Hoagg and D. S. Bernstein, "Discrete-time Adaptive Feedback Disturbance Rejection Using a Retrospective Performance Measure," in *Proc. ACTIVE 04,* Williamsburg, VA, 2004.

[38] J. B. Hoagg and D. S. Bernstein, "Nonminimum-Phase Zeros: Much to Do About Nothing," *IEEE Control Systems Magazine,* Vol. 27, pp. 45–57, June 2007.

[39] J. B. Hoagg and D. S. Bernstein, "Cumulative Retrospective Cost Adaptive Control with RLS-based Optimization," *Proc. Amer. Contr. Conf.,* pp. 4016–4021, Baltimore, MD, July 2010.

[40] J. B. Hoagg and D. S. Bernstein, "Retrospective Cost Model Reference Adaptive Control for Nonminimum-Phase Discrete-Time Systems, Part 1: The Ideal Controller and Error System; Part 2: The Adaptive Controller and Stability Analysis," *Proc. Amer. Contr. Conf.*, pp. 2927–2938, San Francisco, CA, June 2011.

[41] J. B. Hoagg and D. S. Bernstein, "Retrospective Cost Model Reference Adaptive Control for Nonminimum-Phase Systems," *AIAA J. of Guid. Contr. Dyn.,* Vol. 35, No. 6, pp. 1767–1786, 2012.

[42] J. B. Hoagg, D. S. Bernstein, S. L. Lacy, and R. Venugopal, "Adaptive Control of a Flexible Membrane Using Acoustic Excitation and Optical Sensing," in *Proc. Guid. Nav. Contr. Conf.,* Austin, TX, 2003, AIAA-2003-5430.

[43] J. B. Hoagg, M. A. Santillo, and D. S. Bernstein, "Discrete-Time Adaptive Command Following and Disturbance Rejection With Unknown Exogenous Dynamics," *IEEE Transactions on Automatic Control*, Vol. 53, pp. 912–928, 2008.

[44] J. B. Hoagg, M. A. Santillo, and D. S. Bernstein, "Internal Model Control in

the Shift and Delta Domains," *IEEE Transactions on Automatic Control*, Vol. 53, pp. 1066–1072, 2008.

[45] N. Hovakimyan, and C. Cao, L_1 *Adaptive Control Theory: Guaranteed Robustness with Fast Adaptation,* SIAM, 2010.

[46] A. Ilchmann, *Non-Identifier-Based High-Gain Adaptive Control*, Springer-Verlag, 1993.

[47] P. A. Ioannou, and B. Fidan, *Adaptive Control Tutorial,* SIAM, 2006.

[48] P. A. Ioannou, and A. Datta, "Robust Adaptive Control: A Unified Approach," *Proceedings of the IEEE,* Vol. 79, No. 12, pp. 1735–1768, 1991.

[49] P. A. Ioannou, and J. Sun, "Theory and Design of Robust Direct and Indirect Adaptive Control Schemes," *International Journal of Control,* Vol. 47, No. 3, pp. 775–813, 1988.

[50] P. A. Ioannou, and J. Sun, *Robust Adaptive Control,* Prentice-Hall, 1996.

[51] T. Ionescu and R. Monopoli, "Discrete Model Reference Adaptive Control with an Augmented Error Signal," *Automatica,* Vol. 13, pp. 507-517, 1977.

[52] C. D. Johnson, "Accommodation of External Disturbances in Linear Regulator and Servomechanism Problems," *IEEE Transactions on Automatic Control,* Vol. 16, No. 6, pp. 635-644, December 1971.

[53] I. Kanellakopoulos, P. V. Kokotovic, and A. S. Morse, "Systematic Design of Adaptive Controllers for Feedback Linearizable Systems," *IEEE Transactions on Automatic Control,* Vol. 36, No. 11, pp. 1241–1253, November 1991.

[54] N. Karcanias and C. Giannakopoulos, "Necessary and Sufficient Conditions for Zero Assignment by Constant Squaring Down," *Linear Algebra and Its Applications* Vol. 122–124, pp. 415-446, 1989.

[55] N. Karcanias and B. Kouvaritakis, "The Output Zeroing Problem and its Relationship to the Invariant Zero Structure: A Matrix Pencil Approach," *International Journal of Control,* Vol. 30, No. 3, pp. 395–415, 1979.

[56] H. K. Khalil, *Nonlinear Systems: Third Edition,* Prentice-Hall, 2002.

[57] R. E. Kalman, Y. C. Ho, and K. S. Narendra, "Controllability of Linear Systems," *Contributions to Differential Equations*, Vol. 1, No. 2, pp. 189–213, Interscience, New York.

[58] P. V. Kokotovic, I. Kanellakopoulos, and A. S. Morse, "Adaptive Feedback Linearization of Nonlinear Systems," *Lecture Notes in Control and Information Sciences,* Vol. 160, pp. 309–346, 1991.

[59] B. Kouvaritakis and A. G. J. MacFarlane, "Geometric Approach to Analysis and Synthesis of System Zeros, Part 1: Square Systems, Part 2: Nonsquare Systems," *International Journal of Control,* Vol. 23, No. 2, pp. 149–181, 1976.

[60] M. Krstic, and P. V. Kokotovic, "Control Lyapunov Functions for Adaptive Nonlinear Stabilization," *Systems and Control Letters,* Vol. 26, pp. 17–23, 1995.

[61] B. C. Kuo, *Digital Control Systems*, HRW, 1980.

[62] B. C. Kuo, *Automatic Control Systems*, Sixth Edition, Prentice Hall, 1991

[63] S. M. Kuo, and D. R. Morgan, *Active Noise Control Systems: Algorithms and DSP Implementations,* Wiley, 1995.

[64] S. M. Kuo, and D. R. Morgan, "Active Noise Control: A Tutorial Review," *Proceedings of the IEEE,* Vol. 87, No. 6, June 1999.

[65] I. D. Landau, *Adaptive Control: The Model Reference Approach,* Marcel Dekker, 1979.

[66] I. D. Landau, R. Lozano, and M. M'Sadd, *Adaptive Control,* Springer, 1998.

[67] G. Langholz and Y. Bar-Ness, "On Observability of Sampled-Data Systems," *Int. J. Systems Sci.,* Vol. 8, No. 6, pp. 697–704, 1977.

[68] K. Latawiec, S. Banka, and J. Tokarzewski, "Control Zeros and Nonminimum Phase LTI MIMO Systems," *Annual Reviews in Control,* Vol. 24, pp. 105–112, 2000.

[69] E. Lavretsky, "Adaptation Along Prescribed Directions," in *Proc. Amer. Contr. Conf.,* pp. 1748–1752, San Francisco, CA, June 2011.

[70] A. G. J. MacFarlane and N. Karcanias, "Poles and Zeros of Linear Multivariable Systems: A Survey of the Algebraic, Geometric and Complex-Variable Theory," *Int. J. Control,* Vol. 24, No. 1, pp. 33–74, 1976.

[71] J. M. Maciejowski, *Multivariable Feedback Design*, Addison-Wesley, 1989.

[72] "Mechanical Simulation Corporation," http://www.carsim.com.

[73] P. Misra, "A Computational Algorithm For Squaring-Up Part I: Zero Input-Output Matrix," in *Proc. Conf. Dec. Contr.,* pp. 149–150, Tucson, AZ, December 1992.

[74] P. Misra, "Numerical Algorithms For Squaring-Up Non-Square Systems Part II: General Case," in *Proc. Amer. Contr. Conf.,* pp. 1573–1577, San Francisco, CA, June 1993.

[75] E. Mosca, *Optimal Predictive and Adaptive Control,* Prentice Hall, 1995.

[76] S. M. Naik, P.R. Kumar, and B.E. Ydstie, "Robust Continuous Time Adaptive Control by Parameter Projection," *IEEE Transactions on Automatic Control,* Vol. 37, No. 2, pp. 182–198, 1992.

[77] K. S. Narendra, and A. M. Annaswamy, "Robust Adaptive Control in the Presence of Bounded Disturbances," *IEEE Transactions on Automatic Control,* Vol. 31, No. 4, pp. 306–315, 1986.

[78] K. S. Narendra, and A. M. Annaswamy, "A New Adaptive Law for Robust Adaptation without Persistent Excitation," *IEEE Transactions on Automatic Control,* Vol. 32, No. 2, February 1987.

[79] K. S. Narendra and A. M. Annaswamy, *Stable Adaptive Systems,* Prentice-Hall, 1989.

[80] R. Ortega, and T. Yu, "Robustness of Adaptive Controllers: A Survey," *Automatica,* Vol. 25, No. 5, pp. 651–678, 1989.

[81] S. L. Osburn and D. S. Bernstein, "An Exact Treatment of the Achievable Closed-Loop H_2 Performance of Sampled-data Controllers: from Continuous-time to Open-loop," *Automatica*, Vol. 31, No. 4, pp. 617–620, 1995.

[82] D. Patt, L. Liu, J. Chandrasekar, D. S. Bernstein, and P. P. Friedmann, "The Higher-Harmonic-Control Algorithm for Helicopter Vibration Reduction Revisited," *AIAA J. Guid. Contr. Dyn.,* Vol. 28, pp. 918930, 2005.

[83] M. Prandini, and M. C. Campi, "Adaptive LQG Control of Input-Output Systems–A Cost-Biased Approach," *SIAM J. Contr. Optim.,* Vol. 39, No. 5, pp. 1499–1519, 2001.

[84] C. E. Rohrs, L. Valavani, M. Athans, and G. Stein, "Robustness of Continuous-Time Adaptive Control Algorithms in the Presence of Unmodeled Dynamics," *IEEE Trans. Autom. Contr.,* Vol. 30, No. 9, pp. 881–889, Sep 1985.

[85] H. H. Rosenbrock, *State-space and Multivariable Theory,* Wiley, 1970.

[86] H. Sane, R. Venugopal, and D. S. Bernstein, "Disturbance Rejection Using AR-MARKOV Adaptive Control with Simultaneous Identification," *IEEE Trans. Contr. Sys. Tech.,* Vol. 9, pp. 101-106, 2001.

[87] M. A. Santillo, "Adaptive Control Based on Retrospective Cost Optimization," PhD Thesis, University of Michigan, 2009.

[88] M. A. Santillo and D. S. Bernstein, "Adaptive Control Based on Retrospective Cost Optimization," *AIAA J. Guid. Contr. Dyn.*, Vol. 33, pp. 289–304, 2010.

[89] M. A. Santillo and D. S. Bernstein, "A Retrospective Correction Filter for Discrete-Time Adaptive Control of Nonminimum Phase Systems," *Proc. Conf. Dec. Contr.,* Cancun, Mexico, December 2008, pp. 690-695.

[90] M. S. Santina, A. R. Stubberud, and G. H. Hostetter, *Digital Control System Design*, Second Edition, Oxford University Press, 1995.

[91] S. Sastry and M. Bodson, *A*daptive Control: Stability, Convergence, and Robustness, Prentice Hall, 1989.

[92] C. B. Schrader and M. K. Sain, "Research on System Zeros: A Survey," *International Journal of Control,* Vol. 50, No. 4, pp. 1407-1433, 1989.

[93] C. E. Shannon, "Communication in the Presence of Noise," *Proc. Institure of Radio Eng.,* Vol. 37, No. 1, pp. 10–21, January, 1949.

[94] S. M. Shinners, *Modern Control System Theory and Application*, Addison-Wesley, 1978.

[95] S. Skogestad and I. Postlethwaite, *Multivariable Feedback Control: Analysis and Design,* 2nd Edition, Wiley, 2005.

[96] T. Soderstrom and P. Stoica, *System Identification,* Prentice Hall, 1989.

[97] E. D. Sumer, and D. S. Bernstein, "Retrospective Cost Adaptive Control with Error-Dependent Regularization for MIMO Systems with Uncertain Nonminimum-Phase Transmission Zeros," *AIAA Guid. Nav. Contr. Conf.,* Minneapolis, MN, August 2012, AIAA-2012-4670-123.

[98] E. D. Sumer, and D. S. Bernstein, "Adaptive Control of Flexible Structures with Uncertain Dynamics and Uncertain Disturbance Spectra," in *AIAA Guid. Nav. Contr. Conf.,* Minneapolis, MN, August 2012, AIAA-2012-4437-323.

[99] E. D. Sumer, and D. S. Bernstein, "Adaptive Decentralized Noise and Vibration Control with Conflicting Performance Objectives," in *Proc. DSCC,* Fort Lauderdale, FL, October 2012, DSCC2012–MOVIC2012–8752.

[100] E. D. Sumer and D. S. Bernstein, "Robust Sampled-Data Adaptive Control of Rohrs Counterexamples," *Proc. Conf. Dec. Contr.,* pp. 7273–7278, Maui, HI, December 2012.

[101] E. D. Sumer, and D. S. Bernstein, "Aliasing Effects in Direct Digital Adaptive Control of Plants with High-Frequency Dynamics and Disturbances," in *Proc. Amer. Contr. Conf.,* Washingon, DC, June 2012.

[102] E. D. Sumer, A. M. D'Amato, and D. S. Bernstein, "Robustness of Retrospective Cost Adaptive Control to Markov Parameter Uncertainty," in *Proc. Conf. Dec. Contr.,* pp. 6085–6090, Orlando, FL, Dec 2011.

[103] E. D. Sumer, M. H. Holzel, A. M. D'Amato, and D. S. Bernstein, "FIR-Based Phase Matching for Robust Retrospective-Cost Adaptive Control," in *Proc. Amer. Contr. Conf.,* pp. 2707-2712, Montreal, Canada, June 2012.

[104] E. D. Sumer, J. Lu, D. P. Filev, J. B. Hoagg, and D. S. Bernstein, "Adaptive Road-Following Preview Control Using Radius of Curvature Data," in *Proc. Amer. Contr. Conf.,* pp. 4806–4811, Baltimore, MD, June 2010.

[105] G. Tao, *Adaptive Control Design and Analysis*, Wiley, 2003.

[106] G. Tao, and P. A. Ioannou, "Robust Model Reference Adaptive Control for Multivariable Plants," *International Journal of Adaptive Control and Signal Processing,* Vol. 2, No. 3, pp. 217–248, 1988.

[107] J. Tokarzewski, "A General Solution to the Output-Zeroing Problem For MIMO LTI Systems," *Int. J. Appl. Math. Comput. Sci.,* Vol. 12, No. 2, pp. 161–171, 2002.

[108] J. Tokarzewski, *Finite Zeros in Discrete Time Control Systems,* Springer-Verlag, 2006.

[109] A. I. G. Vardulakis, "Zero Placement and the 'Squaring Down' Problem: A Polynomial Approach," *International Journal of Control,* Vol. 31, No. 5, pp. 821–832, 1980.

[110] R. Venugopal and D. S. Bernstein. "Adaptive Disturbance Rejection Using AR-MARKOV System Representations," *IEEE Trans. Contr. Sys. Tech.*, Vol. 8, pp. 257–269, 2000.

[111] M. Vidyasagar, "Control System Synthesis: A Factorization Approach," M.I.T. Press, 1985.

[112] S. R. Weller, W. Moran, B. Ninness, and A. D. Pollington, "Sampling zeros and the Euler-Frobenius polynomials," *IEEE Trans. Autom. Contr.,* Vol. 46. No. 2, pp. 340-343, 2001.

[113] J. M. Whittaker, "Interpolatory Function Theory," *Cambridge Tracts in Mathematics and Mathematical Physics,* no. 33. Cambridge, UK, Cambridge Univ. Press, ch. IV, 1935.

[114] Y. Yamamato, B. D. O. Anderson, M. Nagahara, and Y. Koyanagi, "Optimizing FIR Approximation for Discrete-Time IIR Filters," *IEEE Signal Processing Letters*, vol. 10, no. 9, pp. 273-276, September 2003.

[115] P. C. Young and J. C. Willems, "An Approach to the Multivariable Servomechanism Problem," *International Journal of Control,* Vol. 15, pp. 961979, 1972.

[116] J. Zhou, and C. Wen, *Adaptive Backstepping Control of Uncertain Systems,* Springer, 2008.

[117] K. Zhou, J. C. Doyle, and K. Glover, *Robust and Optimal Control*, Prentice Hall, 1995.